1.0

2.8 2.5
3.2 2.2
3.6
4.0 2.0

1.1

1.8

1.25 1.4 1.6

MICROCOPY RESOLUTION TEST CHART
NATIONAL BUREAU OF STANDARDS-1963-A
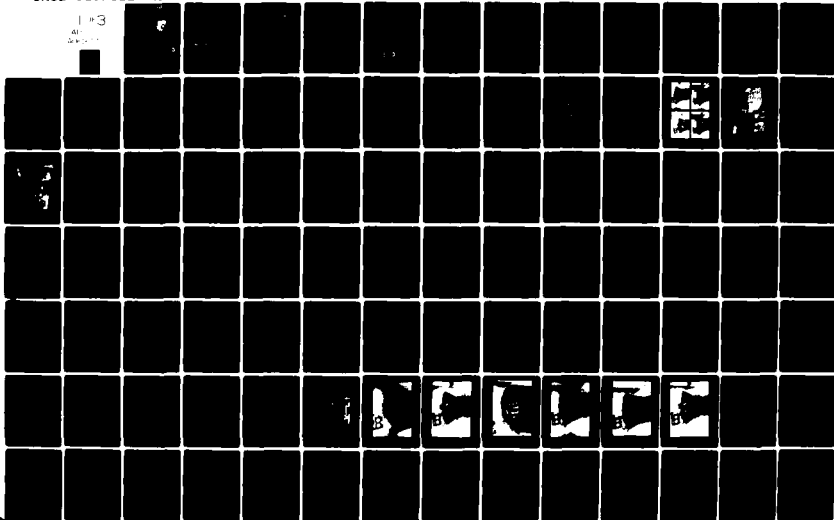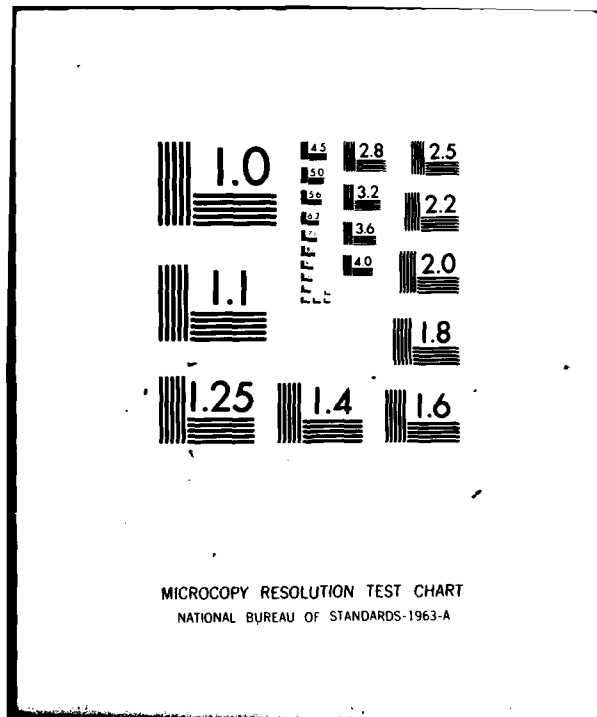
AFWAL-TR-80-3050

② LEVEL Ⅱ

**WEAPON BAY CAVITY NOISE ENVIRONMENTS
DATA CORRELATION AND PREDICTION FOR THE B-1 AIRCRAFT**

AD A089770

Rockwell International Corporation
North American Aircraft Division
P.O. Box 92098
Los Angeles, California 90009

JUNE 1980

Final Report for Period February 1979 to May 1980

Approved for public release; distribution unlimited

DTIC
SELECTED
OCT 1 1980

B

Prepared for

FLIGHT DYNAMICS LABORATORY
AIR FORCE WRIGHT AERONAUTICAL LABORATORIES
AIR FORCE SYSTEMS COMMAND
WRIGHT-PATTERSON AIR FORCE BASE, OHIO 45433

80 9 30 021

NOTICE

When Government drawings, specifications, or other data are used for any purpose other than in connection with a definitely related Government procurement operation, the United States Government hereby incurs no responsibility nor any obligation whatsoever, and the fact that the government may have formulated, furnished, or in any way supplied the said drawings, specifications, or other data, is not to be regarded by implication or otherwise as in any manner licensing the holder or any other person or corporation, or conveying any rights or permission to manufacture, use, or sell any patented invention that may in any way be related thereto.

This technical report has been reviewed and is approved for publication.

LEONARD L. SHAW
Project Manager

DAVEY L. SMITH, Chief
Structural Integrity Branch
Structures & Dynamics Division

FOR THE COMMANDER:

RALPH L. KUSTER, Jr., Colonel, USAF
Chief, Structures & Dynamics Division

"If your address has changed, if you wish to be removed from our mailing list, or if the addressee is no longer employed by your organization please notify AFWAL/FIRE, W-P AFB, OH 45433 to help us maintain a current mailing list."

Copies of this report should not be returned unless return is required by security considerations, contractual obligations, or notice on a specific document.

AIR FORCE/56780/12 September 1980 — 270

REPORT DOCUMENTATION PAGE	READ INSTRUCTIONS BEFORE COMPLETING FORM

1. REPORT NUMBER	2. GOVT ACCESSION NO.	3. RECIPIENT'S CATALOG NUMBER
AFWAL TR-80-3050	AD-A089770	

4. TITLE (and Subtitle)	5. TYPE OF REPORT & PERIOD COVERED
WEAPON BAY CAVITY NOISE ENVIRONMENTS, DATA CORRELATION AND PREDICTION FOR THE B-1 AIRCRAFT	Final Report. February 1979 to May 1980
	6. PERFORMING ORG. REPORT NUMBER
	NA-80-247

7. AUTHOR(s)	8. CONTRACT OR GRANT NUMBER(s)
A. G. Tipton	F33615-79-C-3208

9. PERFORMING ORGANIZATION NAME AND ADDRESS	10. PROGRAM ELEMENT. PROJECT, TASK AREA & WORK UNIT NUMBERS
Rockwell International North American Aircraft Division El Segundo CA P.O. Box 92098, Los Angeles, CA 90009	11541 2401

11. CONTROLLING OFFICE NAME AND ADDRESS	12. REPORT DATE
Flight Dynamics Laboratory (AFWAL/FIBE) Air Force Wright Aeronautical Laboratories Wright-Patterson AFB, Ohio 45433	June 1980
	13. NUMBER OF PAGES
	240

14. MONITORING AGENCY NAME & ADDRESS(if different from Controlling Office)	15. SECURITY CLASS. (of this report)
	Unclassified
	15a. DECLASSIFICATION/DOWNGRADING SCHEDULE

16. DISTRIBUTION STATEMENT (of this Report)

Approved for public release; distribution unlimited

17. DISTRIBUTION STATEMENT (of the abstract entered in Block 20, if different from Report)

18. SUPPLEMENTARY NOTES

19. KEY WORDS (Continue on reverse side if necessary and identify by block number)

Cavity oscillations, pressure oscillations, prediction methods, noise reduction

20. ABSTRACT (Continue on reverse side if necessary and identify by block number)

During development of the B-1 aircraft, an extensive cavity noise measurement and noise reduction program using wind tunnel models and evaluation on a flight-test aircraft was conducted. Substantial cavity noise reduction was achieved with retrofitted spoilers for a mach 0.6 to 1 range for the weapon bay cavity of L/D = 2.2. A substantial amount of cavity unsuppressed and suppressed data were acquired from wind tunnel models and the full-scale aircraft. Data ———over

DD FORM 1473 EDITION OF 1 NOV 65 IS OBSOLETE
1 JAN 73

20. ABSTRACT (Continued)

for weapon bay cavities with internal stores and multiple open cavities was also obtained. The data acquired during development of B-1 cavity noise suppressors are correlated and compared with previously published data. The data are correlated with existing prediction techniques and modifications to the current prediction techniques, and guidelines are recommended.

FOREWORD

This report was prepared by Rockwell International (Rockwell), North American Aircraft Division (NAAD), El Segundo, California, for the Structural Integrity Branch, Structures and Dynamics Division, Flight Dynamics Laboratories, Air Force Wright Aeronautical Laboratories under contract F33615-79-C-3208. This work was conducted under project 2401.

Mr. L. L. Shaw was the Air Force project engineer.

This report concludes work from February 1979 to April 1980 and was submitted for publication in April 1980.

DTIC
SELECTED
OCT 1 1980
B

ACCESSION for

NTIS   White Section

DDC   Buff Section ☐

UNANNOUNCED   ☐

JUSTIFICATION _____

BY

DISTRIBUTION/AVAILABILITY CODES

Dist.   AVAIL. and/or SPECIAL

A

iii

TABLE OF CONTENTS

LIST OF ILLUSTRATIONS

DEFINITION OF SYMBOLS

f	=	frequency, cycles per second
Hz	=	frequency, cycles per second
L	=	cavity length
D	=	cavity depth
V	=	freestream velocity
M	=	freestream mach number
m	=	cavity mode number 1, 2, 3, 4
FO	=	full-open door position
PO	=	part-open door position
γ	=	specific heat rates (1.4)
S	=	strouhal number $\dfrac{fL}{V}$
Q	=	dynamic pressure
P	=	cavity noise level pressure-psi
SPL	=	cavity noise level $20 \log \left(\dfrac{P}{2.9 \times 10^{-9}} \right)$
dB	=	decibel (SPL)
Δ dB	=	decibel difference $SPL_1 - SPL_2$
$\dfrac{dB}{Hz}$	=	noise level power spectral density
x	=	cavity length coordinate
y	=	cavity depth coordinate
FBW	=	filter band width in Hz

Subscripts

1,2,3	=	mode number discrete (m)
RMS	=	root mean square
OA	=	overall level
max	=	maximum level
b	=	broadband

SECTION I

INTRODUCTION

Cavities in the external structural surfaces of aircraft that are exposed to high-speed external flow generate intense pressure fluctuations. The amplitude of these fluctuations can be of such magnitude as to affect the structural integrity of nearby aircraft components, internal stores, and crewmembers comfort.

Substantial previous effort has gone into the study of cavity pressure oscillations, resulting in better understanding of the physical mechanisms and the complex interaction of the cavity external shear layer and the cavity internal fluid medium which is responsible for generation of the highly periodic pressure fluctuations.

In 1970, the aeroacoustic characteristics of shallow rectangular cavities in the mach 0.8 to 3 range were investigated by Heller, Holmes, and Covert in Reference 4. The main result of this study relates nondimensional resonance frequencies and free-stream mach numbers. However, only an upper bound for resonance amplitudes could be derived. At that time, the phenomena were still understood too poorly to reliably predict the occurrence of discrete pressure oscillations and their energy distribution within the cavity.

In 1972, the Air Force conducted extensive flight tests using an RF-4C aircraft with a modified SUU 41 test pod. Results became available[6] on the aeroacoustic environment of shallow cavities in the mach 0.6 to 1.3 range for realistic flight environments (Smith, et al, 1975). It seemed that the previously assumed upper bound level for resonant modes was generally too high. The test data were correlated with previous prediction methods, based on wind tunnel data, and a modified prediction method was established, based on measured aircraft levels for cavities with length/depth (L/D) ratios between 4 and 7.

In 1975, Heller and Bliss[5] evaluated cavity oscillation and suppression concepts in order to improve understanding of the complex interaction of shear layer and cavity internal fluid medium that results in high-intensity pressure fluctuations. Wind tunnel tests were conducted for cavities in the L/D 2.3 to 5.5 range and mach 0.8 to 2 range. Several concepts for pressure oscillation suppression were developed and evaluated. The empirical wind tunnel and previous Air Force data were correlated with prediction techniques that use Mach number, dynamic pressure (Q), L/D, and fL/V_∞.

In 1975, R. Clark[13] evaluated weapons bay turbulence and reduction techniques, using several weapon bay geometries for the Mach 0.7 to 0.9 range. The internal cavity pressures were expressed as a function of Q, cavity length, angle of attack, and mach number.

In 1979, L. Shaw (Reference 15) reported the results of a flight test which evaluated the effectiveness of several suppression concepts for a mach number range of 0.6 to 1.3. Reductions as large as 30dB overall, obtained with the most effective concept of leading edge spoiler and rear bulkhead slant, were achieved.

1

During development of the B-1 aircraft in the mid 1970's, Rockwell International (Rockwell) conducted an extensive cavity noise measurement and noise reduction program, using wind tunnel models and evaluation on a flight-test aircraft. Substantial cavity noise reduction was achieved with retrofitted spoilers for the weapon bay cavity of L/D = 2.2. A substantial amount of cavity unsuppressed and suppressed data were acquired from wind tunnel models and the full-scale aircraft. The data acquired during development of B-1 cavity noise suppressors are correlated and compared with previously published data. The data are correlated with existing prediction techniques and modifications to the current prediction techniques, and guidelines are recommended.

SECTION II

REVIEW CAVITY OSCILLATION MECHANISMS

The theory of cavity pressure oscillations has been evaluated by a number of investigators and published in literature. A summary of the published information concerning the cavity oscillation phenomena is presented in the following paragraphs.

Plumblee, et al (1962), hypothesized that the environment inside the cavity is induced by forced acoustic response of the cavity.

Experimental results of Karamecheti (1955) and Heller, et al (1970), have cast doubt on the assumption that the forcing mechanisms which drive the cavity are provided by fluctuations in the turbulent boundary layer. Cavity oscillations are most intense when the boundary layer upstream is laminar. Thickening the boundary layer has the effect of reducing oscillation intensity (Heller, 1970). Rossiter (1966) also concurs, pointing out that when a small spoiler is placed upstream of the cavity it reduces oscillation intensities.

Since excitation frequencies of shallow cavities do not agree with the acoustic modal frequencies of the enclosure, investigators have sought an excitation mechanism that is not strongly dependent on the detailed acoustics in the shallow cavity. Rossiter (1966) suggested such a mechanism, based on feedback similar to that used by Powell (1961), to describe the production of edge tones. Using a shadowgraph, Rossiter observed that periodic density fluctuations travel downstream over the cavity mouth. These fluctuations were assumed to be vortices shed from the leading edge of the cavity. The shadowgraphs also show acoustic waves in the cavity whose primary source is near the trailing edge. Assuming that the vortices were shed when an acoustic disturbance reached the leading edge of the cavity and that acoustic disturbances were generated when the vortices reached the cavity trailing edge, Rossiter was able to determine a frequency relation at which oscillation might occur. Although this frequency relation requires two empirically determined constants, a reasonable agreement with experimental data can be obtained over a moderate mach number range. Heller, et al (1970), improved this result by correcting for the speed of sound in the cavity.

Pressure oscillation in shallow cavities was believed to result from the unstable shear layer which spans the cavity being forcibly displaced by disturbances that are generated at, or near the cavity trailing edge. These disturbances were thought to arise from the interaction of the oscillating shear layer with the trailing edge.

Although these disturbances should force the shear layer along the entire cavity length, models that assumed coupling to occur only at the leading edge of the cavity have given good predictions for allowable frequencies of oscillation. Thus, the shear layer is most sensitive to perturbations at the leading edge, where it is thinnest.

Although the preceding feedback mechanism, as suggested by Rossiter and modeled by Bilanin, estimated possible excitation frequencies, it did not predict whether any of these will occur. Selection of the excited frequency was thought to be based on a gain criterion; i.e., the frequency or frequencies at which a cavity responds must correspond to the mode or modes receiving sufficient gain along the feedback loop.

To illustrate this idea, let us suppose that for a given geometry and external velocity the possible frequencies of oscillation are estimated using the preceding feedback model. The shear layer is then forced at the leading edge with a periodic pressure fluctuation with frequency corresponding to a possible excitation frequency. The shear layer is displaced, and vorticity waves propagate aft and interact with the trailing edge of the cavity, causing a pressure disturbance to be generated. Upon reaching the leading edge of the cavity, this pressure disturbance will have the same phase as the forcing pressure (the frequency chosen is a possible excitation frequency), but the amplitude of the disturbance will not, in general, equal the forcing amplitude. If the returning pressure disturbance is of smaller amplitude than that of the forcing pressure (gain 1.0), it can be anticipated that this mode cannot sustain oscillation. However, if the returning disturbance is of greater amplitude than the forcing (gain 1.0), the oscillation amplitude will be increased until nonlinear effects have reduced the gain to unity. The amplitude at which a cavity will oscillate is that amplitude at which the gain is unity; i.e., when the energy addition to the feedback loop from the external flow just balances the energy losses through viscosity and radiation. If other possible frequencies of excitation can meet this gain criterion, then the excitation of simultaneous discrete frequencies, as observed in practice, is possible.

The physical mechanism of cavity oscillations and shear layer interaction is further described by Heller and Bliss (1975):

> "The flow separates at the sharp leading edge of the cavity, and a shear layer grows downstream. At the rear bulkhead, the flow stagnates and splits. Part of the shear layer enters the cavity, and the rest passes over the cavity trailing edge and continues downstream as part of the downstream boundary layer. In the laminar flow case a streamline divides the flow which enters the cavity from that which does not. The same fluid always remains in the cavity. The fluid that is entrained from the cavity by the shear layer over the cavity mouth is returned to the cavity by the trailing-edge stagnation process. The same is essentially true when the shear layer is turbulent, although there will actually be some change in which fluid elements occupy the cavity. This exchange of fluid occurs because of the turbulent diffusion across the dividing steamline. The mass addition and removal process at the cavity trailing edge is caused by unsteady motion of the shear layer. This process produces a piston-like effect at the rear bulkhead, which sets up the internal wave structure that forces the shear layer. This shear layer motion is responsible for the trailing-edge mass addition and removal. The wave motion of the shear layer and the wave structure within the cavity are strongly coupled and cannot be considered separately as long as the wave length is comparable to or exceeds the cavity depth. The cavity internal wave structure is composed primarily of upstream and downstream traveling wavetrains. Their combination produces a modal unsteady pressure field in the cavity. The fluid motion within the cavity is governed by the solution of the wave equation in a region bounded by a rigid front bulkhead and floor, with a free shear layer on top, and a rear bulkhead, which oscillates like a piston. This oscillating bulkhead approximates the pseudopiston effect of mass addition and removal at the trailing edge."

4

SECTION III

CORRELATION OF B-1 DATA

The acoustic environments in the weapons bays were studied extensively during the B-1 design and development program. Figure 1 indicates the location and geometry of the three weapons bays.

The B-1 weapons bay doors have two modes of operation, fully open and approximately half open. The internal bay geometry is shown in Figure 2. The microphone installation on the bay forward and aft bulkheads and sidewalls was the same for all three weapon bay cavities and is shown in Figure 3.

The acoustic levels in the weapons bays resulted in potential problems for open-bay operation at high dynamic pressures, including acoustic fatigue of the internal bay structure, high vibration levels at the crew station and, possibly, excessive vibrations of the weapons and other aircraft equipment. The most severe problem was vibration of the weapons bay doors, due to coincidence of the natural vibration frequencies of the doors and the cavity resonance frequencies. The near coincidence of the frequencies caused a forced vibration of the doors which would have resulted in structural failure of the doors in a very short time if the doors had been opened at high dynamic pressure.

The potential problems caused by the high acoustic levels made it necessary to incorporate cavity resonance suppression devices on the weapons bays. Preliminary wind tunnel test data indicated that cavity noise could be reduced by spoilers in front of the weapons bays.

Subsequent evaluation of cavity noise suppression devices was carried out in wind tunnel tests in April and June of 1975. The emphasis in these tests was on developing a spoiler configuration which could be retracted and was feasible for installation within the space limitations imposed by the aircraft. Several configurations were tested. These included 70-degree ramps, 90-degree fences, porous panels, panels which did not span the full width of the weapons bays, and panels with gaps at the base to reduce buffeting of the panel. Some of these configurations are shown in Figure 4.

It was uncertain how reliable small-scale (1/10-scale) wind tunnel tests of the noise suppression devices could be for predicting full-scale performance. Therefore, design of a flight-test spoiler configuration which could be quickly installed on the actual aircraft was initiated. The flight-test configuration was designed to allow testing with variations in ramp angle, gap size, and spoiler span. The initial test installation is shown in Figure 5 with all four of the individually actuated spoiler panels deployed. Both porous and solid spoiler panels were evaluated. The porous panel is shown in Figure 6. Extensive open-bay flight tests were then conducted with the flight-test spoiler configurations on aircraft 1 and 3 for empty bays, several internal store configurations, and full- and part-open doors.

The final test configuration adopted for installation on the aircraft was a 90-degree porous fence, spanning approximately half the weapons bay width, extending 14 inches below the fuselage, and having a 3-1/2 inch gap at the base of the panel. The spoiler was installed at the front of the bay as shown in Figure 7.

Aft bay

Center bay

Fwd bay
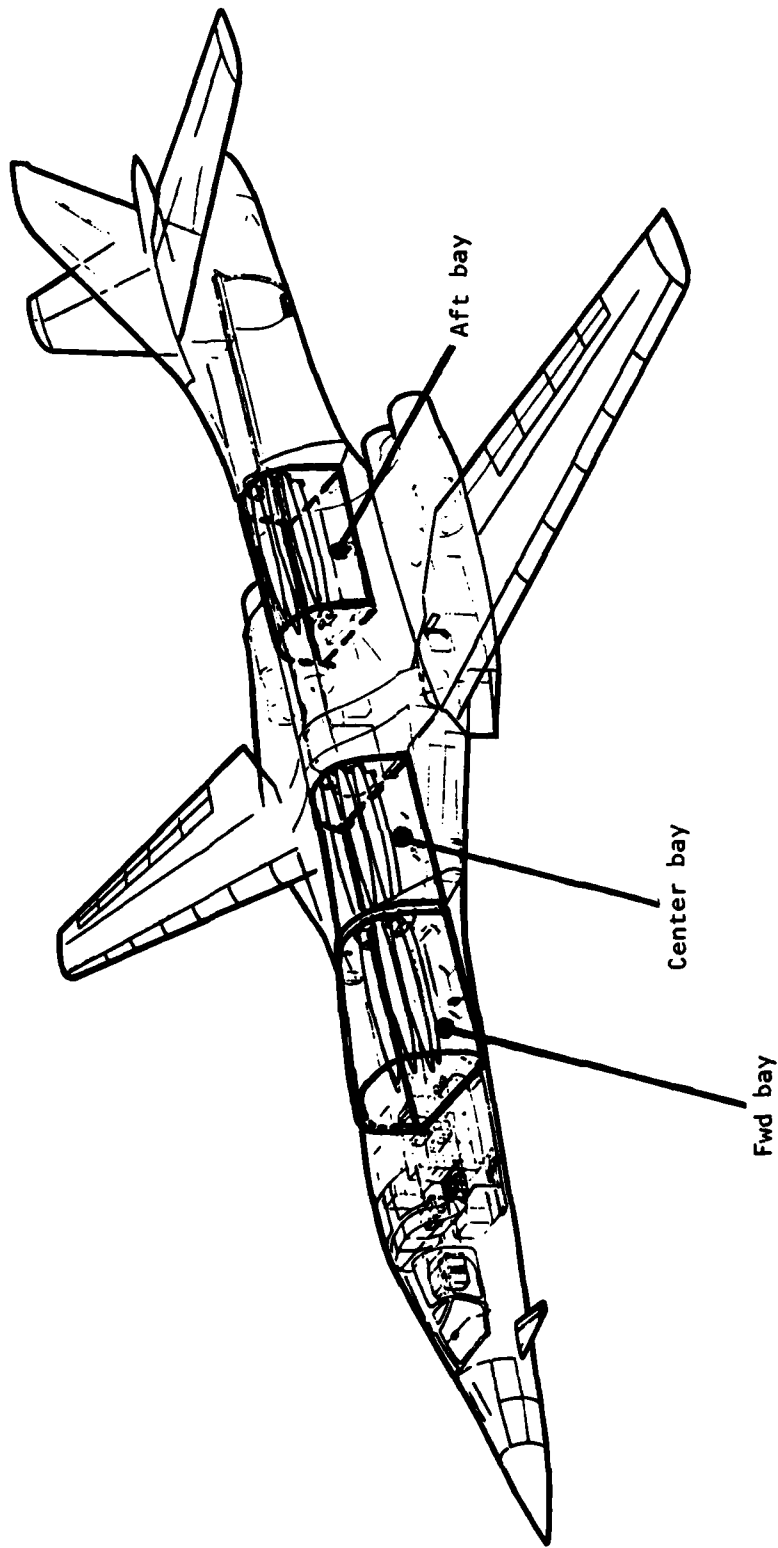
Figure 1. View Indicating Weapons Bay Locations
With Respect to Complete Aircraft
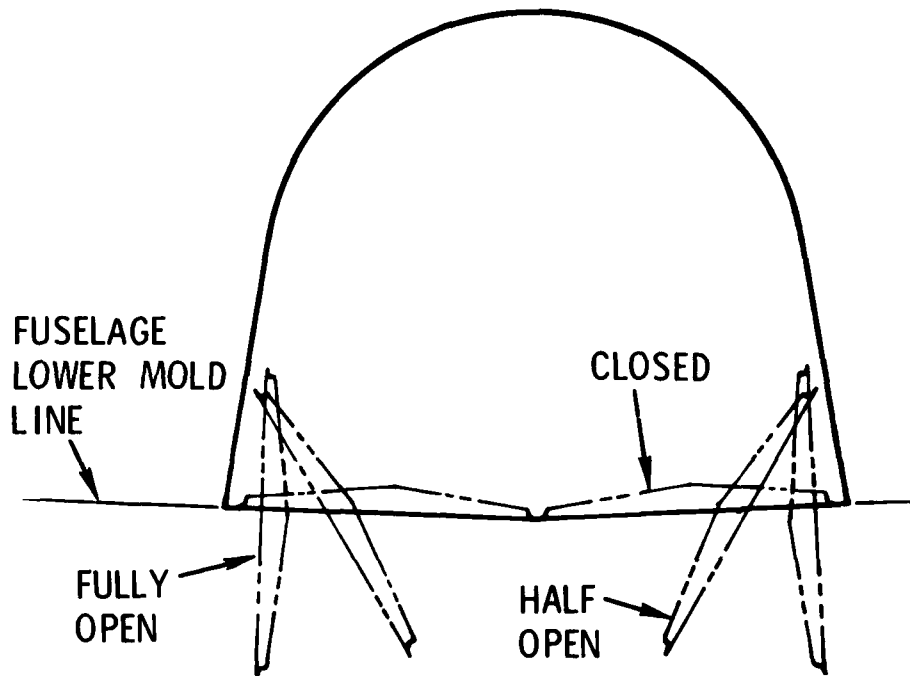
Figure 2. Weapons Bay Door Positions
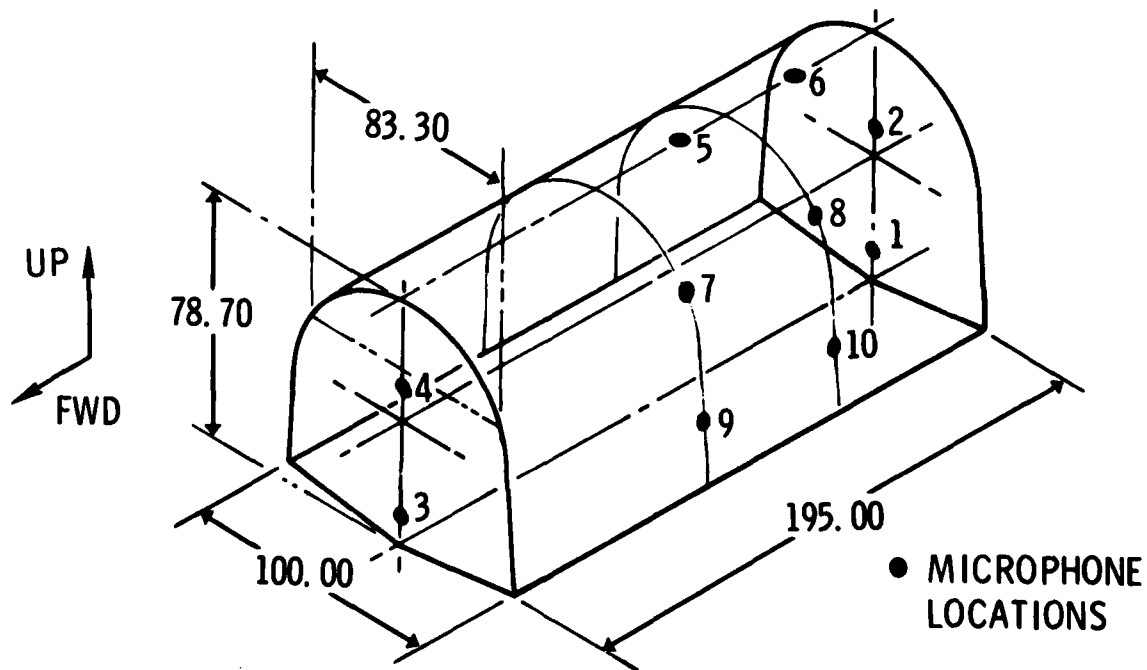
Figure 3. Weapons Bay Geometry and Microphone Locations

7
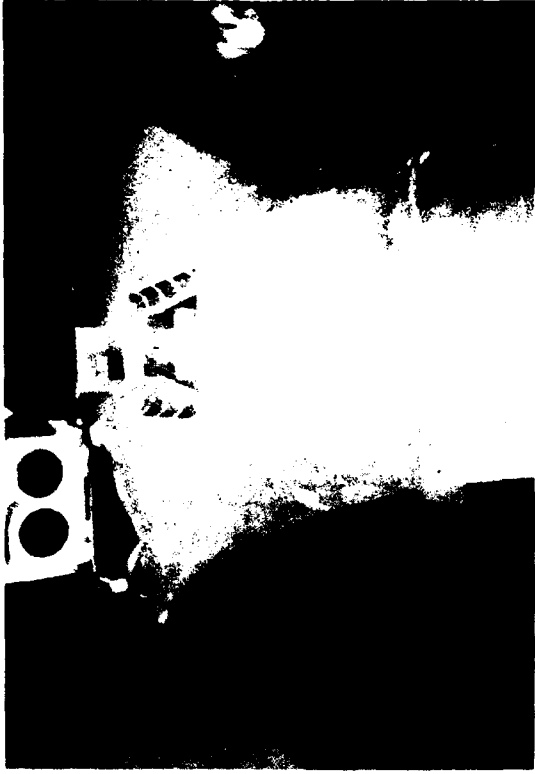
Figure 4. Suppressor Evaluation - 0.10 Scale Wind Tunnel Test

Figure 5. 70° Solid Spoiler Installation

9

Figure 6. View of Perforated Spoiler Assembly
Central Weapons Bay - A/C-1

10
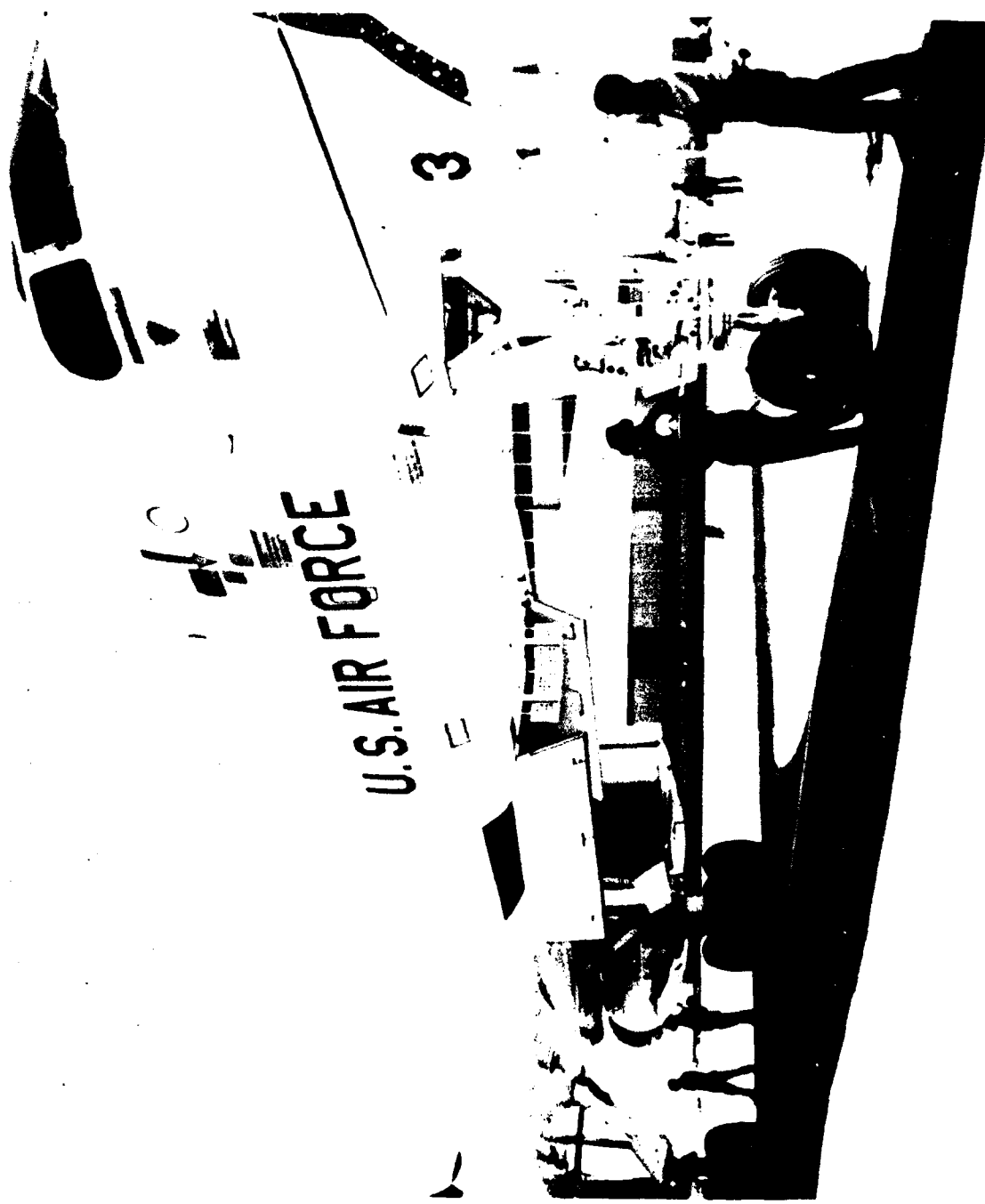
Figure 7. 90° Porous Spoiler Installation

11

Extensive data were obtained in wind tunnels and on the full-scale aircraft over a range of subsonic and supersonic mach numbers for several cavity configurations. Data were recorded with and without noise reduction spoilers, with full- and part-open doors, with internal stores, and for two open cavities in close proximity.

The B-1 cavity noise data will be grouped to illustrate characteristics of the noise level for specific cavity configurations as a function of mach number and dynamic pressure. The configurations are:

1. Empty cavity without noise suppression devices

2. Empty cavity with noise suppression devices

    a. 70° solid spoiler combinations of inboard and outboard

    b. 70° porous spoiler combinations of inboard and outboard

    c. 90° porous spoiler

3. Cavity/store configurations without noise suppression devices

4. Cavity/store configurations with noise suppression devices

5. Two adjacent cavities

Cavity noise level measurements for the full-scale aircraft have been recorded incrementally for a range of mach 0.6 to 1.5 and dynamic pressures from 250 to 1070 psf. The noise level distribution within the cavity for each cavity configuration and flight data point has been recorded with 10 internal microphones. The wind tunnel data were recorded for similar cavity configurations for a range of Mach 0.6 to 2.2 and dynamic pressures from 500 to 1,700 psf.

EMPTY CAVITIES WITHOUT SUPPRESSION

The noise level in open cavities consists of periodic oscillations and broadband random pressure levels with a continuous frequency distribution. The periodic pressures occur at specific frequencies which relate to cavity size and flow conditions over the cavity opening. Typical cavity noise spectra are shown in Figure 8 illustrating the periodic and random characteristics of cavity noise. The noise level is shown for full- and part-open doors. For the part-open door positions, three periodic discrete modes are shown superimposed on the broadband random noise level. The full-open door shows four discrete modes but with the first mode noise level at a greater magnitude. The pressure level of the various cavity modes and the broadband noise level vary with mach number and dynamic pressure. The pressure level for both the discrete modes and the broadband noise varies within the cavity enclosure. The pressure level variations as a function of mach number and location within the cavity for the broadband and discrete cavity mode are illustrated separately. The overall broadband noise level is computed from the spectral density data by eliminating the discrete components and integrating only the broadband pressures to obtain the pure random noise level.
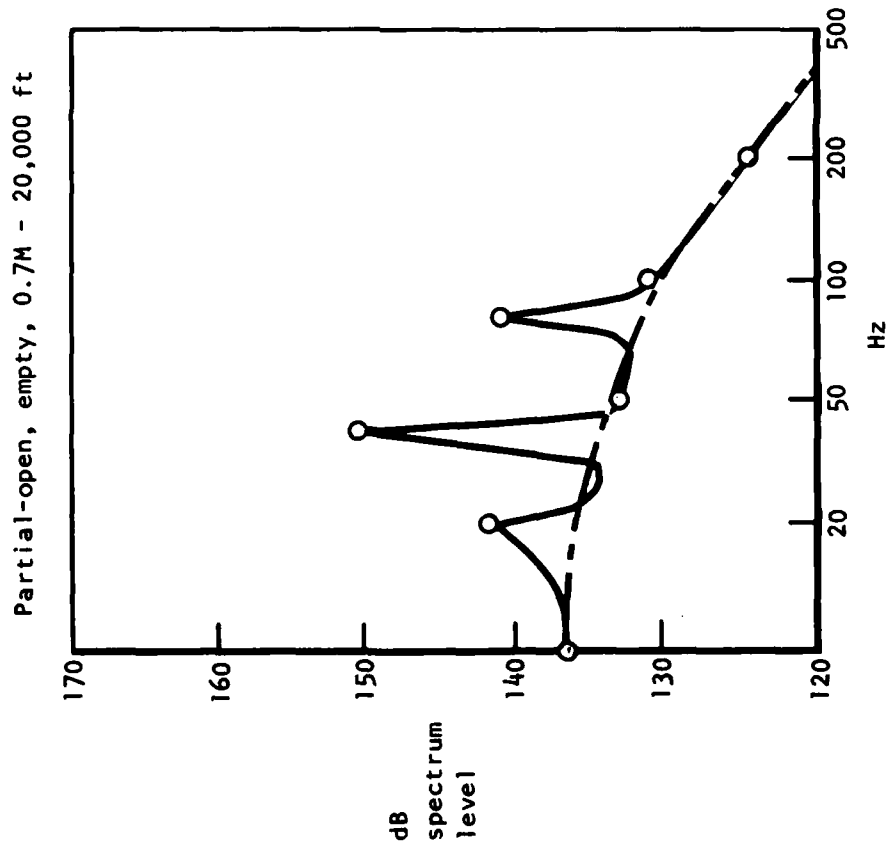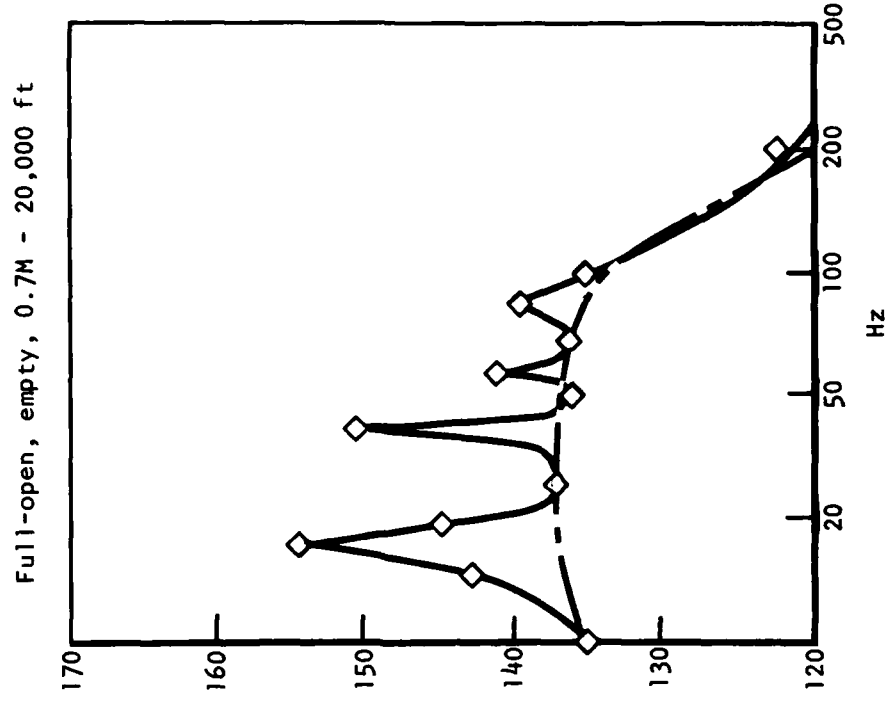
Figure 8. Weapons Bay Acoustic Levels - Unsuppressed

DISCRETE MODE VERSUS MACH NUMBER

The data in Figures 9 through 18 illustrate the magnitude variation of the significant cavity modes as a function of mach number at constant dynamic pressure. Both full-scale and wind tunnel model data are shown for part- and full-open door positions. The full-scale aircraft data also show cavity noise measured in the aft weapons bay cavity between the engine nacelles.

The first two modes in the intermediate bay show the highest level at subsonic speeds and are reduced in amplitude as mach number increases. The pressure magnitude of higher frequency modes 3 and 4 are lower in level and relatively constant with mach number. The noise levels in the forward weapon bay cavity are the same as for the intermediate bay when only a single bay is open.

The variation in pressure level in the aft weapon bay cavity between the nacelles shows a different trend with mach number. The noise levels for part-open doors shown in Figures 9 through 12 are slightly higher in the aft bay at subsonic speeds, but at supersonic speeds the third mode is significantly higher in the aft weapon bay cavity. The noise levels for full-open doors illustrated in Figures 13 through 16 show higher noise levels in the aft cavity except for the first mode in the intermediate bay, which shows a noise level peak in the transonic mach number range that exceeds the levels in the aft bay by an order of magnitude. It is suspected that the noise levels in the aft weapon bay cavity are influenced by the engine nacelles and therefore will not be correlated with the other published data and cavity noise prediction technique in Section IV. The cavity noise level in the forward and intermediate weapon bay cavities are similar and are not affected by disturbances upstream or adjacent ot the cavities that are peculiar to the B-1 aircraft configuration and would therefore have more general applicability in terms of noise level correlation and prediction.

Wind tunnel data for the intermediate weapon bay cavity are shown in Figures 17 and 18. At part-open door positions, the second mode is dominant for both the full-scale and model data but shows peak levels occurring at supersonic speed for the model and subsonic speeds for the full scale. On the average, the magnitude of the model noise levels are higher than the full scale at constant dynamic pressure.

For full-open door positions, the model and full-scale data correlate reasonably well except for slightly higher noise levels for the model.

BROADBAND NOISE VERSUS MACH NUMBER

The overall broadband noise levels for the full-scale aircraft and wind tunnel models are shown plotted in Figures 19 through 24 as a function of mach number. Data are plotted for a variety of conditions, and therefore the noise level is normalized to dynamic pressure. The symbols plotted in Figures 19 through 24 are correlated in Table 1 with dynamic pressure, mach number, and whether obtained in wind tunnel models or the full-scale aircraft. Data are illustrated for part- and full-open door positions for the aft bulkhead and forward bulkhead of the cavity.
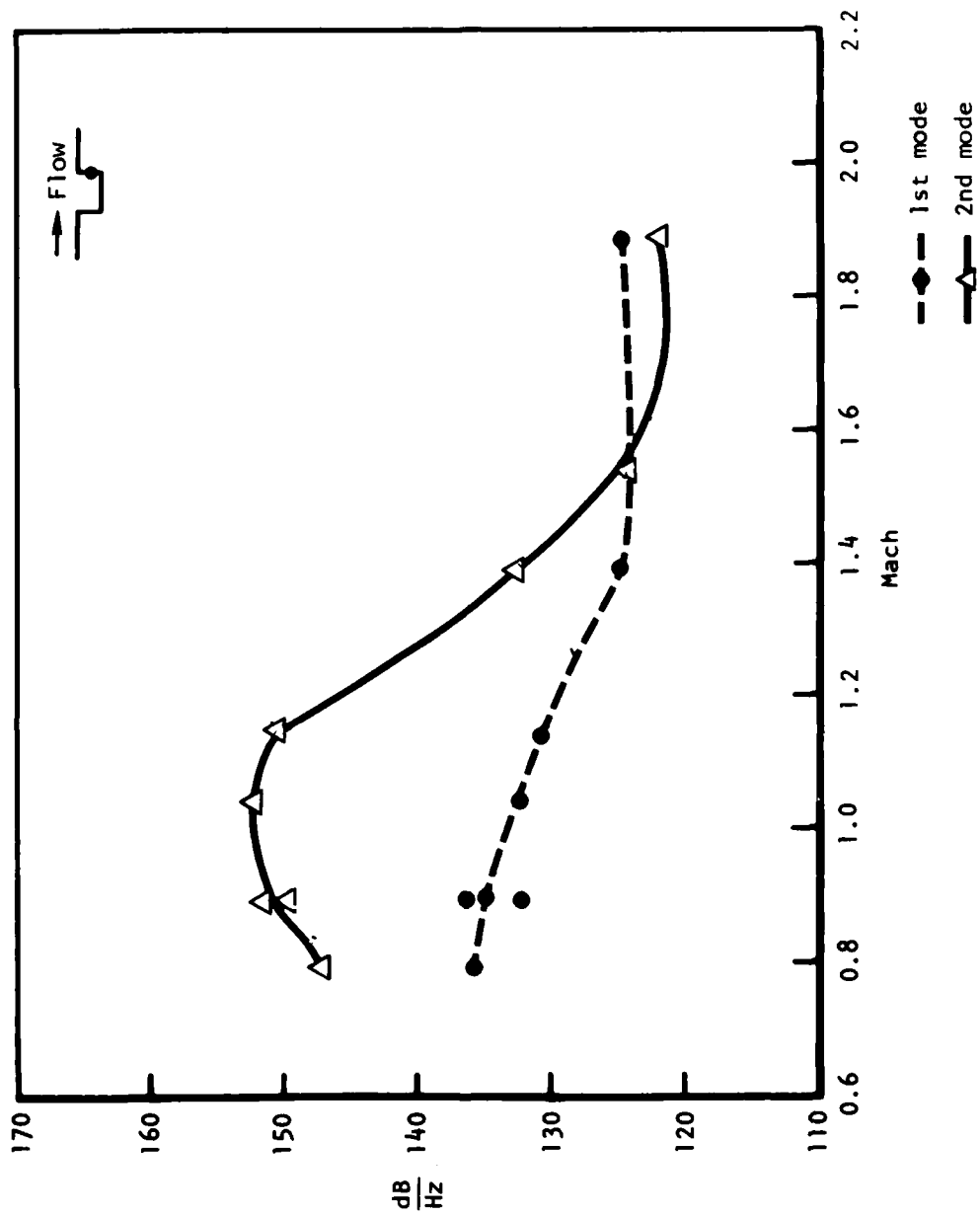
Figure 9.   Center Bay Unsuppressed, Aft Bulkhead Upper, Part Open, Q = 500 psf

15
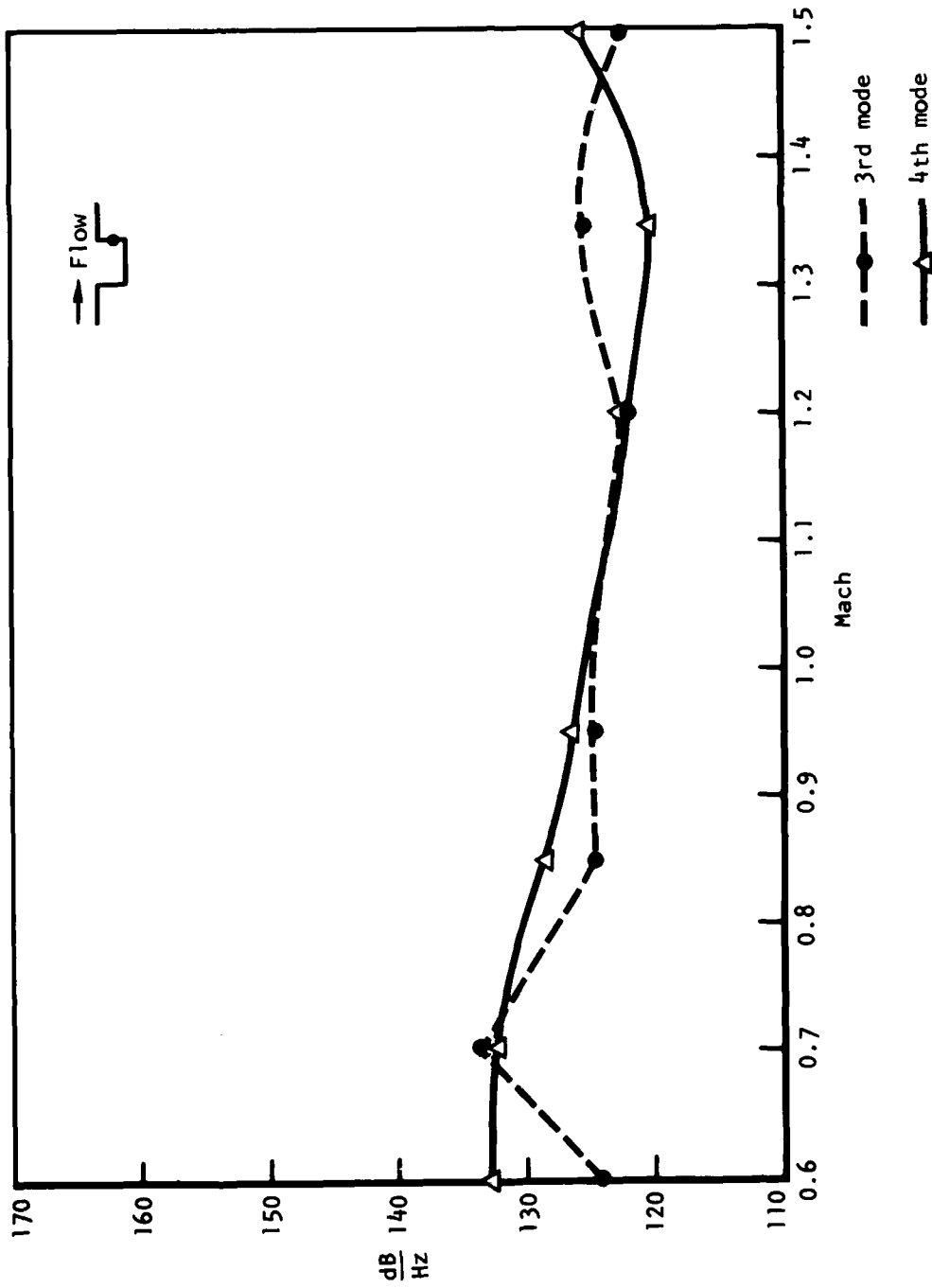
Figure 10. B-1 Full-Scale Flight Data Unsuppressed, Aft Bulkhead Upper, Part-Open, Q = 500 psf, Center Bay
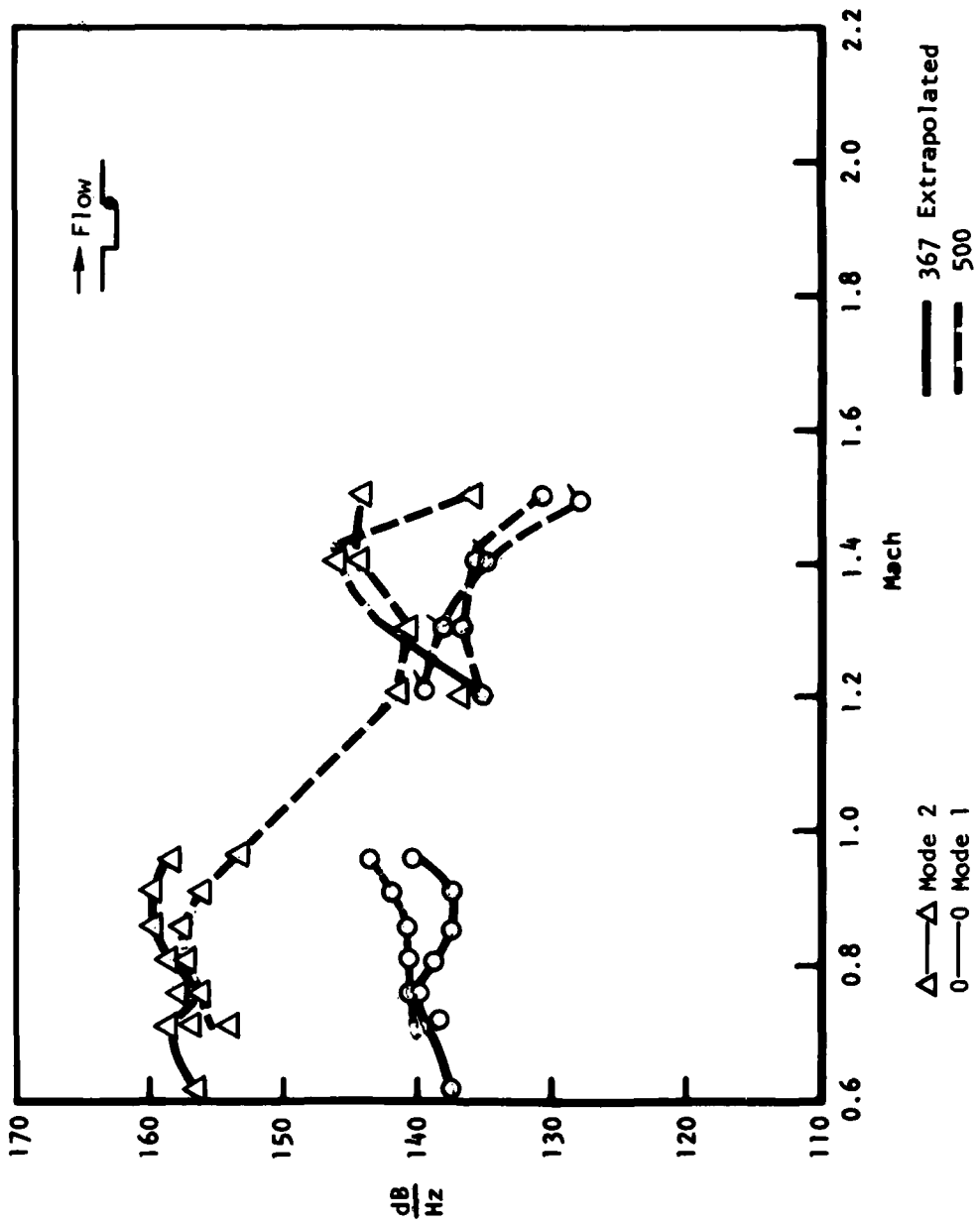
Figure 11. Aft Bay Unsuppressed, Aft Bulkhead Upper, Part-Open, Q = 500 psf
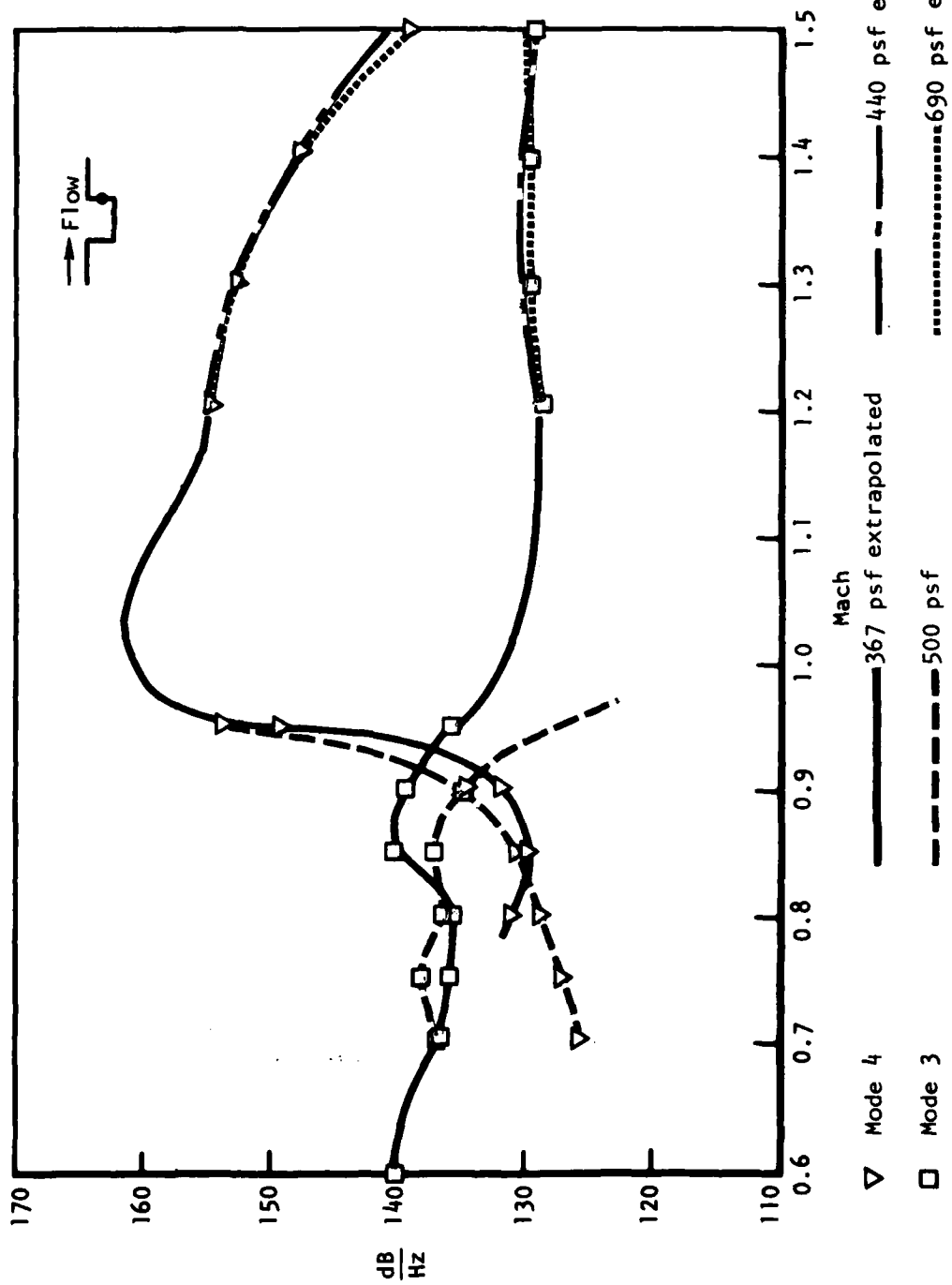
Figure 12. Aft Bay Unsuppressed, Aft Bulkhead Upper, Part-Open, Q = 500 psf

18
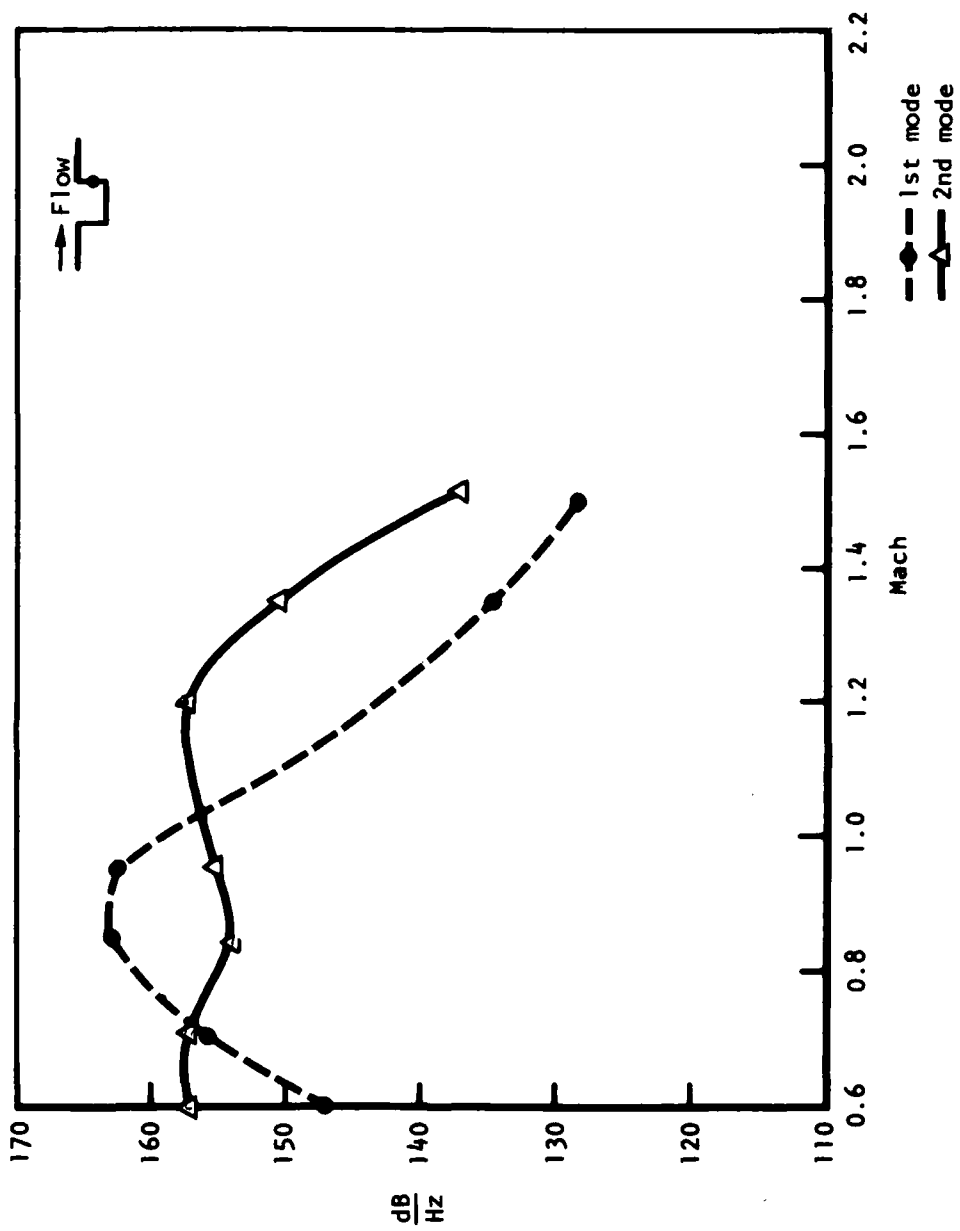
Figure 13. Center Bay Unsuppressed, Aft Bulkhead Upper, Full-Open, Q = 500 psf

19
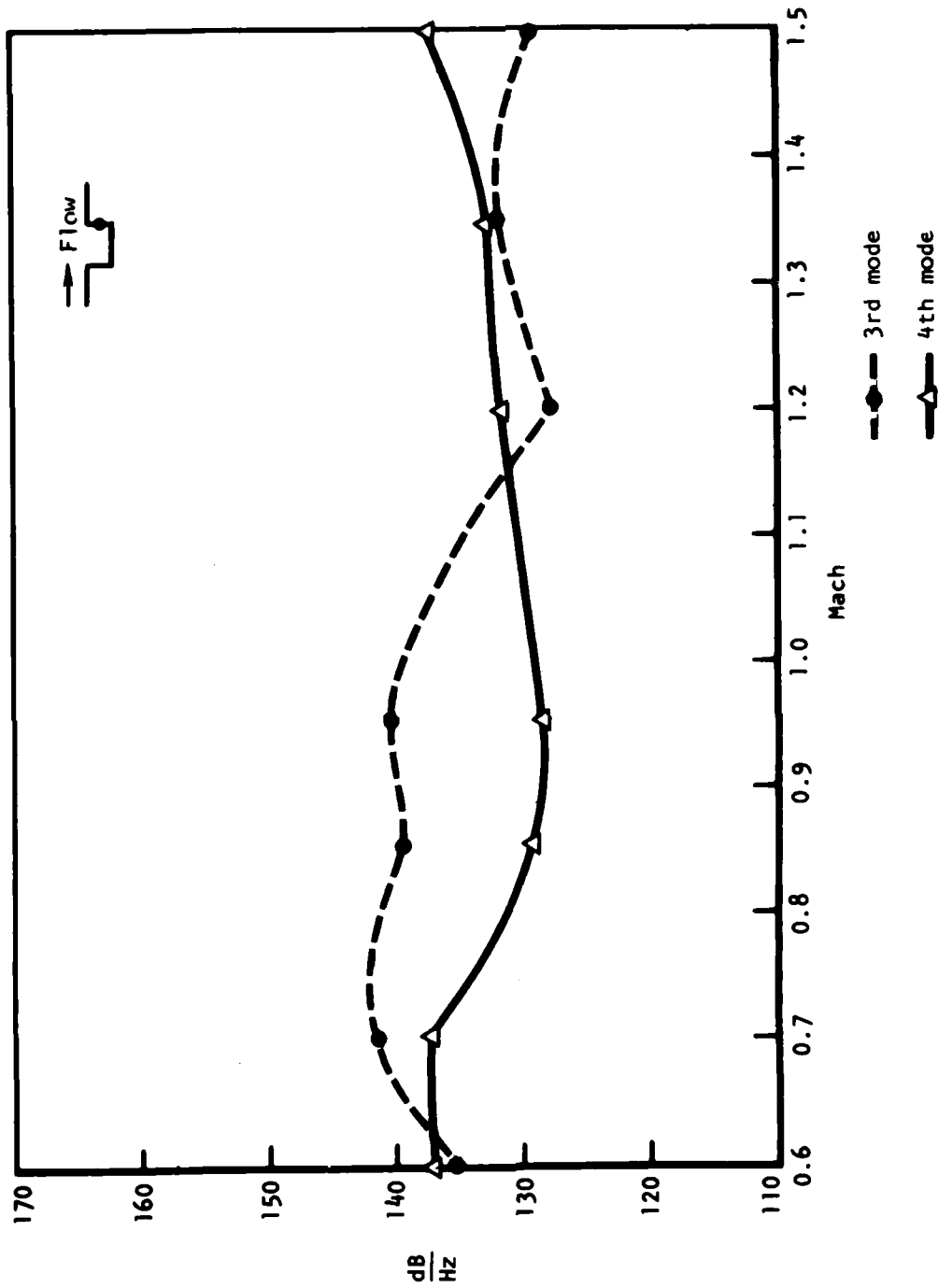
Figure 14.   B-1 Full-Scale Flight Data, Unsuppressed, Aft Bulkhead Upper, Full-Open, Q = 500 psf, Center Bay

20
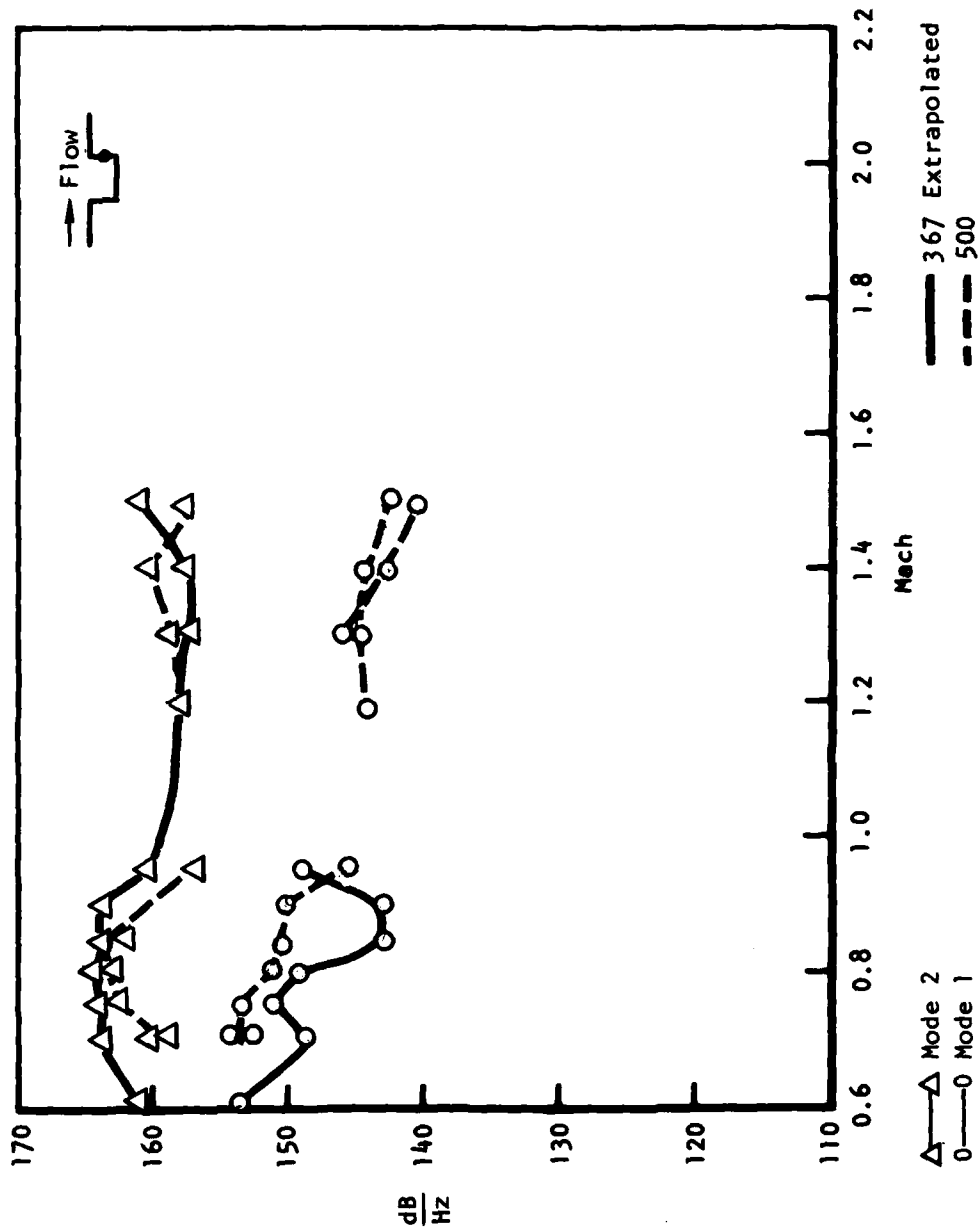
Figure 15. Aft Bay Unsuppressed, Aft Bulkhead Upper, Full-Open, Q = 500 psf

21
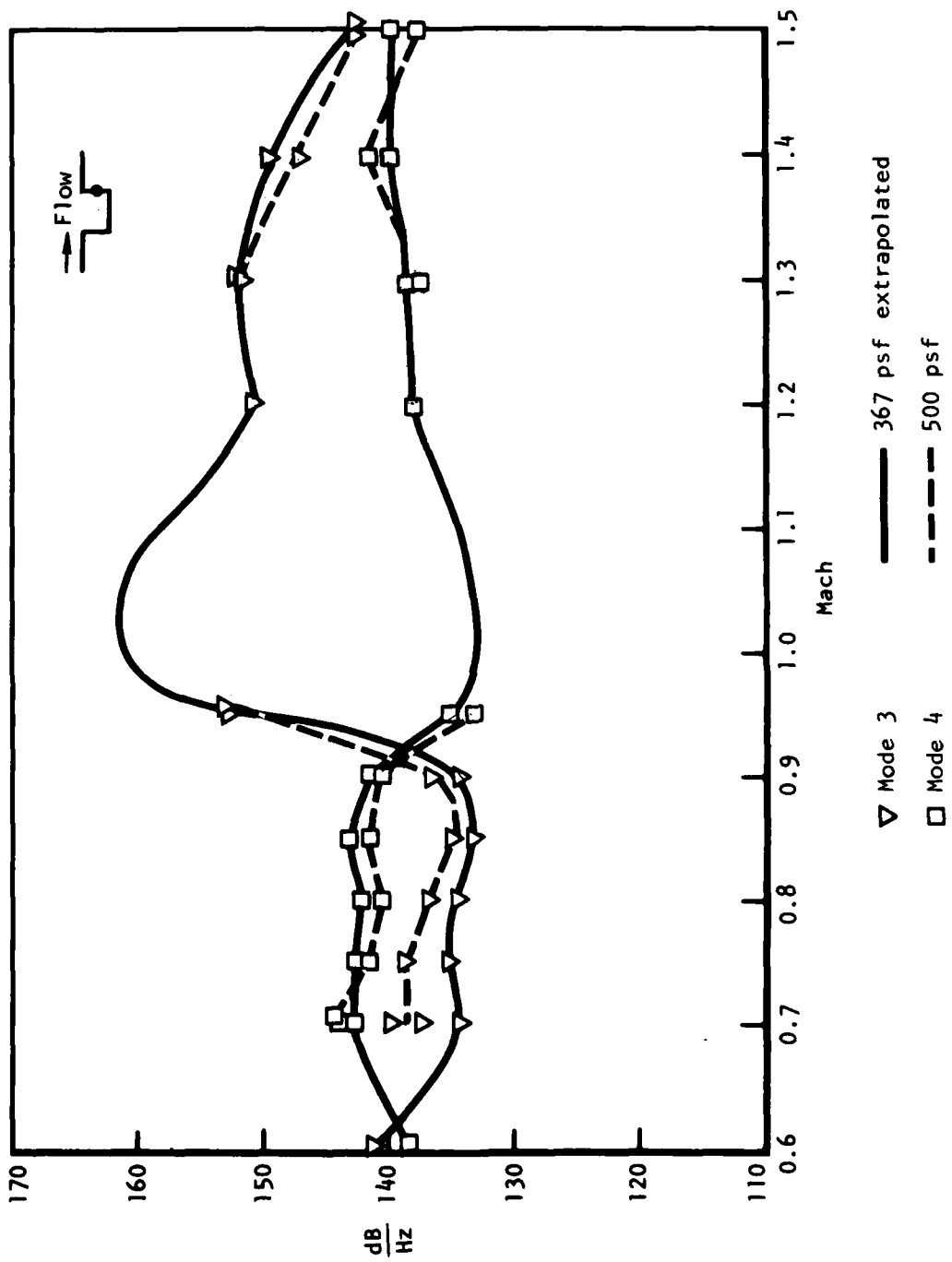
Figure 16. Aft Bay Unsuppressed, Aft Bulkhead Upper, Full Open, Q = 500 psf
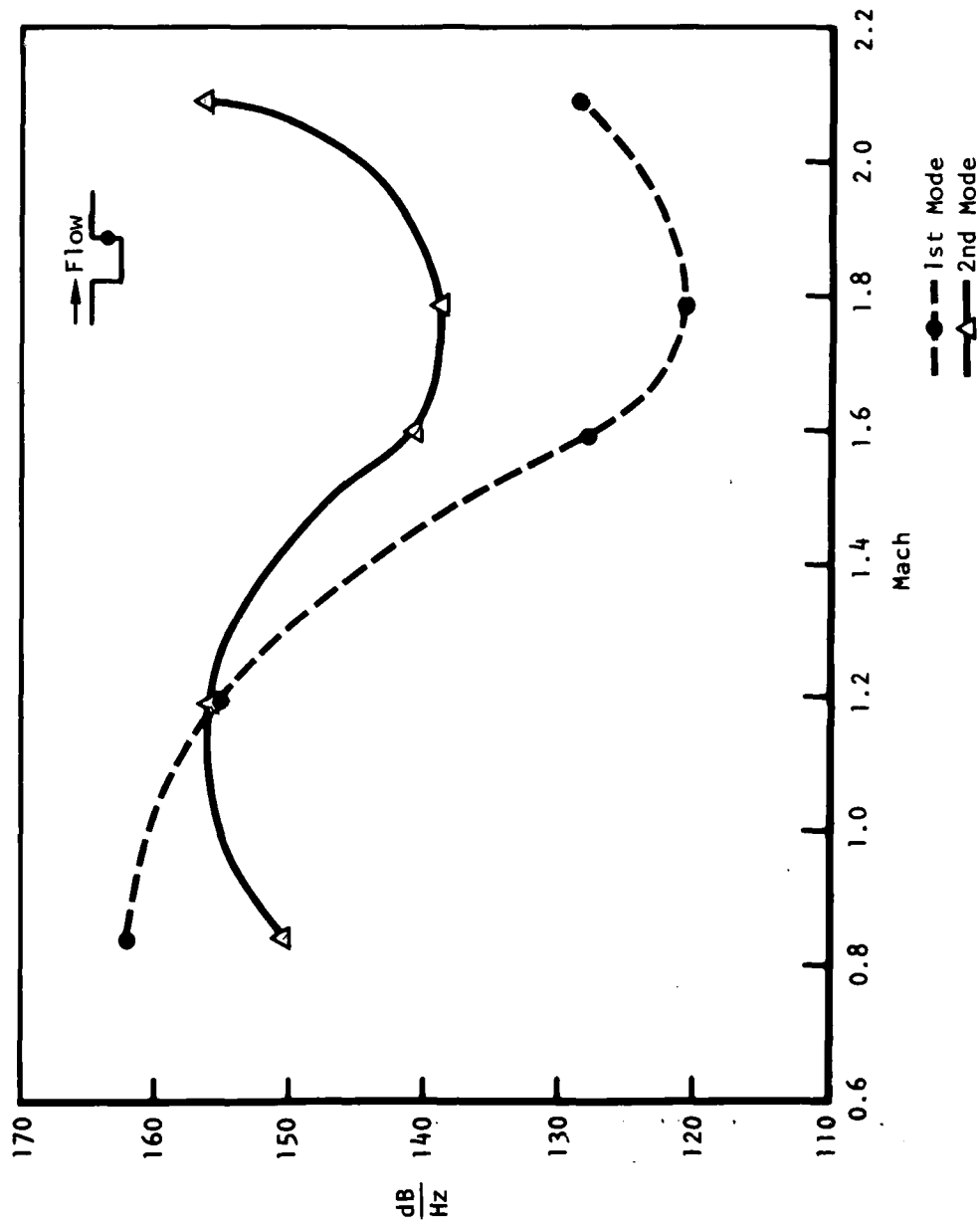
Figure 17. 0.1-Scale Model Data - Unsuppressed Full-Open, Aft Bulkhead Upper, Q = 500 psf, Center Bay
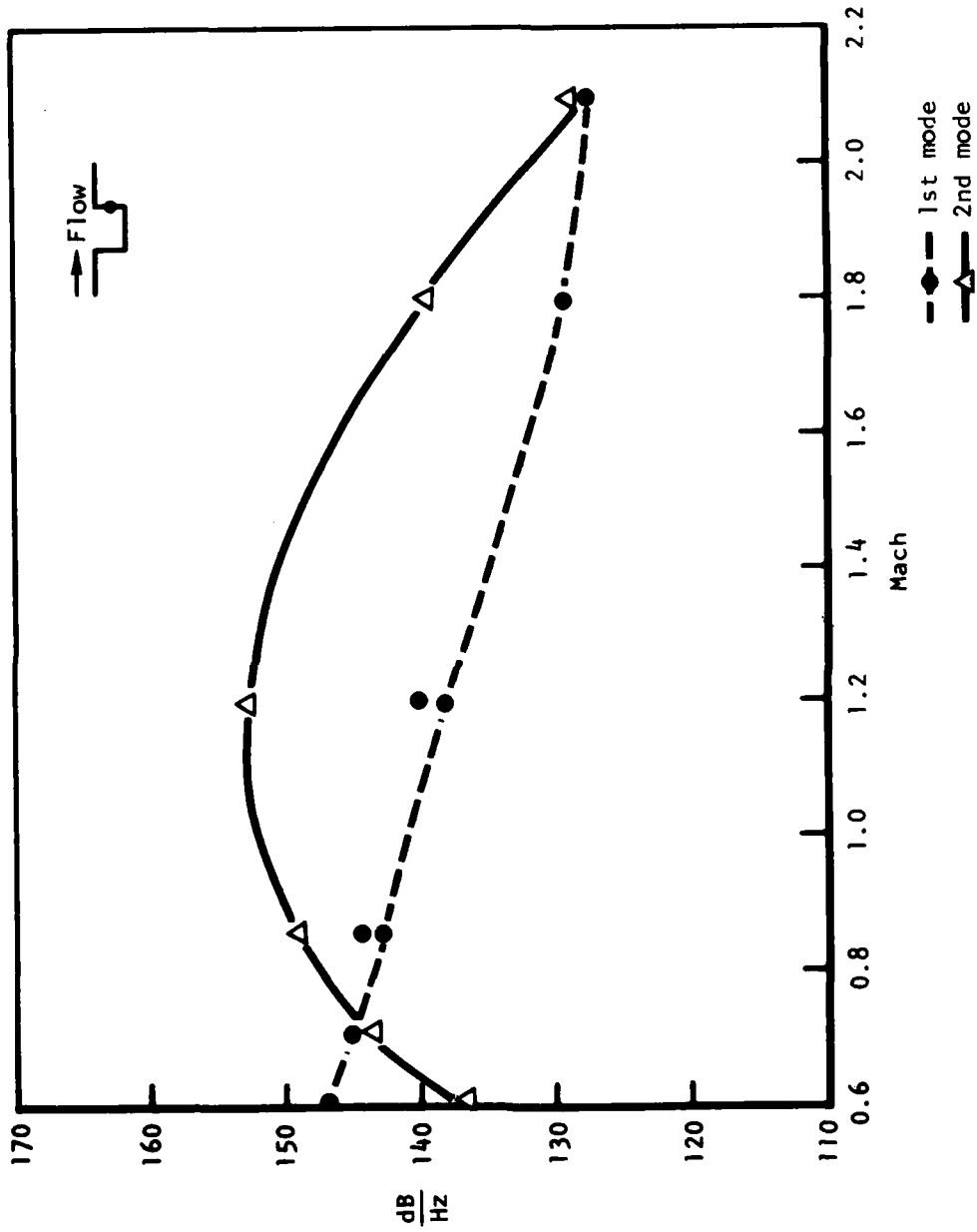
Figure 18. 0.1-Scale Model Data - Unsuppressed Part-Open, Aft Bulkhead Upper, Q = 500 psf, Center Bay

24
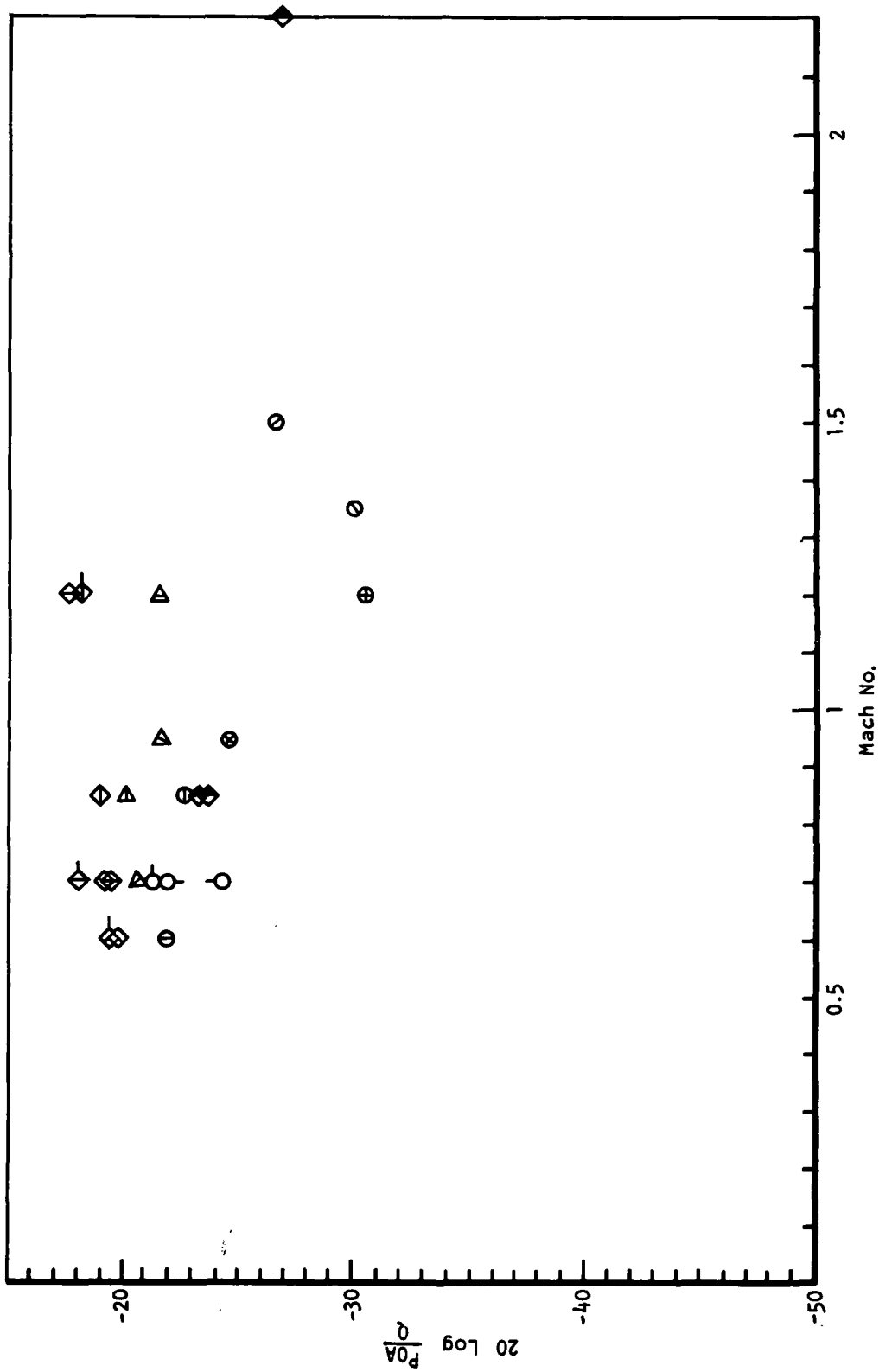
Figure 19. Overall Broadband Pressure Level, Part-Open, Aft Bulkhead Lower

25
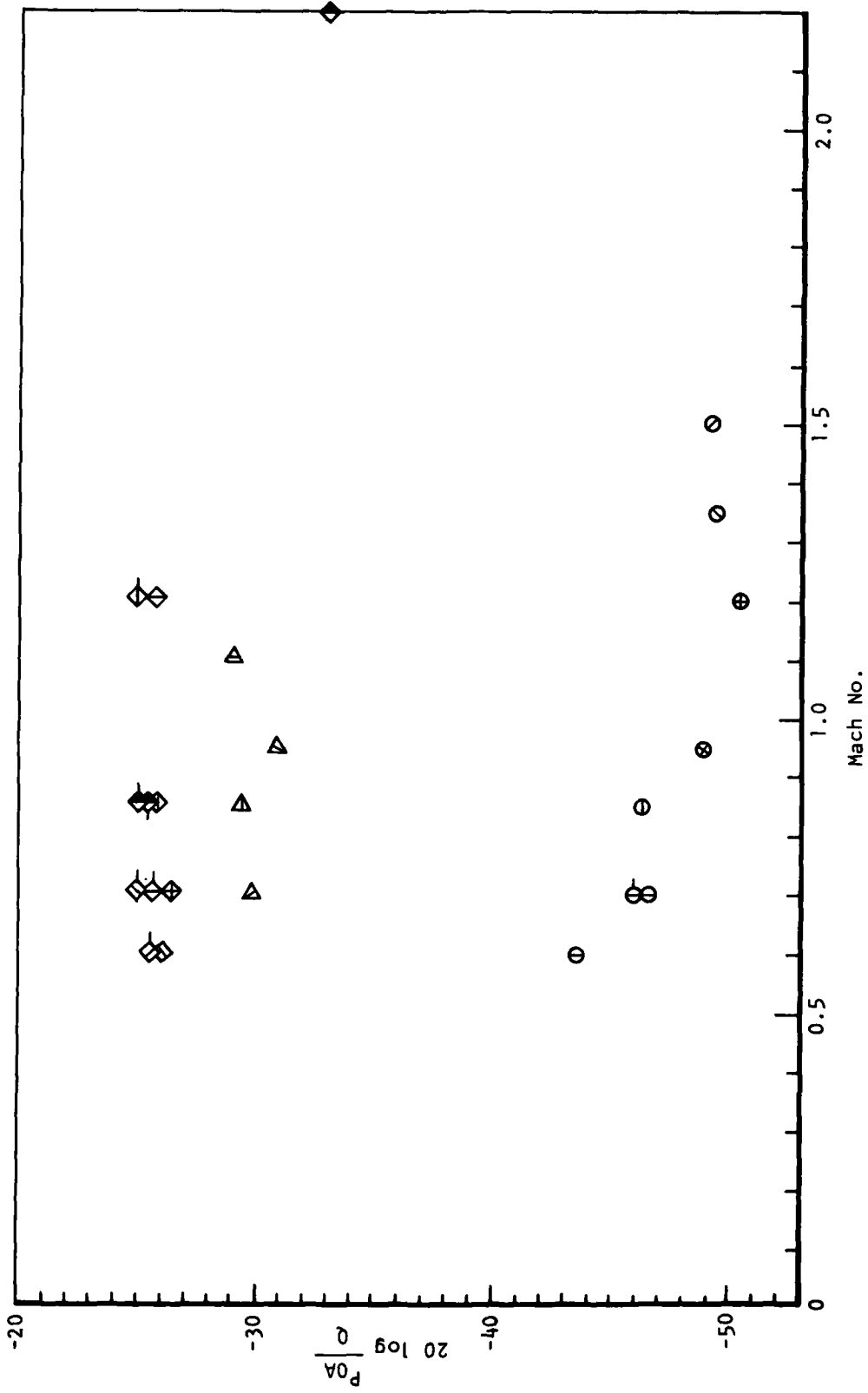
Figure 20. Overall Broadband Pressure Level, Part Open, Aft Bulkhead, Upper

26
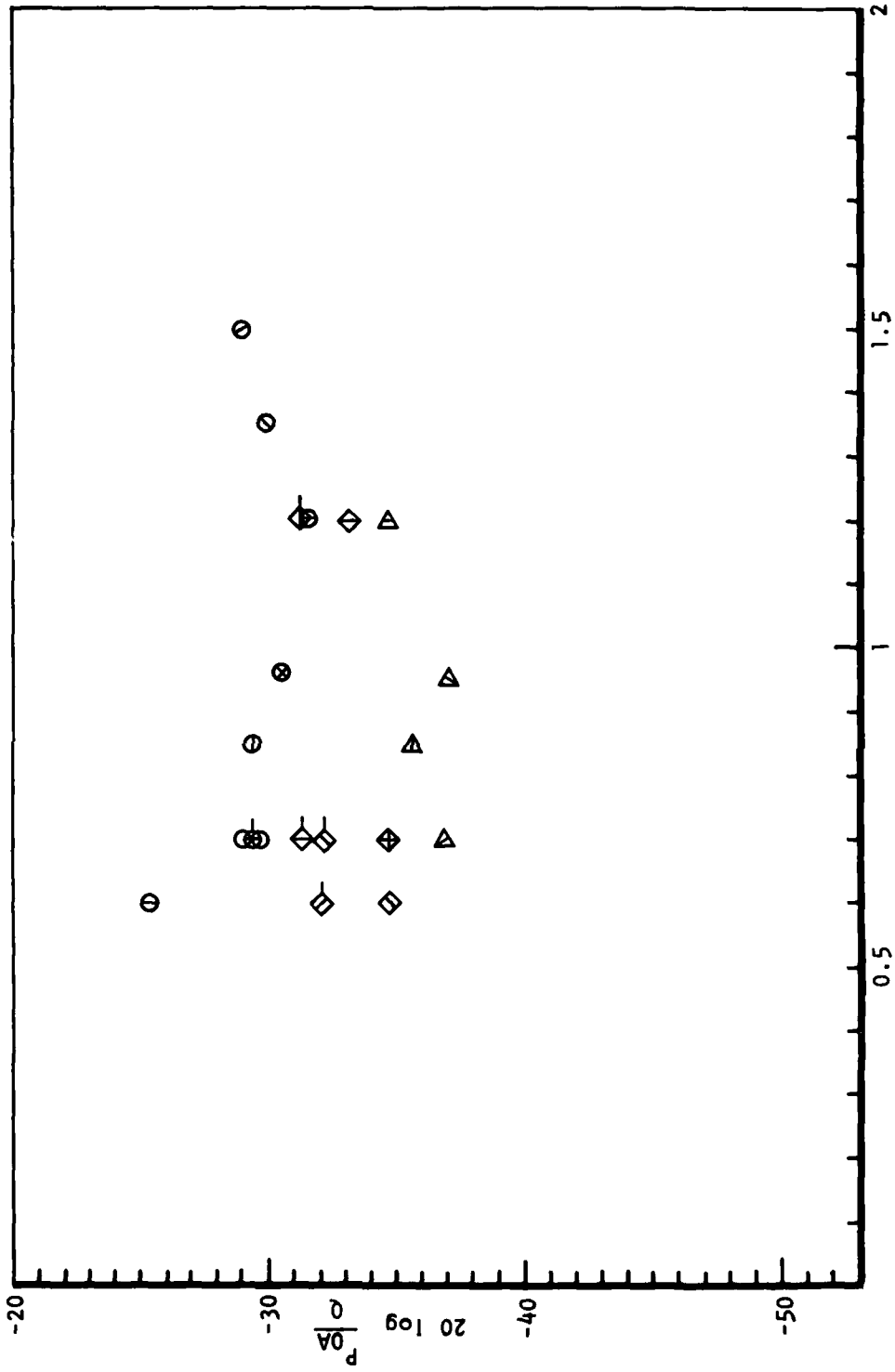
Figure 21. Overall Broadband Pressure Level, Part-Open, Forward Bulkhead, Upper

Mach No.
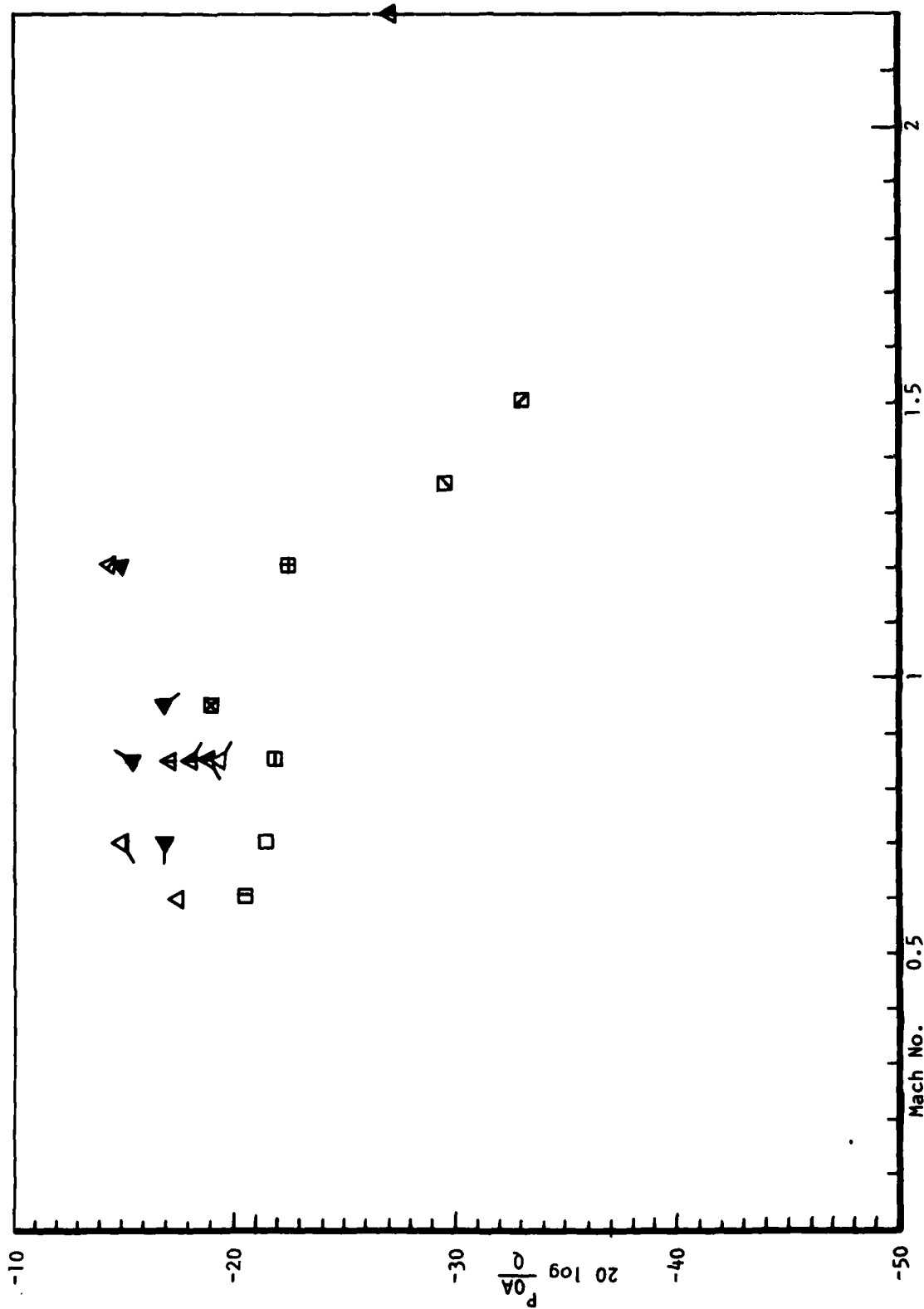
Figure 22. Overall Broadband Pressure Level, Full-Open, Aft Bulkhead Upper
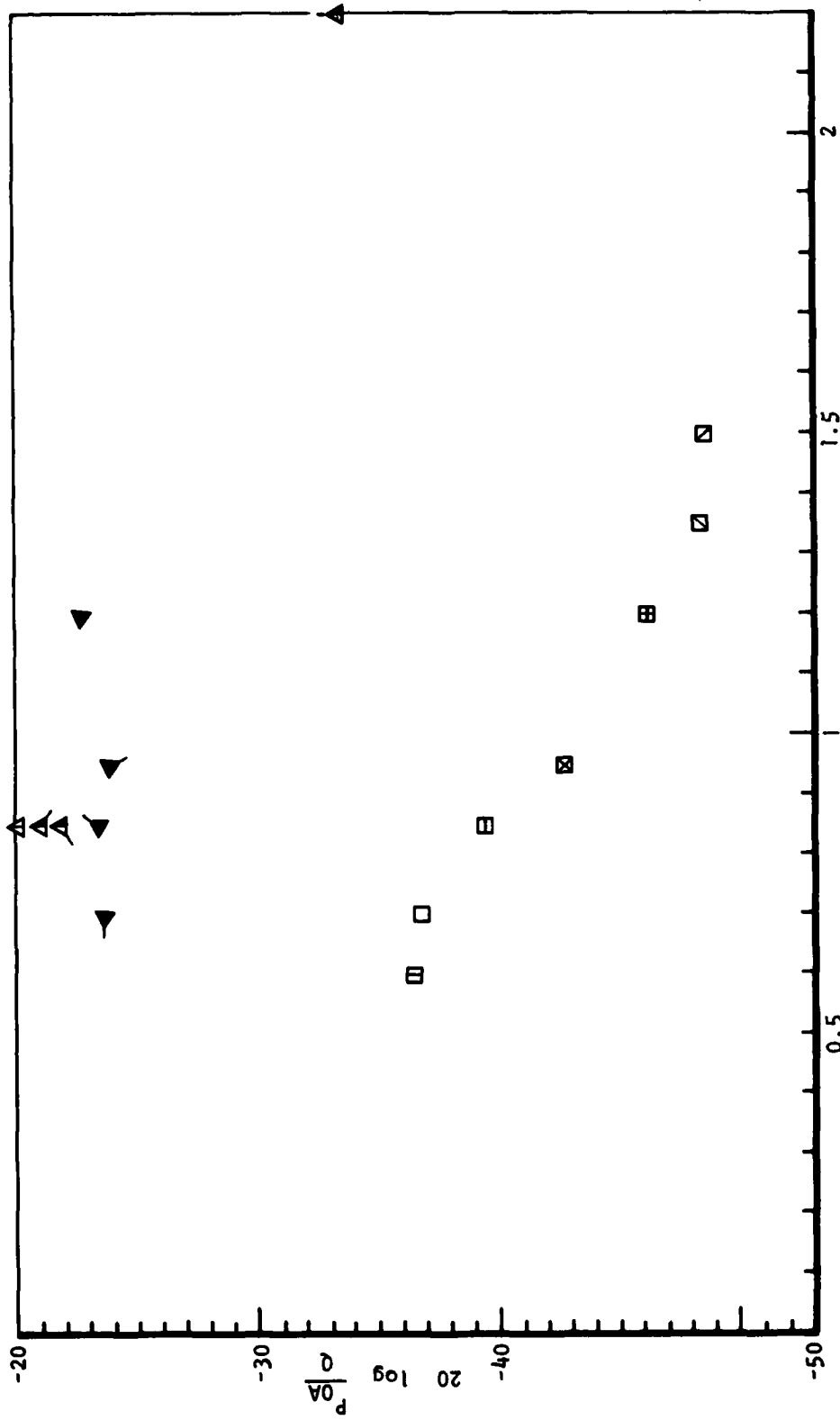
Figure 23. Overall Broadband Pressure Level, Full-Open, Aft Bulkhead Upper
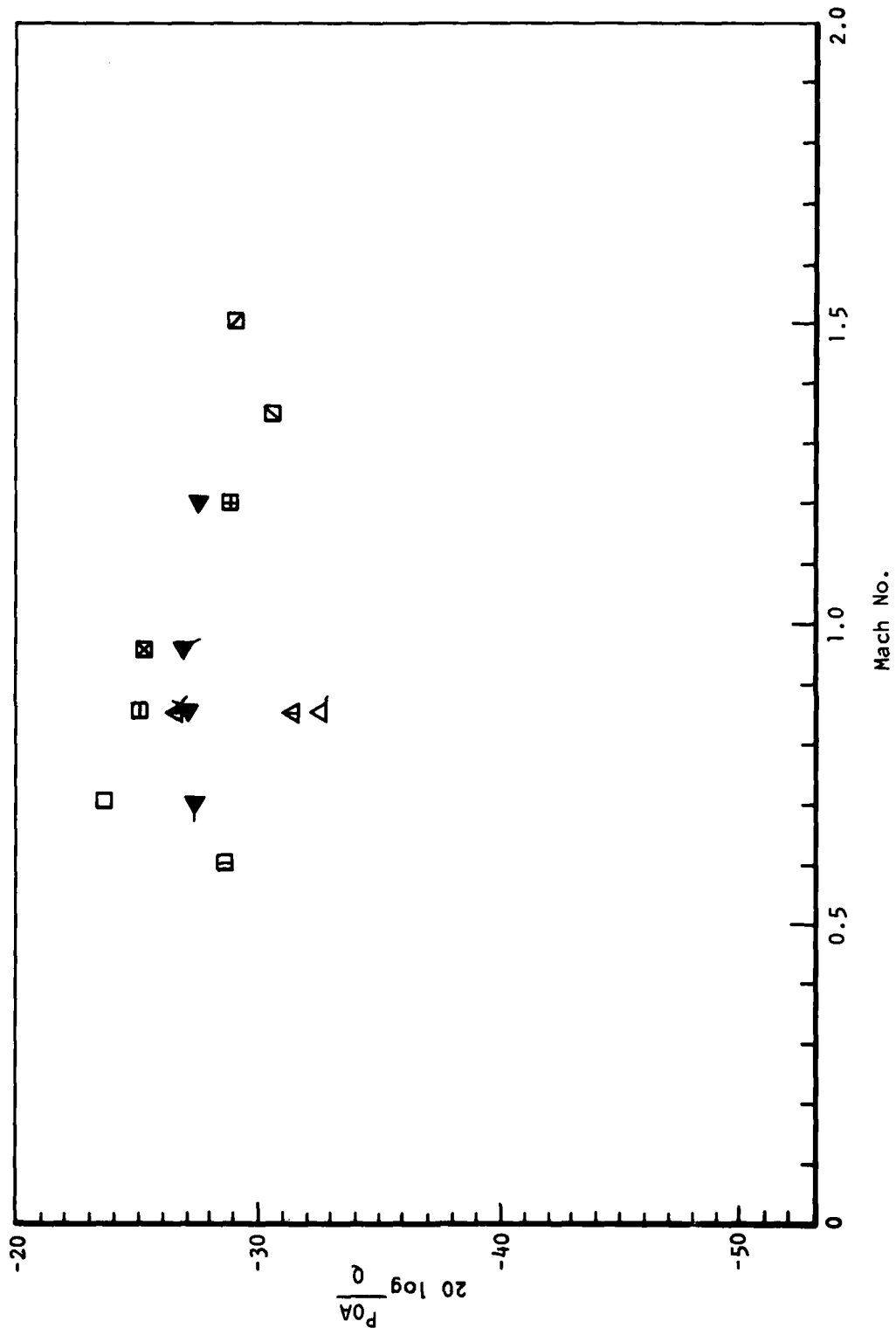
Figure 24. Overall Broadband Pressure Level, Full-Open, Forward Bulkhead Lower

30

TABLE 1. SYMBOLS

Full-scale Flt 1-37

<table>
<tr><td colspan="3" align="center"><u>Door PO</u></td><td colspan="3" align="center"><u>Door FO</u></td></tr>
<tr><td>M</td><td>Q(psf)</td><td></td><td>M</td><td>Q(psf)</td><td></td></tr>
<tr><td>0.6</td><td>367</td><td>⦶</td><td>0.6</td><td>367</td><td>⊞</td></tr>
<tr><td>0.7</td><td>367</td><td>○</td><td>0.7</td><td>367</td><td>□</td></tr>
<tr><td>0.7</td><td>500</td><td>⦶</td><td>0.85</td><td>350</td><td>⊟</td></tr>
<tr><td>0.7</td><td>690</td><td>○</td><td>0.95</td><td>350</td><td>⊠</td></tr>
<tr><td>0.85</td><td>350</td><td>⊖</td><td>1.2</td><td>440</td><td>⊞</td></tr>
<tr><td>0.95</td><td>350</td><td>⊗</td><td>1.35</td><td>440</td><td>⊘</td></tr>
<tr><td>1.2</td><td>440</td><td>⊕</td><td>1.5</td><td>440</td><td>◨</td></tr>
<tr><td>1.35</td><td>440</td><td>⊘</td><td></td><td></td><td></td></tr>
<tr><td>1.5</td><td>440</td><td>⊘</td><td></td><td></td><td></td></tr>
</table>

0.1-Scale TWT 302

Blow	M	Q (psf)	Door	
49	0.85	907	CLFO	▲
50	1.2	1,325	CLFO	△
70	1.2	1,325	CLPO	◇
82	0.85	907	CLPO	◈
83	0.7	677	CLPO	◈
84	0.6	504	CLPO	◇
163	0.6	504	POCL	◇–
164	0.7	677	POCL	◇–
168	0.7	677	POOCL	◇–
169	1.2	1,325	POCL	◇–

Full-scale flt 1-36

<u>Door PO</u>

M	Q (psf)	
0.85	352	○

<u>Door FO</u>

M	Q (psf)	
0.85	352	●

0.1-Scale TWT 261

Run	M	Q(psf)	Door	
159	0.842	900	CLFO	▲
159	0.848	910	CLFO	▲
160	0.842	895	CLPO	◈
160	0.848	906	CLPO	◈–
168	2.197	1,736	CLPO	◈
169	2.197	1,735	CLFO	▲

0.1-Scale model data (WPAFB)

Run	M	Q(psf)	Door	
2	0.6	558	FOCL	△
7	0.7	695	FOCL	△
12	0.85	697	} FOCL △	
14	0.85	697		
15	0.85	697		

0.2-Scale model data

Run	M	Q(psf)	Door	
112	0.7	726	CLPO	▷
113	0.7	726	CLFO	◀
120	0.85	1,071	CLPO	▷
121	0.85	1,071	CLFO	◀
127	0.95	1,338	CLPO	▷
128	0.95	1,338	CLFO	◀
134	1.2	1,483	CLPO	▷
135	1.2	1,483	CLFO	◀

In general, the data amplitude collapses to an acceptable scatter for the various conditions plotted except for the upper aft bulkhead position, where the full-scale data are considerably below the wind tunnel data. In general, the broadband data have the highest amplitude on the lower aft bulkhead. The data for full-open door positions are slightly higher in amplitude then for part-open doors. The noise level on the forward bulkhead is approximately 10 db below the noise level on the aft bulkhead. The maximum noise level of the aft lower bulkhead peaks in the subsonic range and generally decreases with increased mach number.

NOISE VERSUS CAVITY LENGTH AND DEPTH

The noise distribution within the cavity is expressed in terms of normalized length and depth ratios x/L and y/H. Figure 25 shows the three cavity depths (lower plane, upper plane, and top center) used for data correlation. At each of the three depths, the noise was shown for several length ratios x/L. The magnitude of the noise level was normalized with free-stream dynamic pressure for each data plot. The overall broadband noise levels are shown for full- and part-open doors in Figures 26 through 31. The cavity discrete frequencies are shown in Figures 32 through 43 for modes 1 and 2 for full- and part-open doors. The data plotted in Figure 26 through 43 represent full-scale and model data identified by the symbols in Table 1.

The overall noise correlation in Figures 26 through 31 versus cavity length shows the highest levels on the aft bulkhead and the lowest on the forward bulkhead. In general, the noise level differential between the front and back of the cavity is approximately 10 to 15 db. The noise level variation with cavity depth shows that the lower position of the cavity near the opening is generally higher, with decreasing values near the upper and top of the cavity away from the opening.

The discrete cavity noise versus cavity length shown in Figures 32 through 43 is correlated for the fundamental and the second harmonic modes. The data for mode 1 indicate the highest pressures on the aft bulkhead, with minimum pressures near the center of the cavity and slightly lower pressures on the forward bulkhead. The noise levels shown in Figures 38 through 43 for mode 2 do not indicate a clear data trend.

Data scatter for both random and discrete mode appear significant even after normalizing out dynamic pressure. The data represent model and full-scale data at various dynamic pressures for a constant mach 0.85. At present, it is not understood why the data scatter is so large.

NOISE VARIATION VERSUS ANGLE OF ATTACK

Cavity noise levels for the fundamental resonance mode 1 and the overall broadband pressure level are shown in Figures 44 through 47 for part- and full-open bay doors. The angle of attack varies from 0 to 2 degrees. The noise data are shown on the forward and aft bulkhead. The broadband and discrete levels for part-open doors show very little variation, less than 1 db, with angle of attack. The broadband levels for full-open doors show very little variation with angle of attack. The data for the discrete mode 1, however, show more variation. The noise level variation between 0- and 2-degrees angle of attack is about 4 db for full-open doors as illustrated in Figure 44.
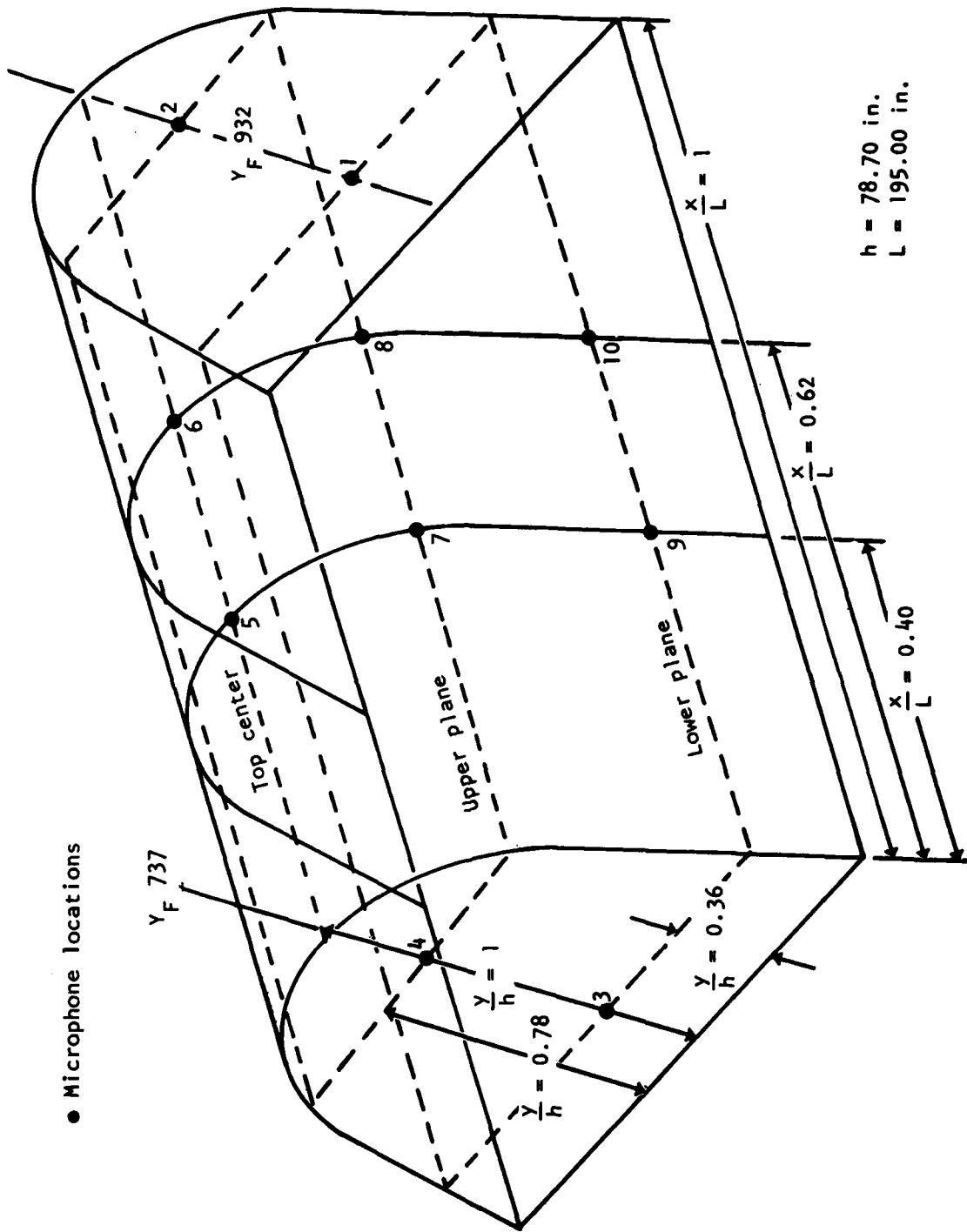
32

Figure 25. Measurement Reference Planes

$\bullet$ Microphone locations

$h = 78.70$ in.
$L = 195.00$ in.
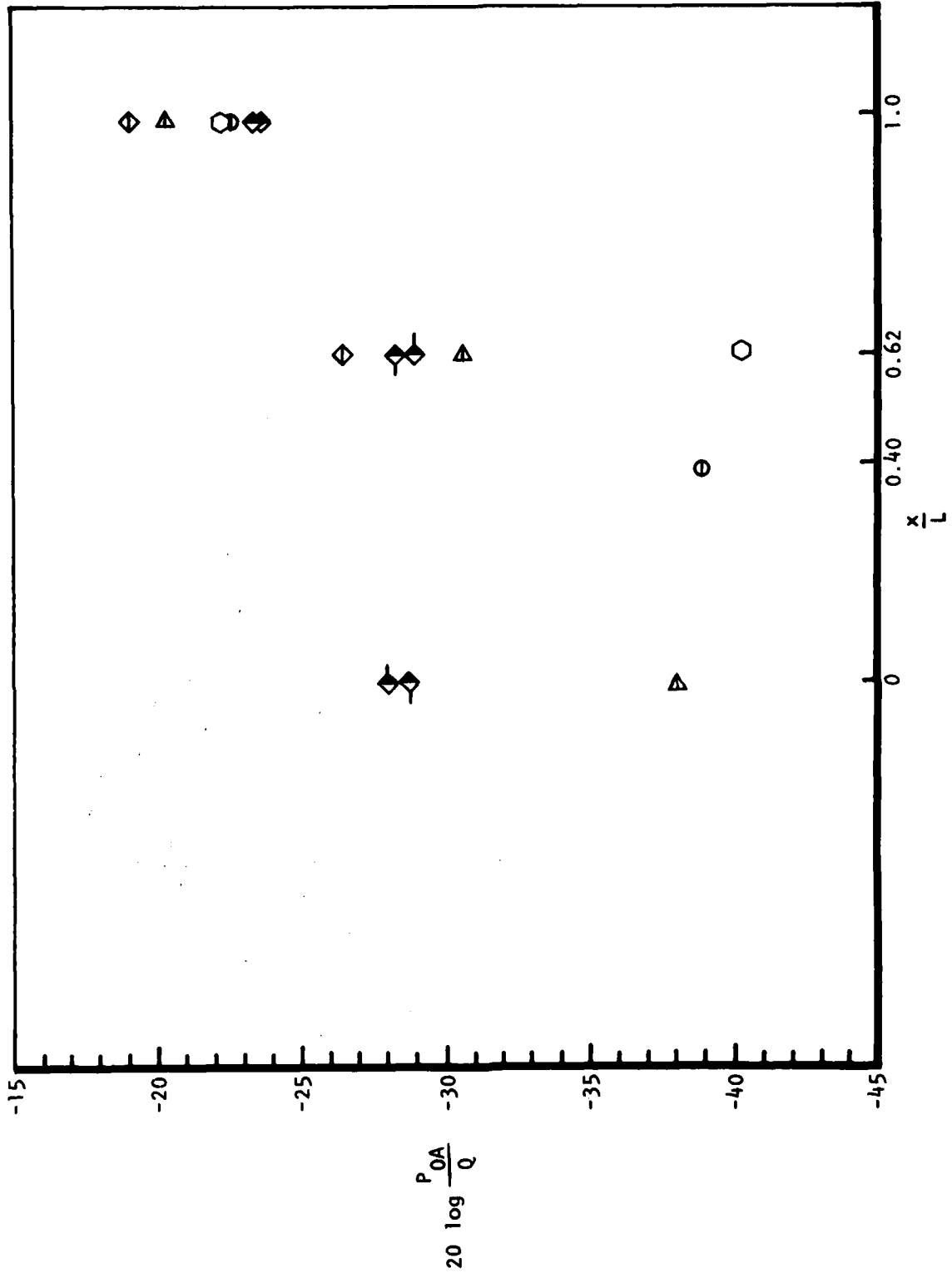
Figure 26. Bulkhead/Sidewall Lower, 0.85M, Part-Open, Overall Broadband Levels Versus Bay Length

34

$20 \log \dfrac{P_{OA}}{Q}$

-15
-20
-25
-30
-35
-40
-45

$\dfrac{x}{L}$

0   0.40   0.62   1.0
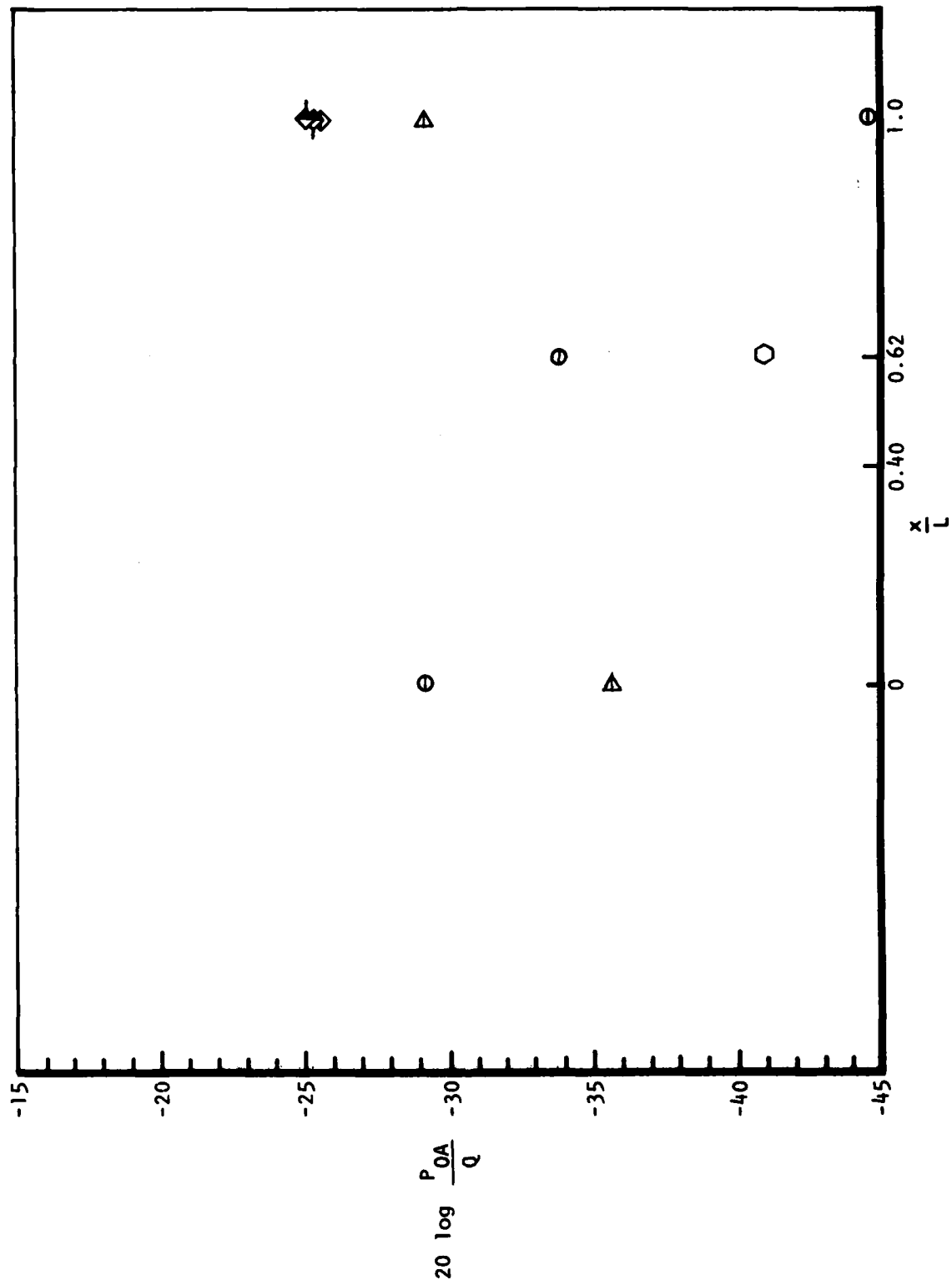
Figure 27. Bulkhead/Sidewall Upper, 0.8SM, Part-Open, Overall Broadband Levels Versus Bay Length
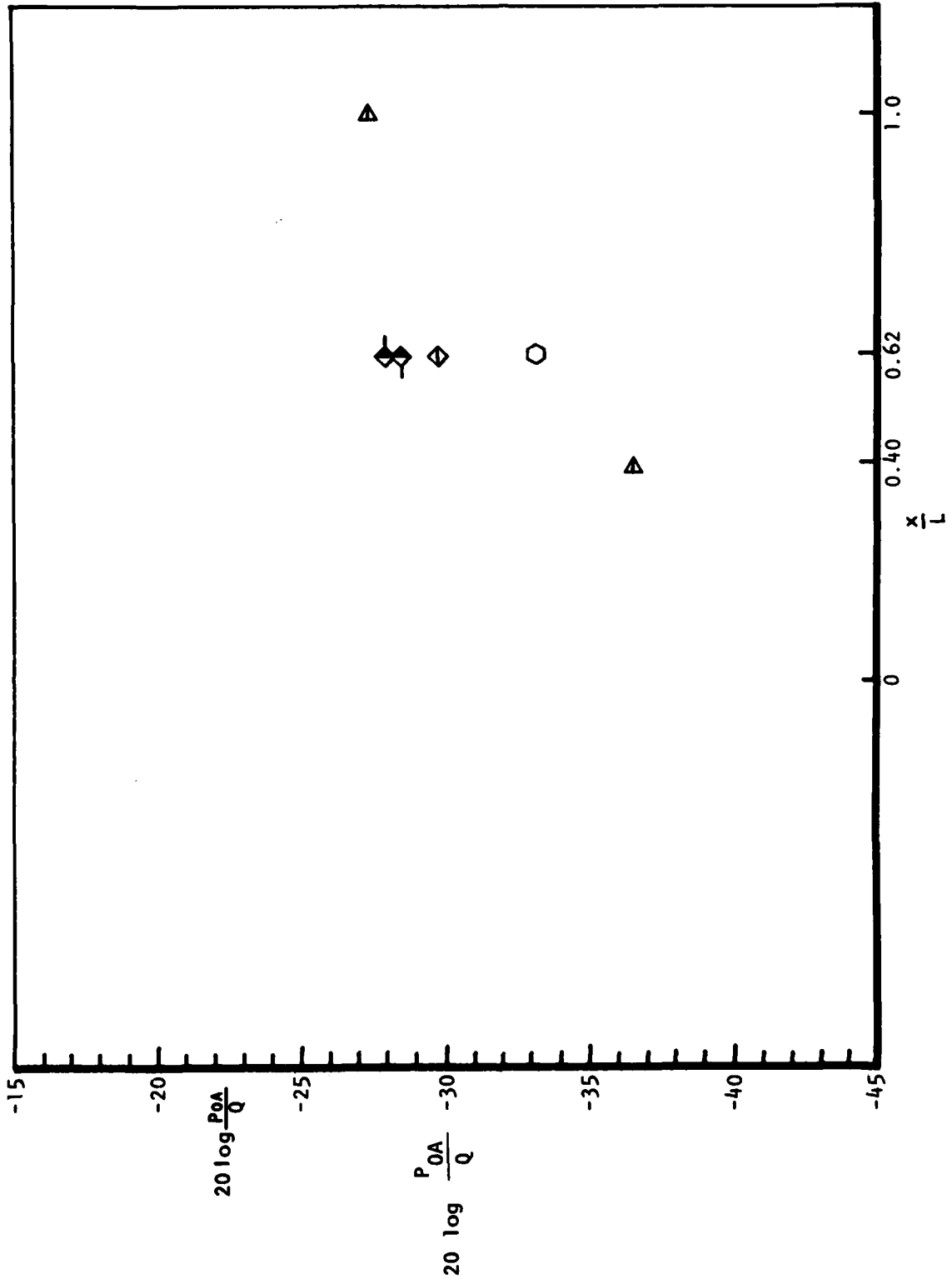
Figure 28. Bulkhead/Sidewall Top Center, 0.85M, Part-Open Overall Broadband Levels Versus Bay Length

36
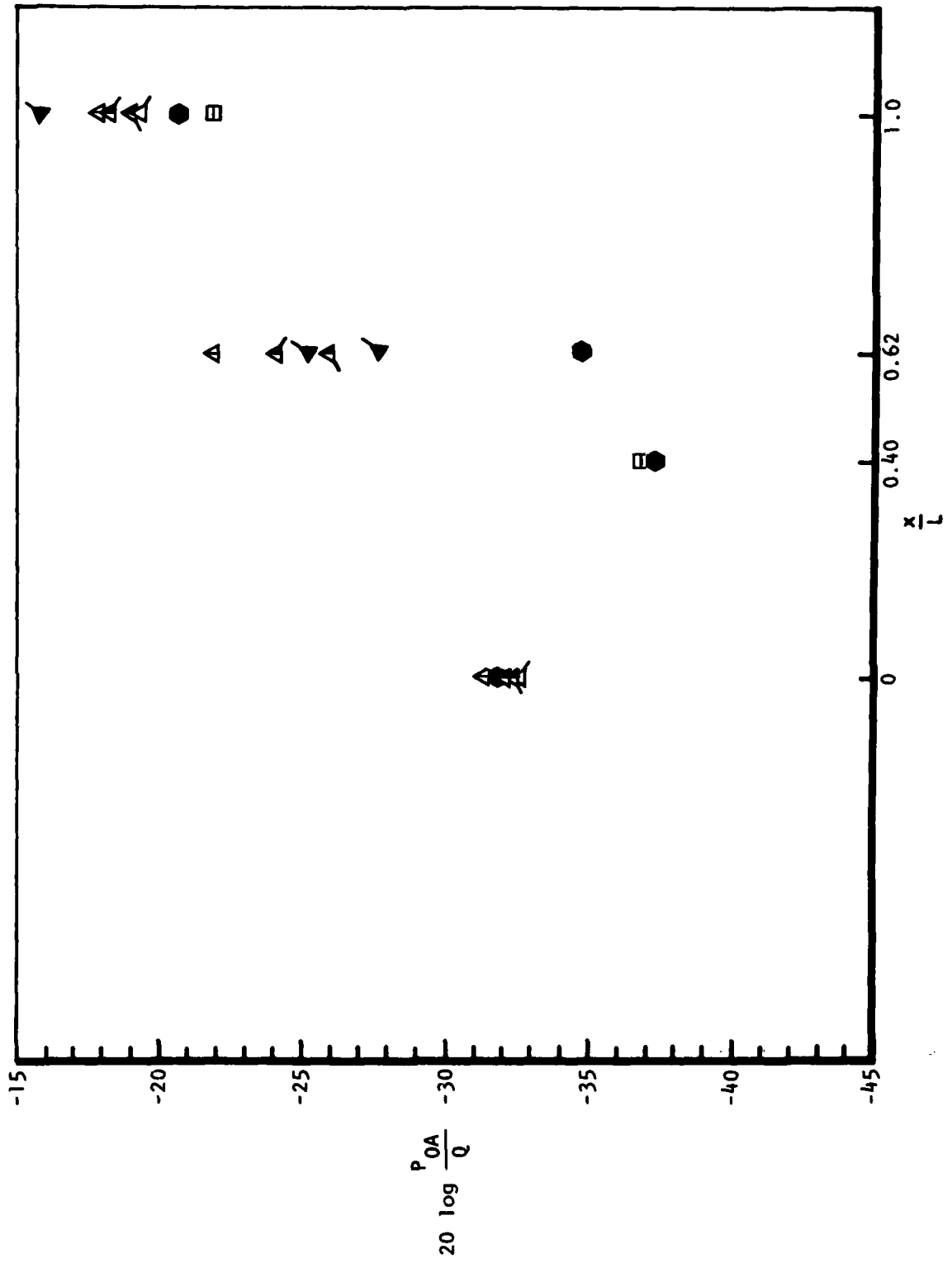
Figure 29. Bulkhead/Sidewall Lower, .85M, Full-Open Overall Broadband Levels Versus Bay Length
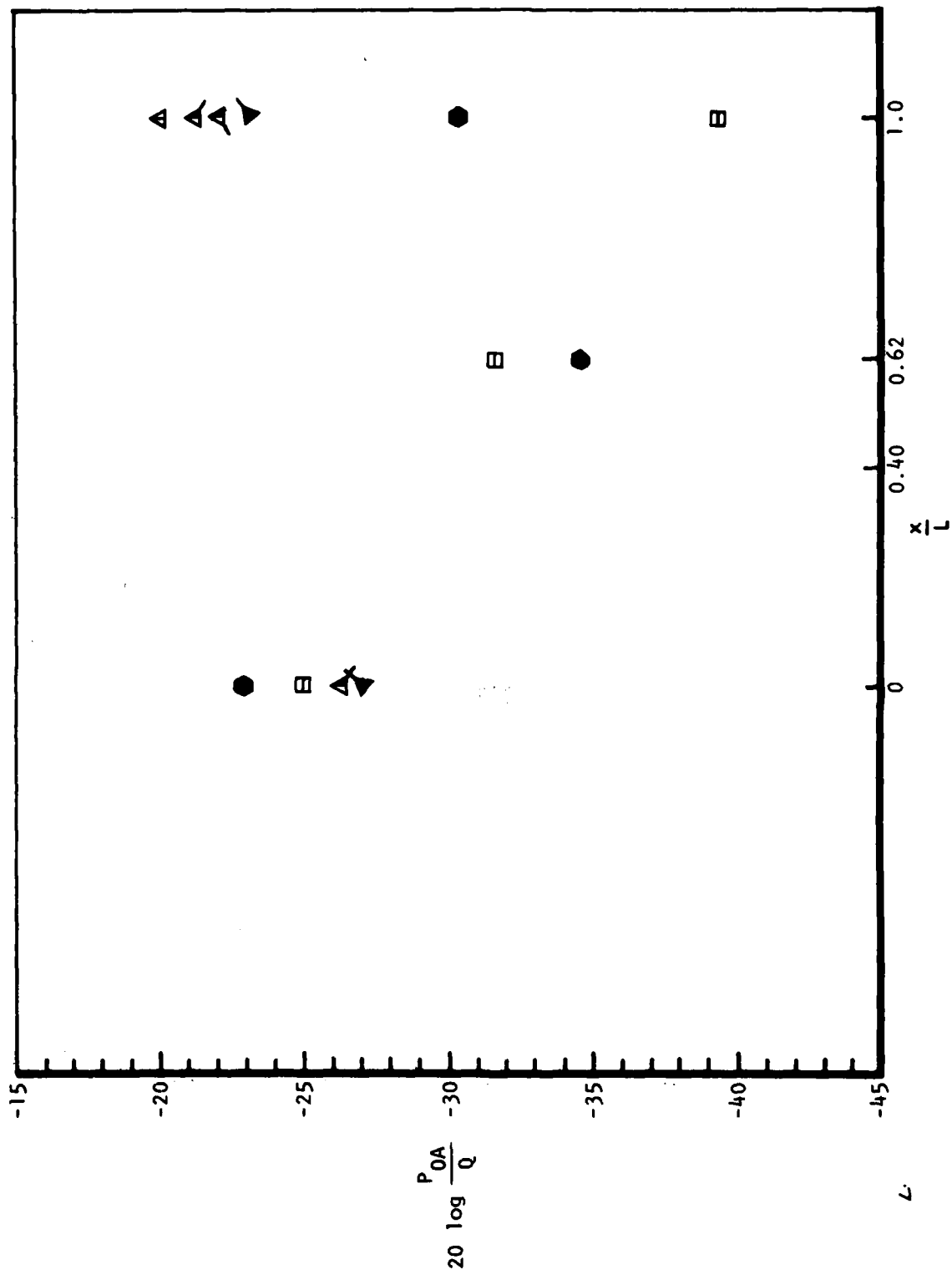
Figure 30. Bulkhead/Sidewall Upper, 0.85M, Full-Open, Overall Broadband Levels Versus Bay Length
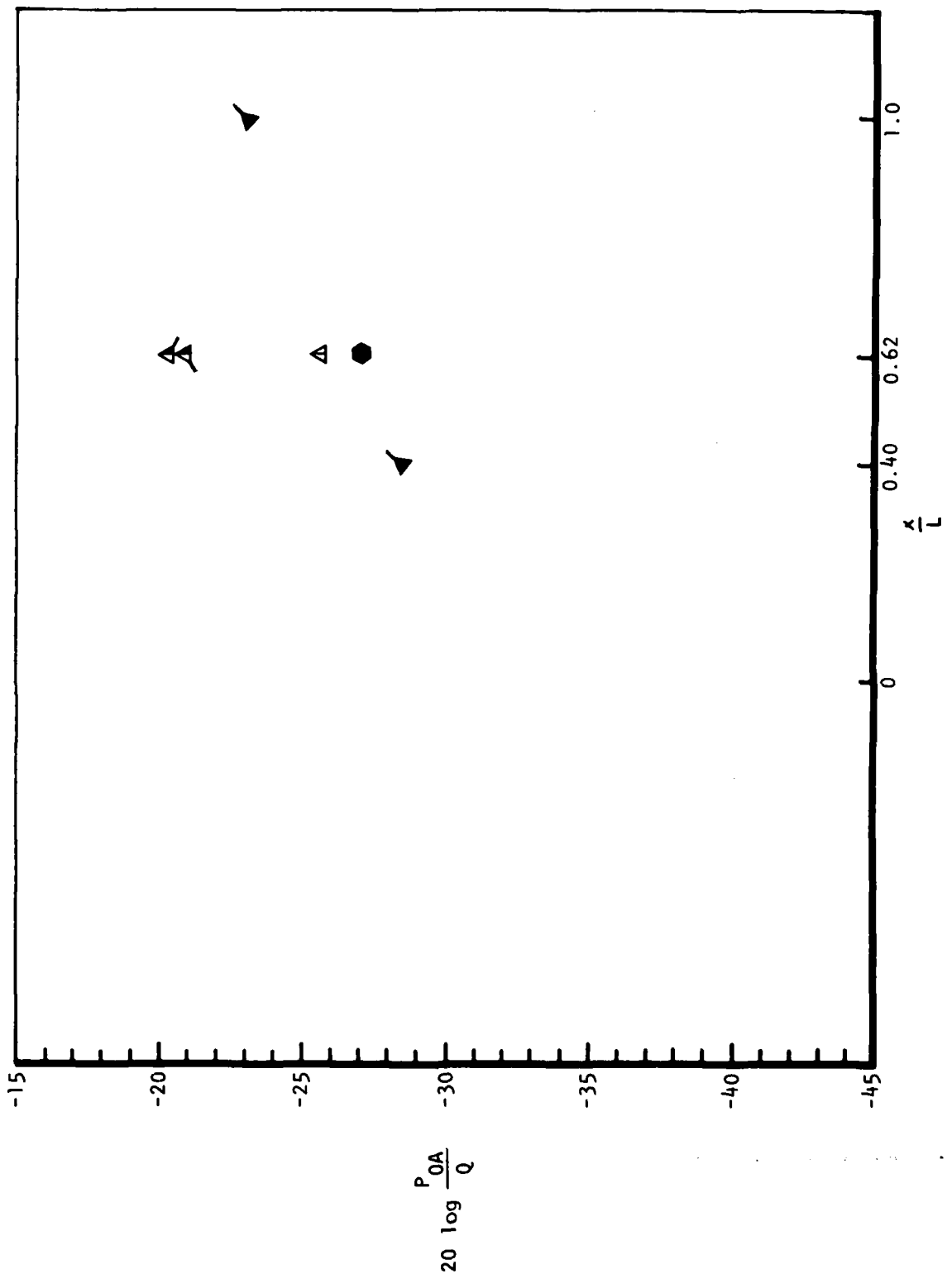
Figure 31. Bulkhead/Sidewall Top Center, 0.85M, Full-Open, Overall Broadband Levels Versus Bay Length

39
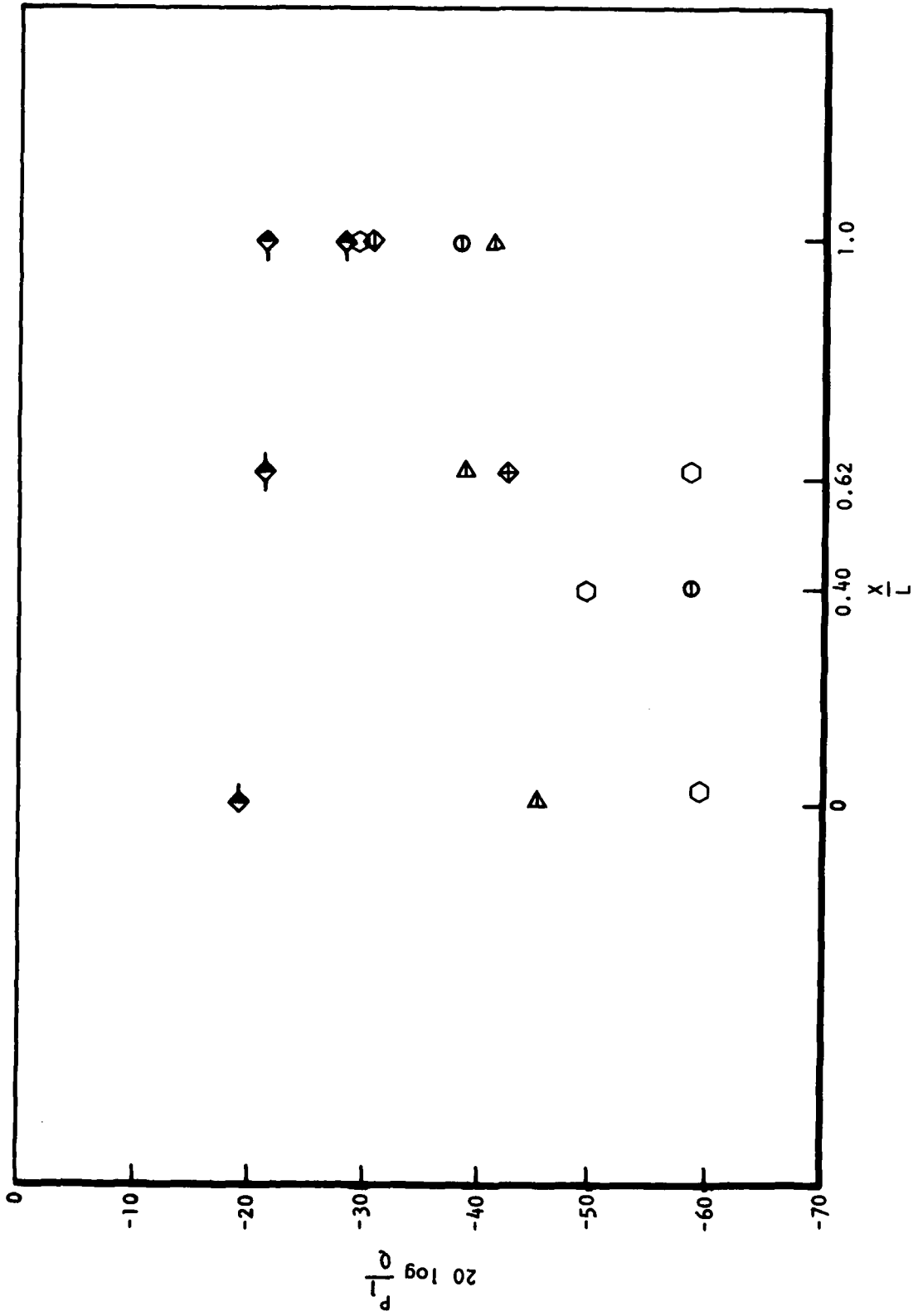
Figure 32. Bulkhead/Sidewall Lower, Mode 1, 0.85M, Part-Open, Discrete Levels Versus Bay Length

40
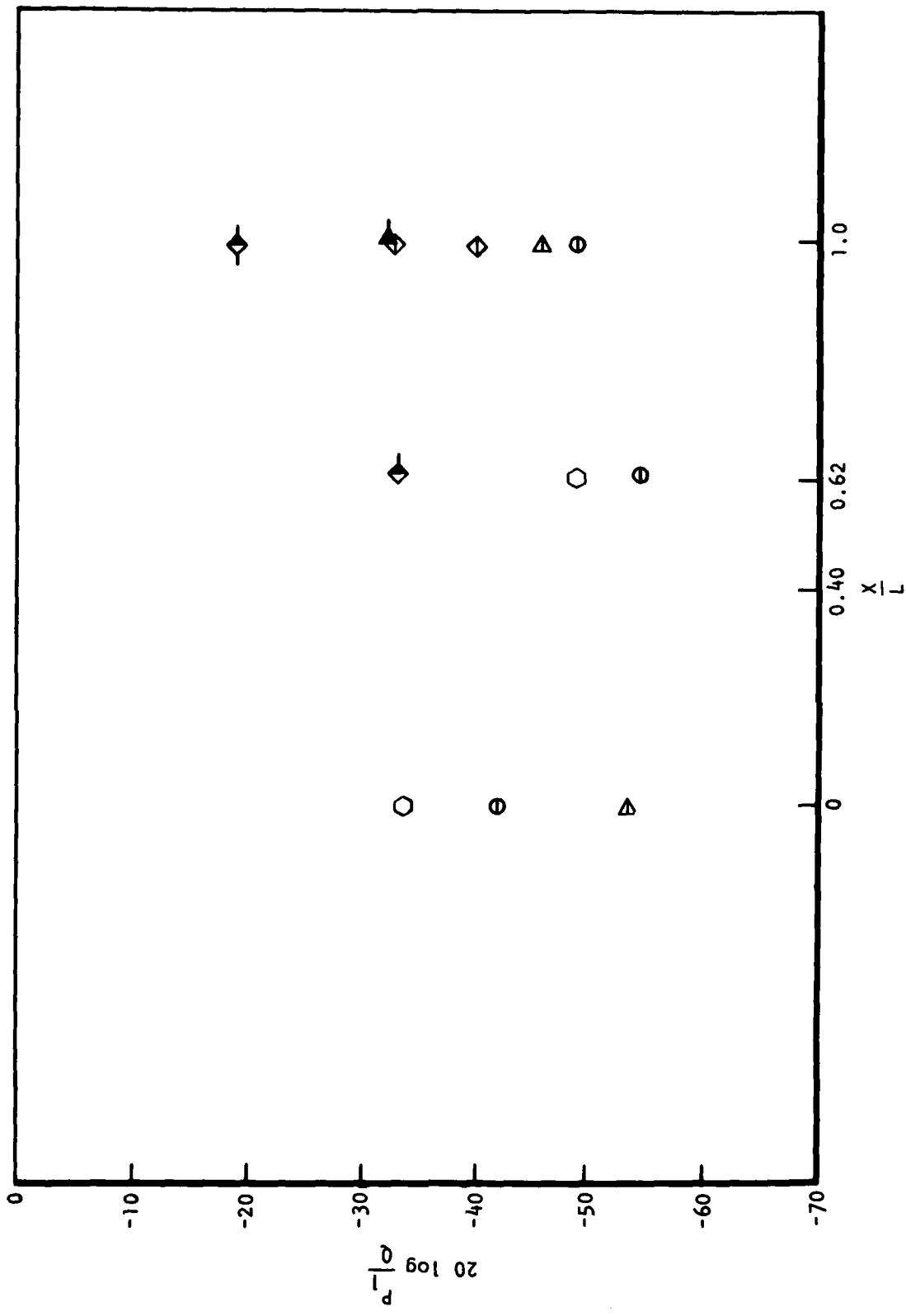
Figure 33. Bulkhead/Sidewall Upper, Mode 1, 0.85M, Part-Open, Discrete Levels Versus Bay Length
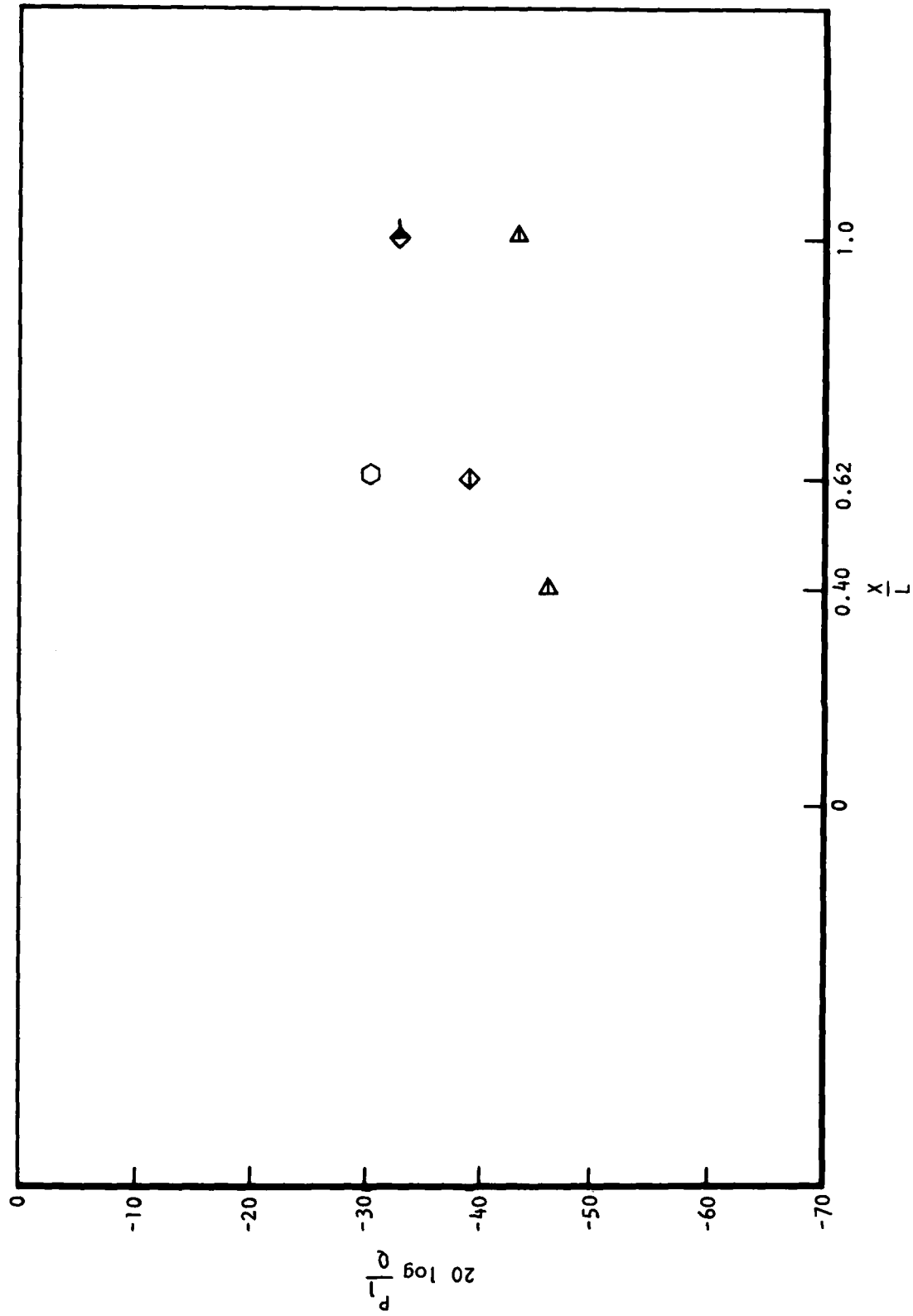
Figure 34. Bulkhead/Sidewall Top Center, Mode 1, 0.85M, Part-Open, Discrete Levels Versus Bay Length

42
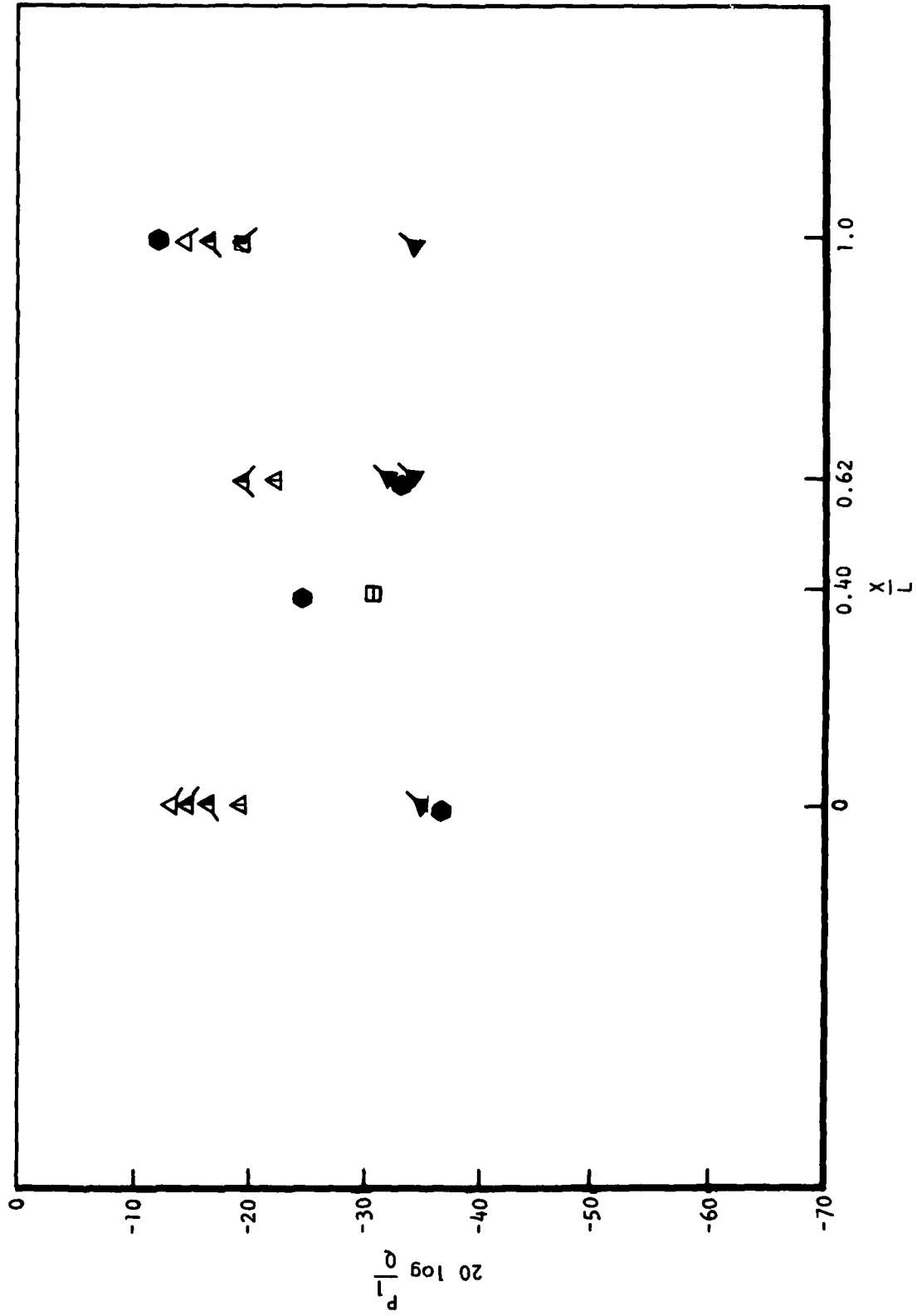
Figure 35. Bulkhead/Sidewall Lower, Mode 1, 0.85M, Full-Open Discrete Levels Versus Bay Length

43
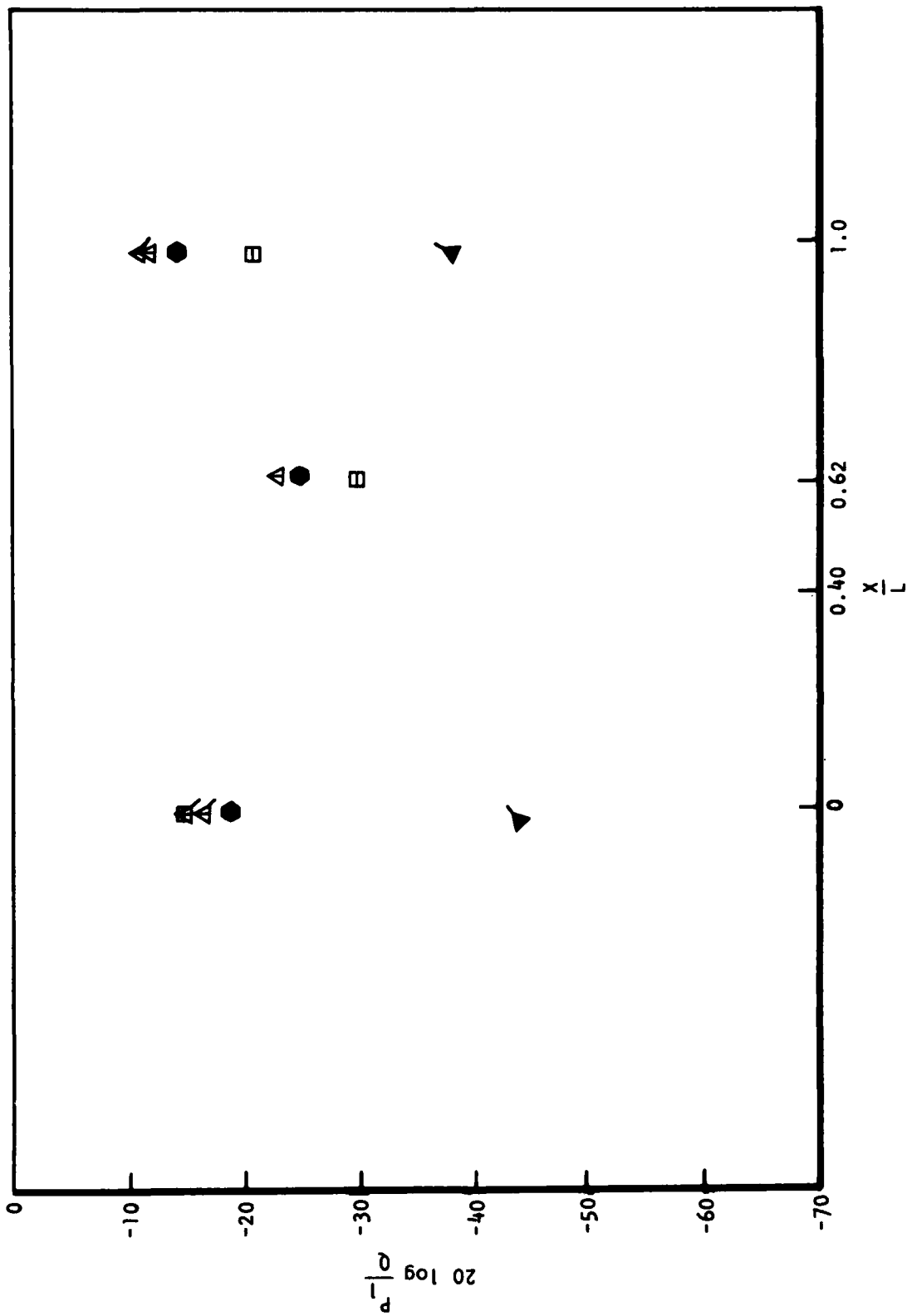
Figure 36.   Bulkhead/Sidewall Upper, Mode 1, 0.85M, Full-Open, Discrete Levels Versus Bay Length
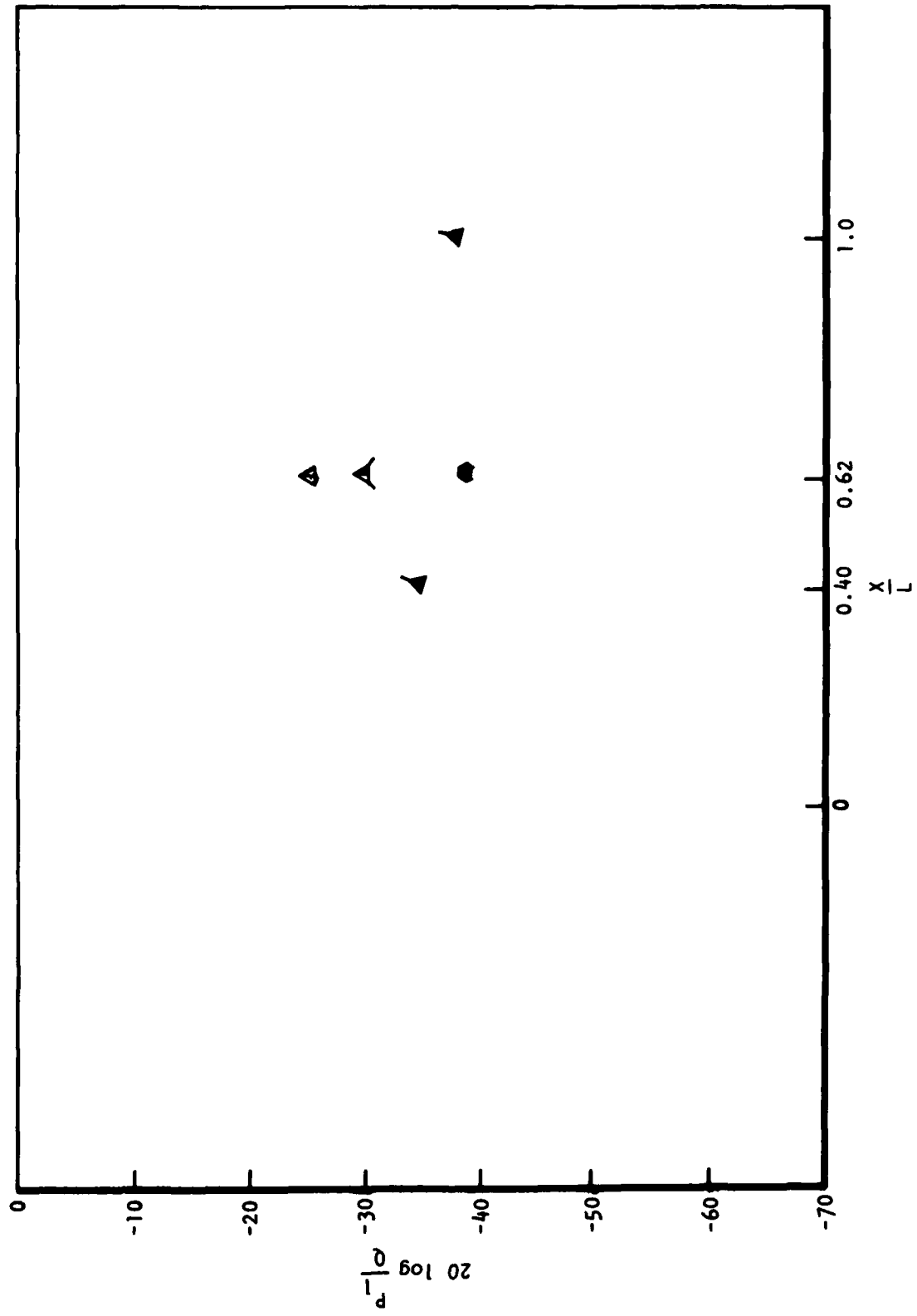
Figure 37. Bulkhead/Sidewall Top Center, Mode 1, 0.85M, Full-Open, Discrete Levels Versus Bay Length
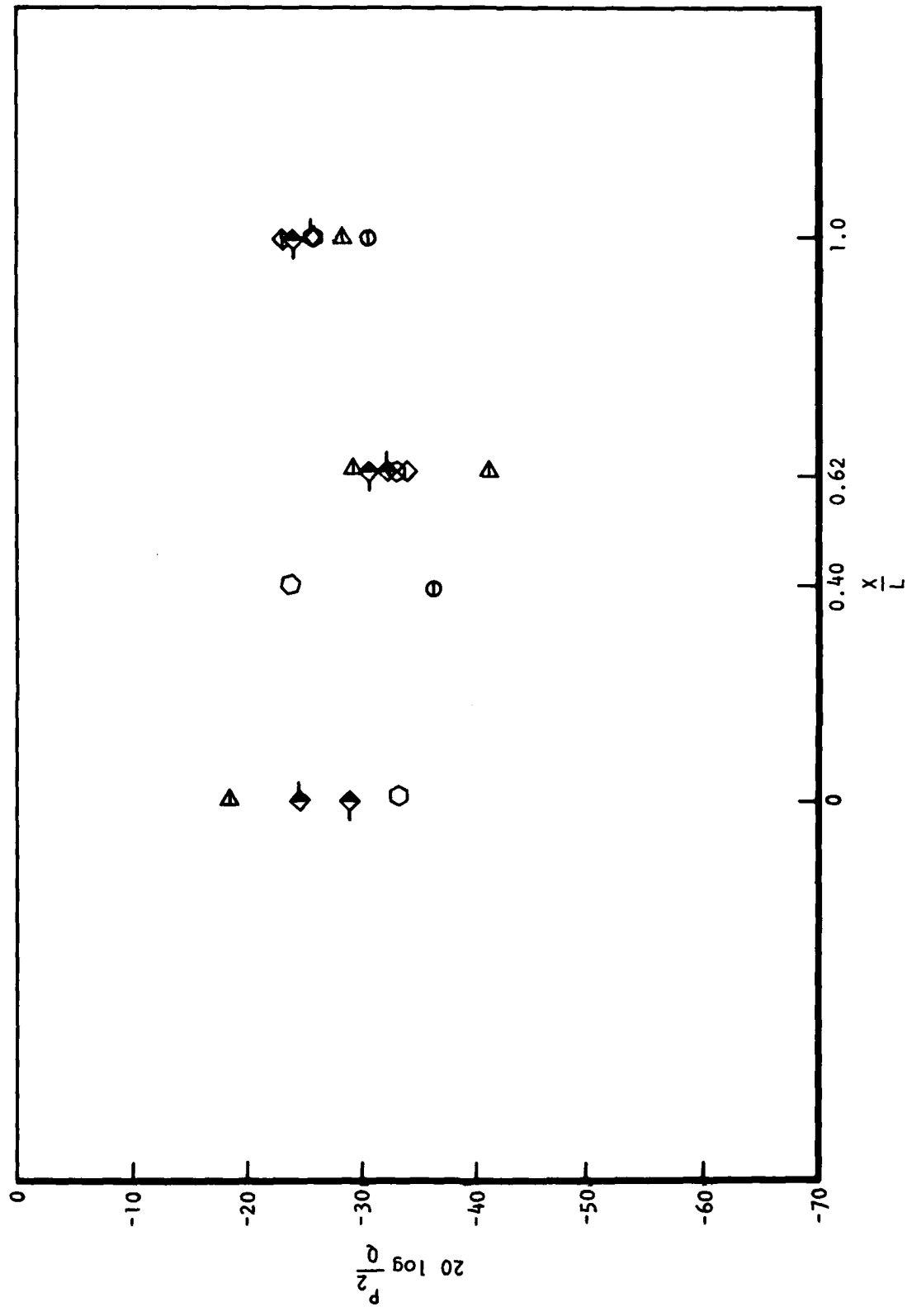
Figure 38. Bulkhead/Sidewall Lower, Mode 2, 0.85M, Part-Open, Discrete Levels Versus Bay Length
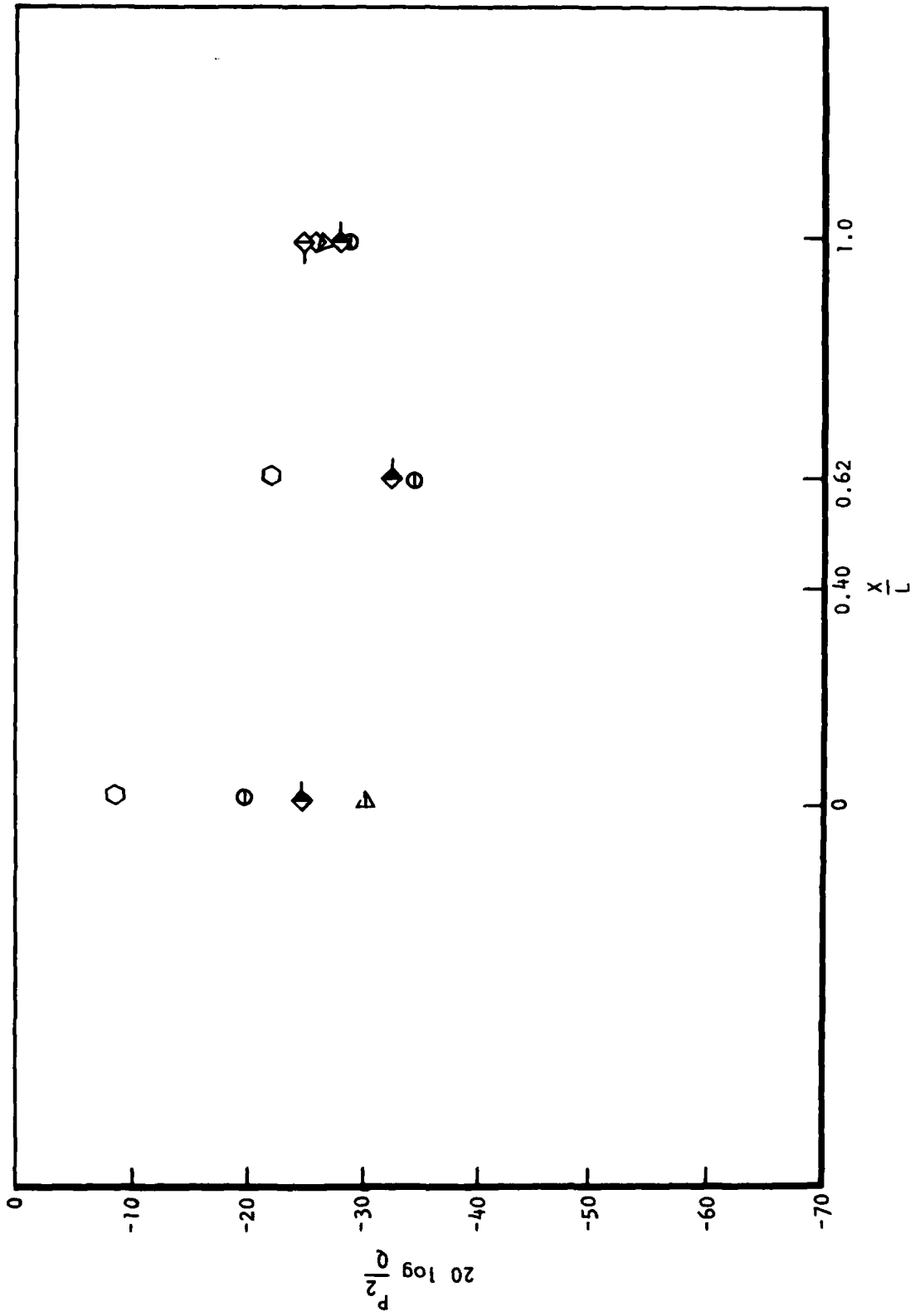
Figure 39. Bulkhead/Sidewall Upper, Mode 2, 0.85M, Part-Open, Discrete Levels Versus Bay Length

47
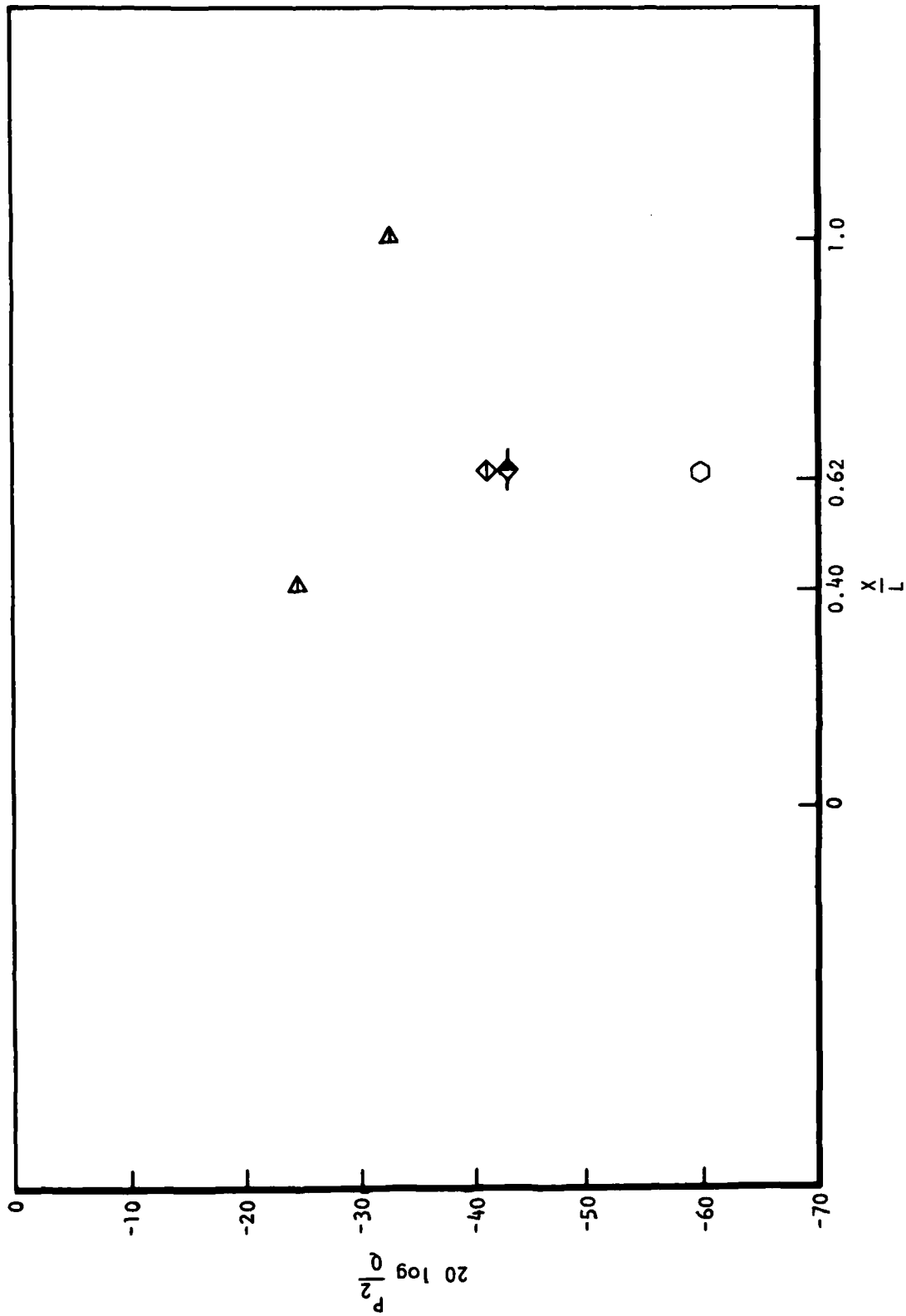
Figure 40. Bulkhead/Sidewall Top Center, Mode 2, 0.85M, Part-Open, Discrete Levels Versus Bay Length

Figure 41. Bulkhead/Sidewall Lower, Mode 2, 0.85M, Full-Open, Discrete Levels Versus Bay Length

49
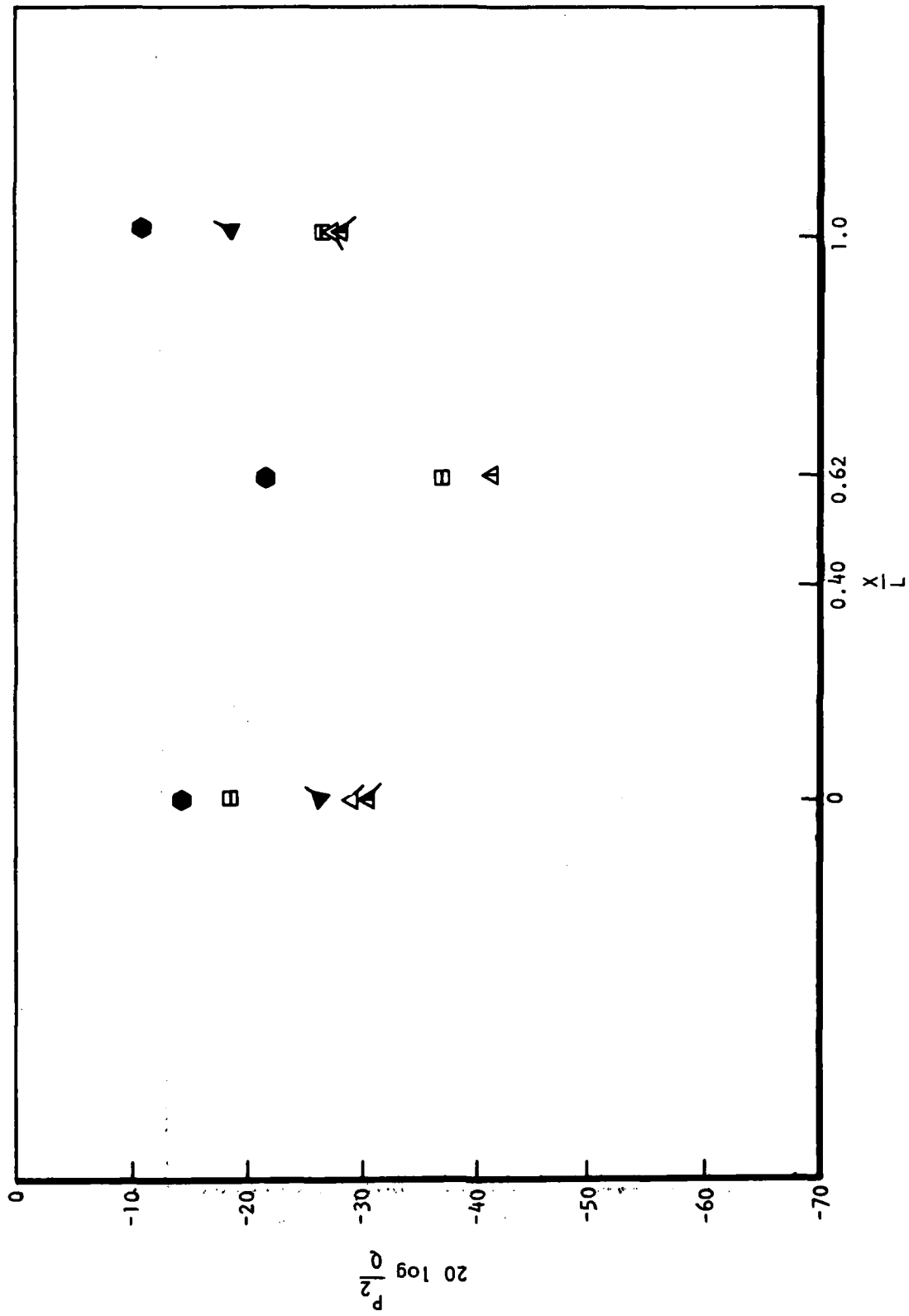
Figure 42. Bulkhead/Sidewall Upper, Mode 2, 0.85M, Full-Open, Discrete Levels Versus Bay Length
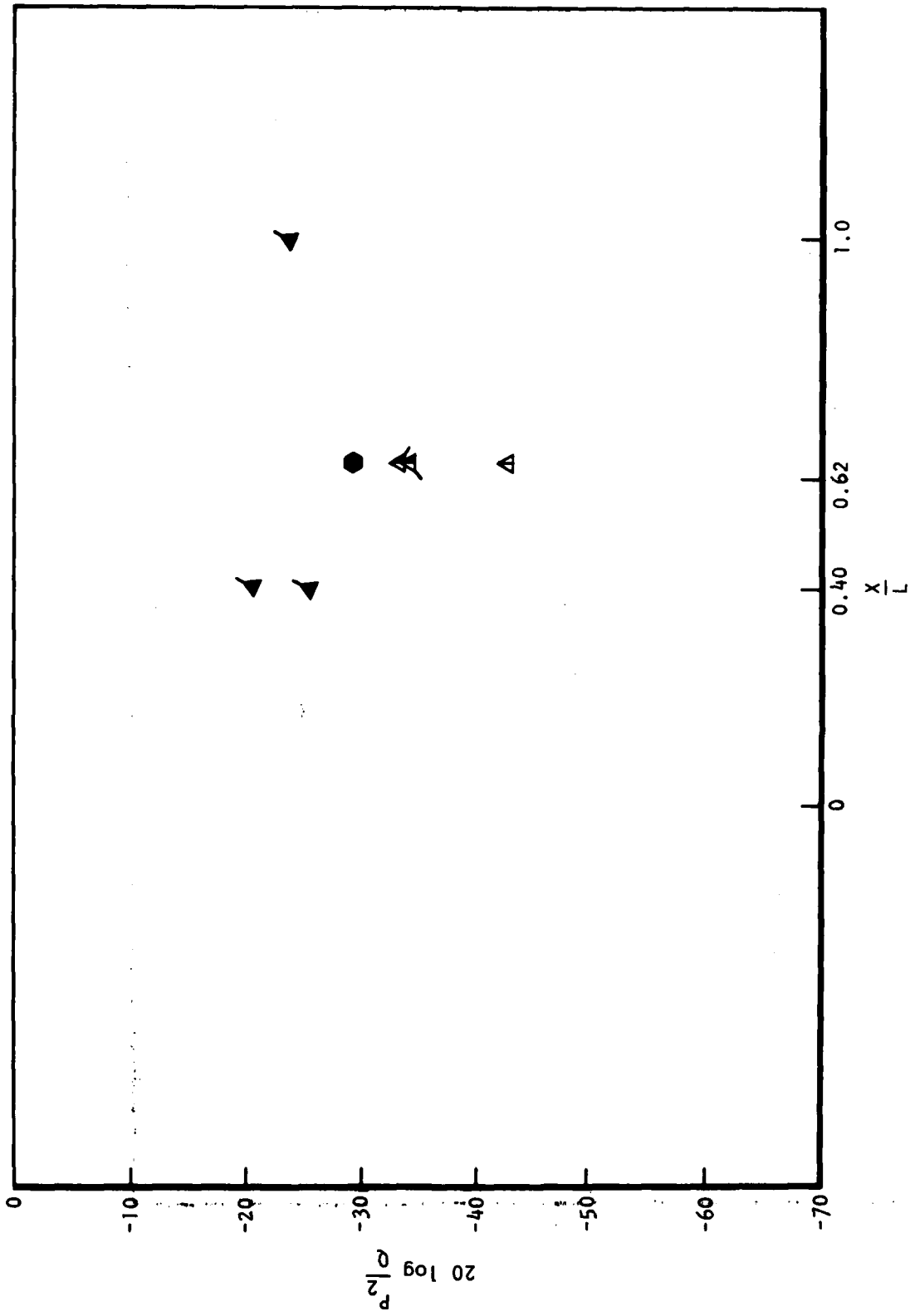
Figure 43. Bulkhead/Sidewall Top Center, Mode 2, 0.85M, Full-Open, Discrete Levels Versus Bay Length

51
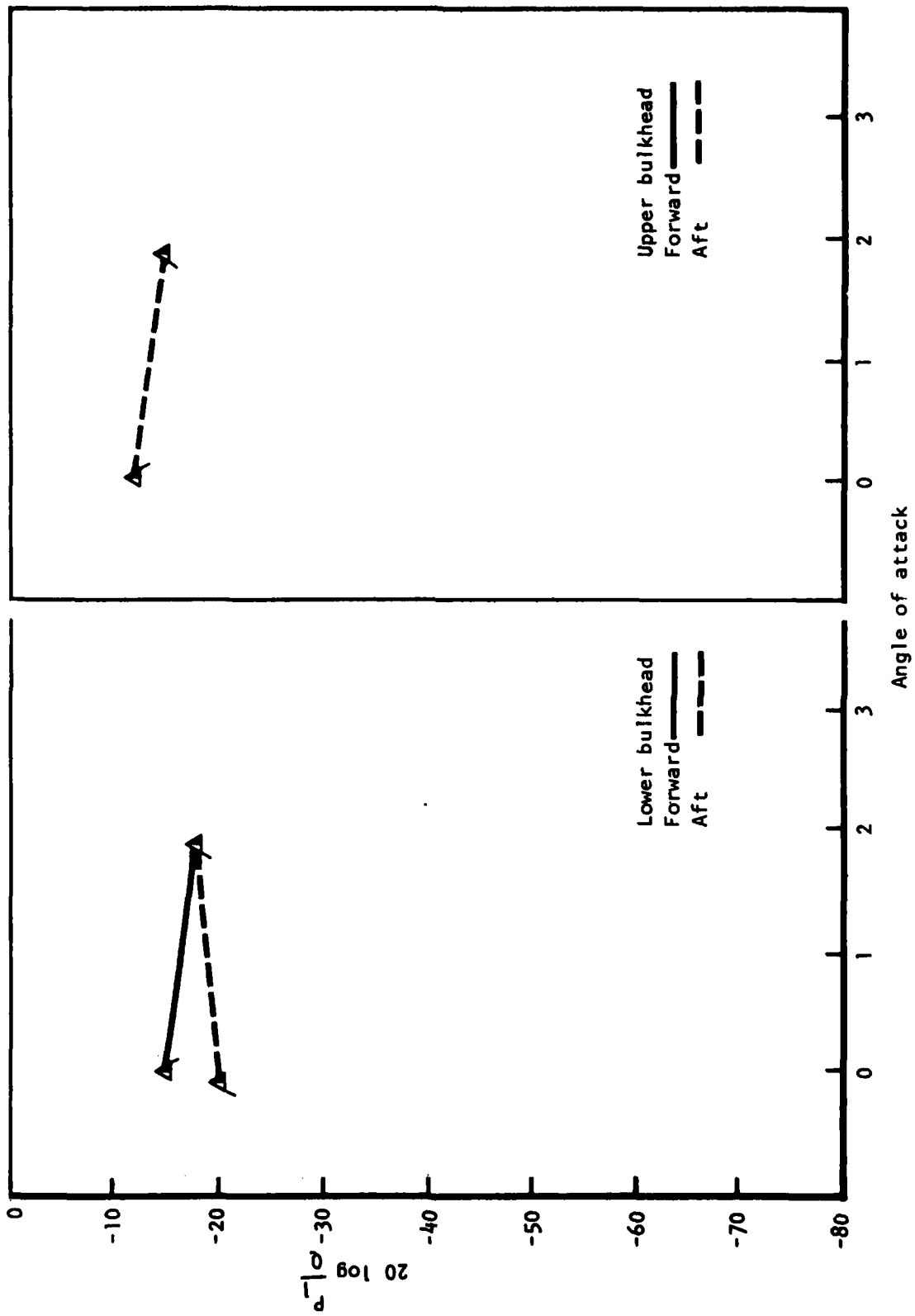
Figure 44.   Angle of Attack Versus Discrete Mode 1 - 0.1-Scale Model Data, 0.85M, Full-Open
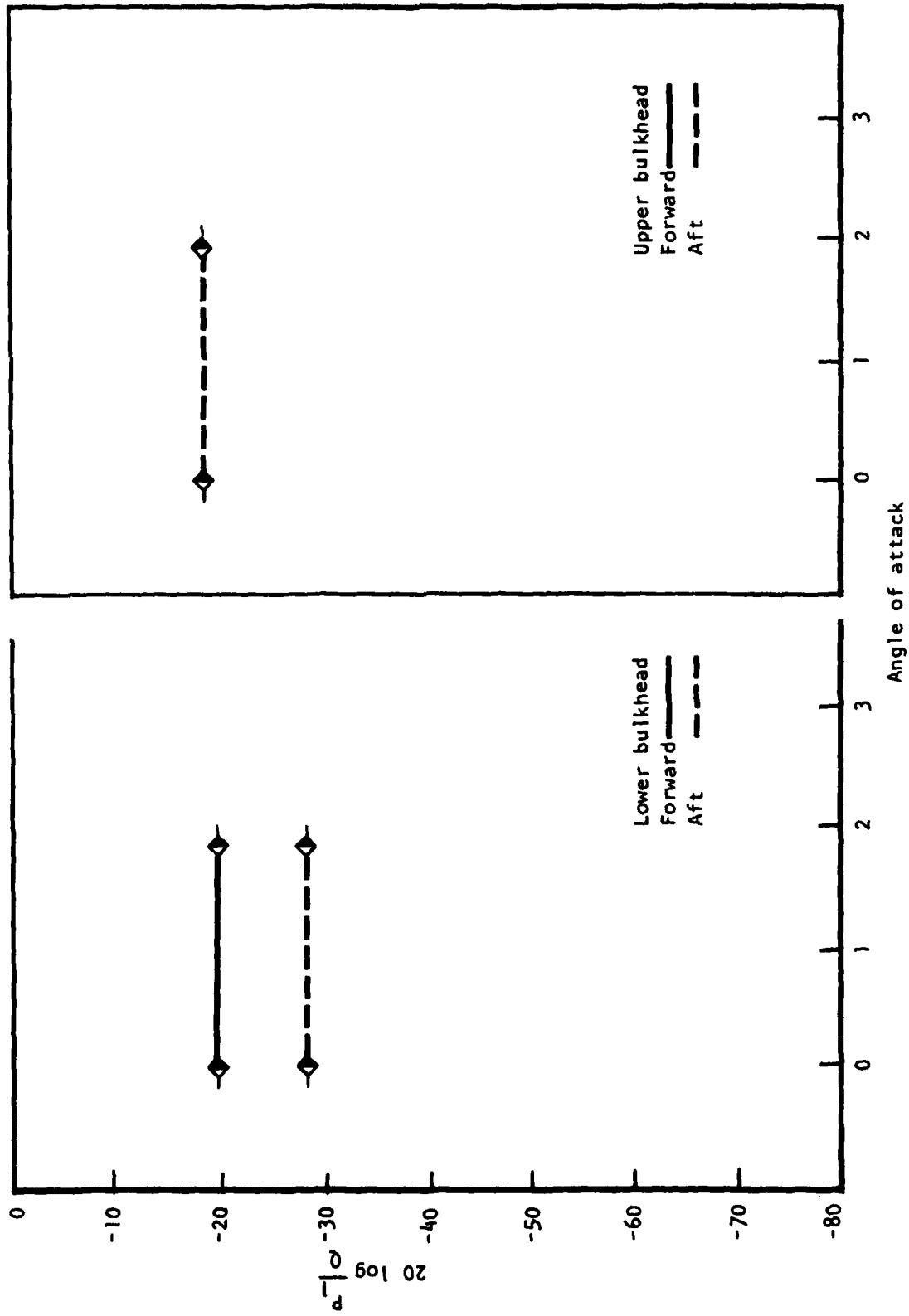
Figure 45. Angle of Attack Versus Discrete Mode 1 - 0.1-Scale Model Data, 0.85M, Part-Open
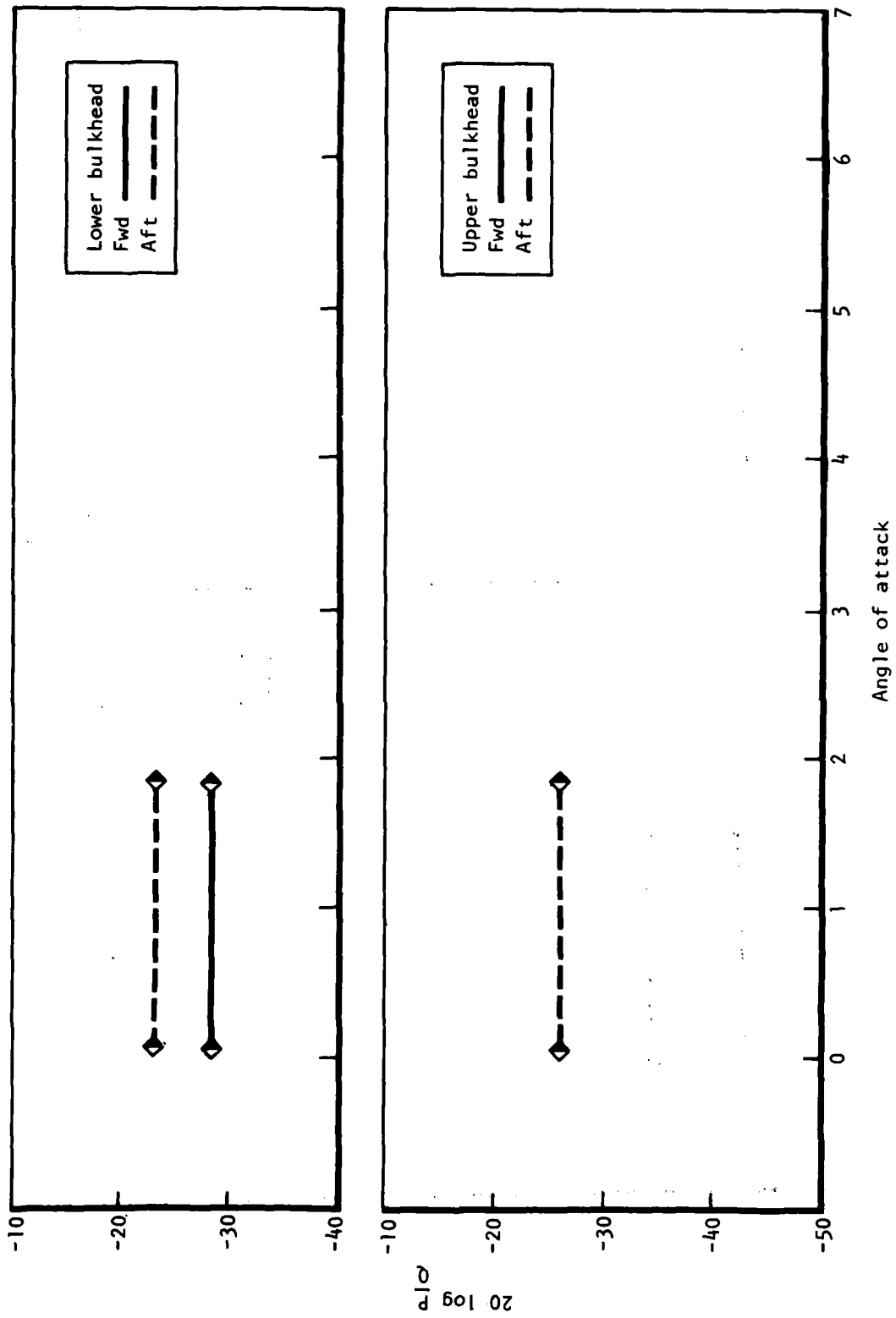
Figure 46. 0.1 Model Data, Angle of Attack Versus Overall Broadband, Mach 0.85, Part Open
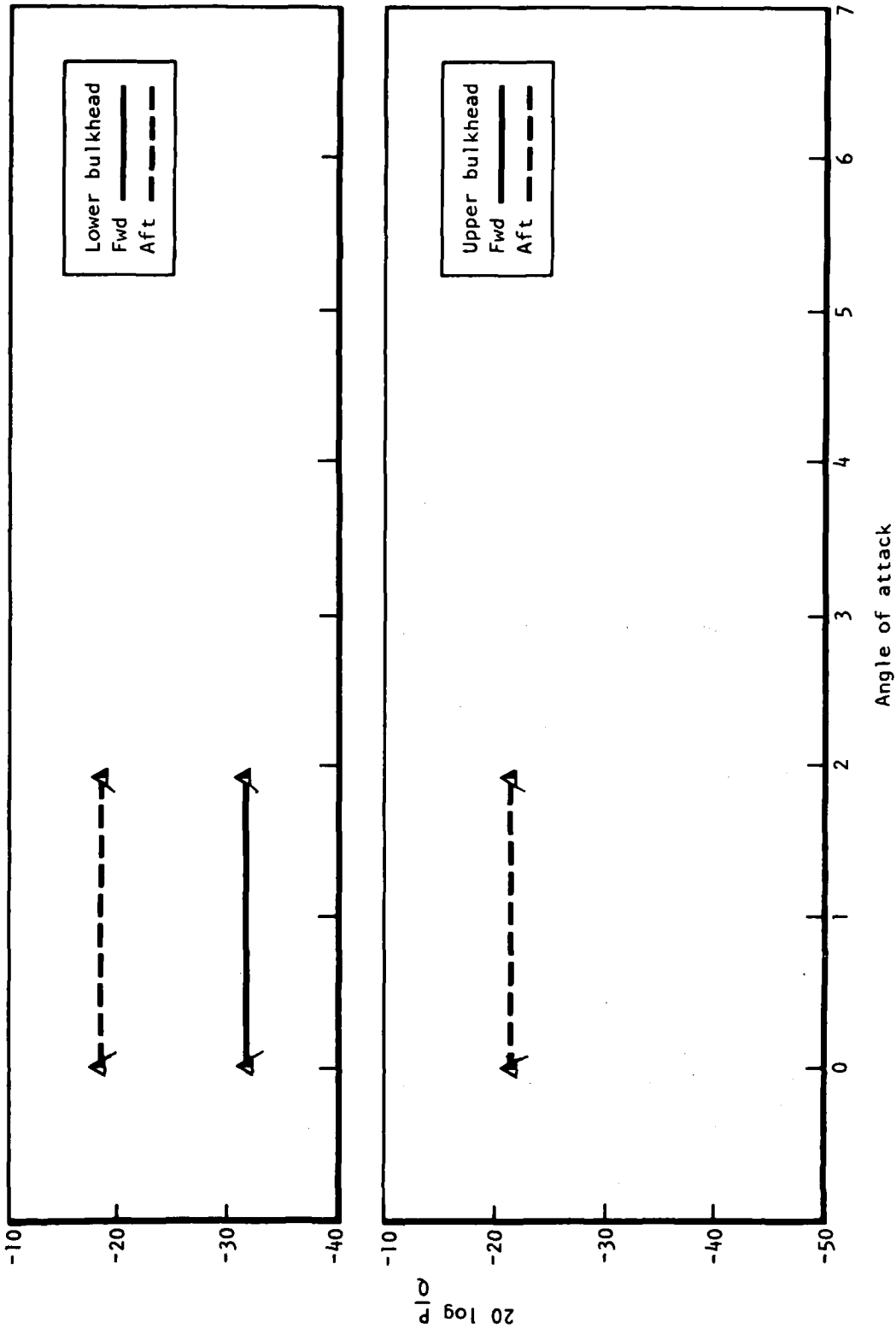
Figure 47. 0.1 Model Data, Angle of Attack Versus Overall Broadband, Mach 0.85, Full Open

55

CAVITY NOISE REDUCTION DEVICES

The data for several cavity noise suppression concepts are presented and correlated with the unsuppressed baseline data for empty cavities. Both wind tunnel and full-scale aircraft data are illustrated for each suppression device. The suppression devices are a 90-degree porous, 90-degree solid, a 70-degree porous, and a 70-degree solid spoiler that spans the cavity width and protrudes approximately 14 inches from the mold line of the full scale. The spoilers were on the leading edge of the weapon bay cavities and were retractable for the full-scale aircraft. Data are plotted for both full- and part-open doors. The spoilers for the full-scale aircraft are shown in Figures 48 and 49. The spoilers tested in the wind tunnel are shown in Figures 50 through 55 for part- and full-open door positions.

The maximum cavity noise reduction was achieved on the aft lower bulkhead, and a typical plot is shown in Figure 56. Significant broadband and discrete frequency noise reduction was achieved for the aft lower bulkhead. Much less attenuation occurred for the broadband noise levels for other positions in the cavity. On the forward bulkhead and near the top of the cavity, very little, if any, broadband noise level reduction occurred. The discrete frequencies were significantly attenuated throughout the cavity.

Cavity noise levels for various configurations of 70- and 90-degree porous and solid spoilers are shown as a function of mach number in Figures 57 through 82. Model data and full-scale data are shown in addition to noise reduction values for each spoiler configuration. The data are shown for the first and second cavity modes, which are the dominant pressures inside the unsuppressed cavity, and for full- and part-open door positions. All data shown are for a constant dynamic pressure of 500 psf at the aft upper bulkhead position. The aft lower bulkhead position would have been preferred for data comparison, but instrumentation problems at supersonic speeds resulted in questionable data at the lower bulkhead position. The absolute magnitude of the discrete pressure level may be slightly higher at the lower position, but the data shown for the upper position illustrate the noise level trends and comparisons of the various spoiler configuration and correlation between full-scale and model data at subsonic and supersonic speeds.

The 90-degree porous spoiler noise data are shown in Figures 57 through 62. The full-scale data show high subsonic noise levels for the full-open door position and approximately the same noise levels at supersonic speeds. The noise reduction for 90-degree porous spoilers is shown in Figures 59 and 60 as a function of mach number for part- and full-open door positions, respectively. Both figures show appreciable subsonic noise reduction, but at supersonic speeds the spoilers appear ineffective. At the part-open door position, the spoilers increase the cavity noise level. Model data for the same spoiler configuration are shown in Figures 61 and 62. The model data in Figure 52 show appreciable spoiler noise reduction at both subsonic and supersonic speeds. The unsuppressed noise levels for the model cavity are significantly higher than for the full-scale data at supersonic speeds and of comparable magnitude at subsonic speeds, as shown in Figures 9 and 18. It appears that cavity noise reduction may be a function of the intensity at which a cavity resonates. The noise level of a highly resonant cavity may be easier to reduce than

Four independently actuated spoilers

FRP

Inboard attenuator
panels

Outboard attenuator panels
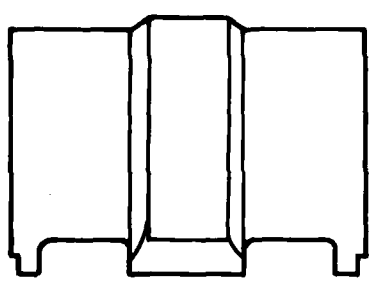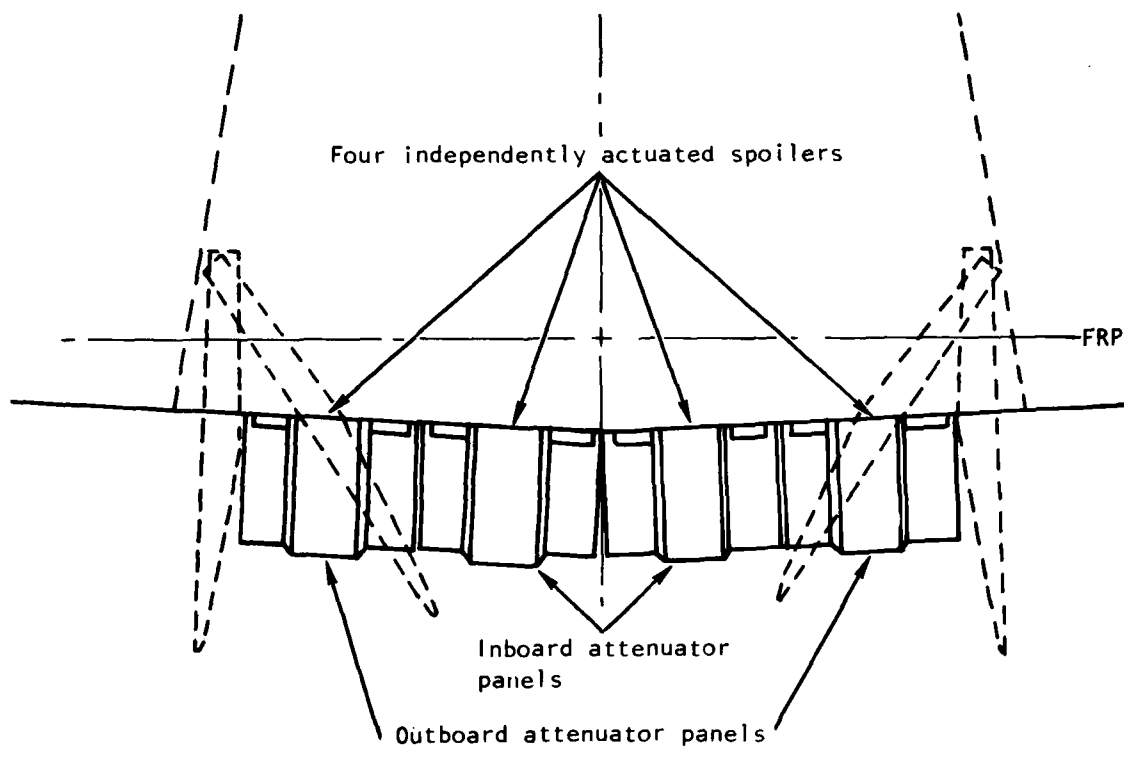
70° solid spoiler

70° porous spoiler

Fwd bulkhead
Bays No. 1 or
No. 2

70°
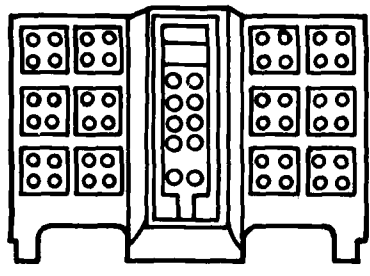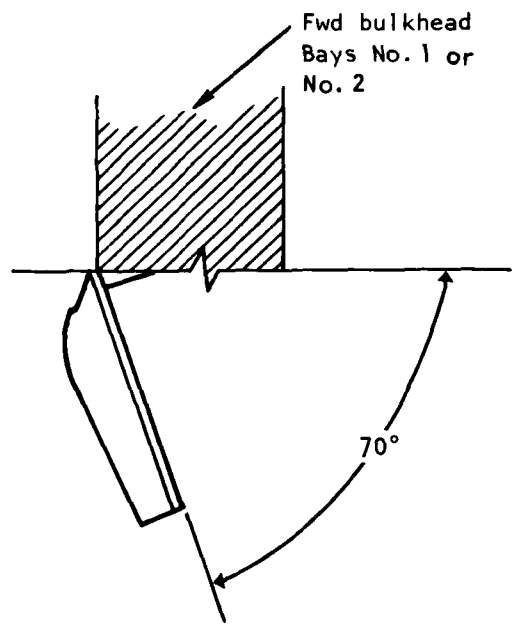
Figure 48.   70-Degree Spoiler Configuration

57

SIDE VIEW
FORWARD
END OF BAY

LWR
FUS ML

RETRACTED

EXTENDED

LWR
FUS ML

HYD
ACTUATOR

42.00

14.00

U.S. AIR FORCE

3
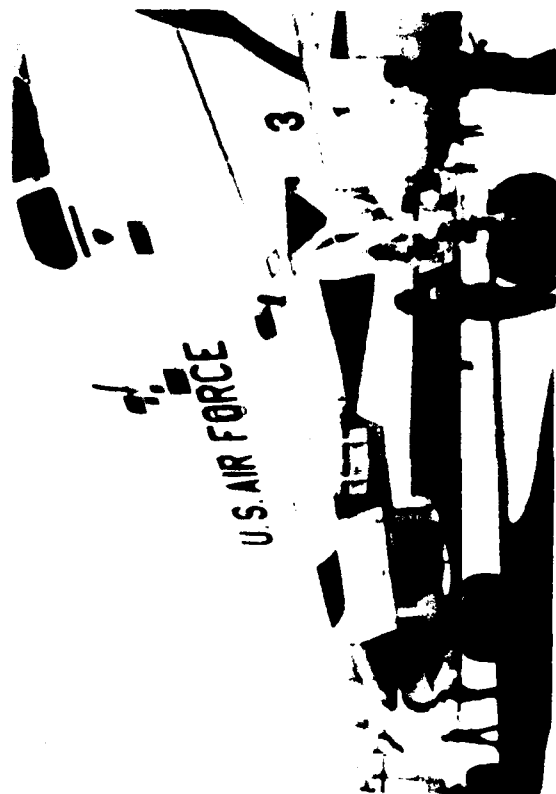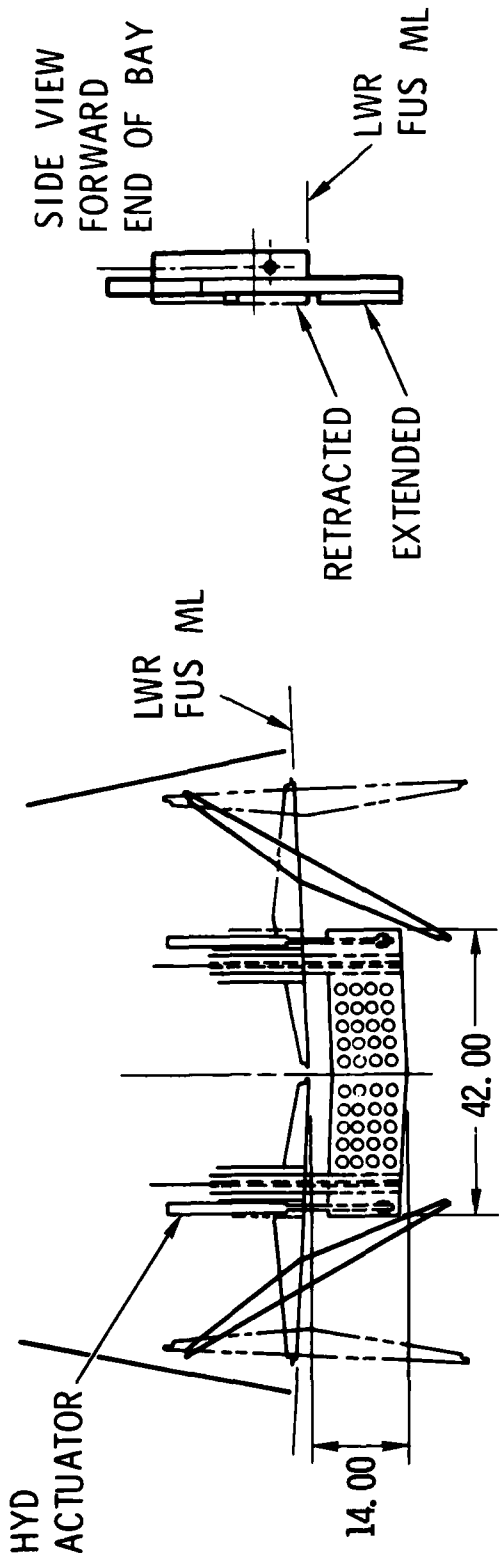
Figure 49.   90-Degree Porous Spoiler Installation

58
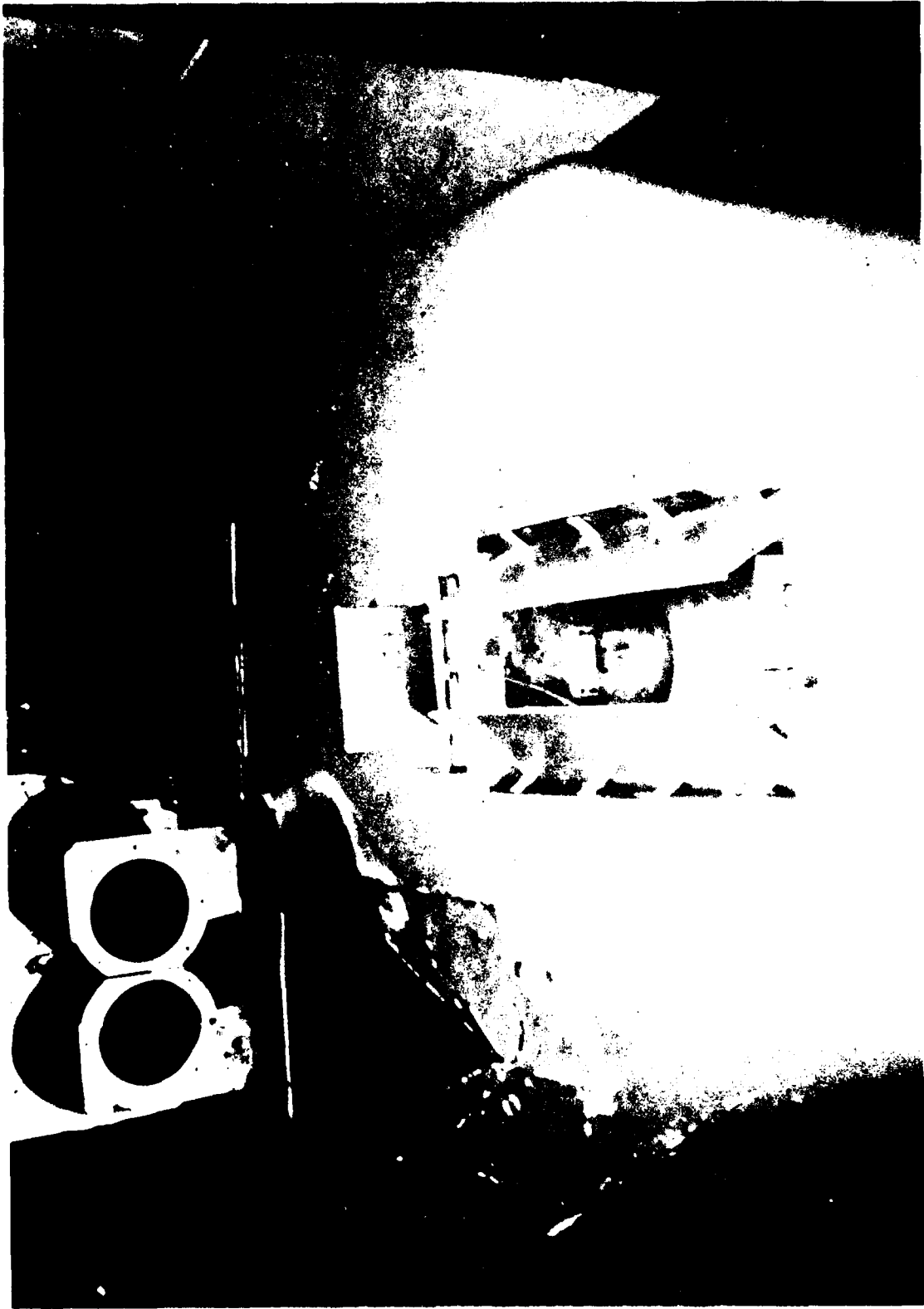
Figure 50. 70 Degree Solid Part Open

59

Figure 51. 70 Degree Solid Full Open

60

Figure 52. 90 Degree Porous Part Open

61
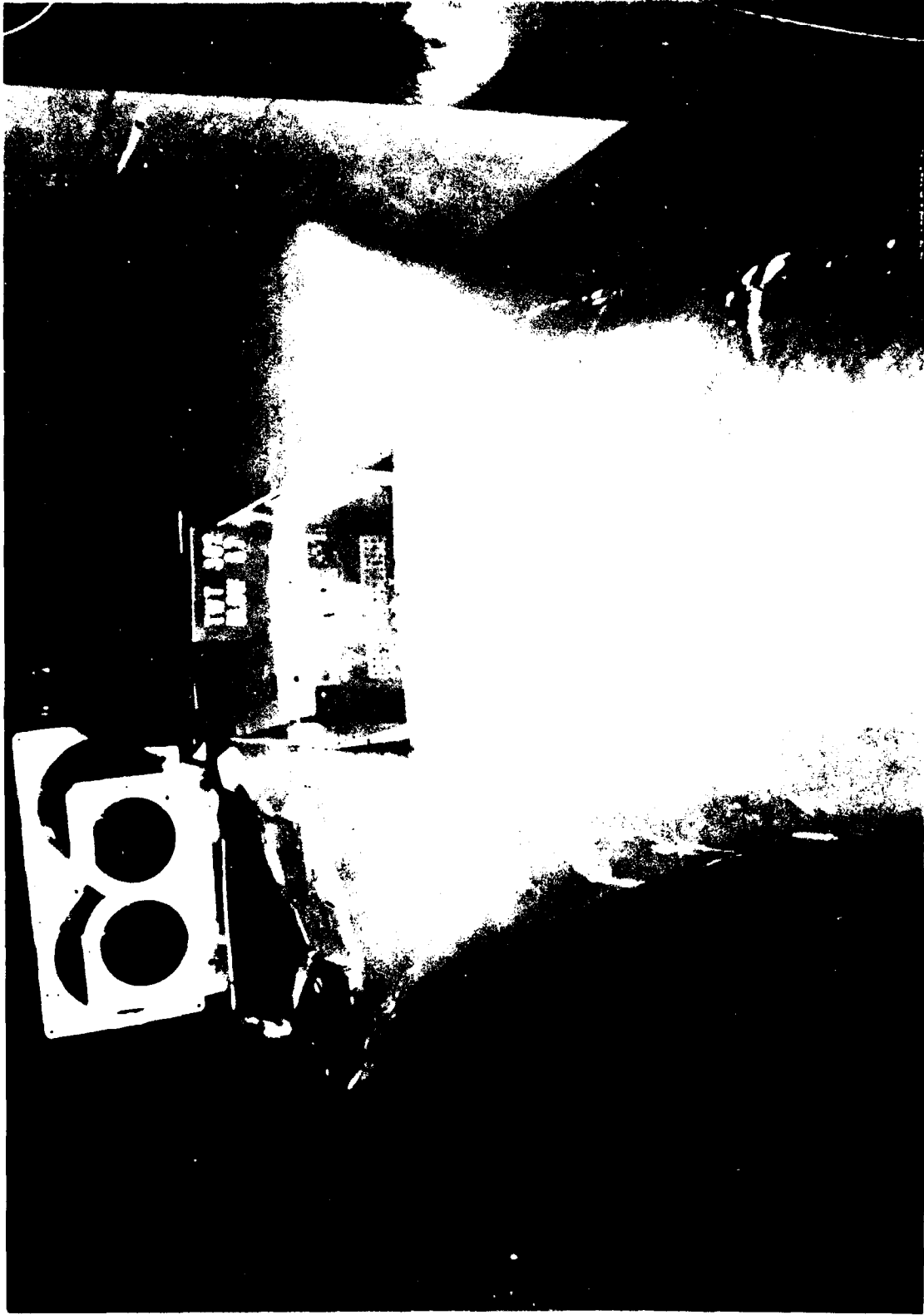
Figure 53. 90 Degree Porous Full Open
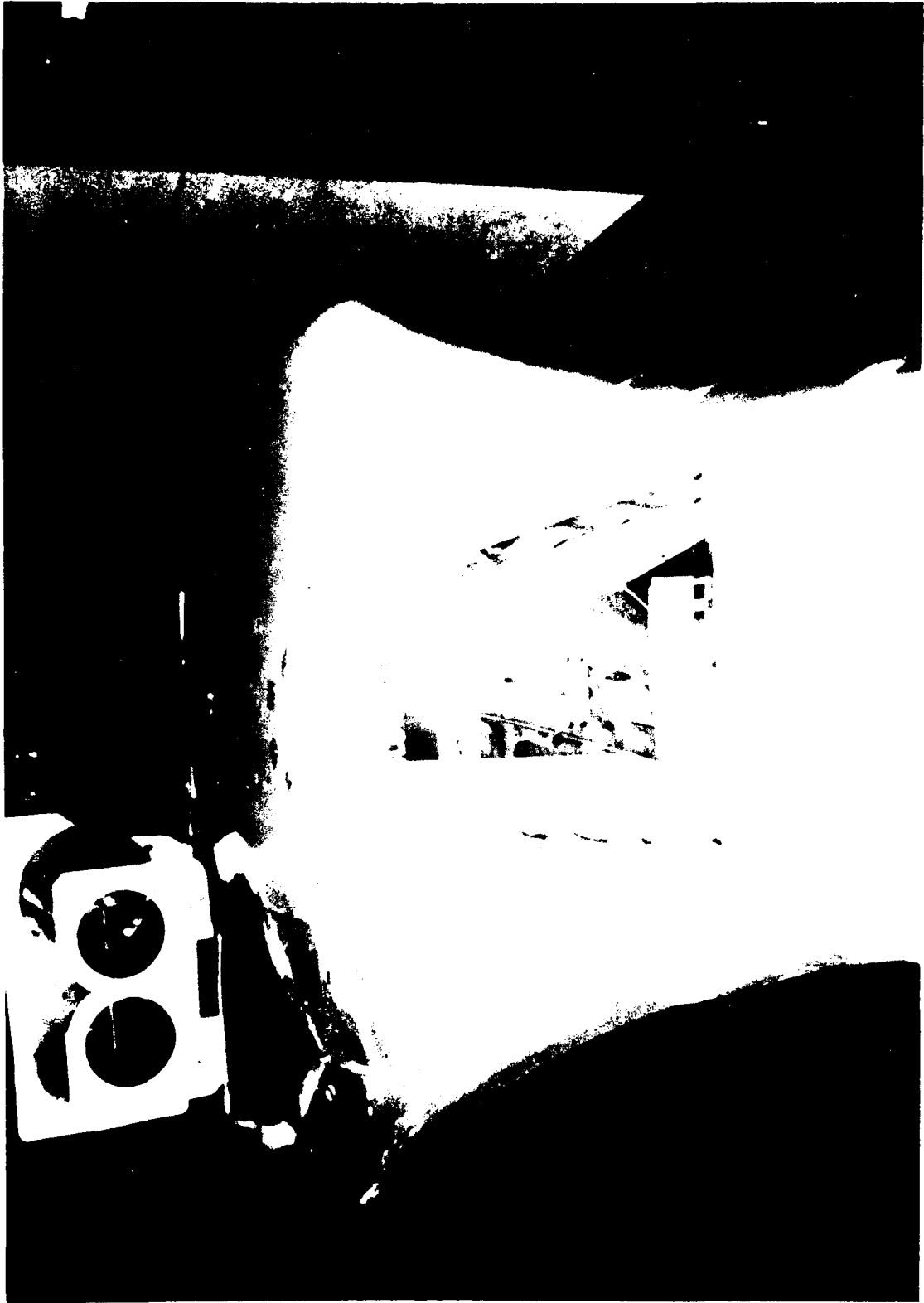
Figure 54. 90 Degree Solid Part Open

63
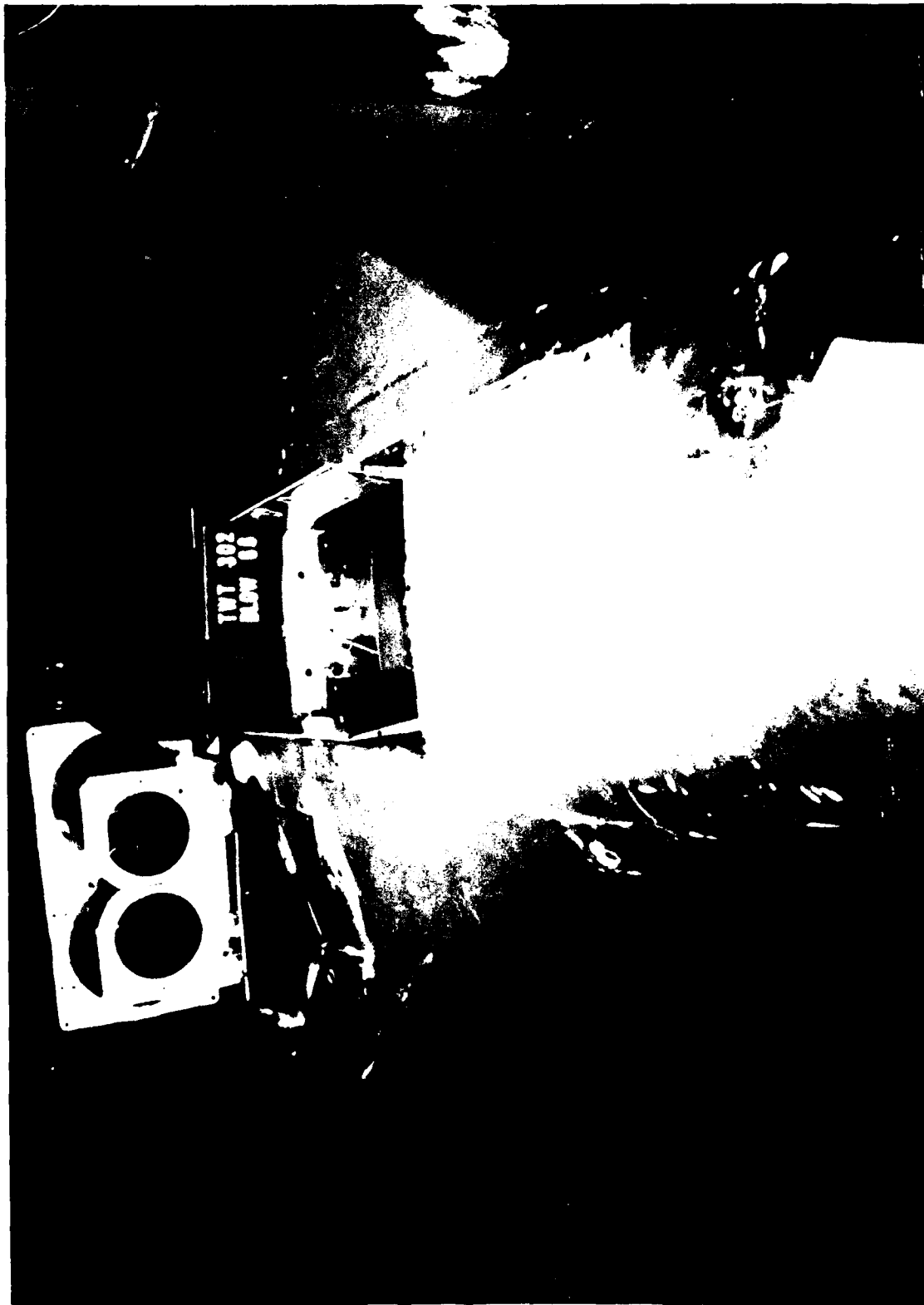
Figure 55. 90 Degree Solid Full Open
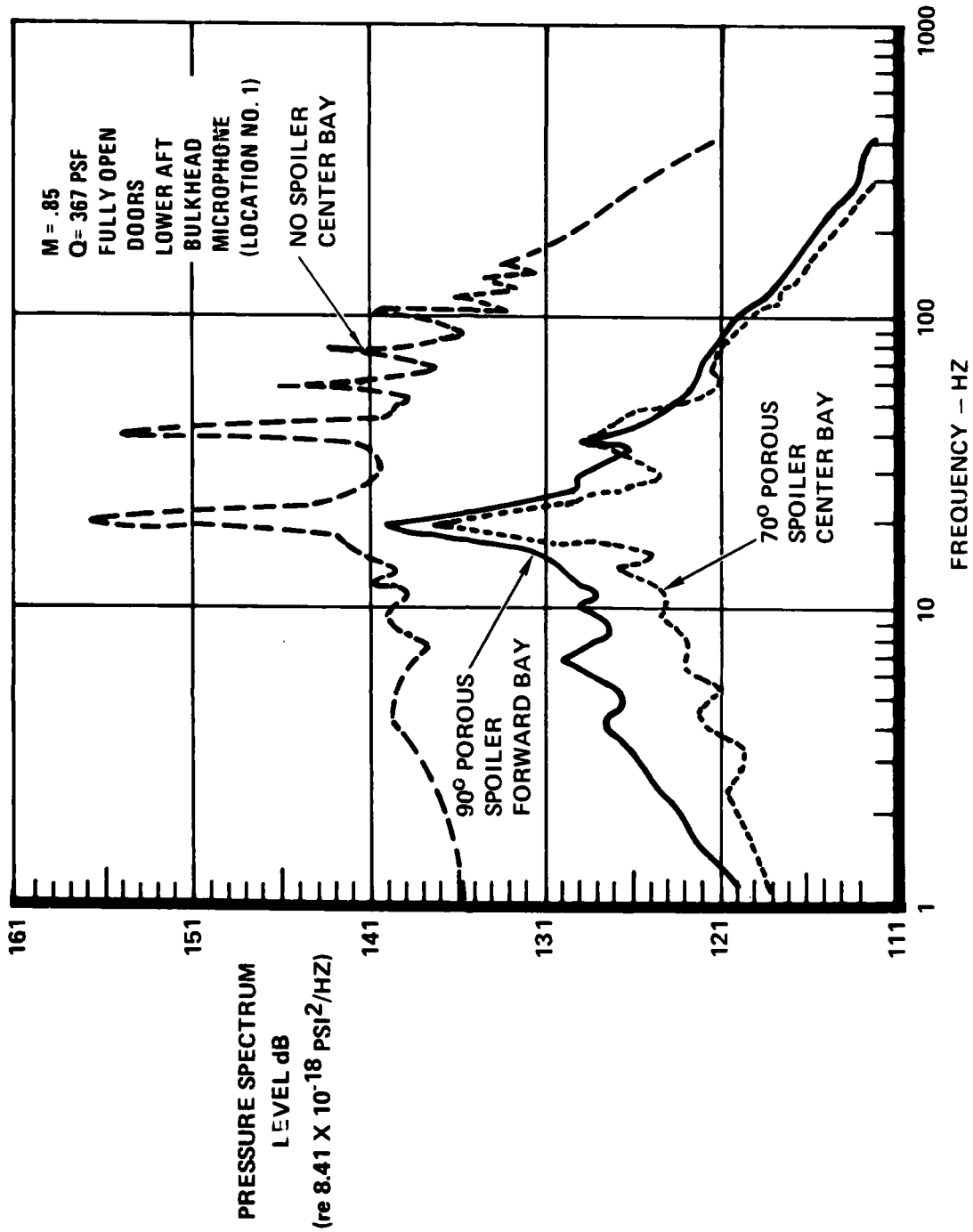
Figure 56. Forward and Center Bay Acoustic Levels
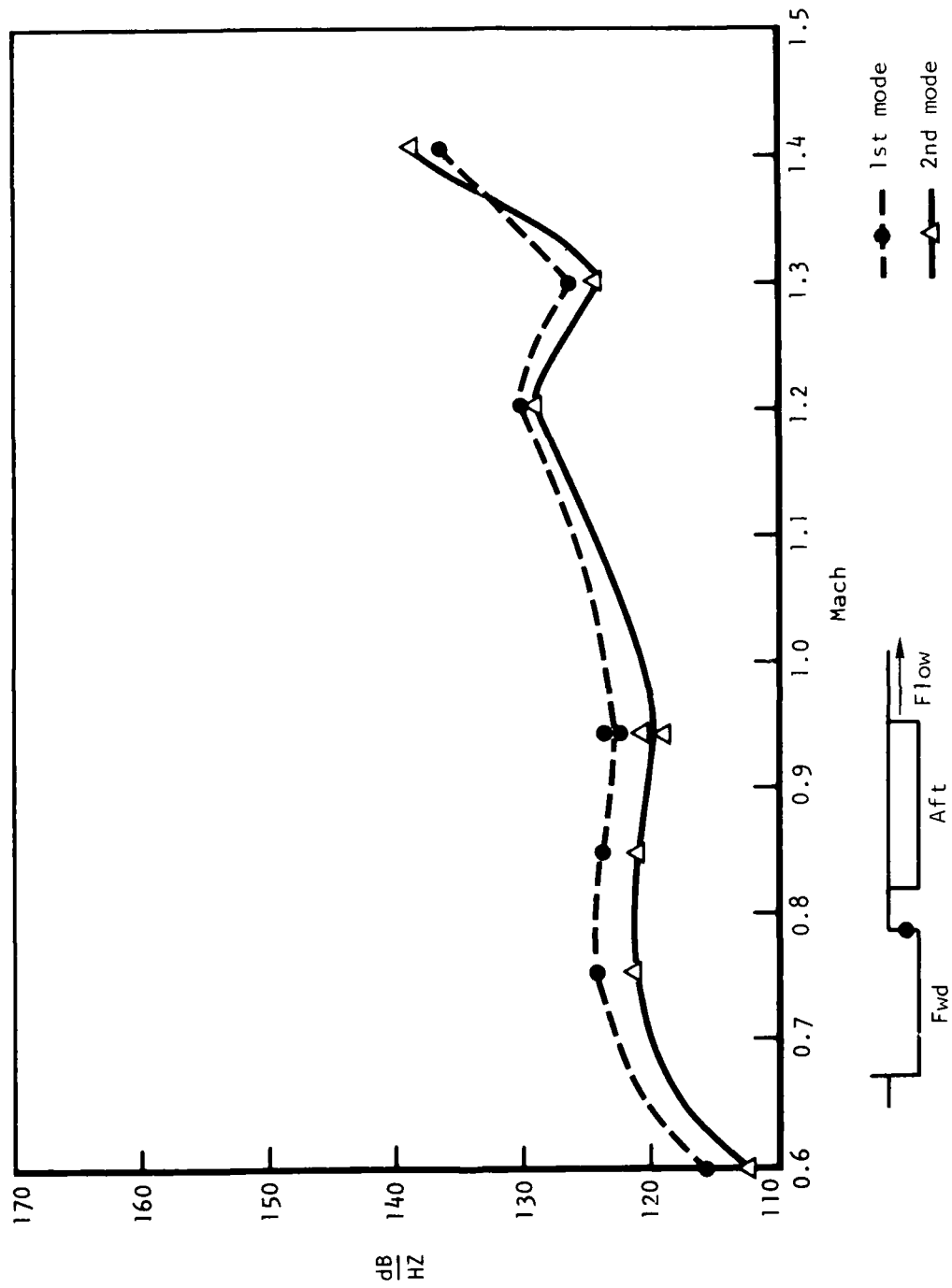
Figure 57. B-1 Full-Scale Flight Data, 90° Porous Spoiler, Forward Bay Part Open, Aft Bulkhead, Upper, Q = 500 psf

66
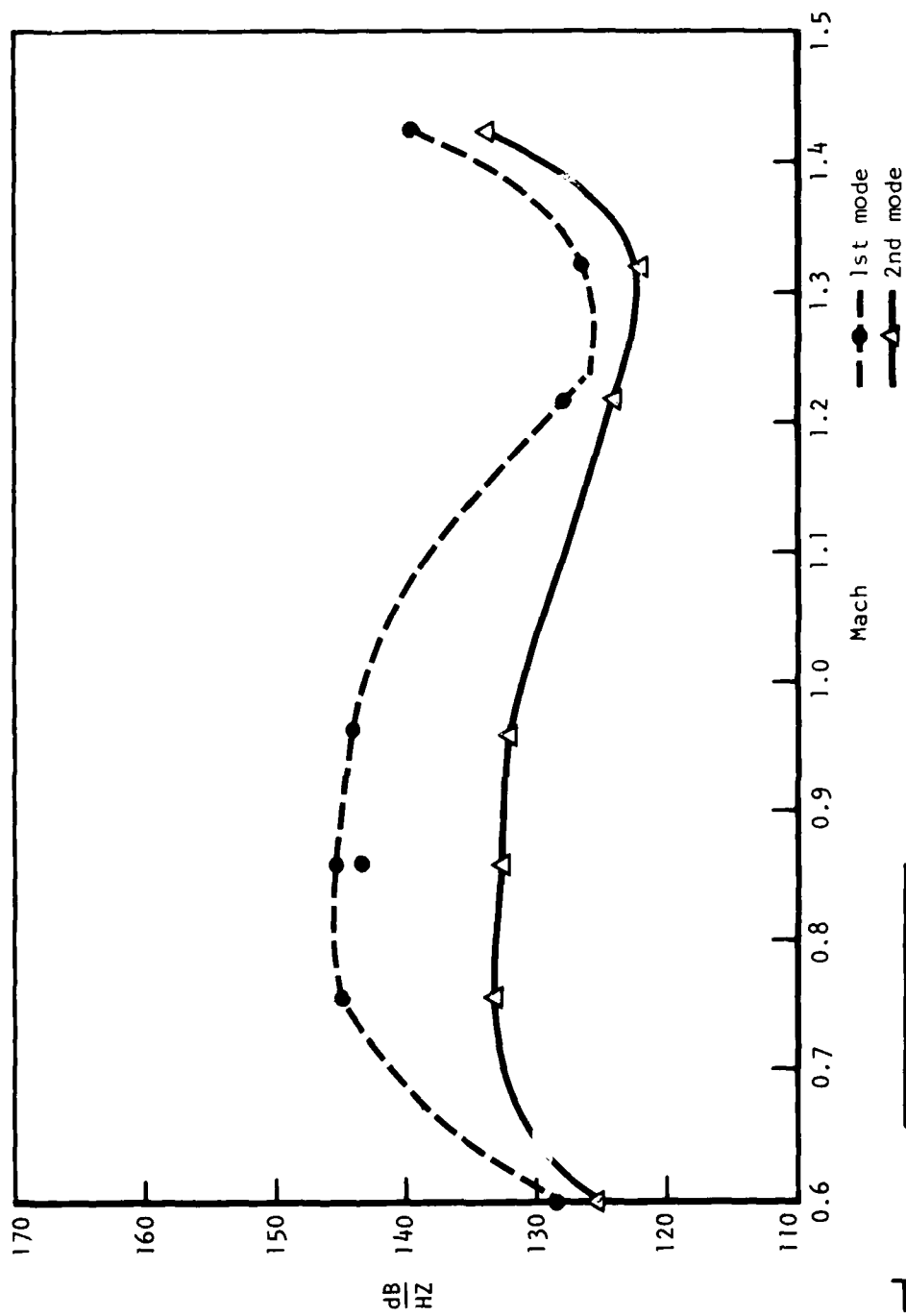
Figure 58. B-1 Full-Scale Flight Data, 90° Porous Spoiler, Forward Bay Full Open, Aft Bulkhead Upper, Q = 500 psf
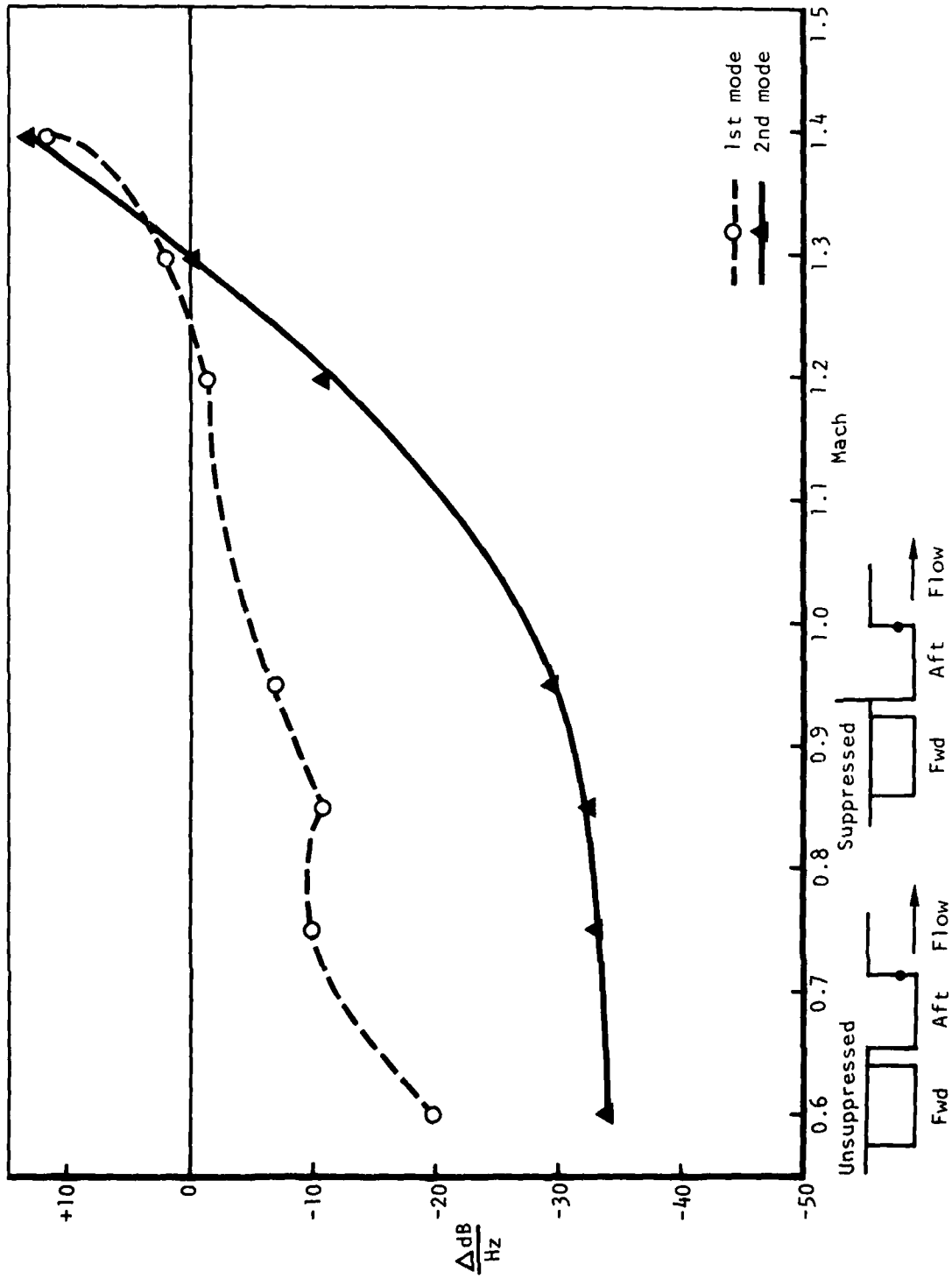
Figure 59. B-1 Full-Scale Flight Data, 90° Porous Spoiler versus Unsuppressed, Part Open, Aft Bulkhead Upper, Q = 500 psf
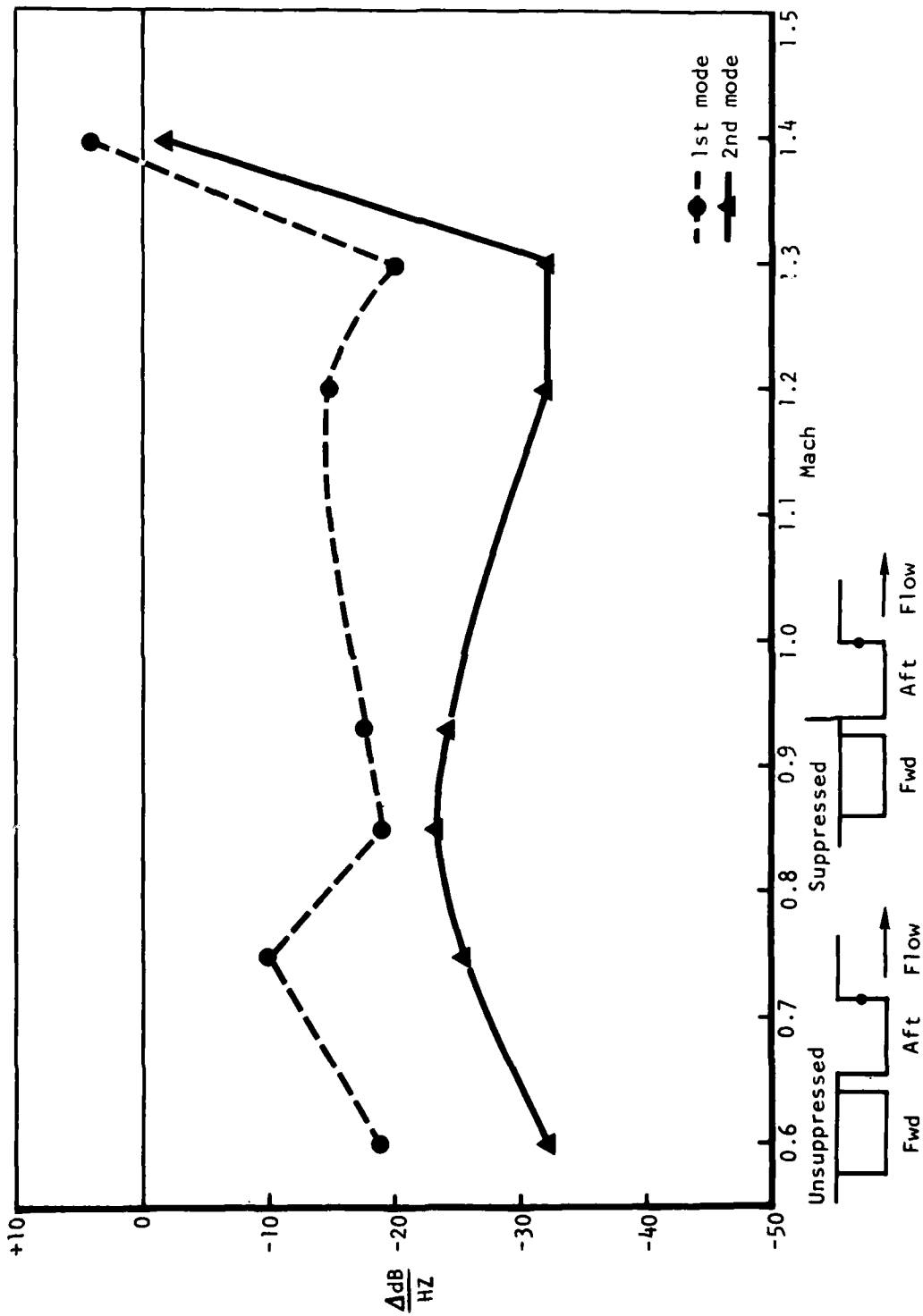
Figure 60. Full-Scale Flight Data, 90° Porous Spoiler versus Unsuppressed, Aft Bulkhead Upper, Full Open, Q = 500 psf
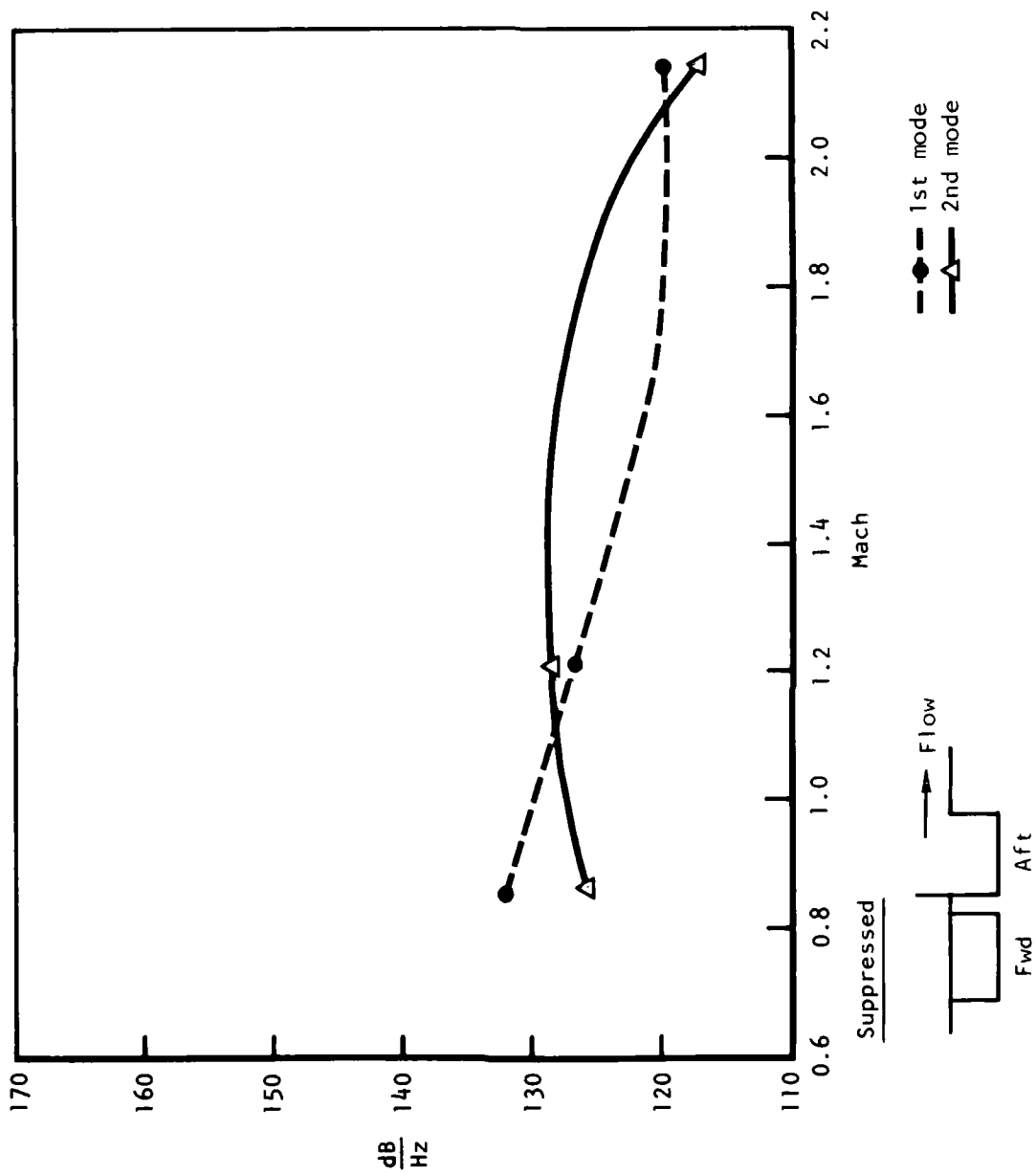
Figure 61. 0.1-Scale Model Data, 90° Porous Spoiler, Part Open, Aft Bulkhead Upper, Q = 500 psf
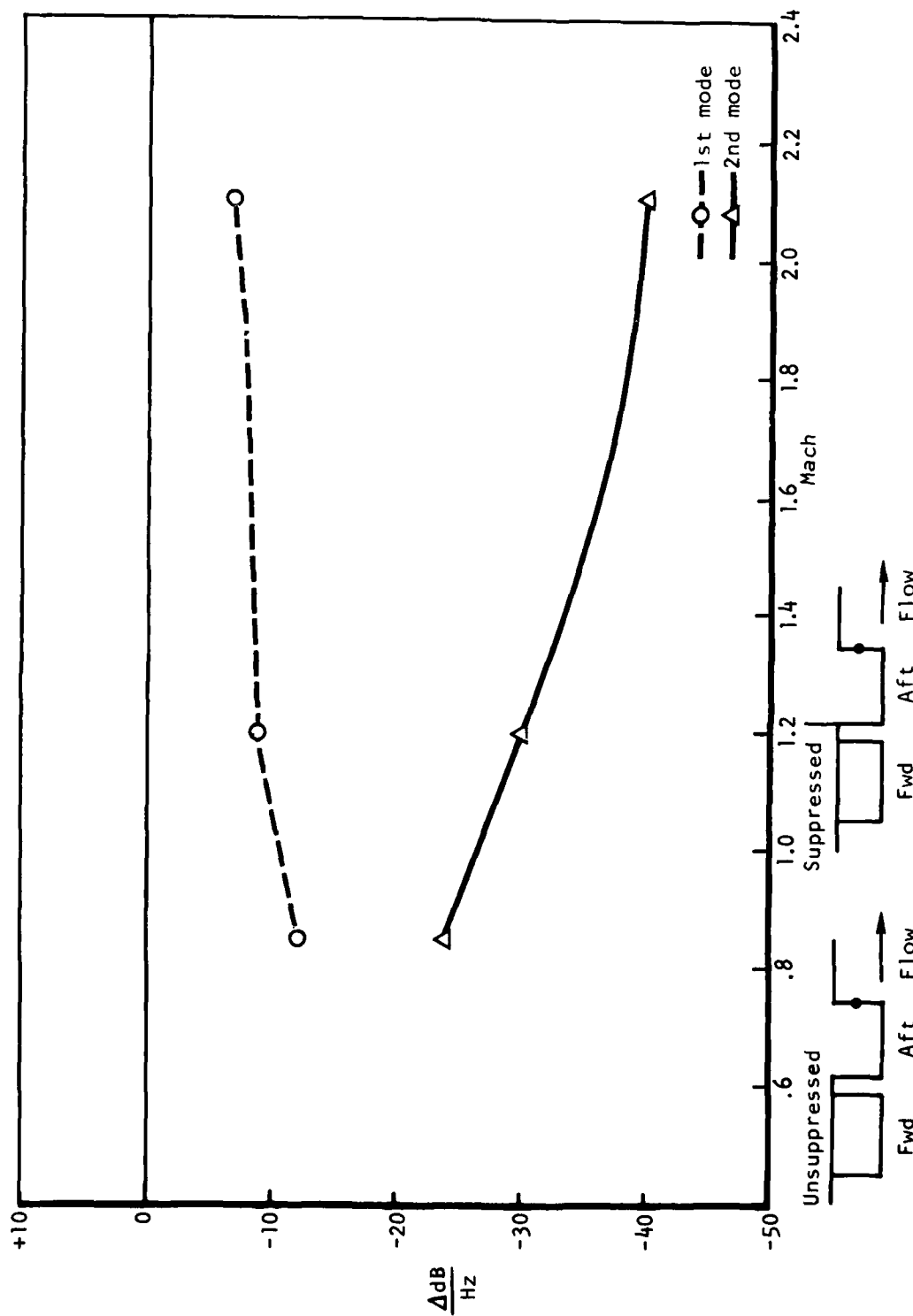
Figure 62. 0.1-Scale Model Data, 90° Porous Spoiler versus Unsuppressed, Part Open, Aft Bulkhead Upper, Q = 500 psf
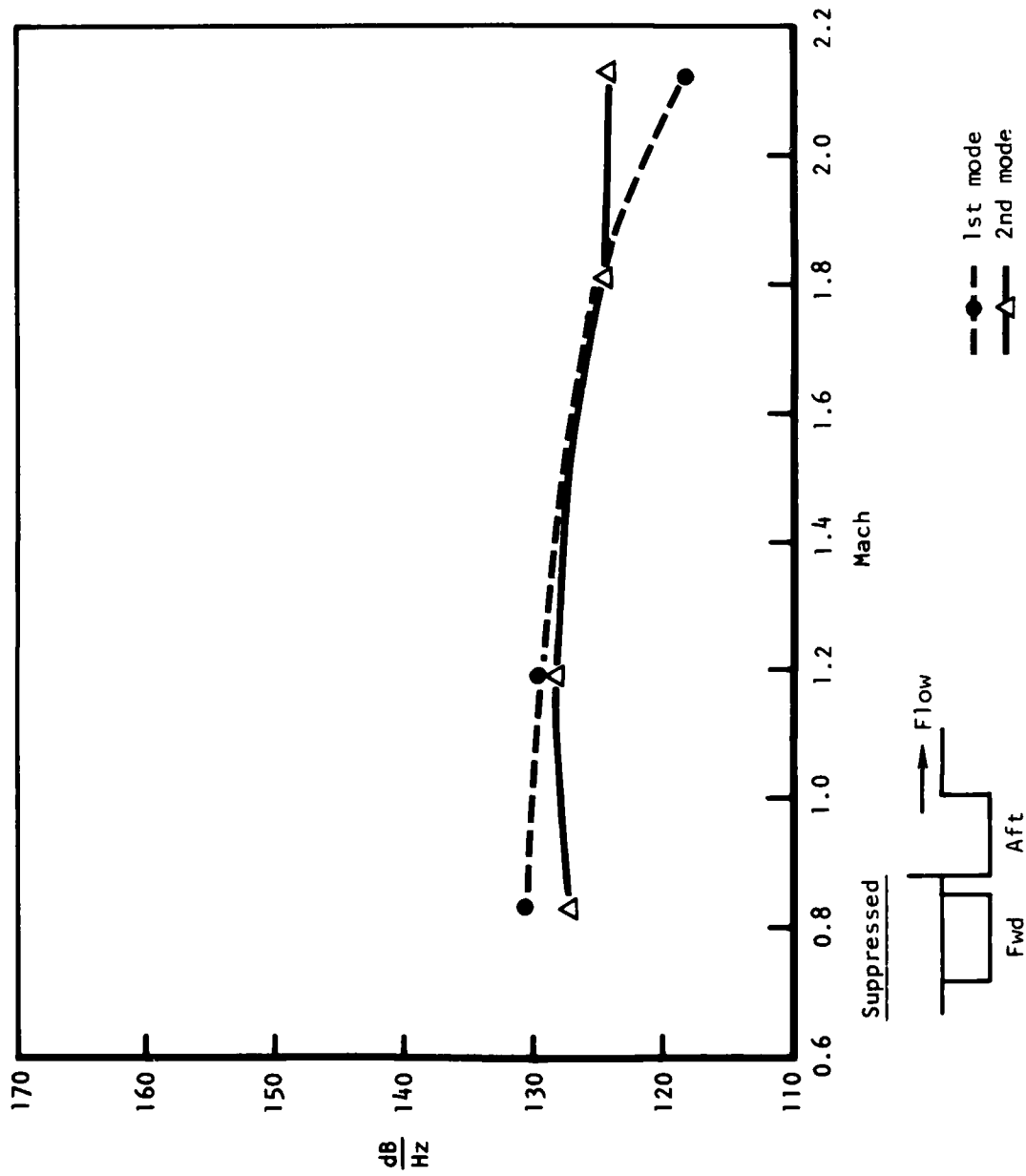
Figure 63. 0.1-Scale Model Data, 90° Solid Spoiler, Part Open, Aft Bulkhead Upper, Q = 500 psf
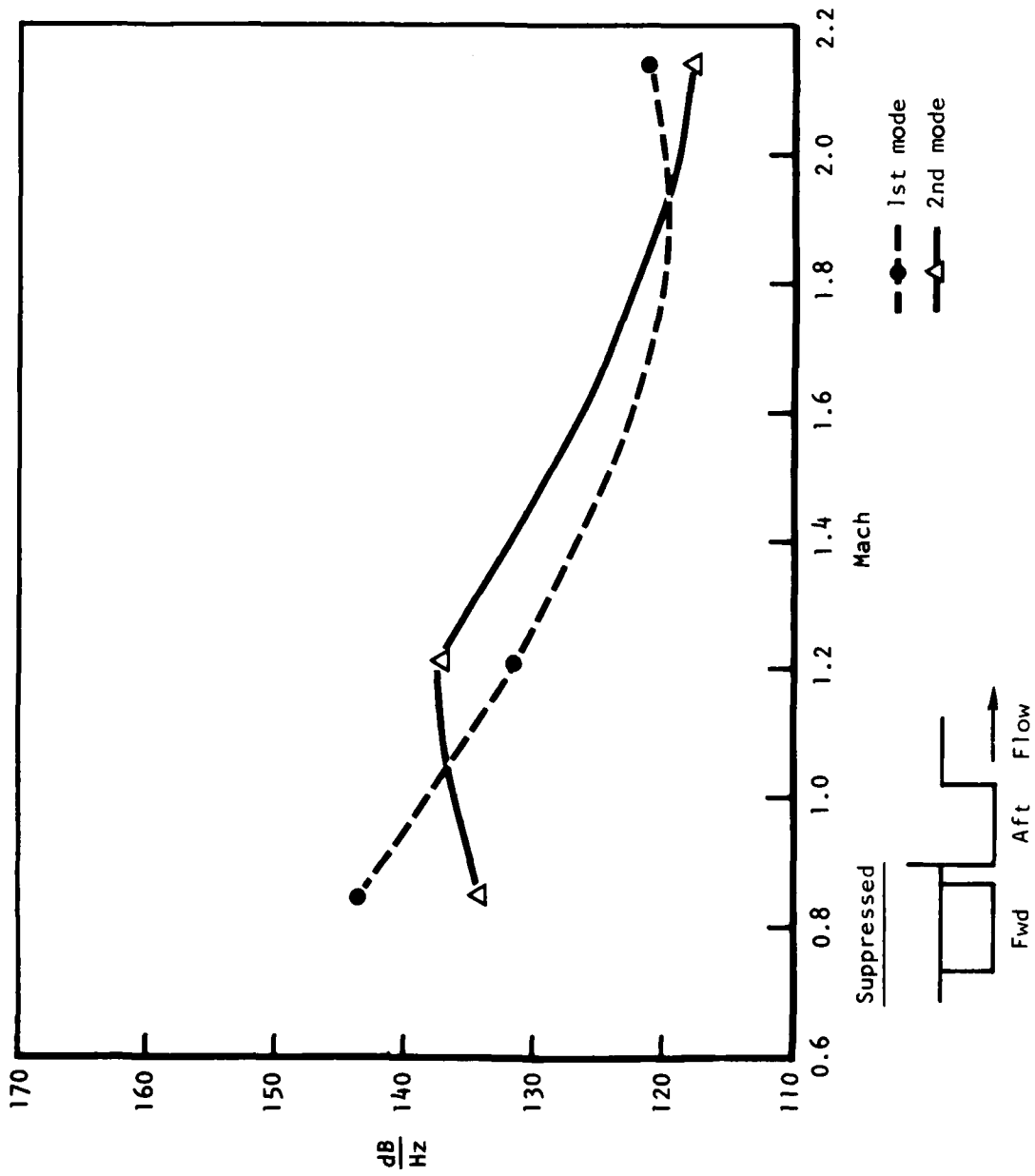
Figure 64. 0.1-Scale Model Data, 90° Solid Spoiler, Full Open, Aft Bulkhead Upper, Q = 500 psf
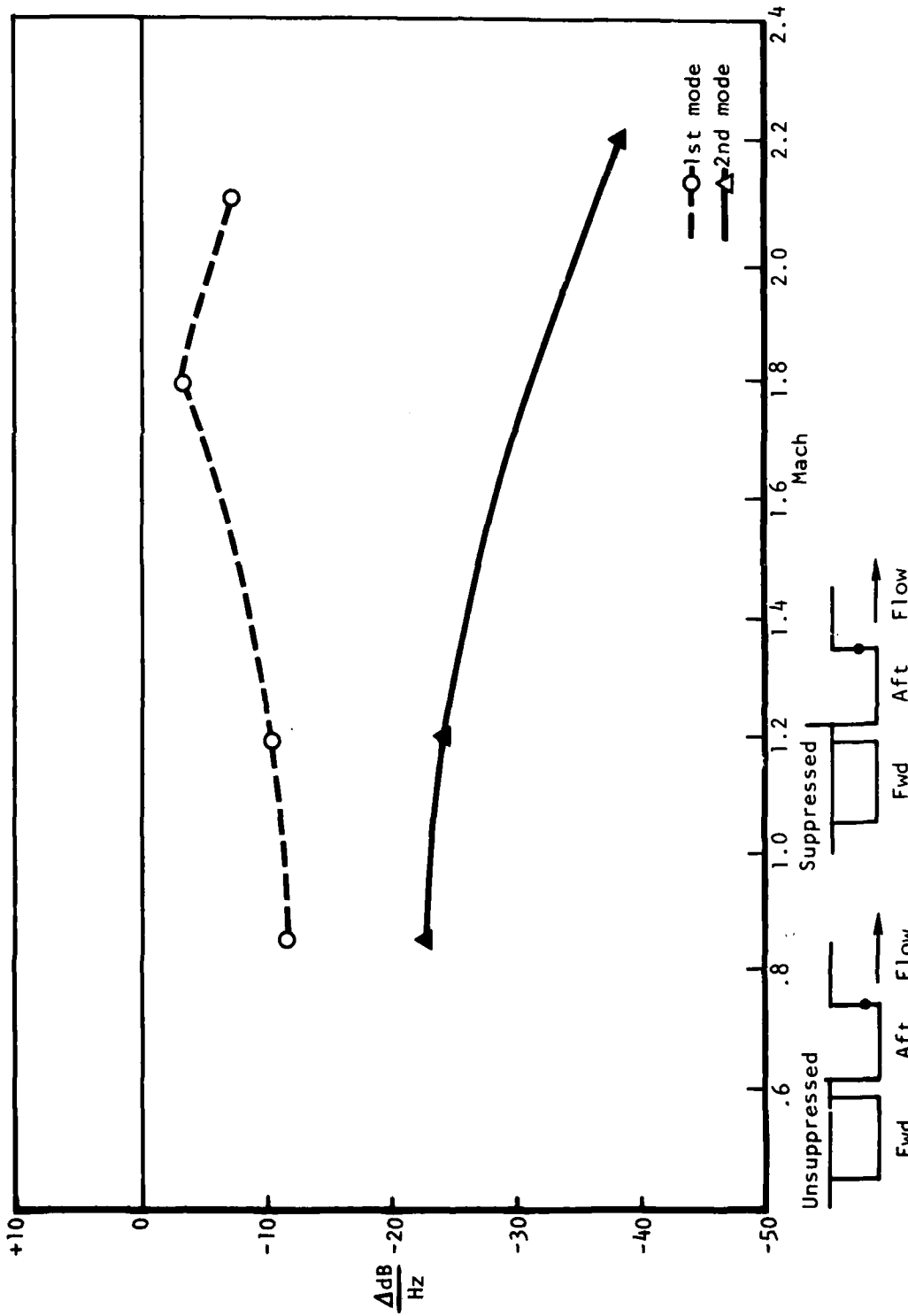
Figure 65. 0.1-Scale Model Data, 90° Solid Spoiler versus Unsuppressed, Part Open, Aft Bulkhead Upper, Q = 500 psf

$\frac{\Delta dB}{Hz}$

+10, 0, -10, -20, -30, -40, -50

Mach: .6, .8, 1.0, 1.2, 1.4, 1.6, 1.8, 2.0, 2.2, 2.4

Unsuppressed — Fwd — Aft — Flow

Suppressed — Fwd — Aft — Flow

1st mode
2nd mode
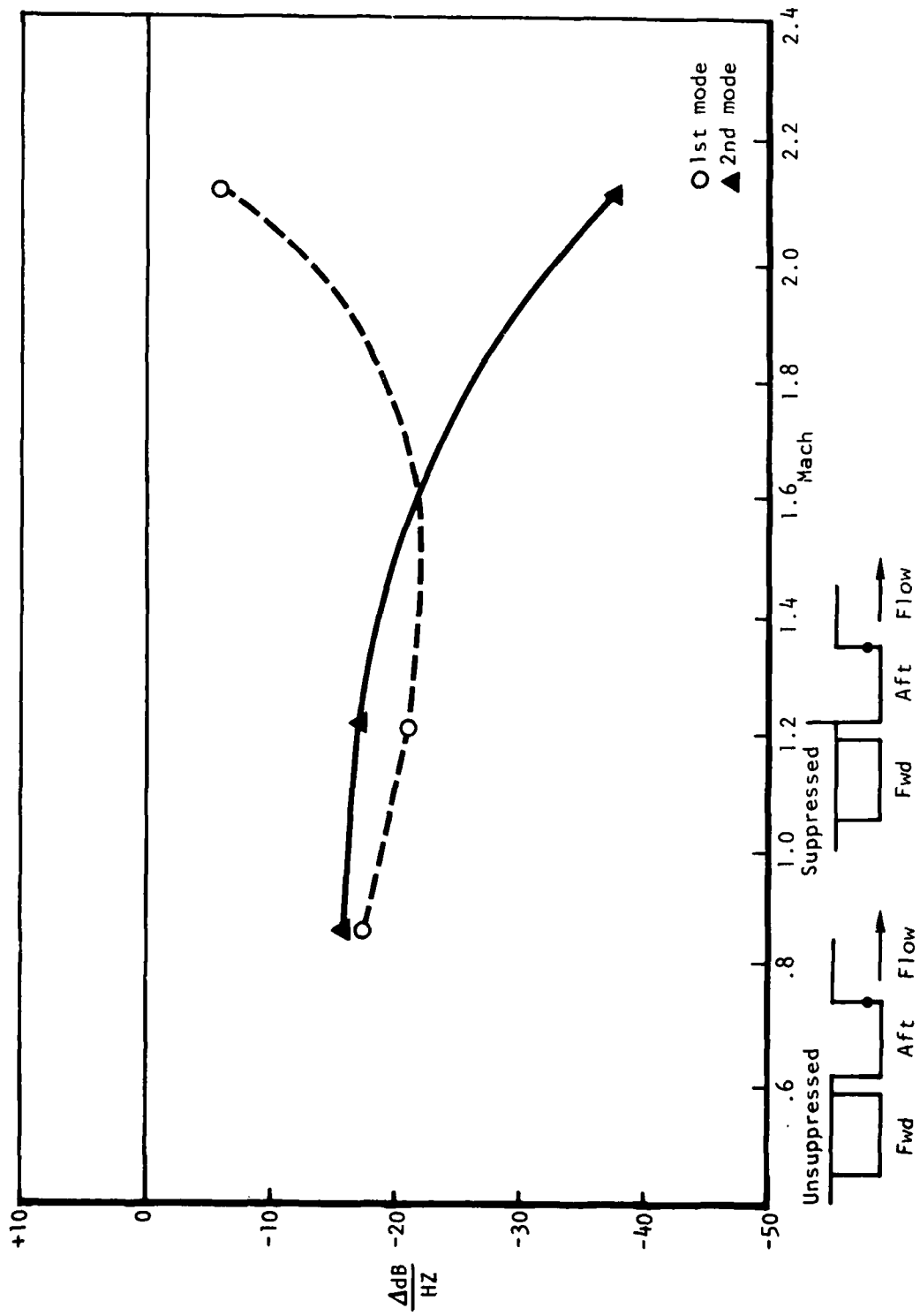
Figure 66. 0.1-Scale Model Data, 90° Solid Spoiler versus Unsuppressed,
Full Open, Aft Bulkhead Upper, Q = 500 psf

75
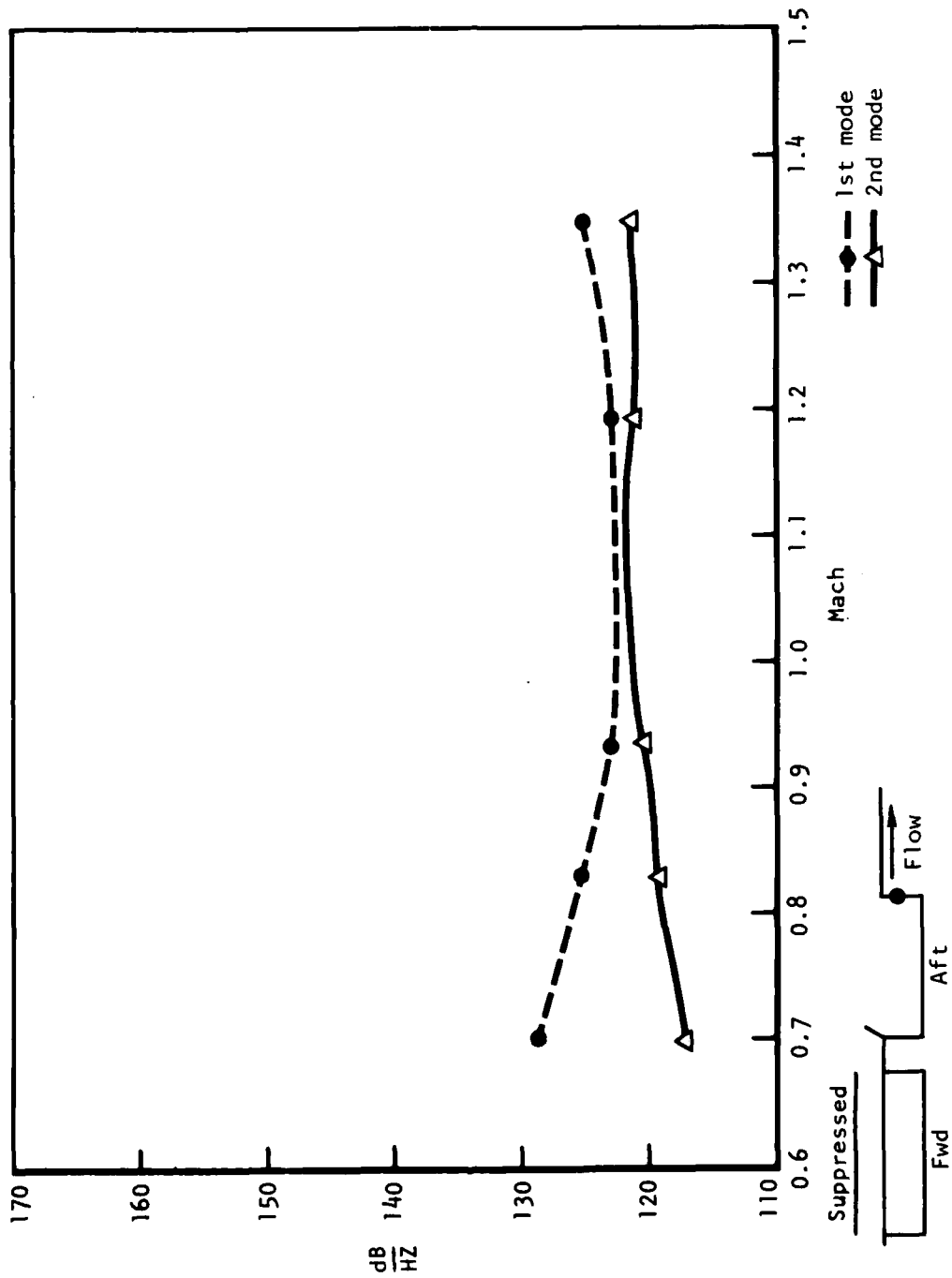
Figure 67. B-1 Full-Scale Flight Data, 70° Porous Spoiler, Aft Bulkhead Upper, Inboard Part Open, Q = 500 psf
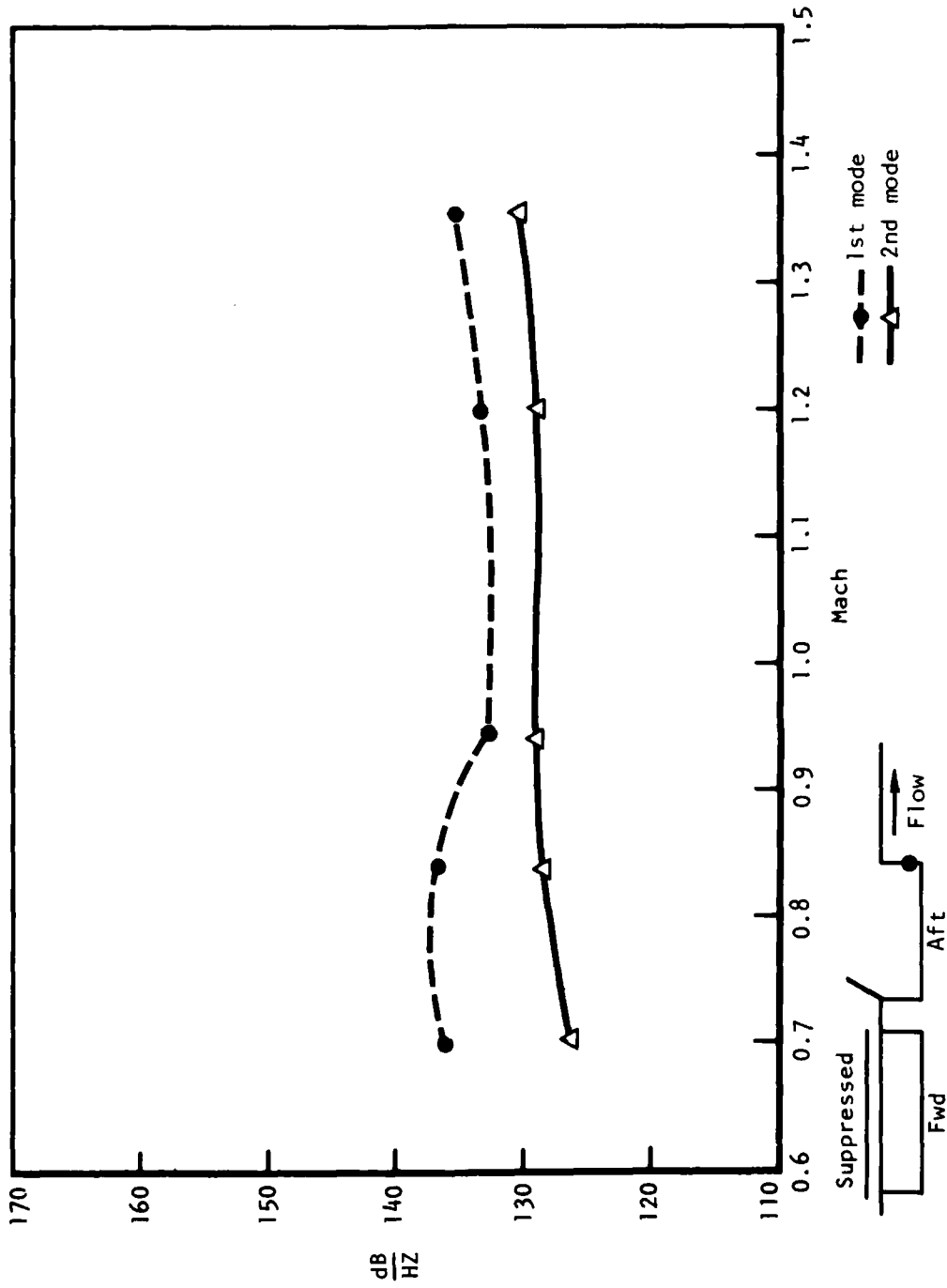
Figure 68. B-1 Full-Scale Flight Data, 70° Porous Spoiler, Aft Bulkhead Upper Inboard Full-Open, Q = 500 psf
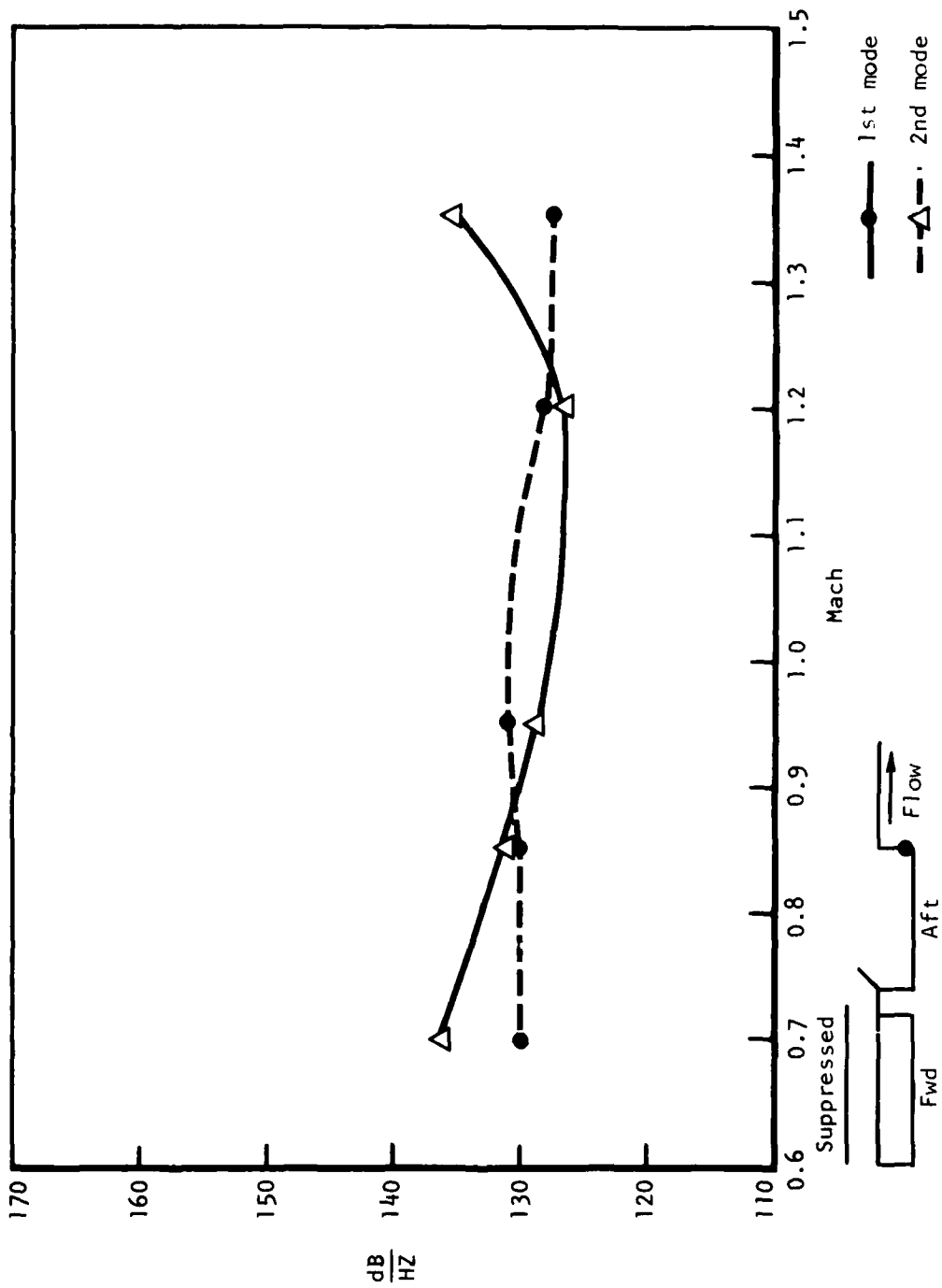
Figure 69. B-1 Full-Scale Flight Data, 70° Porous Spoiler, Aft Bulkhead Upper,
Outboard Part-Open, Q = 500 psf
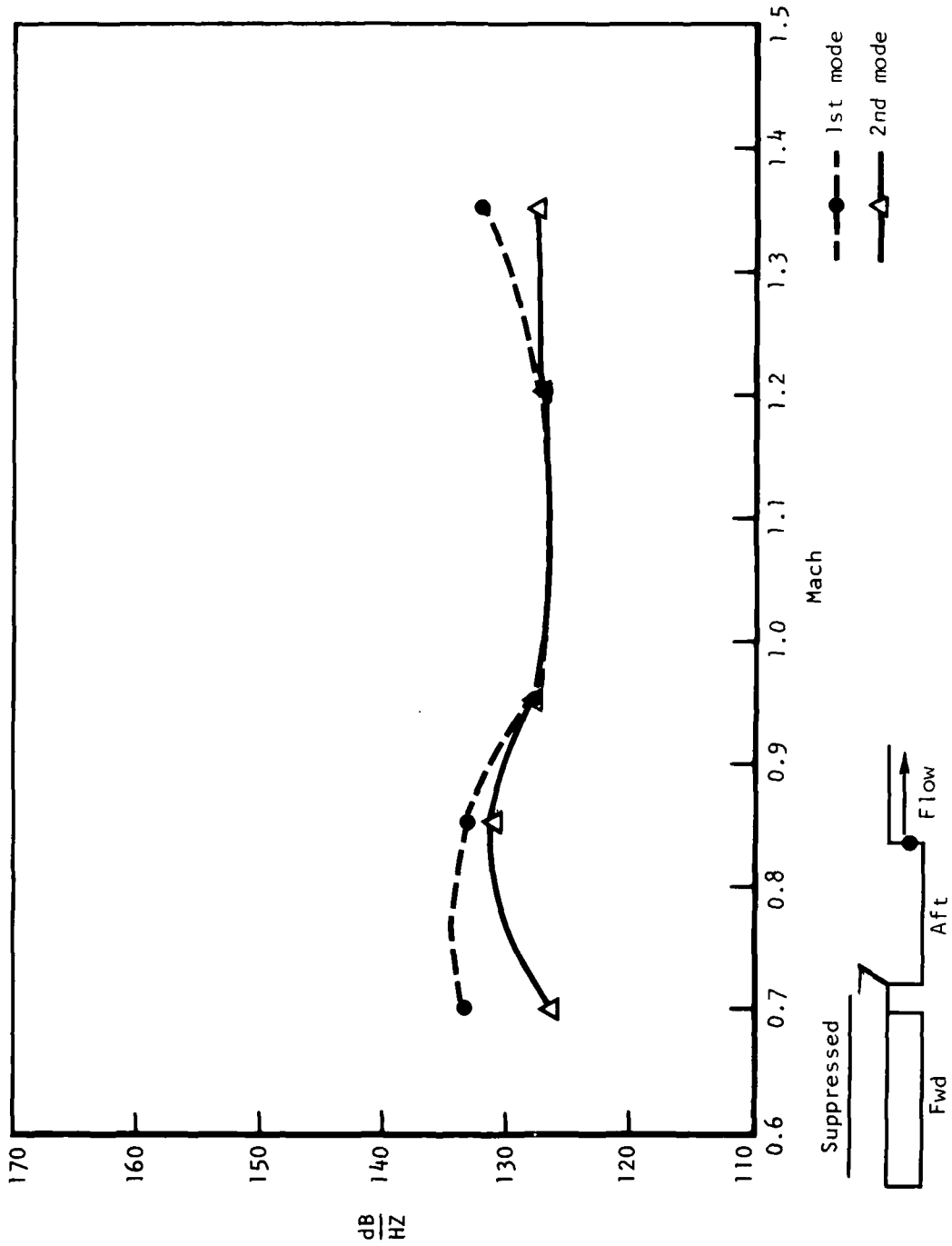
Figure 70. B-1 Full-Scale Flight Data, 70° Porous Spoiler, Aft Bulkhead Upper, Outboard Full-Open, Q = 500 psf
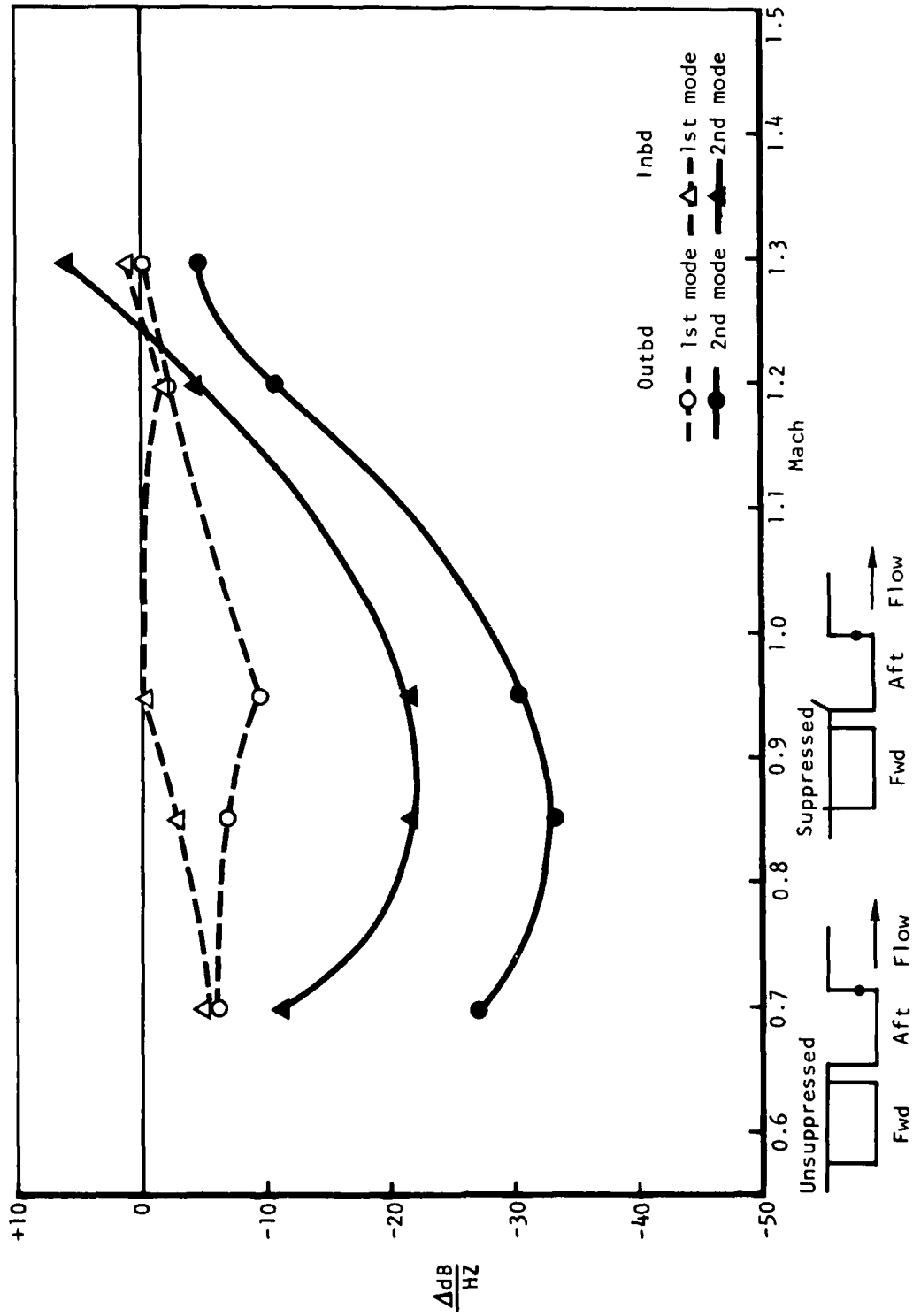
Figure 71. B-1 Full-Scale Flight Data, 70° Porous Spoiler versus Unsuppressed, Part Open, Aft Bulkhead Upper, Q = 500 psf
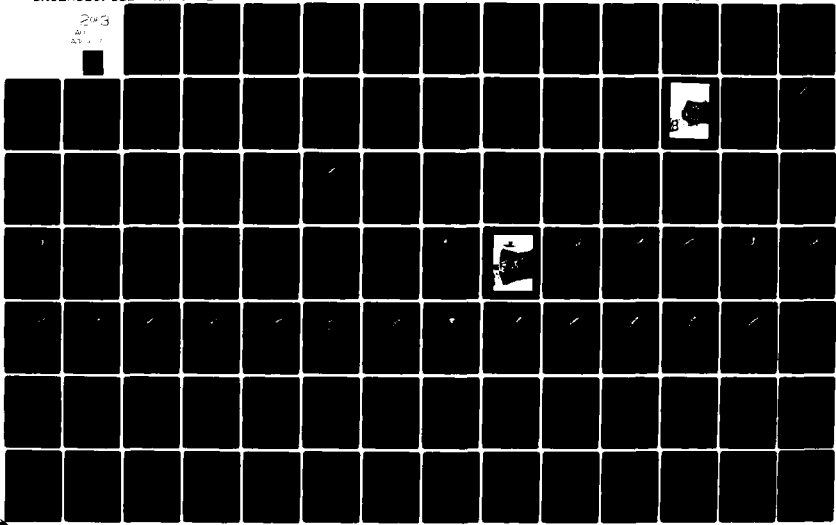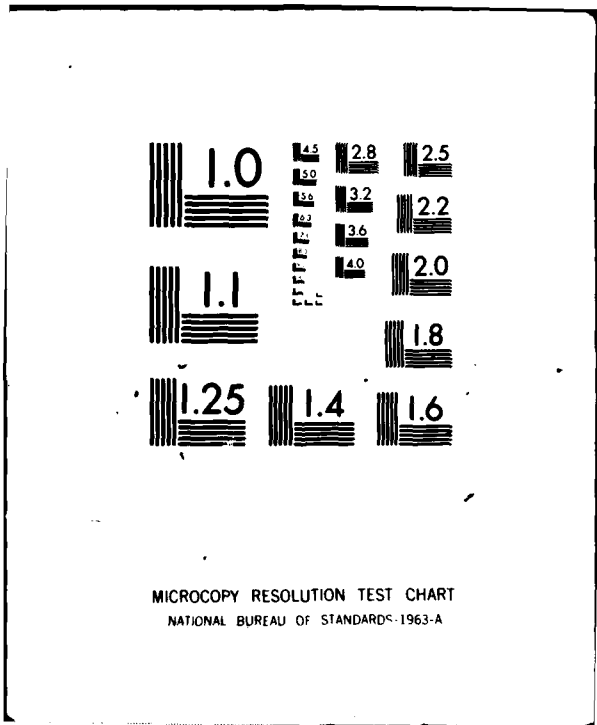
MICROCOPY RESOLUTION TEST CHART

NATIONAL BUREAU OF STANDARDS-1963-A
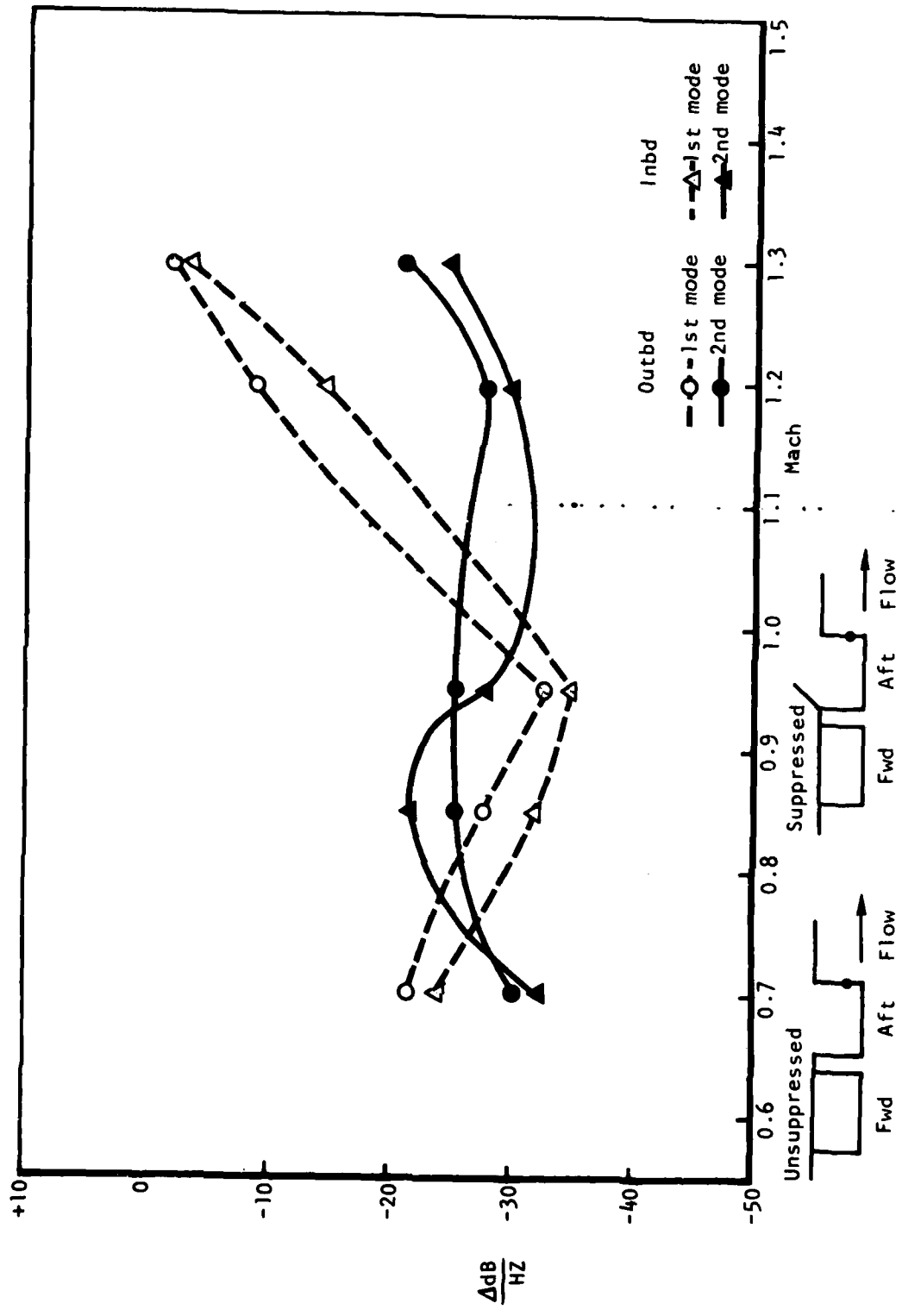
Figure 72. B-1 Full-Scale Flight Data, 70° Porous Spoiler versus Unsuppressed, Aft Bulkhead Upper, Full-Open, Q = 500 psf
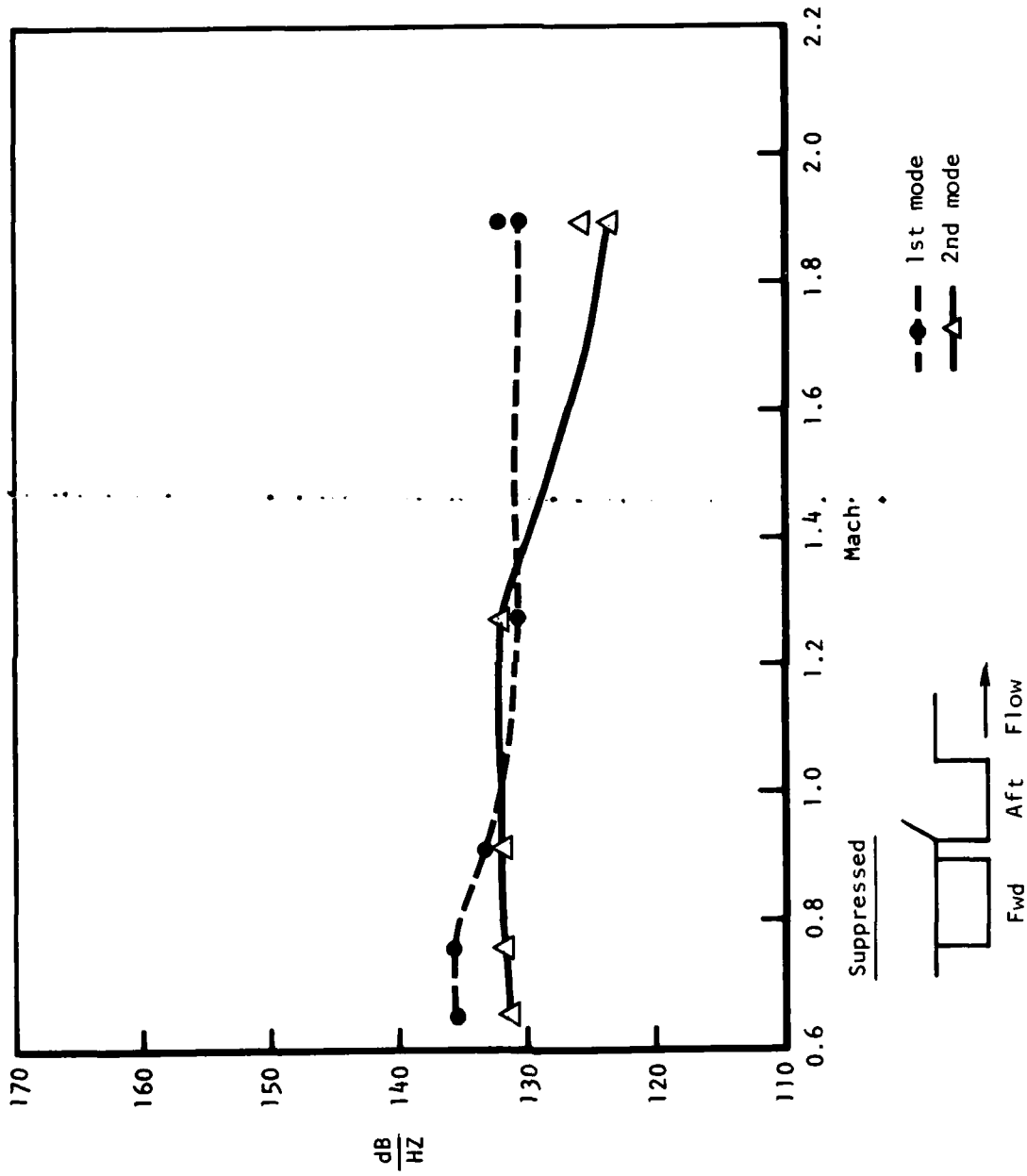
Figure 73. 0.1-Scale Model Data, 70° Solid Inboard Spoiler, Part Open, Aft Bulkhead Upper, Q = 500 psf
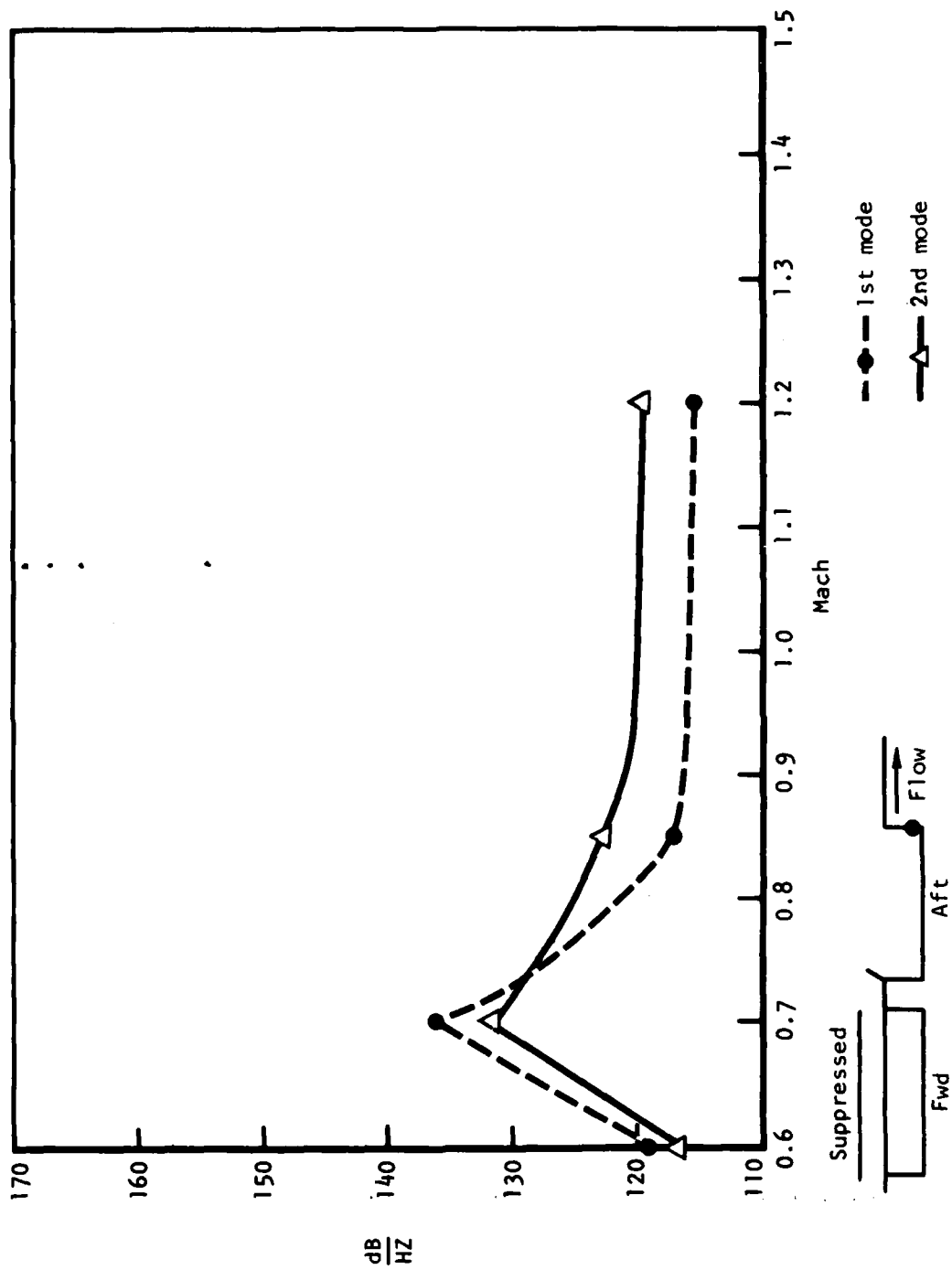
Figure 74. 0.1-Scale Model Data, 70° Solid Inboard Spoiler, Full-Open, Aft Bulkhead Upper, Q = 500 psf

83
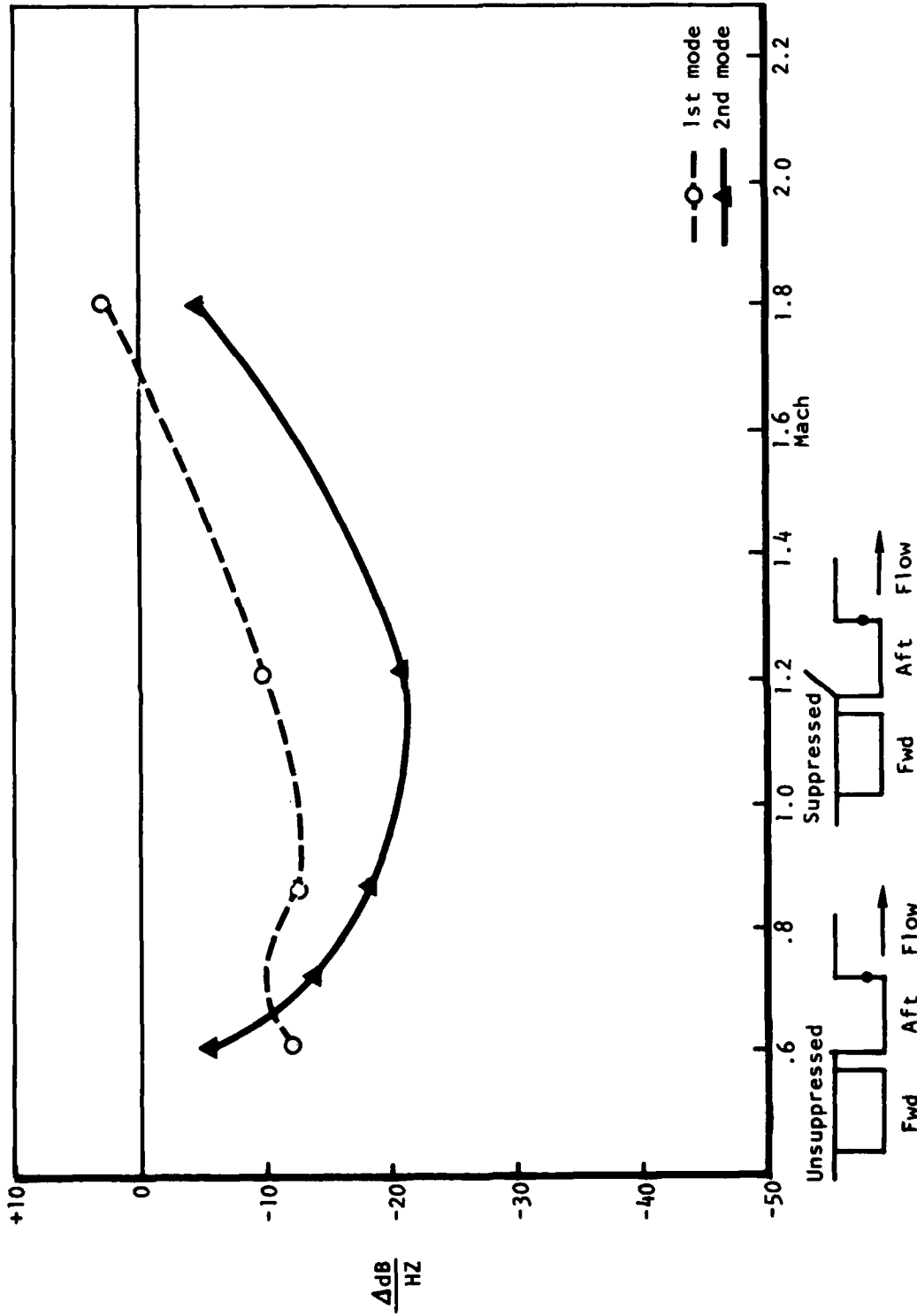
Figure 75. 0.1-Scale Model Data, 70° Solid Inboard Spoiler Versus Unsuppressed, Part Open, Aft Bulkhead Upper, Q = 500 psf
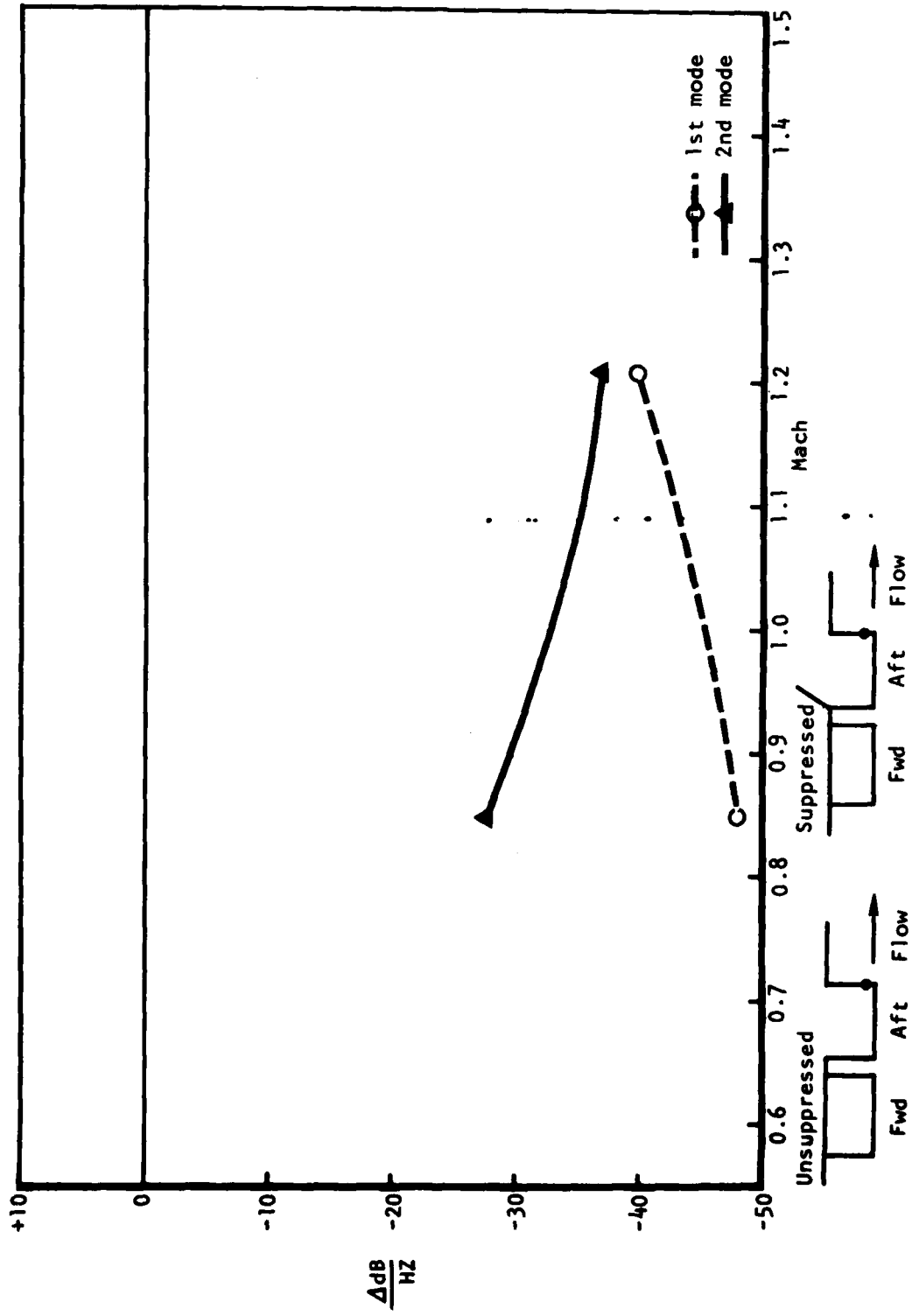
Figure 76. 0.1-Scale Model Data, 70° Solid Inboard Spoiler Versus Unsuppressed, Full Open, Aft Bulkhead Upper, Q = 500 psf
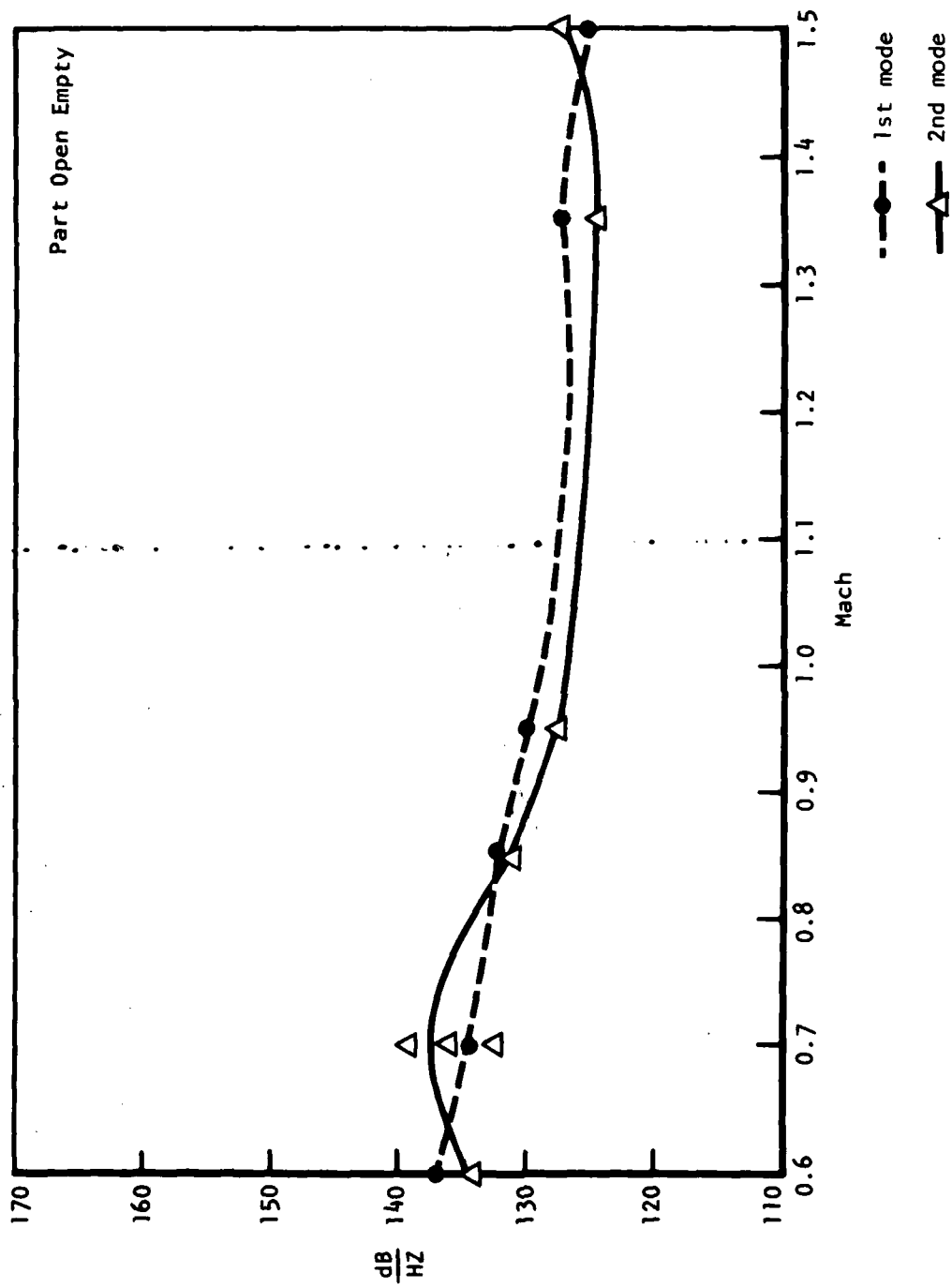
Figure 77. B-1 Aft Bulkhead Upper, 70° Solid Outboard Spoilers, Q = 500 psf

86
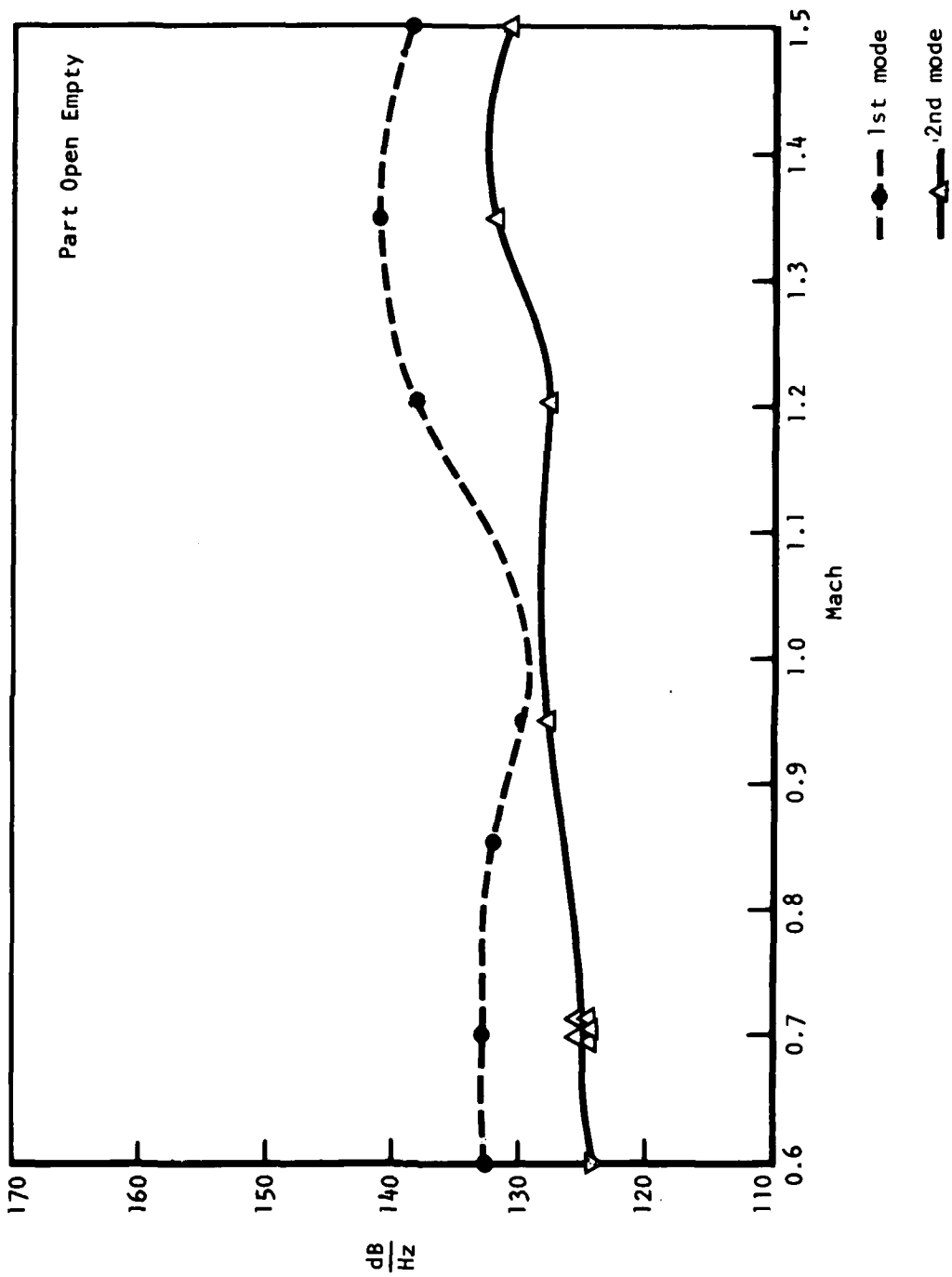
Figure 78. B-1 Aft Bulkhead Upper, 70° Solid Inboard Spoiler, Q = 500 psf
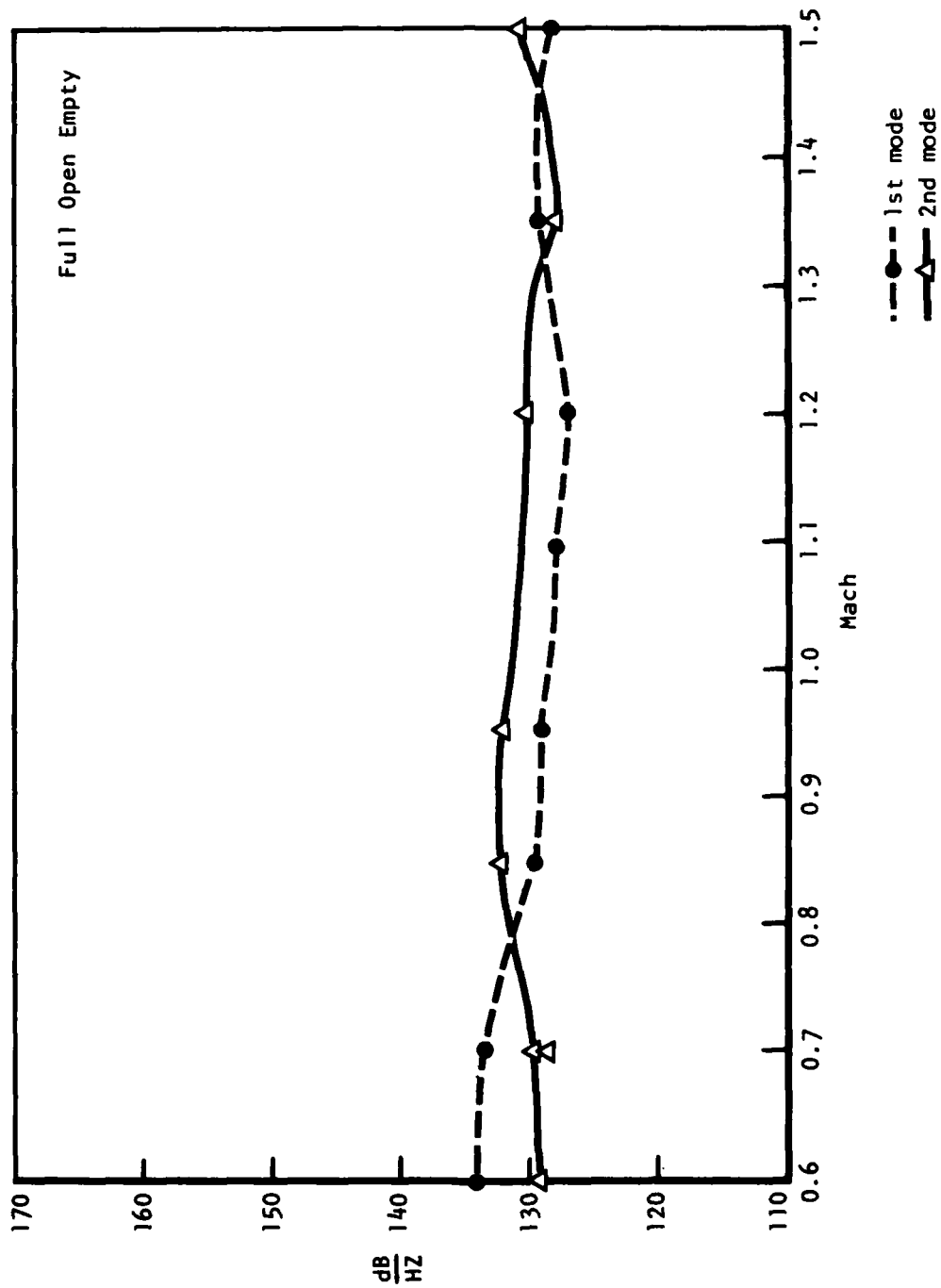
Figure 79. B-1 Aft Bulkhead Upper, 70° Solid Outboard Spoilers, Q = 500 psf
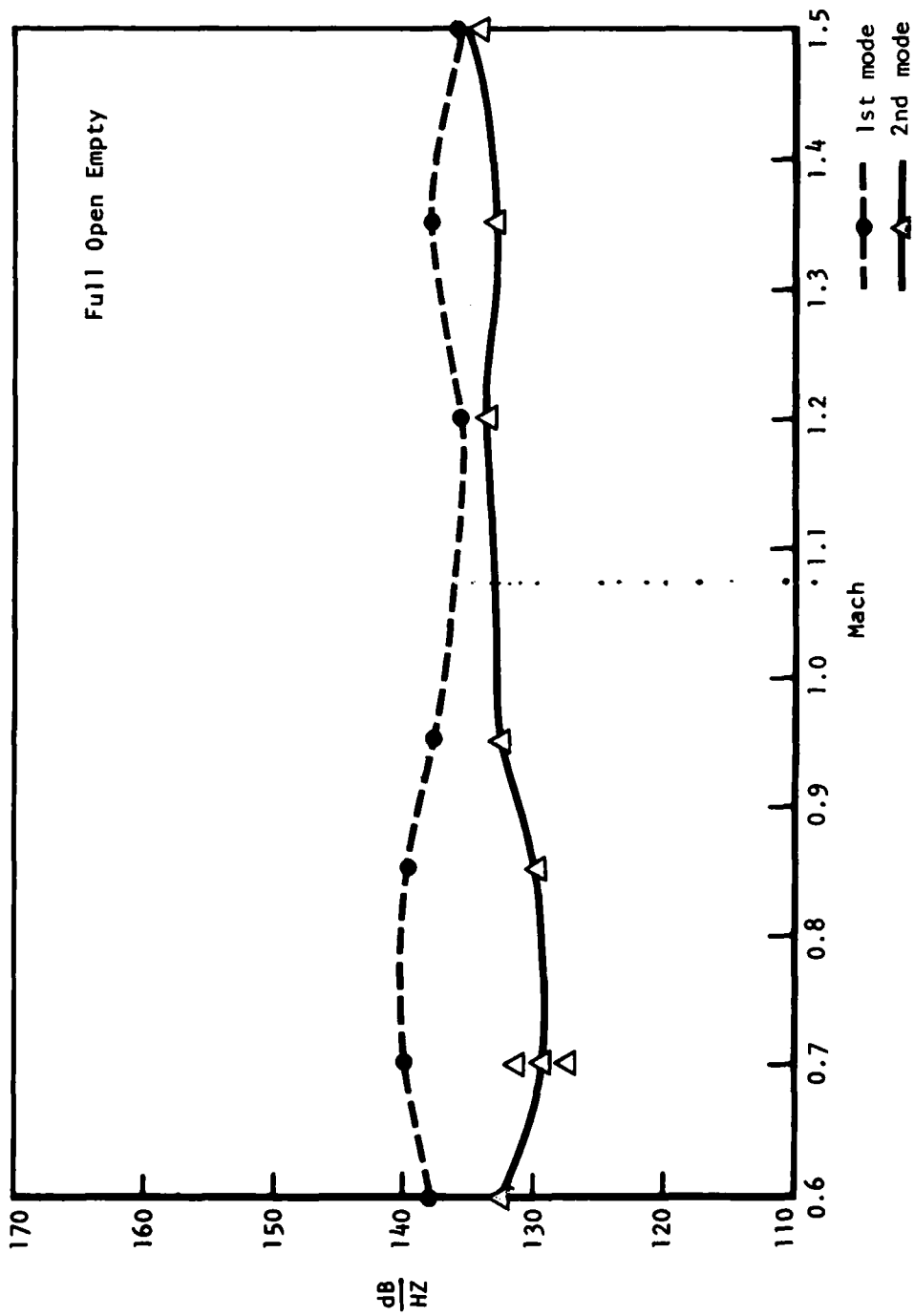
Figure 80. B-1 Aft Bulkhead Upper, 70° Solid Inboard Spoilers, Q = 500 psf
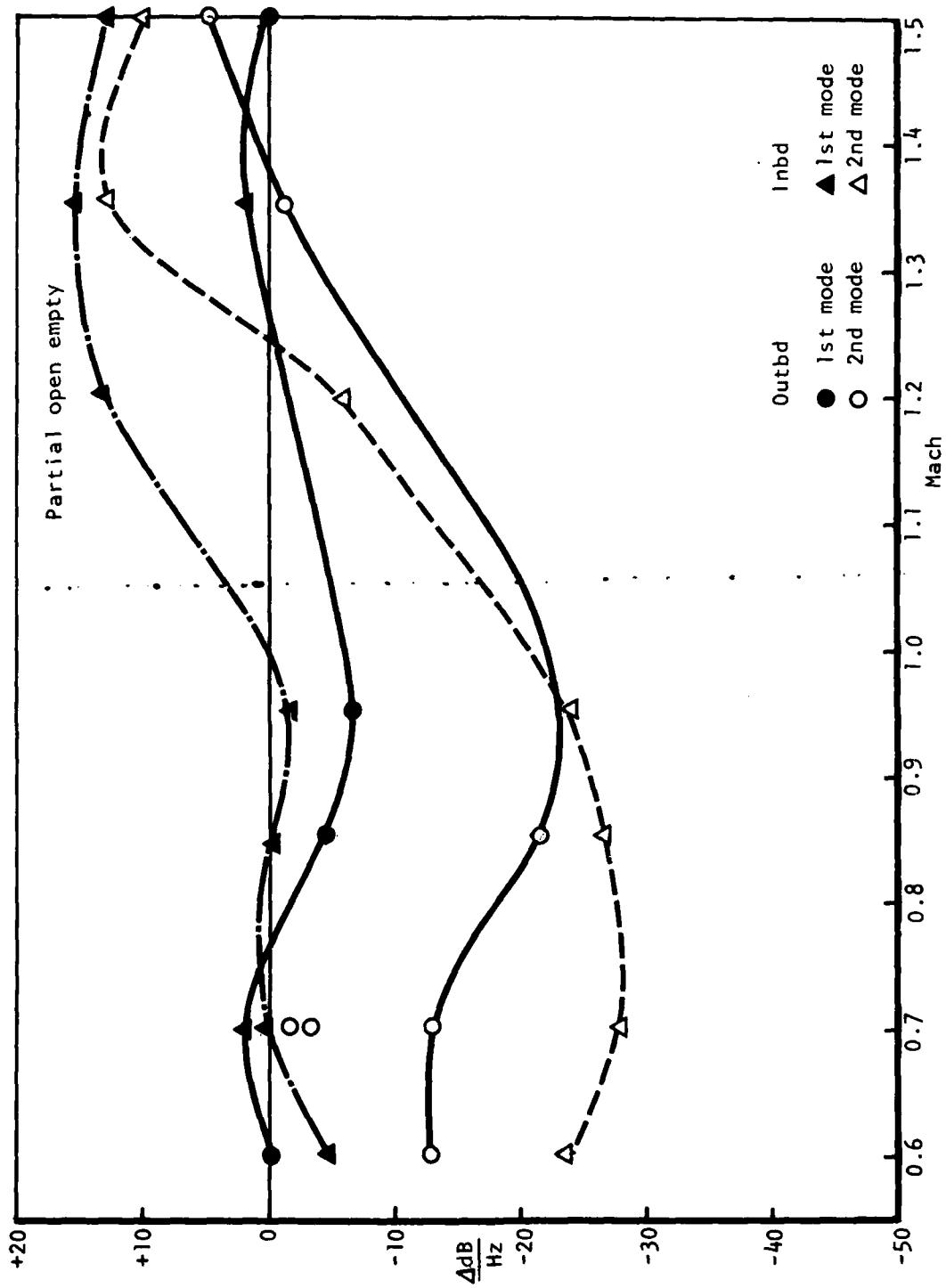
Figure 81. B-1 Full-Scale, 70° Solid Spoiler Versus Unsuppressed
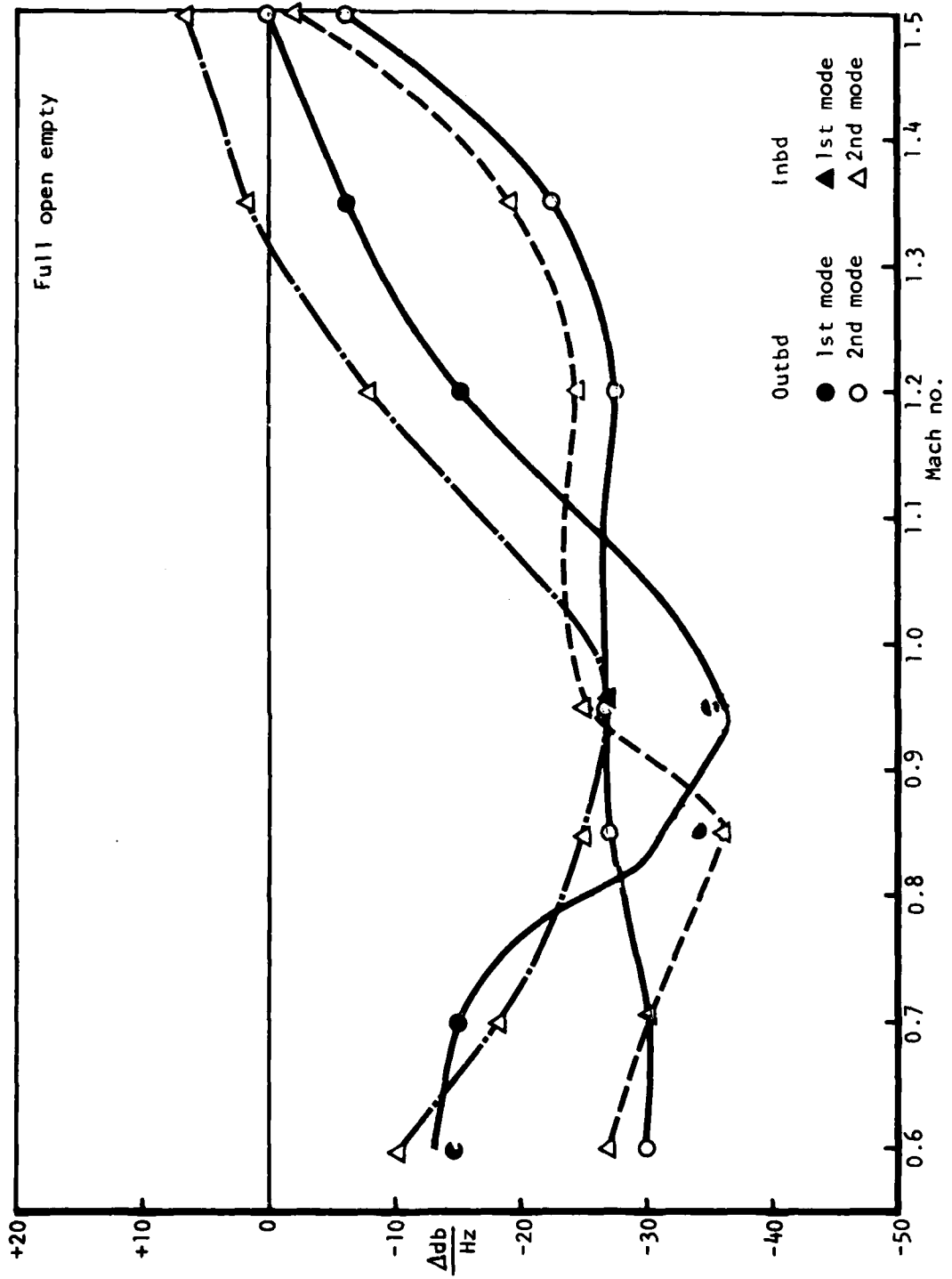
Figure 82. B-1 Full-Scale, 70° Solid Spoiler Versus Unsuppressed

91

for cavities with less intense resonant pressures. In fact, the B-1 data indicate that spoilers may actually increase the noise level for cavities with low initial noise levels as shown in Figure 85. The magnitude of the noise levels in the full-scale B-1 weapon bay cavities at supersonic speeds is considerably lower than for subsonic speeds, and would not require attenuation. Additional test data would be required to define spoiler operation at supersonic speeds, but it appears that the spoiler could simply be retracted at supersonic speeds.

Noise level data for a solid 90-degree spoiler are shown in Figures 63 through 66 for the 0.10-scale model. The noise levels of the porous and solid spoilers appear approximately the same.

Noise levels for a 70-degree porous spoiler are shown in Figures 67 through 72. The data trends are the same as for the 90-degree spoilers. At supersonic speeds, the noise level reduction of the spoilers is much less efficient than for subsonic speeds, where the unsuppressed cavity noise levels are the highest. In general, the inboard spoiler configuration resulted in greater noise reduction than the outboard configuration. The noise reduction of the inboard 70-degree porous spoilers was comparable to the 90-degree porous spoilers.

The cavity noise data for the 70-degree solid spoilers are shown in Figures 73 through 82. The 70-degree solid spoilers appears less effective in reducing noise than the 70-degree porous spoiler. The same trend of reduced spoiler noise reduction occurs at supersonic speeds as for the other spoilers tested on the full-scale aircraft.

A summary of the cavity noise levels for the various suppression devices discussed in the preceding paragraphs is shown in Figures 83 through 93. The overall noise levels are normalized to dynamic pressure and plotted as a function of mach number. The noise levels of an unsuppressed cavity are shown for reference in all data plots. In addition to the aforementioned aft upper bulkhead position, the lower aft and forward upper bulkhead locations are shown for comparison. Model and full-scale data are shown for correlation.

The data trends in the summary plots for the aft lower, aft upper, and forward upper bulkhead positions were similar to those discussed previously for the aft upper bulkhead position. The full-scale data showed appreciable noise level reduction at subsonic speeds and little, if any, at supersonic speeds. The model data showed appreciable noise reduction for subsonic and supersonic speeds. The normalized noise level of the various spoiler configurations was surprisingly similar in magnitude, considering the scatter in cavity noise data. The overall noise level ratio to dynamic pressure was reduced to a factor of approximately of 0.05 for the majority of data points.

CAVITIES WITH INTERNAL STORES

Cavity noise was recorded with several internal store configurations and plotted relative to empty cavities to illustrate the effects of stores on open-cavity noise. The cavity store configurations ranged from a full bay of eight stores to a single store at the drop position in the cavity opening. Data were recorded for the full-scale aircraft and the 0.10-scale model. A photograph of the full cavity load of eight stores is shown in Figure 94.
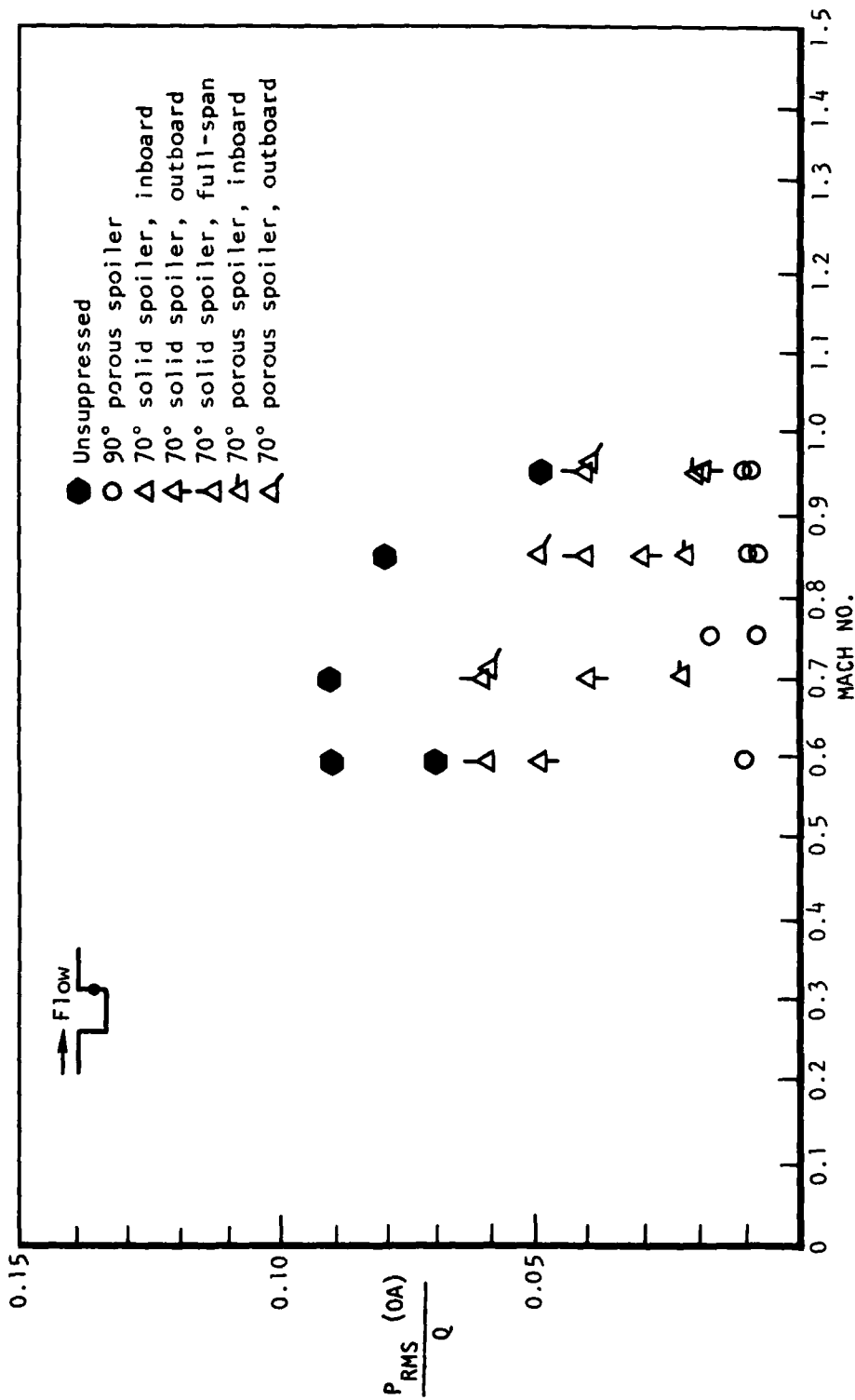
Figure 83. Cavity Noise Reduction, Full-Scale Flight Data, Lower Aft Bulkhead -
Part-Open, Unsuppressed Versus Suppressed
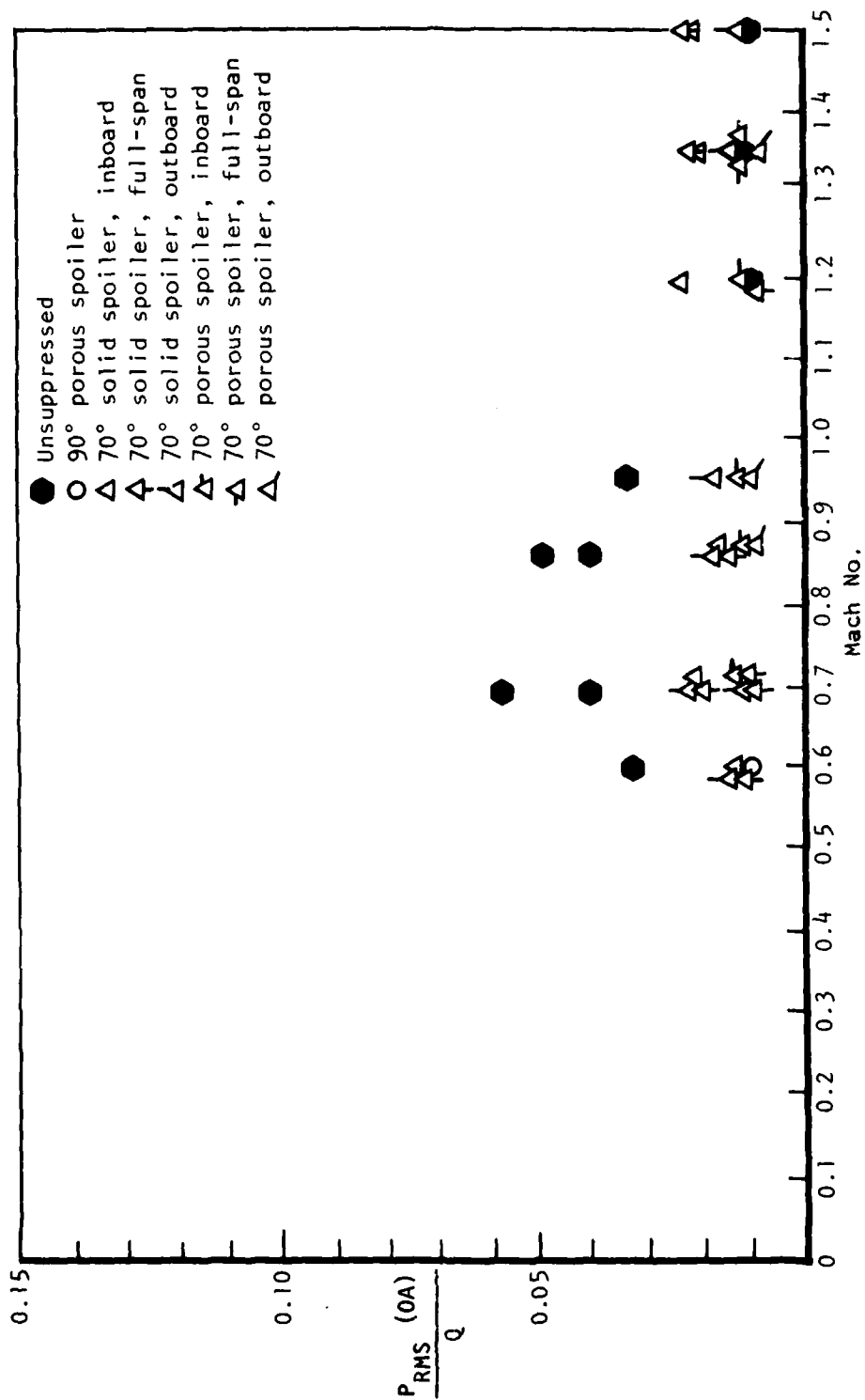
Figure 84. Cavity Noise Reduction, Full-Scale Flight Data, Upper Aft Bulkhead -
Part-Open, Unsuppressed Versus Suppressed

94
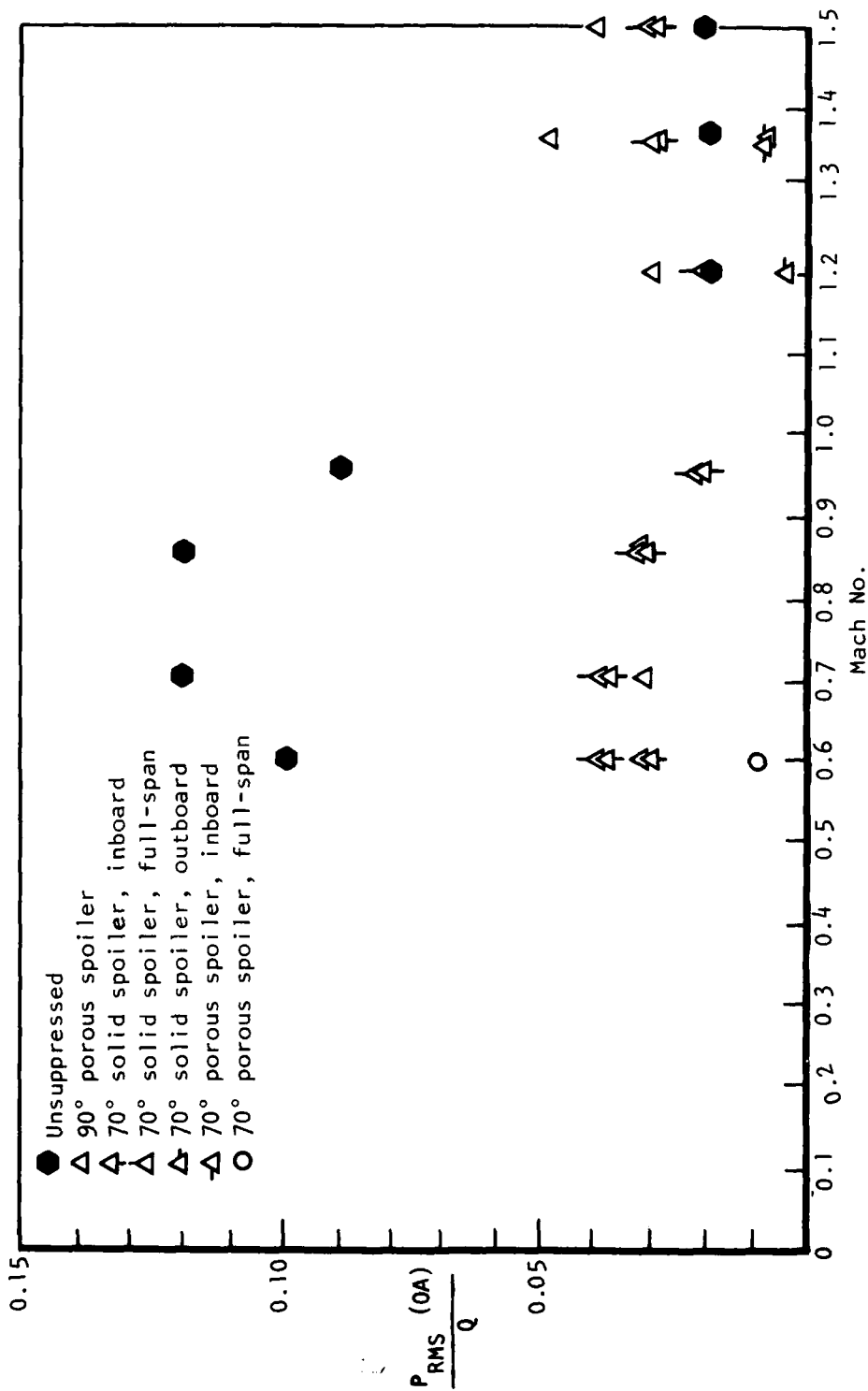
Figure 85. Cavity Noise Reduction, Full-Scale Flight Data, Upper Forward Bulkhead - Part-Open, Unsuppressed Versus Suppressed
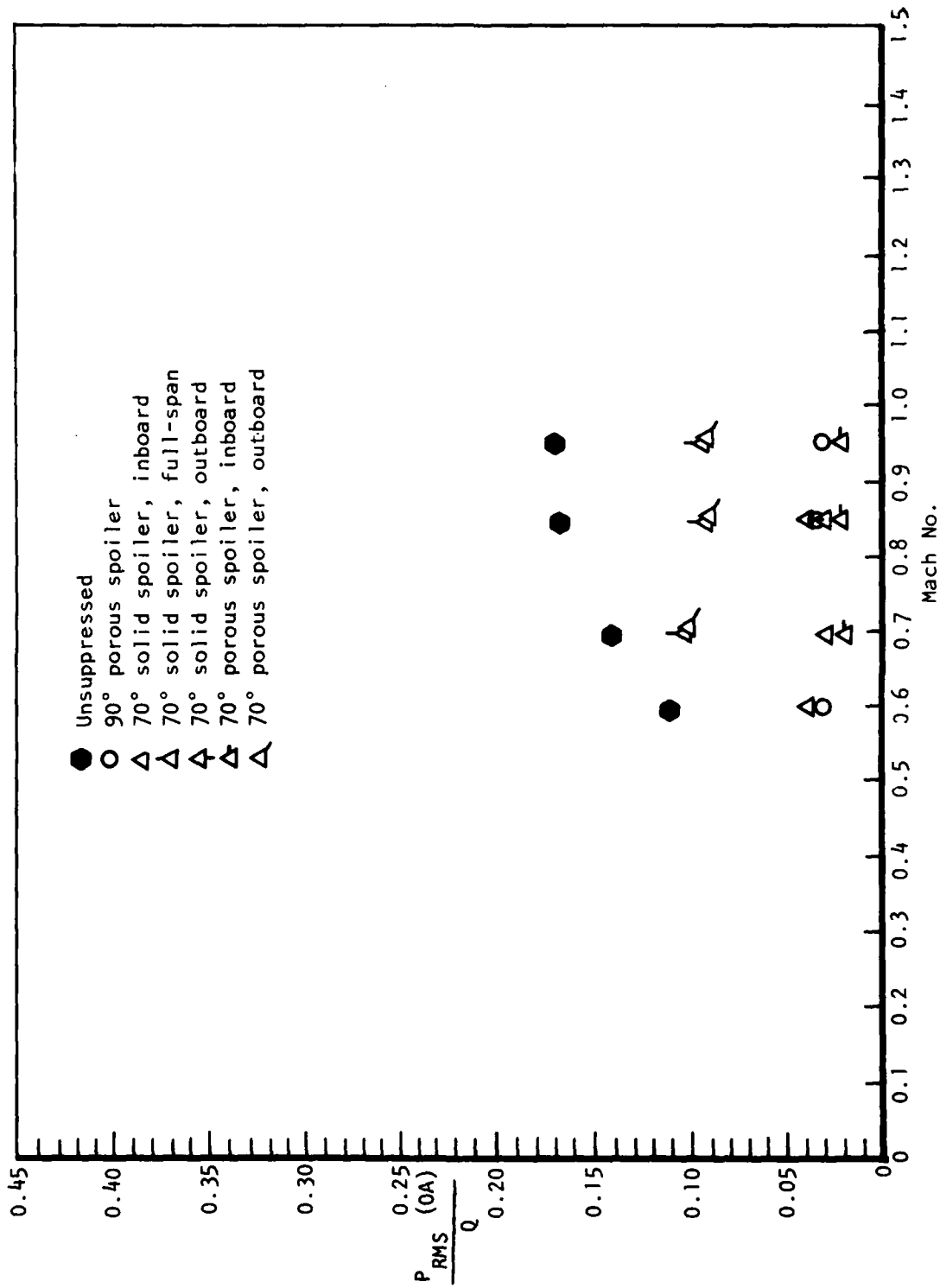
Figure 86. Cavity Noise Reduction, Full-Scale Flight Data, Lower Aft Bulkhead - Full-Open, Unsuppressed Versus Suppressed

Unsuppressed
○ 90° porous spoiler
◁ 70° solid spoiler, inboard
◁ 70° solid spoiler, full-span
◁ 70° solid spoiler, outboard
◁ 70° porous spoiler, inboard
◁ 70° porous spoiler, full-span
◁ 70° porous spoiler, outboard

$\frac{P_{RMS} (OA)}{Q}$

Mach No.
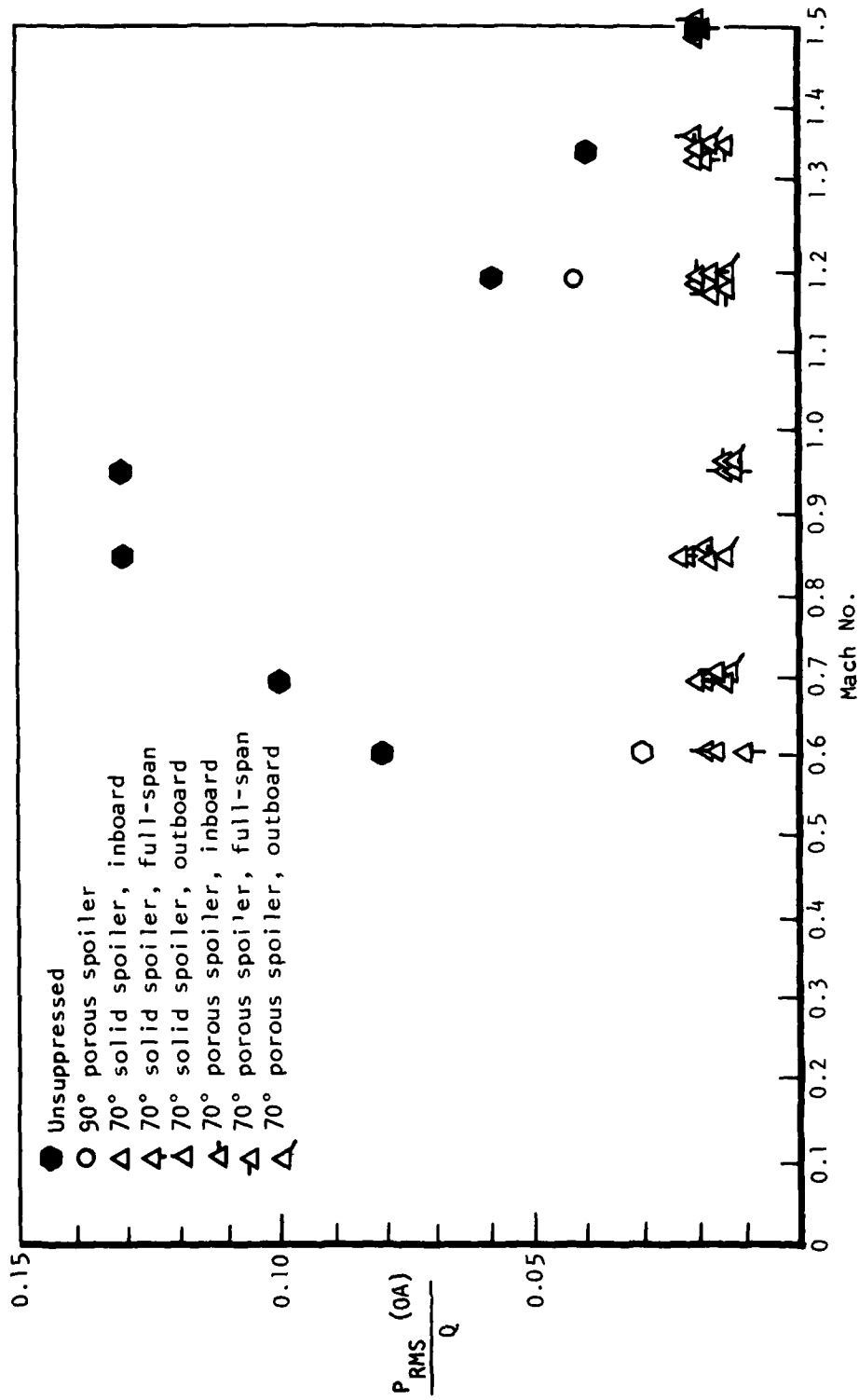
Figure 87. Cavity Noise Reduction, Full-Scale Flight Data, Upper Aft Bulkhead - Full-Open Unsuppressed Versus Suppressed
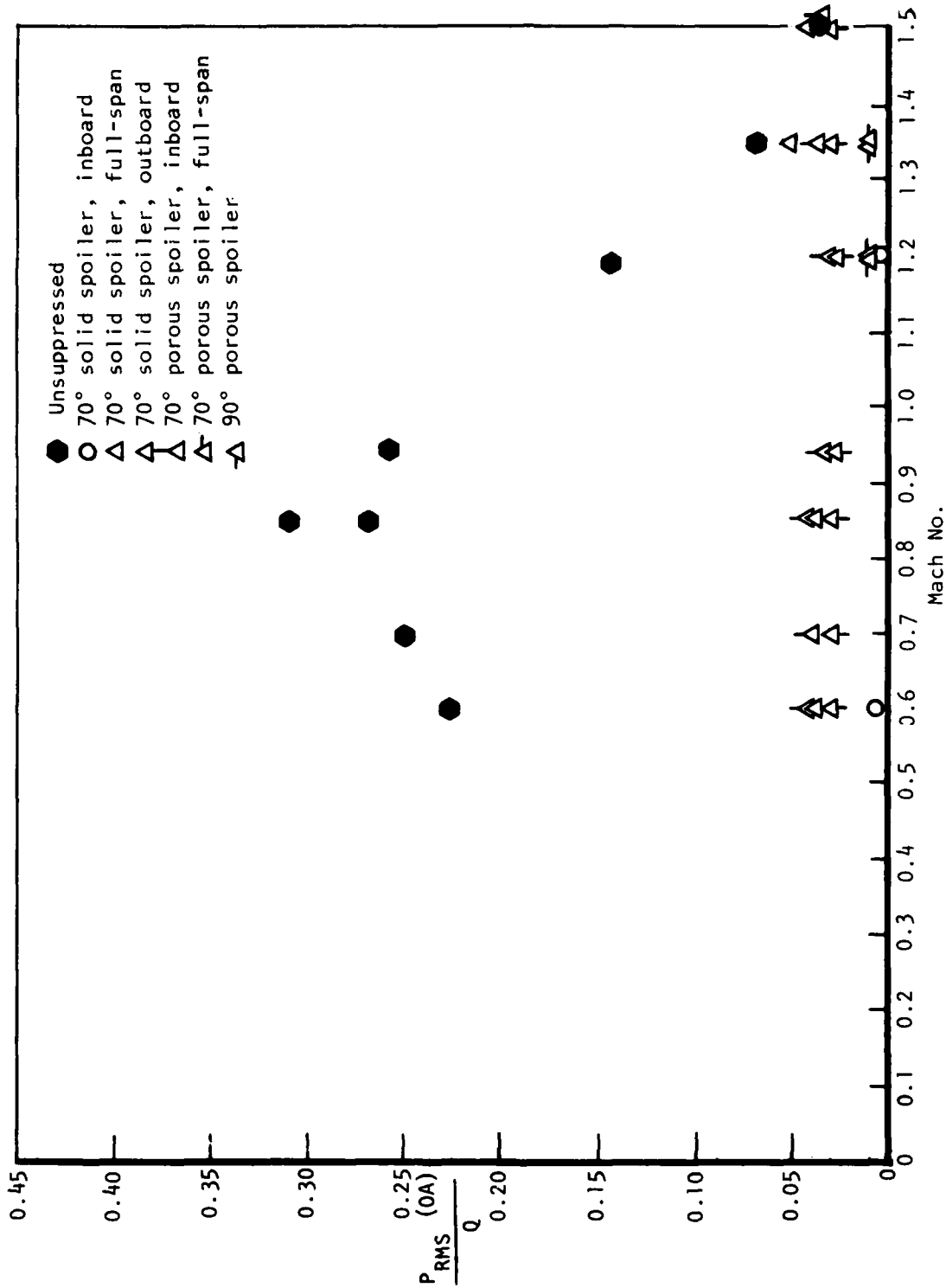
Figure 88. Cavity Noise Reduction, Full-Scale Flight Data, Upper Forward Bulkhead -
Full-Open Unsuppressed Versus Suppressed
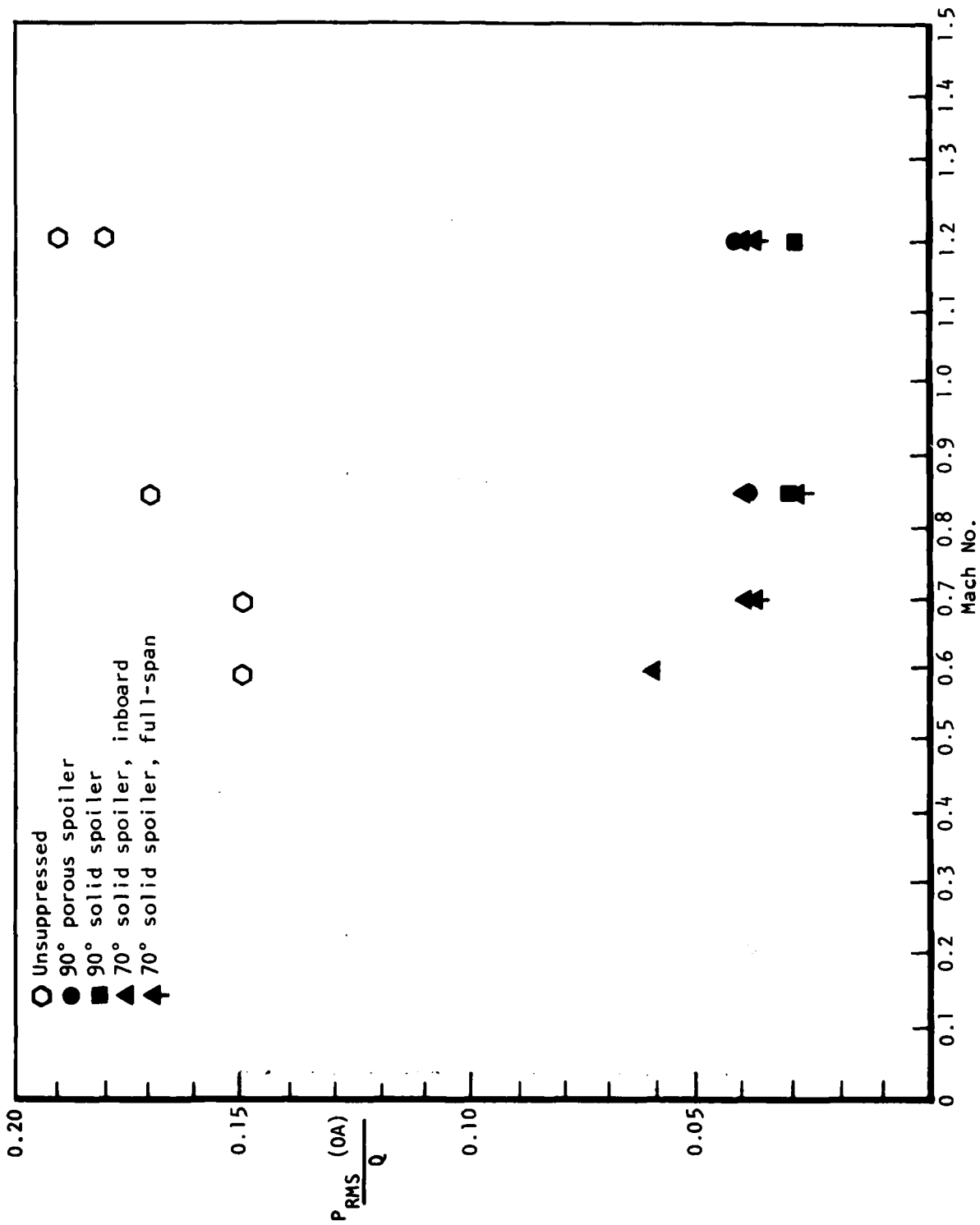
Figure 89. Cavity Noise Reduction, TWT 302, 0.1-Scale Model Data, Lower Aft Bulkhead - Part-Open

Legend:
○ Unsuppressed
● 90° porous spoiler
■ 90° solid spoiler
▲ 70° solid spoiler, inboard
◄ 70° solid spoiler, full-span

Y-axis: $\frac{P_{RMS} (OA)}{Q}$

X-axis: Mach No.
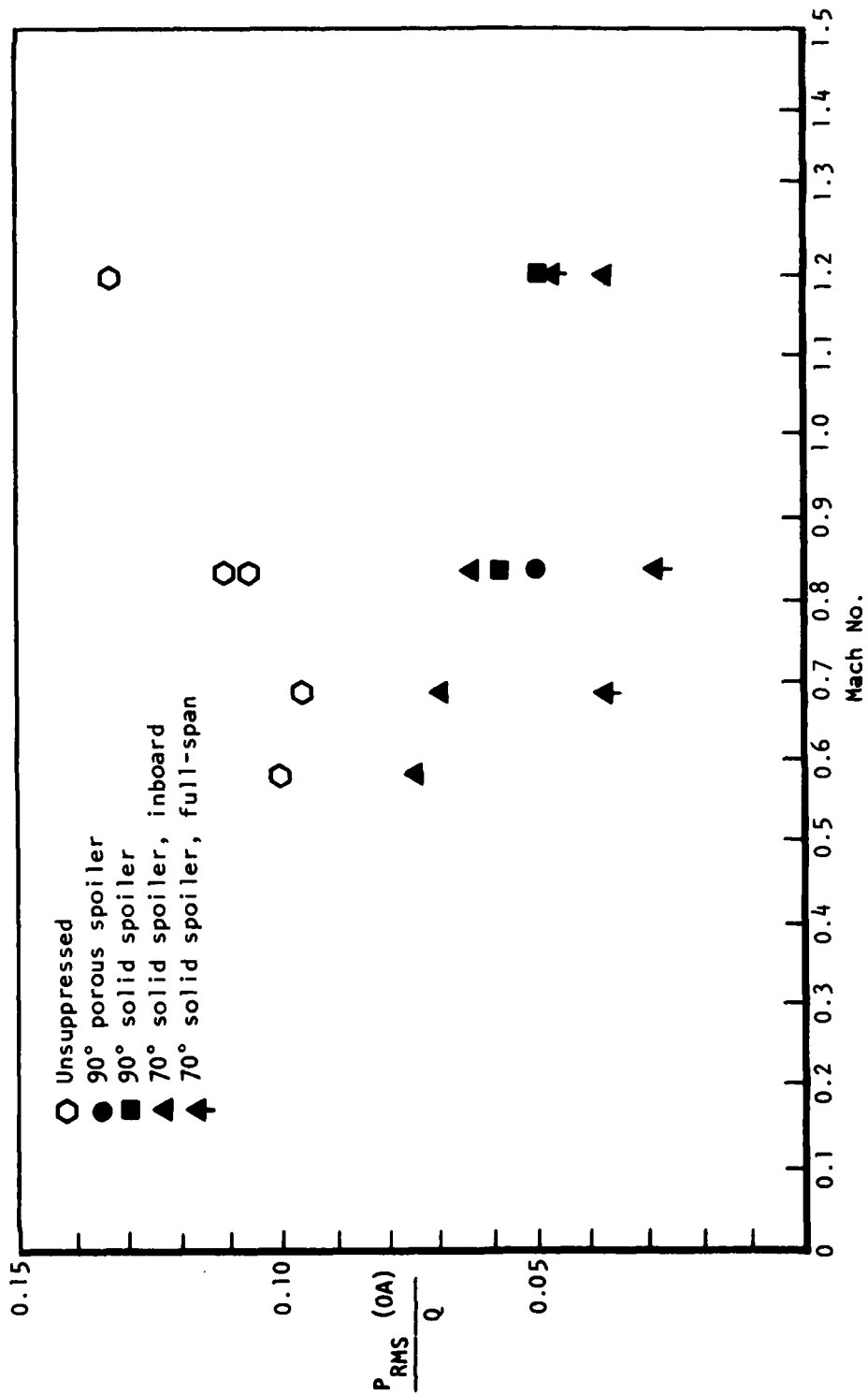
Figure 90. Cavity Noise Reduction, TWT 302, 0.1-Scale Model Data, Upper Forward Bulkhead-Part-Open

100
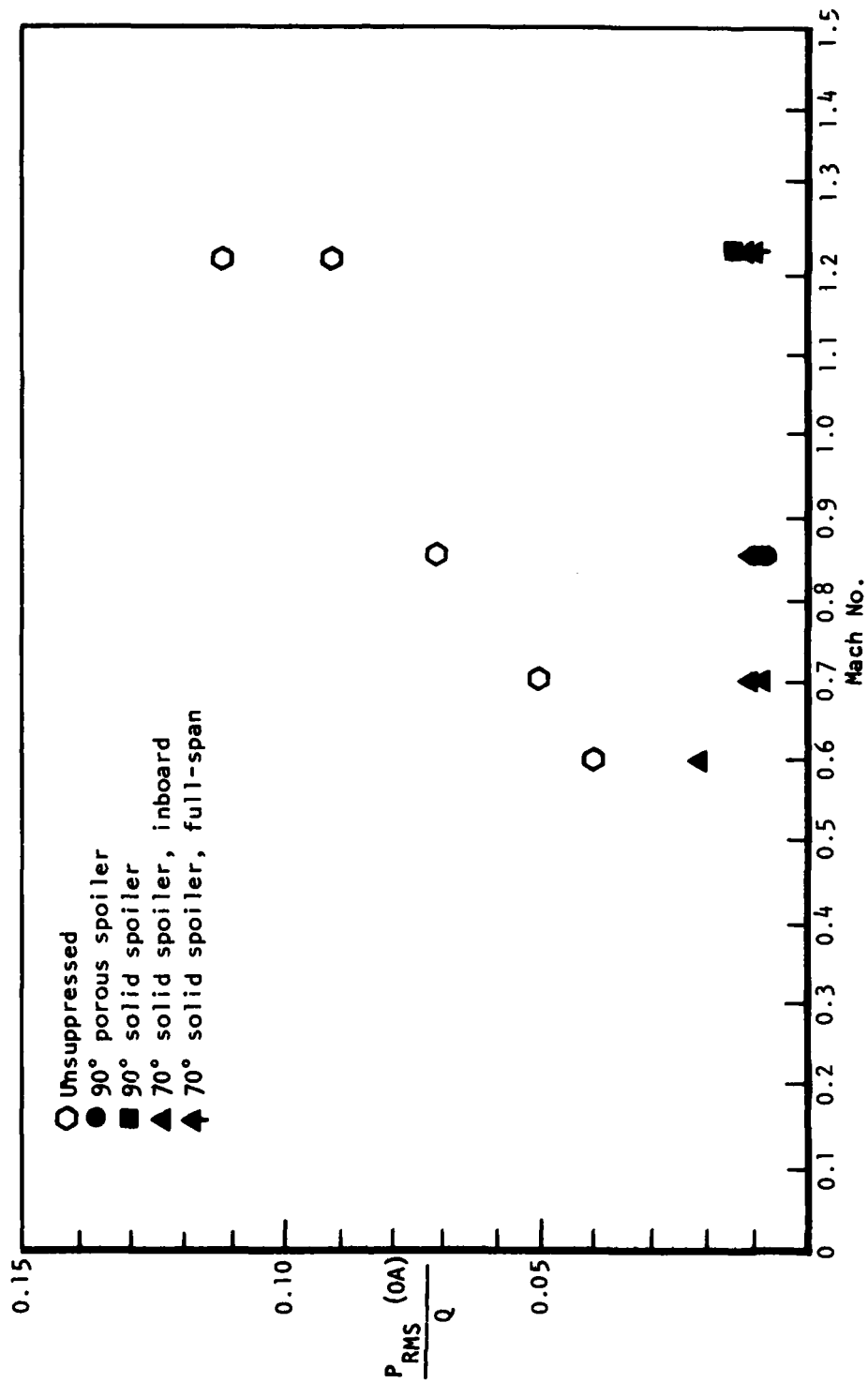
Figure 91. Cavity Noise Reduction, TWT 302, 0.1-Scale Model Data,
Upper Forward Bulkhead - Part-Open
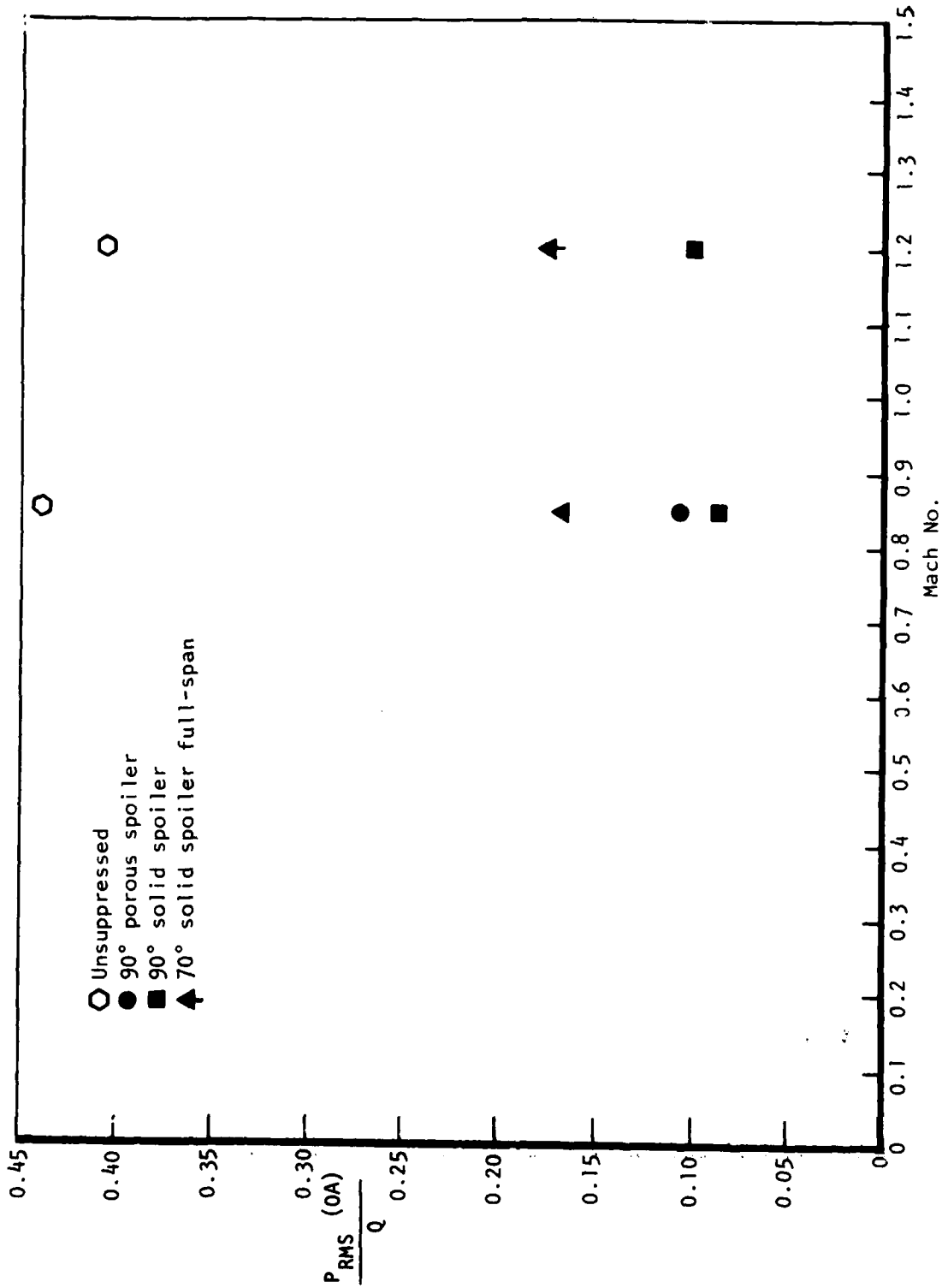
Figure 92. Cavity Noise Reduction TWT 302, 0.1-Scale Model Data
Lower Aft Bulkhead-Full-Open

P_RMS (OA) / Q axis: 0.45, 0.40, 0.35, 0.30, 0.25, 0.20, 0.15, 0.10, 0.05, 0

$$\frac{P_{RMS} \text{ (OA)}}{Q}$$

Mach No. axis: 0, 0.1, 0.2, 0.3, 0.4, 0.5, 0.6, 0.7, 0.8, 0.9, 1.0, 1.1, 1.2, 1.3, 1.4, 1.5

Mach No.

○ Unsuppressed
● 90° porous spoiler
■ 90° solid spoiler
◀ 70° solid spoiler, inboard
◀ 70° solid spoiler, full-span
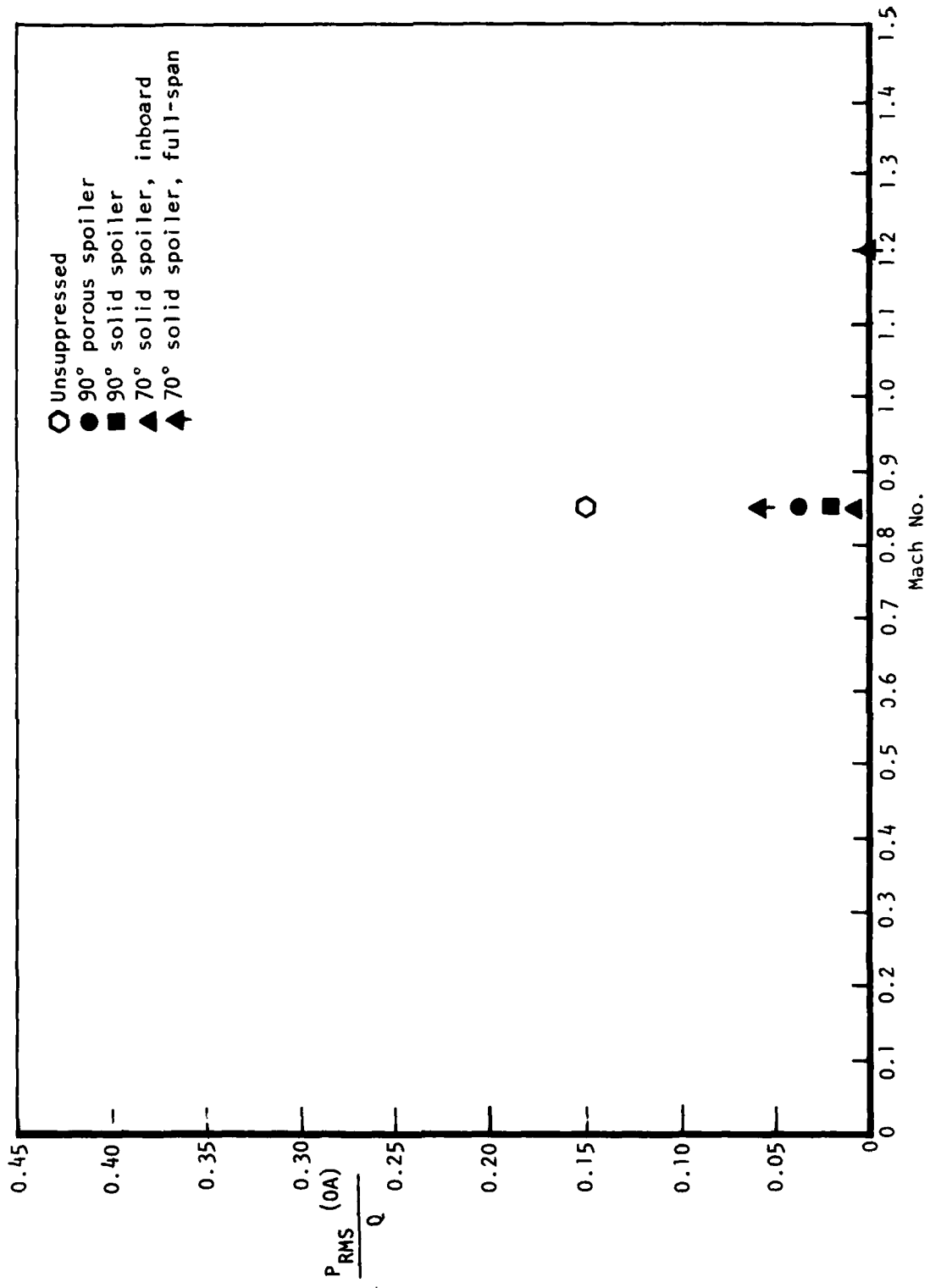
Figure 93. Cavity Noise Reduction. TWT 302, 0.1-Scale Model Data, Upper Forward Bulkhead Full-Open
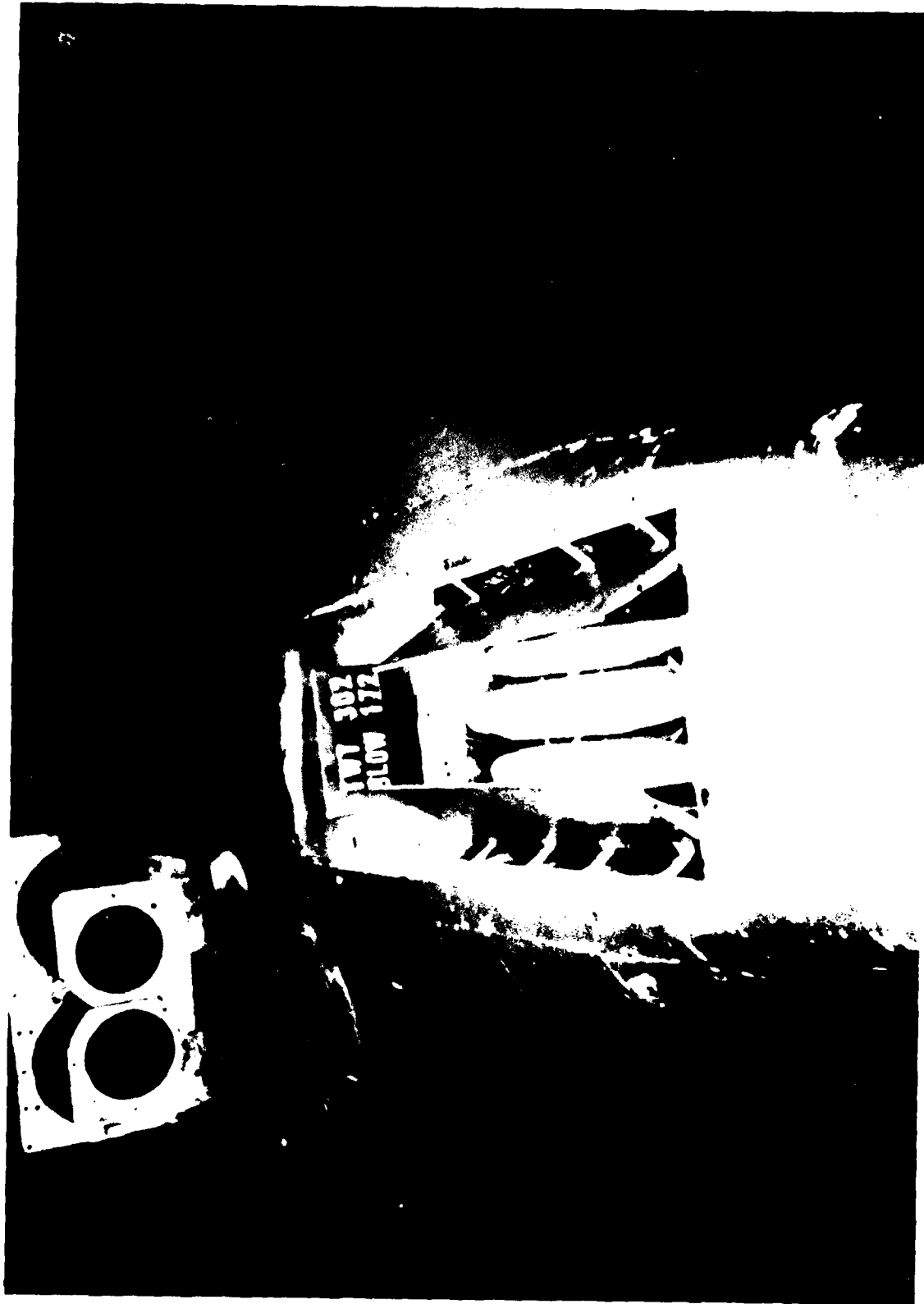
Figure 94. Unsuppressed Part Open 8 SRAMS

104

EIGHT-STORE CAVITY CONFIGURATION UNSUPPRESSED

The noise level data are shown in Figures 95 through 105 for the full-scale aircraft and the 0.10-scale wind tunnel model. The full-scale data show noise level reductions with eight SRAM's in the cavity relative to the empty cavity. A typical power spectral density plot is shown in Figure 95 for the full-scale, and in Figure 101 for the model data. The spectral density of the unsuppressed cavity noise levels with and without internal stores shows narrow-band cavity resonances superimposed on broadband random noise levels. The eight SRAM's inside the weapon bay cavity reduced the magnitude of the discrete cavity resonances, but on the average had little effect on the broadband noise levels. The full-scale data show about an order of magnitude reduction in the dominant cavity resonant frequency pressure level with a full load of eight internal stores. The model and full-scale data show that the second mode corresponding to 30 Hz for the full-scale and 300 Hz for the 0.10-scale model is the dominant cavity mode. The fundamental cavity resonant frequency which corresponds to 15 Hz full scale and 150 Hz for the model is excited at higher magnitudes for the 0.10-scale model than for the full-scale data. The model data in Figure 101 showed significant reduction for the fundamental cavity resonance with eight internal stores, but an increase for the second and most dominant mode. The model data on the average indicated greater attenuation of the random broadband noise than occurred for the full scale.

A summary of the overall cavity noise level is shown in Figures 96 through 100 for the full scale, and Figures 102 through 105 for the 0.10-scale model. In general, the presence of internal stores reduces the amplitude of the overall noise level in the cavity. The model data show less noise level reduction than the full-scale data. In some cases, the model showed slight increases in cavity noise level with the presence of internal stores.

Data with cavity noise suppression devices have been recorded with internal stores. In general, the presence of stores does not affect the noise levels inside cavities with noise suppressors.

THREE-STORE CAVITY CONFIGURATION

The data for three SRAM's in the upper portion of the cavity ceiling away from the doors are shown in Figures 108 through 110. The three-SRAM configuration represents approximately one-third of a full cavity store loading. The overall summary plots in Figures 106 through 109 show the effects of the stores for unsuppressed cavities and the 70-degree solid inboard spoiler for full- and part-open doors at two locations inside the cavity. The data are plotted relative to the empty cavity baseline configuration. The overall summary plots for part-open doors indicate a negligible effect on cavity noise level for the three stores configuration relative to the baseline empty cavity. The full-open door case, however, indicates increased noise levels with the three store configuration relative to empty cavity baseline configuration at supersonic speeds. The spectral density plot in Figure 110 is typical of the increased noise level at supersonic speeds due to the presence of the internal stores. For cavities with noise suppressors, the internal stores had no effect on new noise-level.
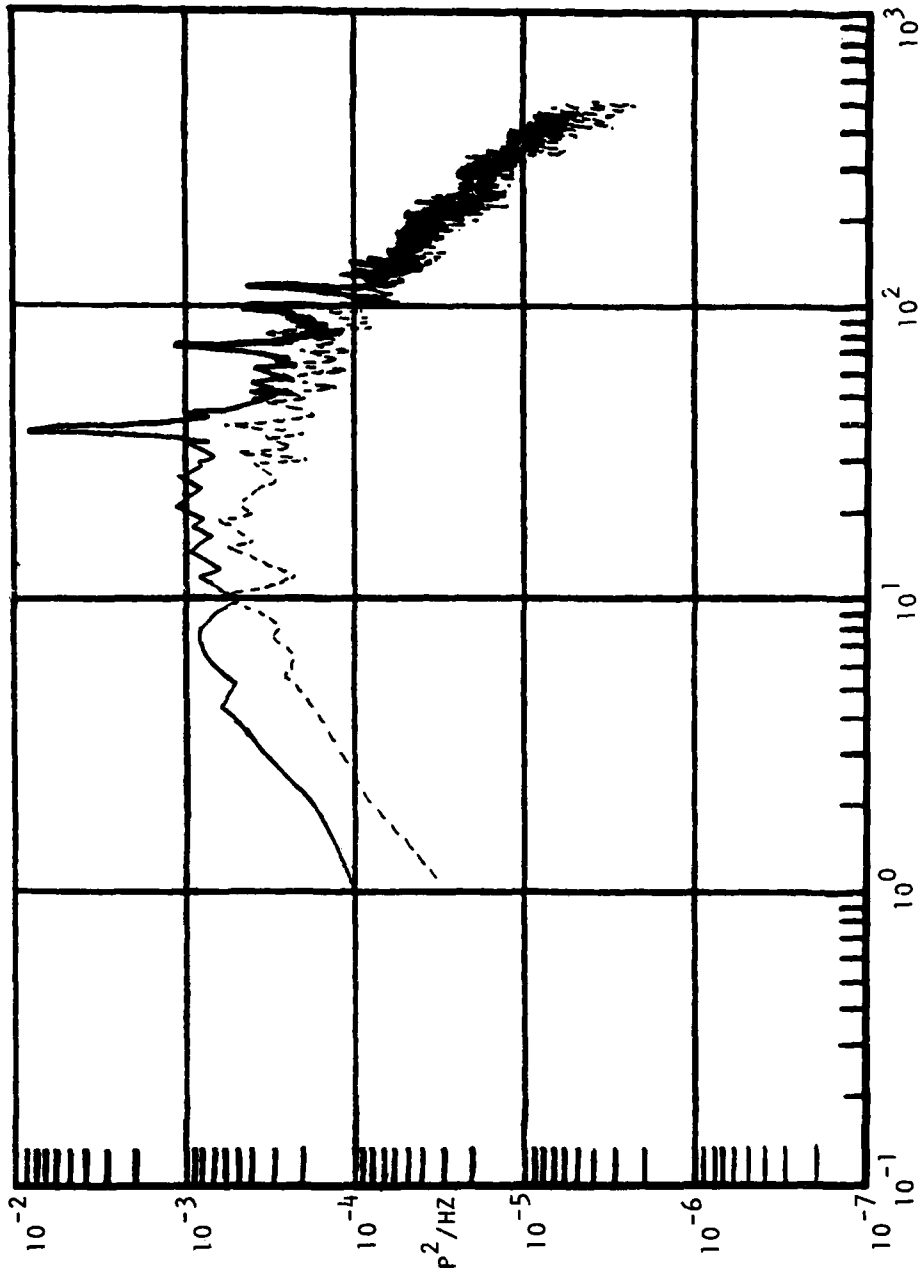
Figure 95. Full-Scale Flight Data, Unsuppressed, Stores Mach 0.7, Part-Open, Aft Bulkhead Lower
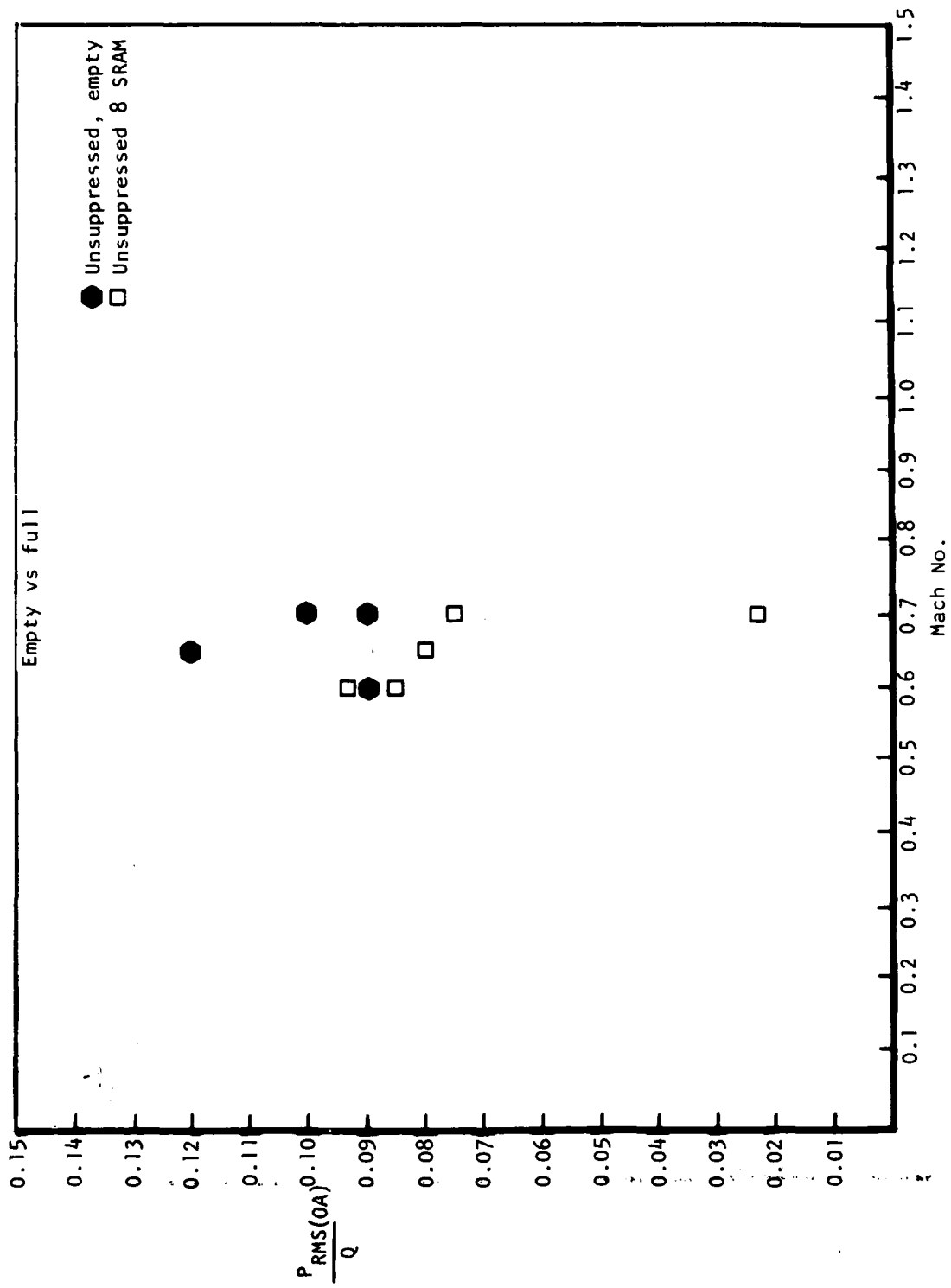
Figure 96. Cavity Noise Internal Stores, Full-Scale Flight Data, Lower Aft Bulkhead-Part-Open
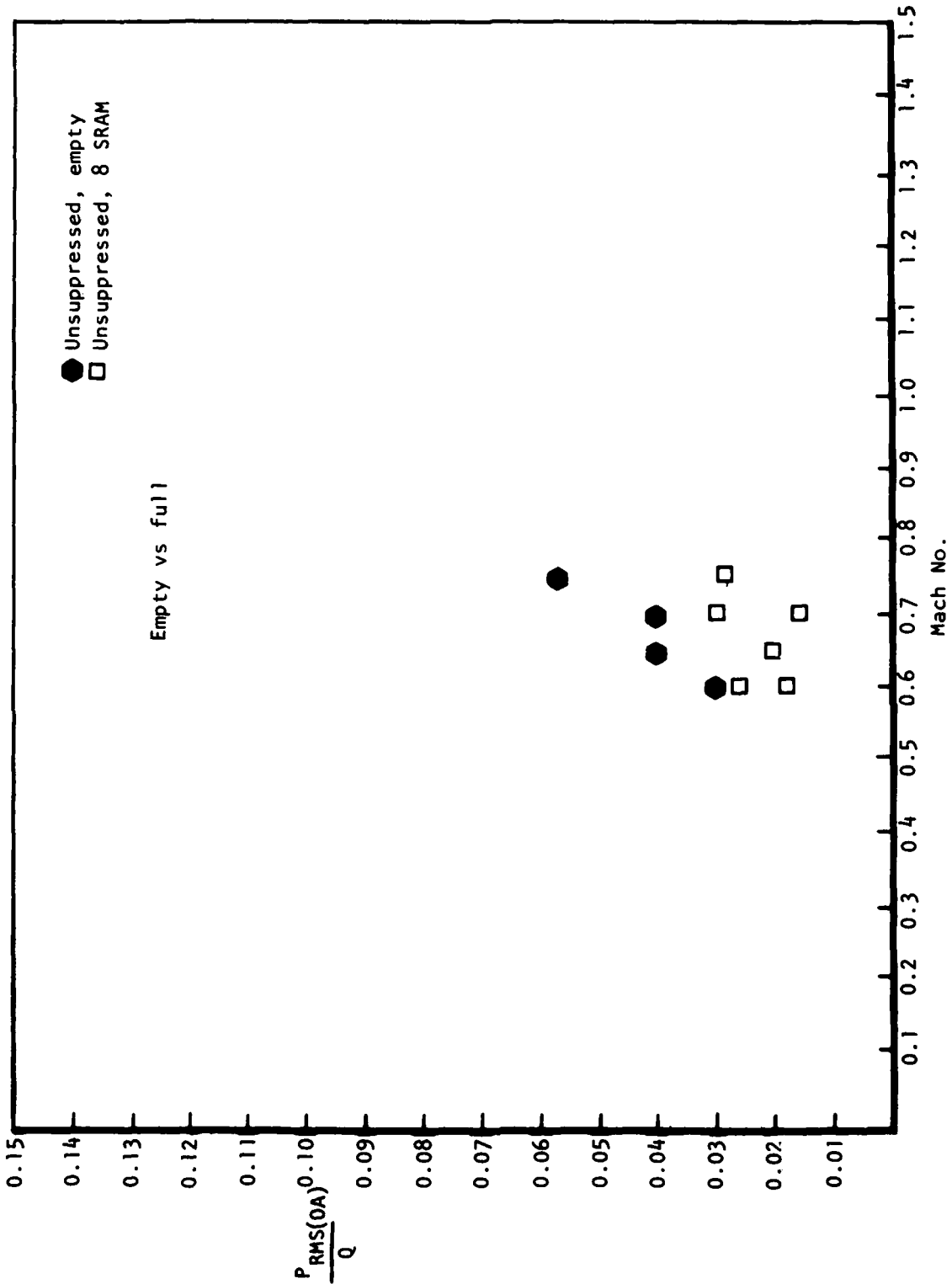
Figure 97. Cavity Noise Internal Stores, Full-Scale Flight Data,
Upper Aft Bulkhead-Part-Open
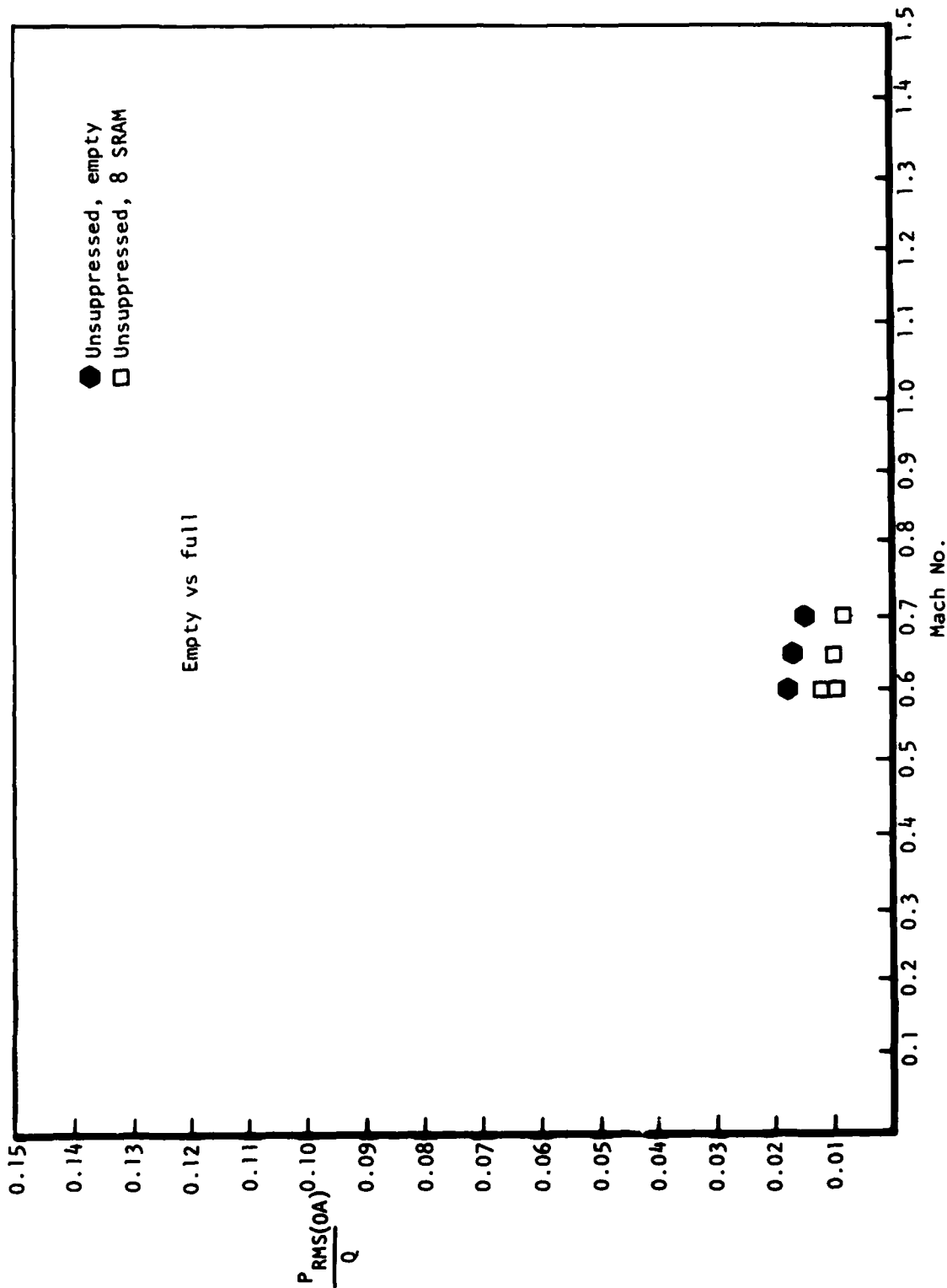
Figure 98. Cavity Noise Internal Stores, Full-Scale Flight Data, Upper Aft Bulkhead-Part-Open
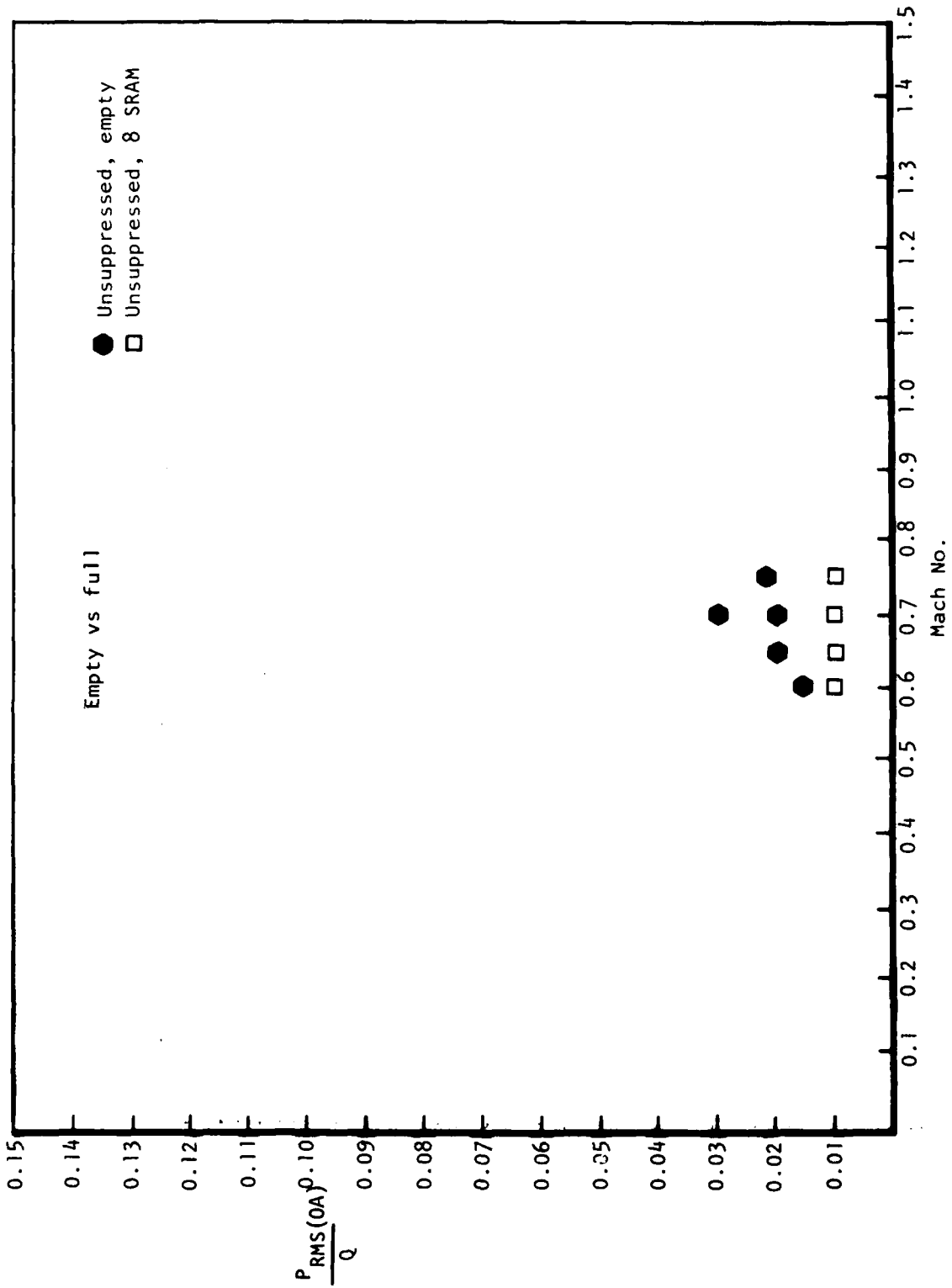
Figure 99. Cavity Noise Internal Stores, Full-Scale Flight Data,
Lower Forward Sidewall–Part-Open

110
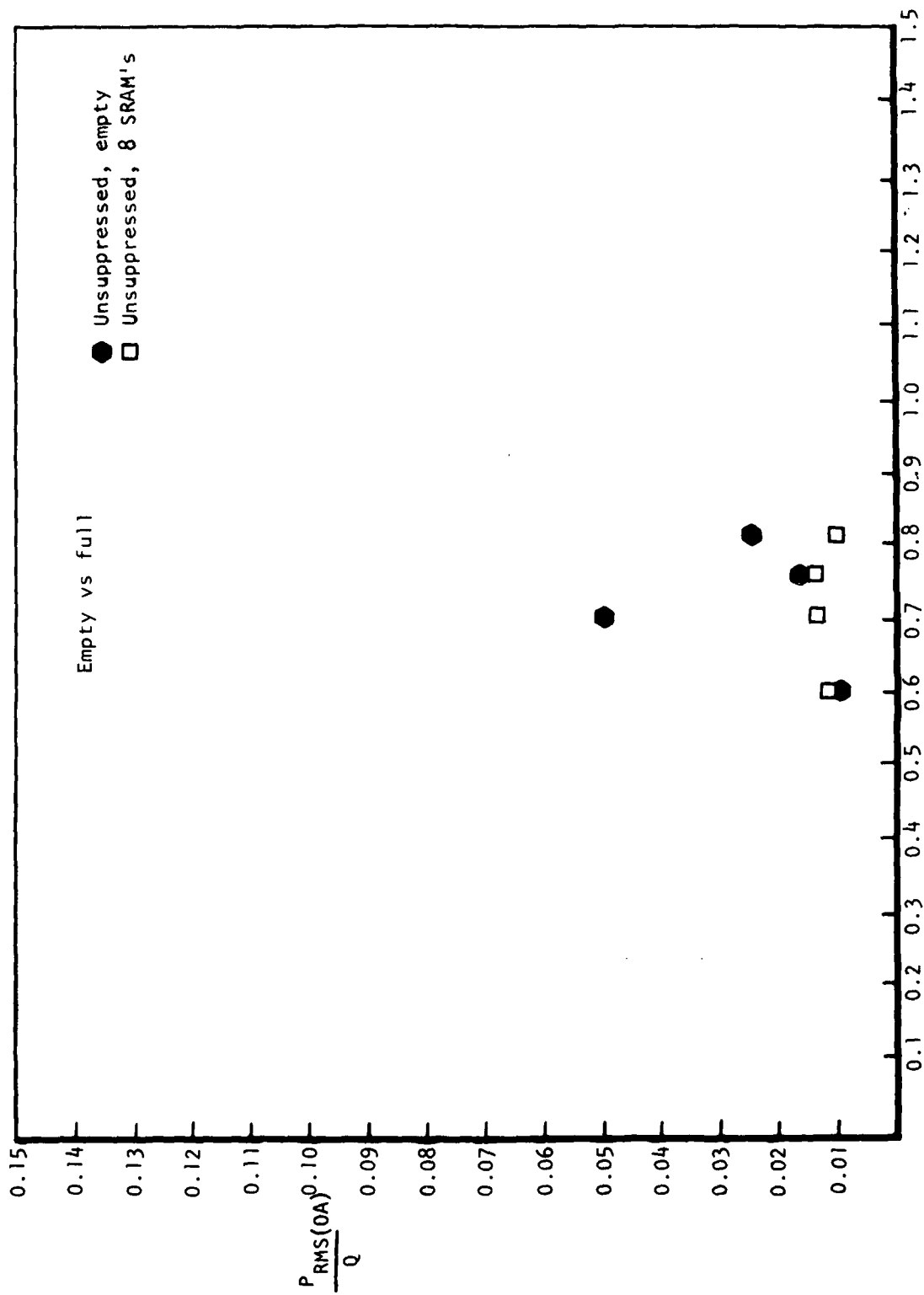
Figure 100. Cavity Noise Internal Stores, Full-Scale Flight Data, Lower Forward Bulkhead - Part-Open
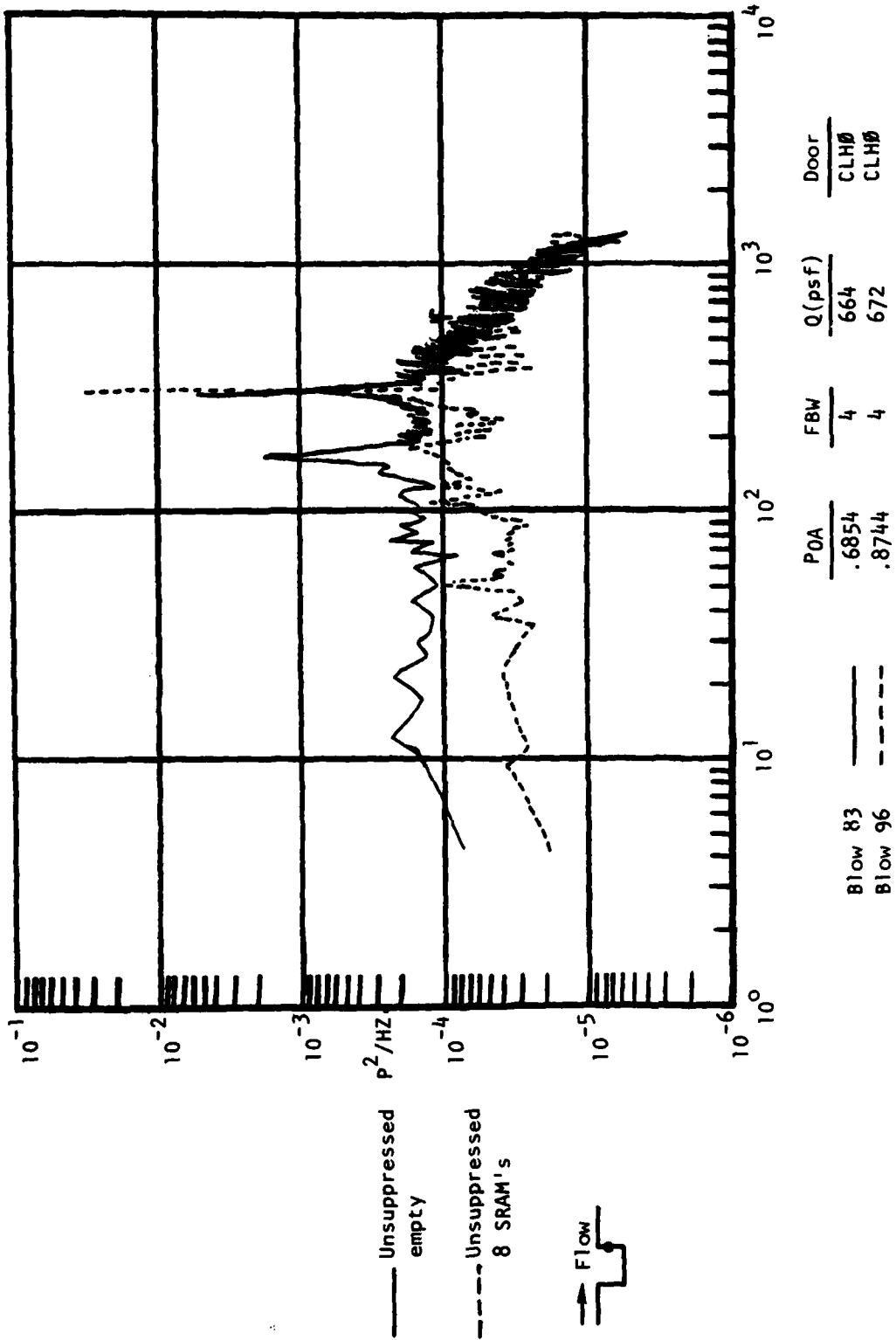
Figure 101. TWT 302 0.1-Scale Model Data, Mach 0.7, Part-Open, Aft Bulkhead Lower

112
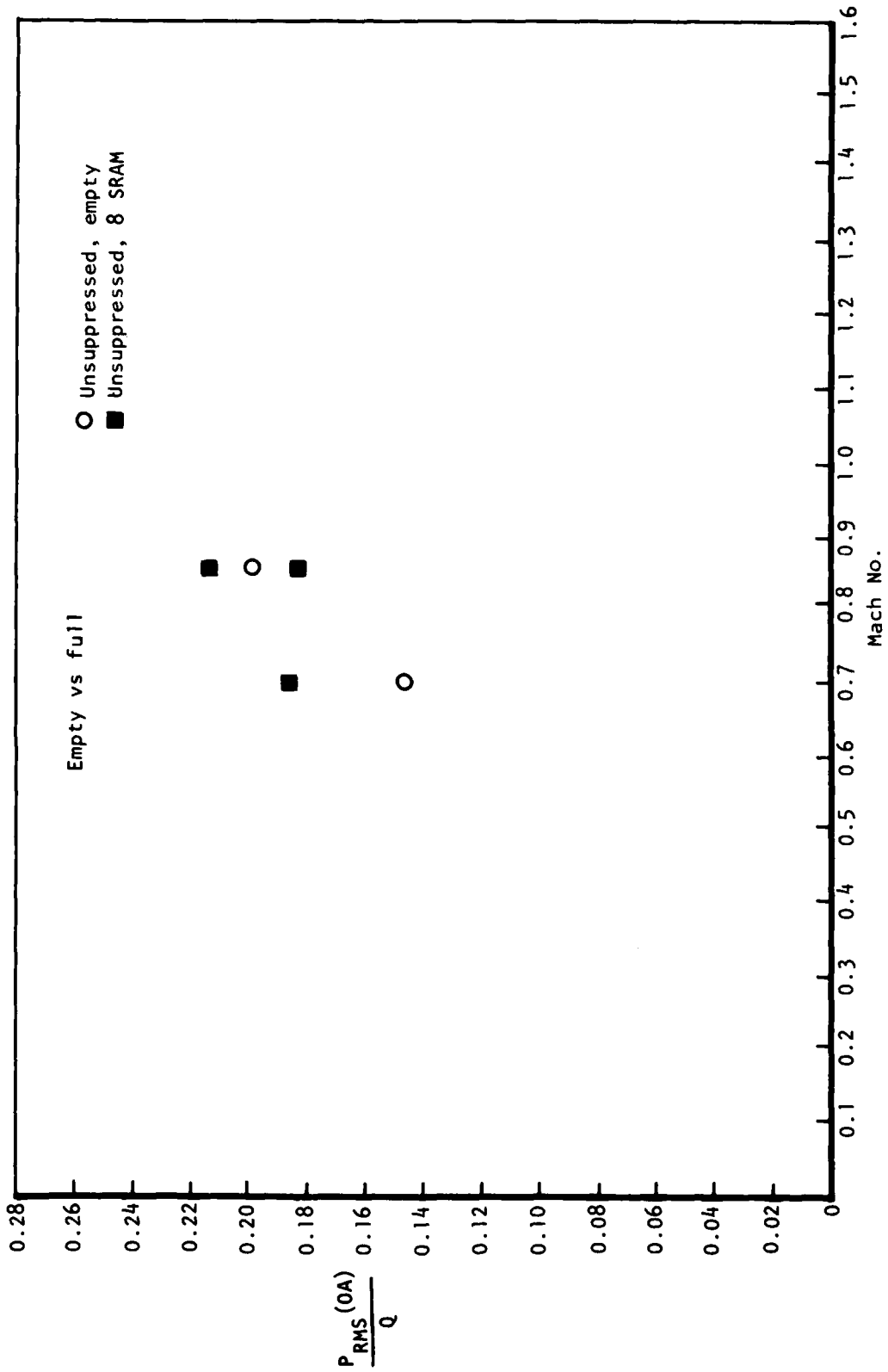
Figure 102. Cavity Noise Internal Stores, TWT 302. 0.1-Scale Model Data, Lower Aft Bulkhead - Part-Open
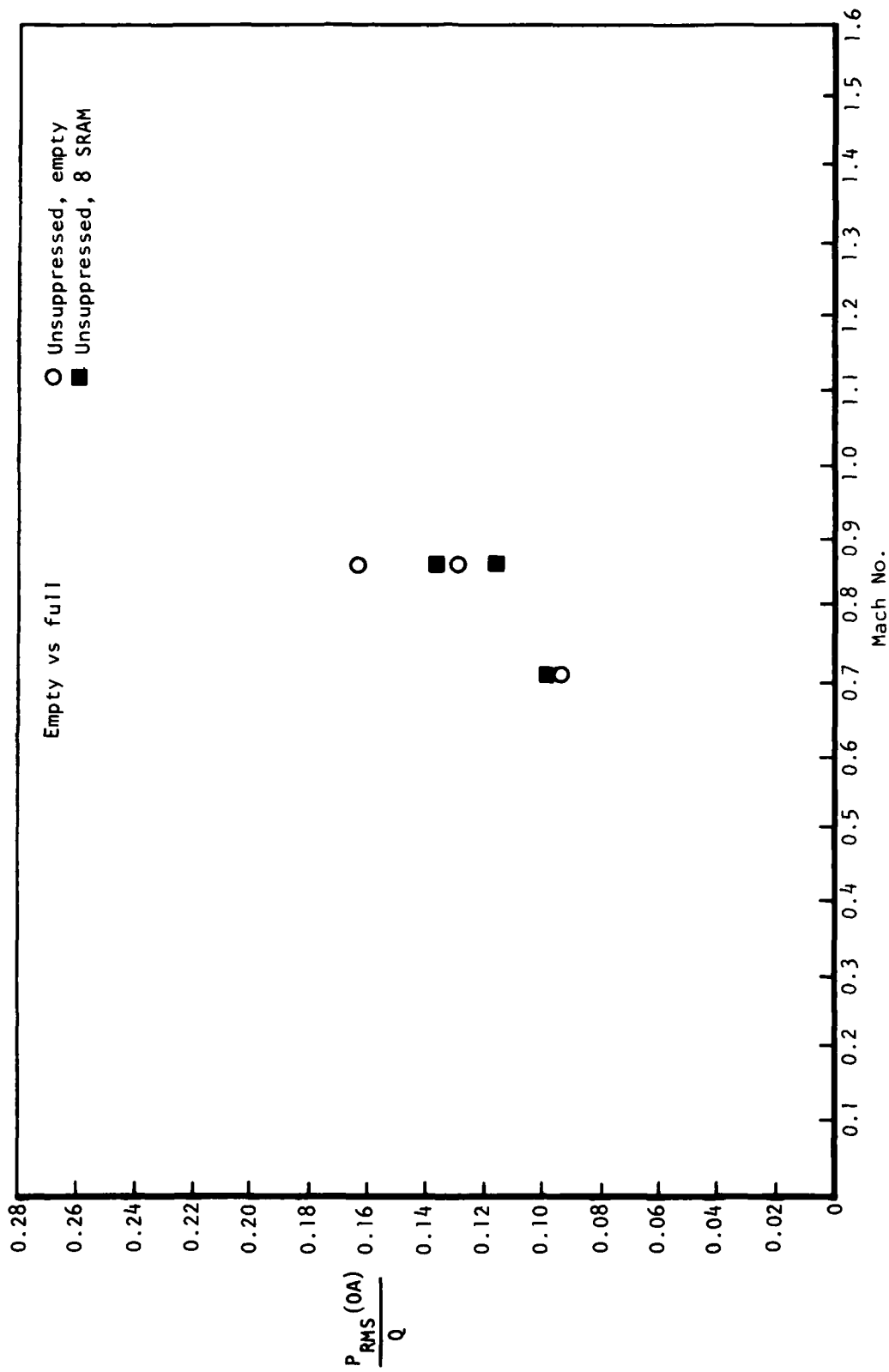
Figure 103. Cavity Noise Internal Stores, TWT 302, 0.1-Scale Model Data, Upper Aft Bulkhead – Part-Open

Figure 104. Cavity Noise Internal Stores, TWT 302, 0.1-Scale Model Data,
Lower Aft Sidewall - Part-Open

Empty vs full

○ Unsuppressed, empty
■ Unsuppressed, 8 SRAM

Mach No.

$\frac{P_{RMS}(OA)}{Q}$

115
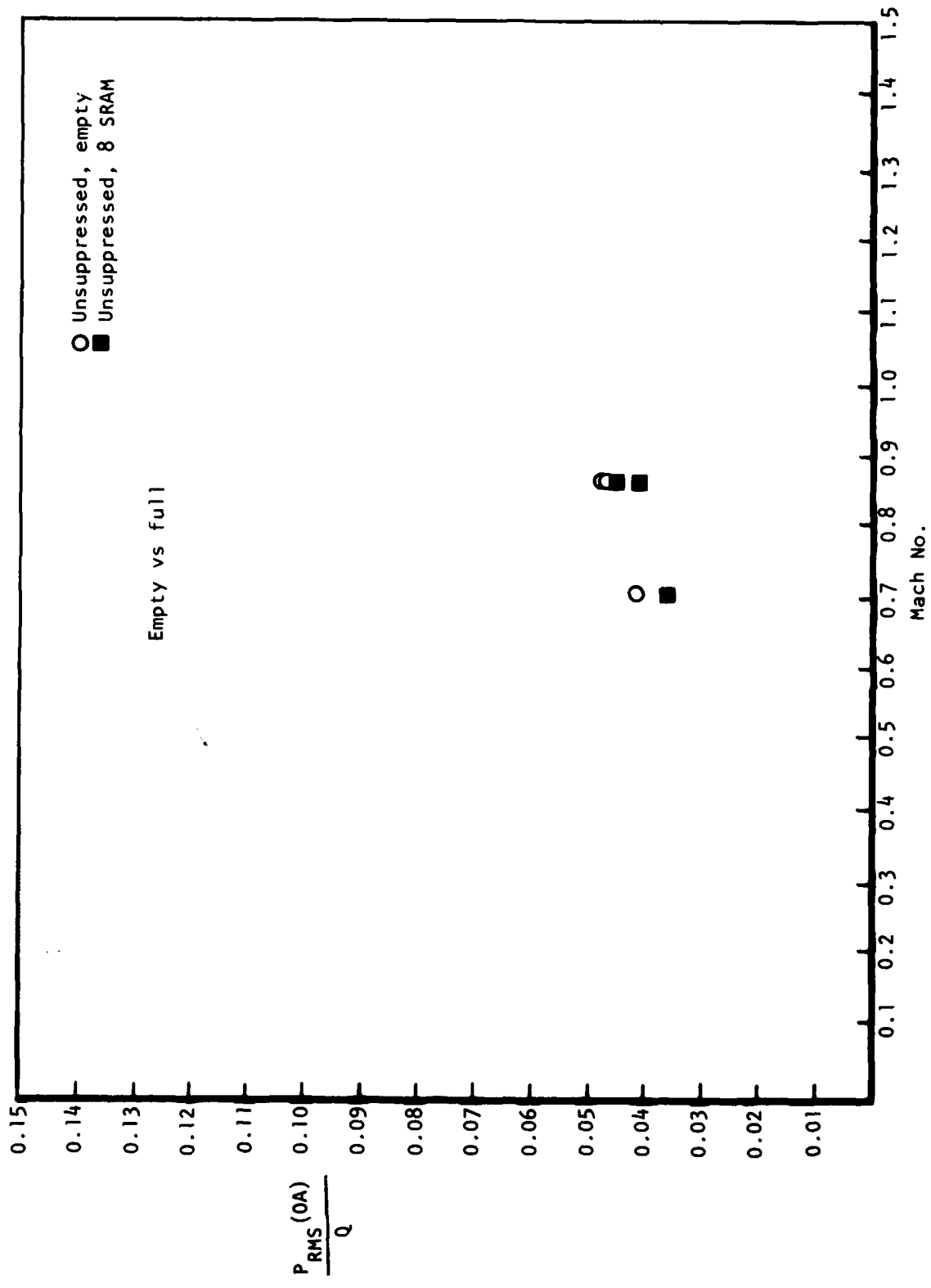
Figure 105. Cavity Noise Internal Stores, TWT 302, 0.1-Scale Model Data,
Upper Aft Sidewall - Part-Open
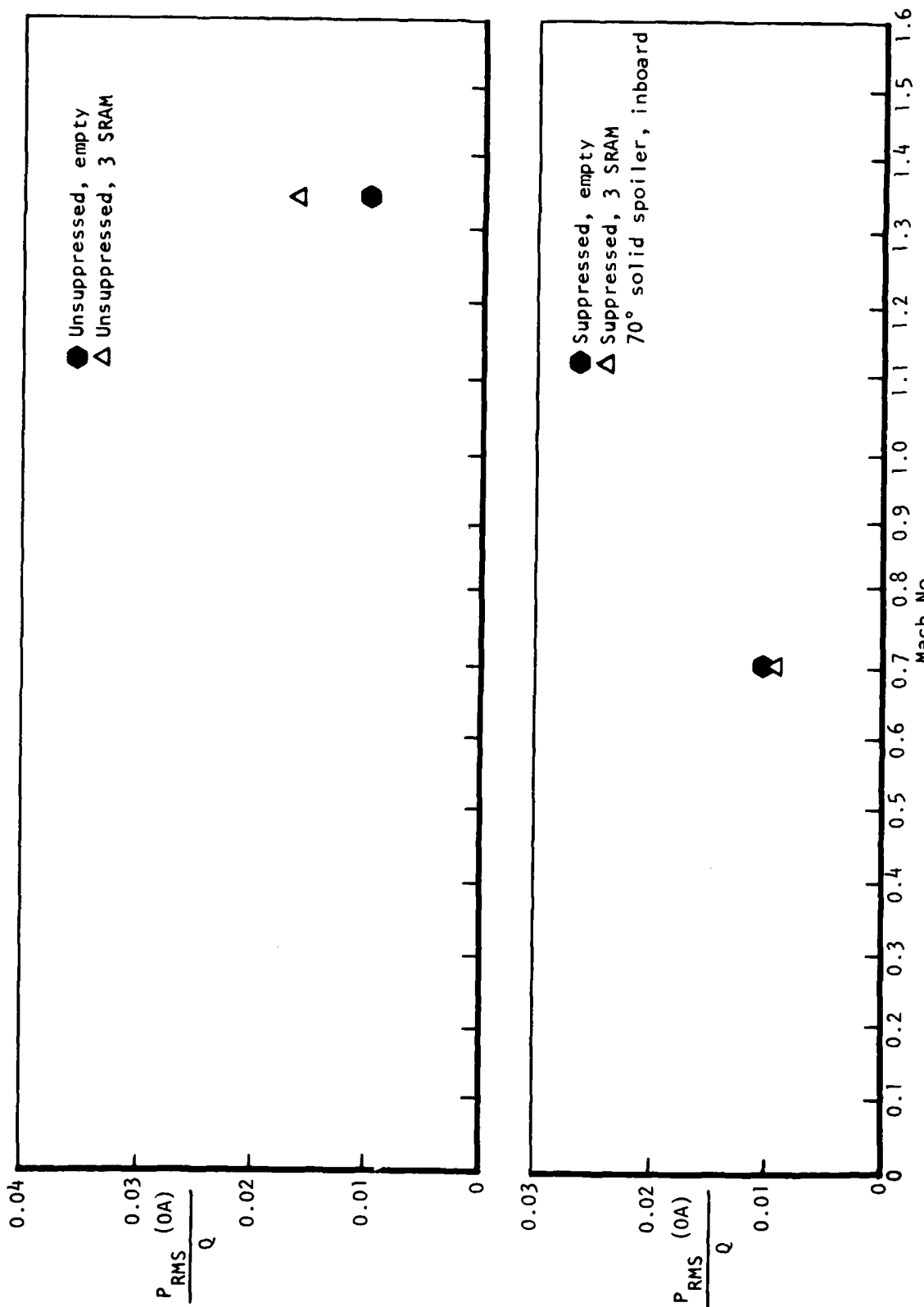
Figure 106. Cavity Noise Internal Stores, Full-Scale Flight Data,
Upper Aft Bulkhead - Part-Open

117
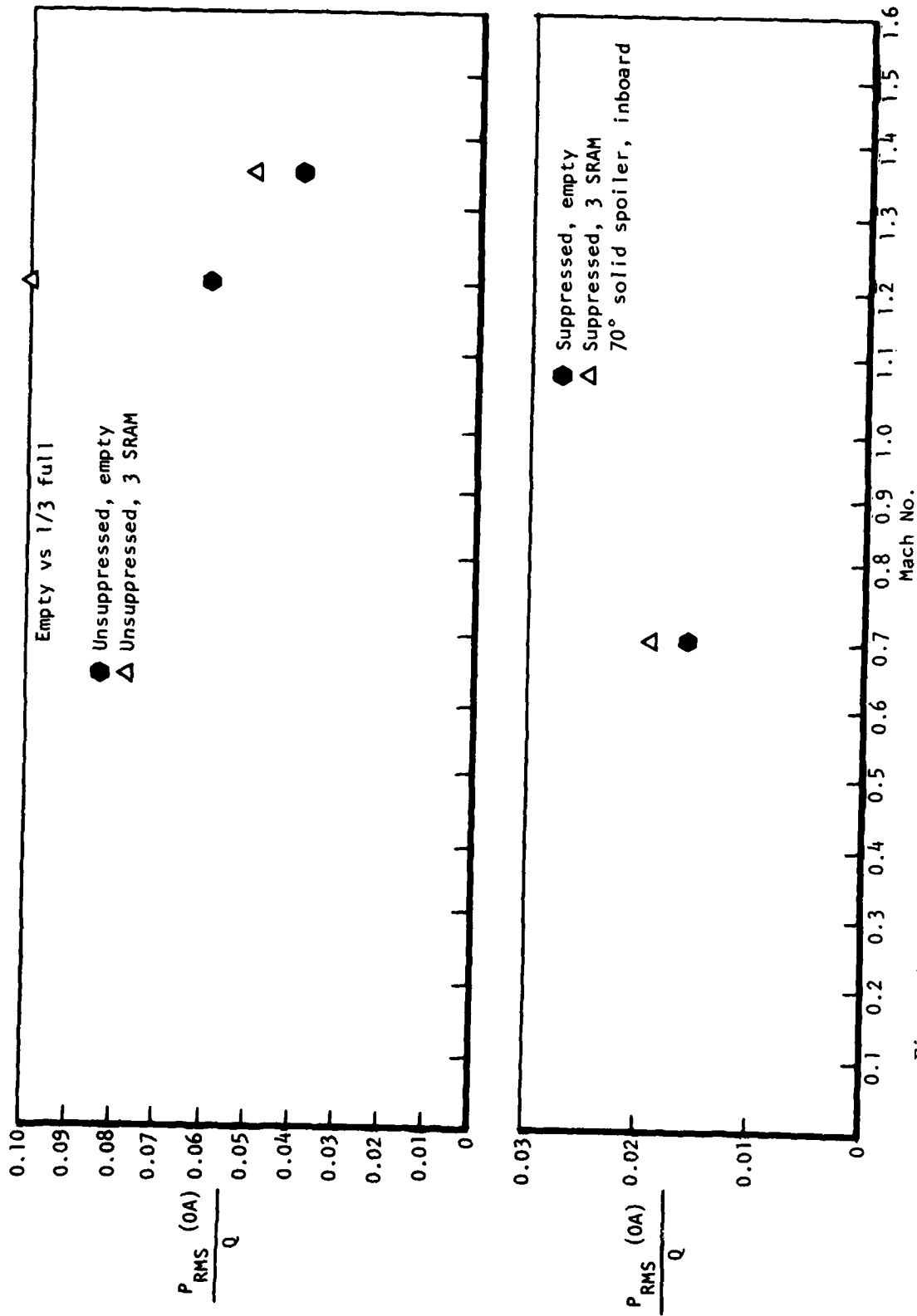
Figure 107. Cavity Noise Internal Stores, Full-Scale Data,
Upper Aft Bulkhead - Full-Open

118

Empty vs 1/3 full

● Unsuppressed, empty
△ Unsuppressed, 3 SRAM

$\dfrac{P_{RMS}\ (OA)}{Q}$

Suppressed, empty
Suppressed, 3 SRAM
70° solid spoiler, inboard

$\dfrac{P_{RMS}\ (OA)}{Q}$

Mach No.
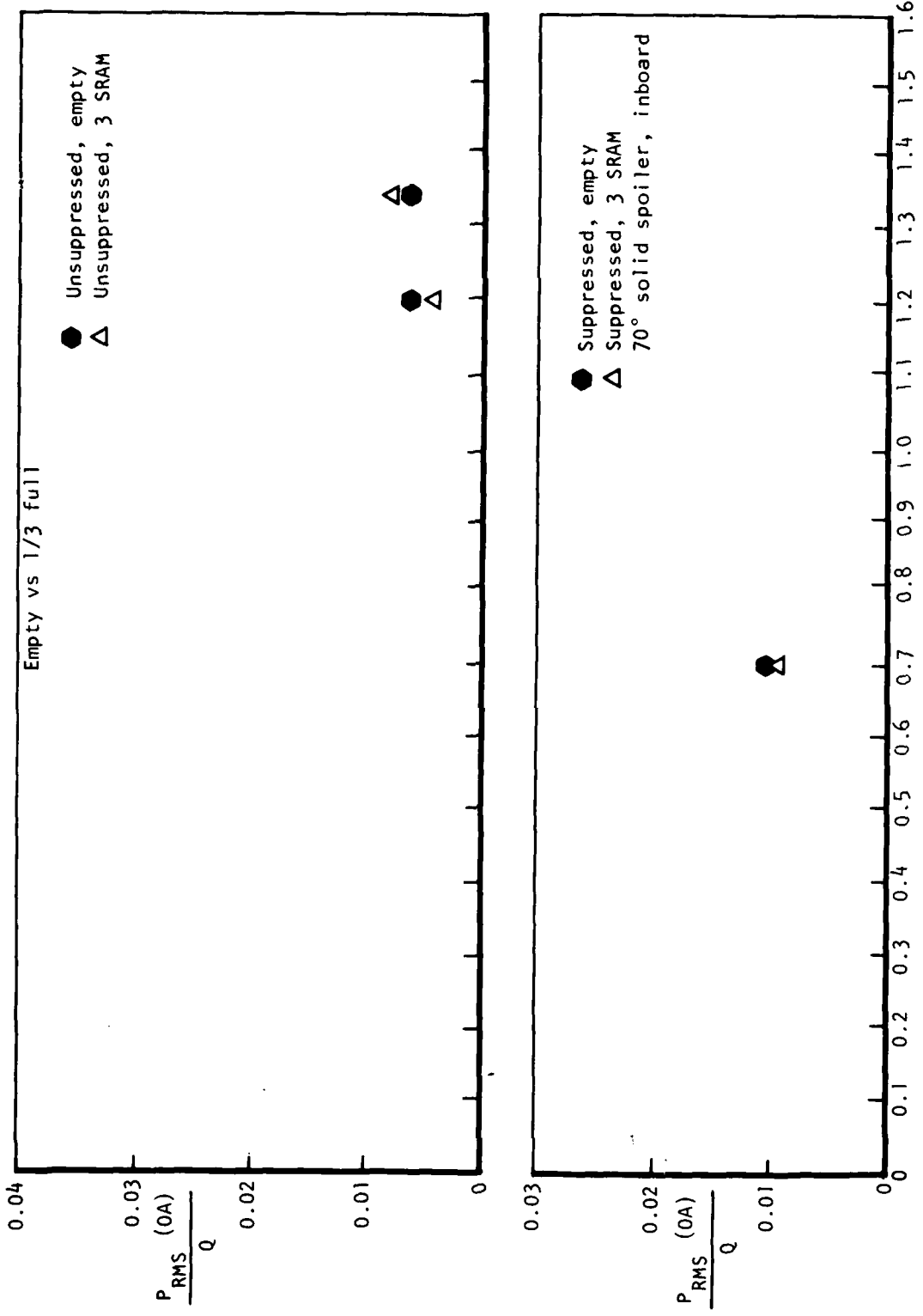
Figure 108. Cavity Noise Internal Stores, Full-Scale Flight Data, Lower Forward
Sidewall - Part-Open

119

Empty vs 1/3 full

● Unsuppressed, empty
□ Unsuppressed, 3 SRAM

$\frac{P_{RMS}\ (OA)}{Q}$

0.04

0.03

0.02

0.01

0

● Suppressed, empty
△ Suppressed, 3 SRAM
70° solid spoiler, inboard

$\frac{P_{RMS}\ (OA)}{Q}$

0.03

0.02

0.01

0   0.1   0.2   0.3   0.4   0.5   0.6   0.7   0.8   0.9   1.0   1.1   1.2   1.3   1.4   1.5   1.6

Mach No.
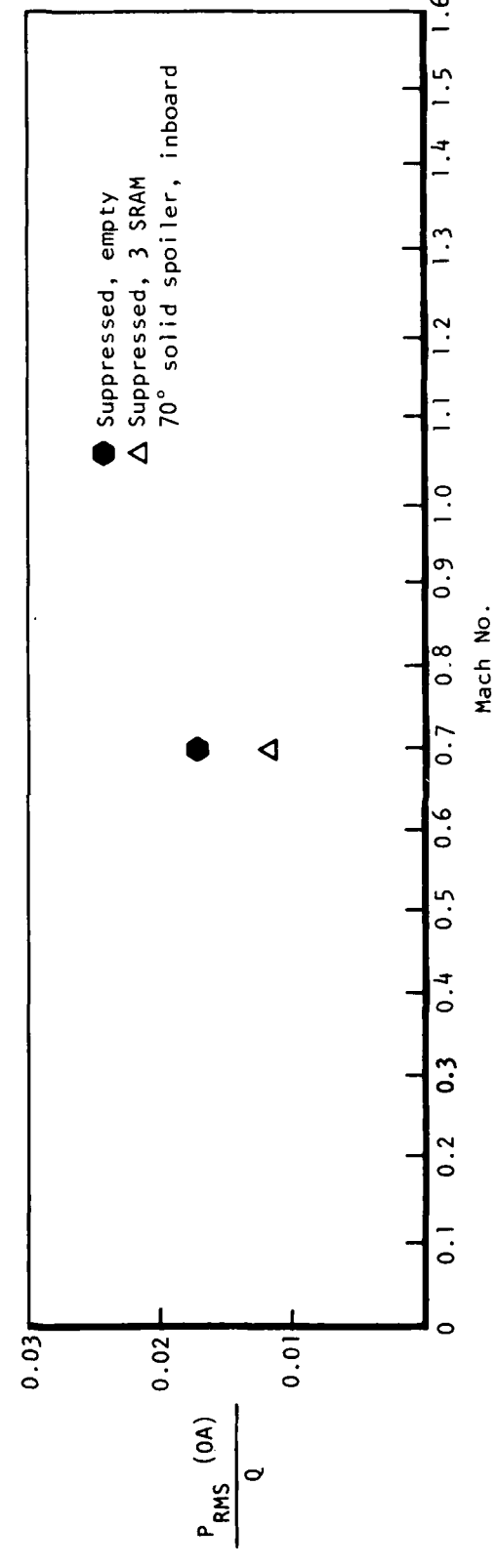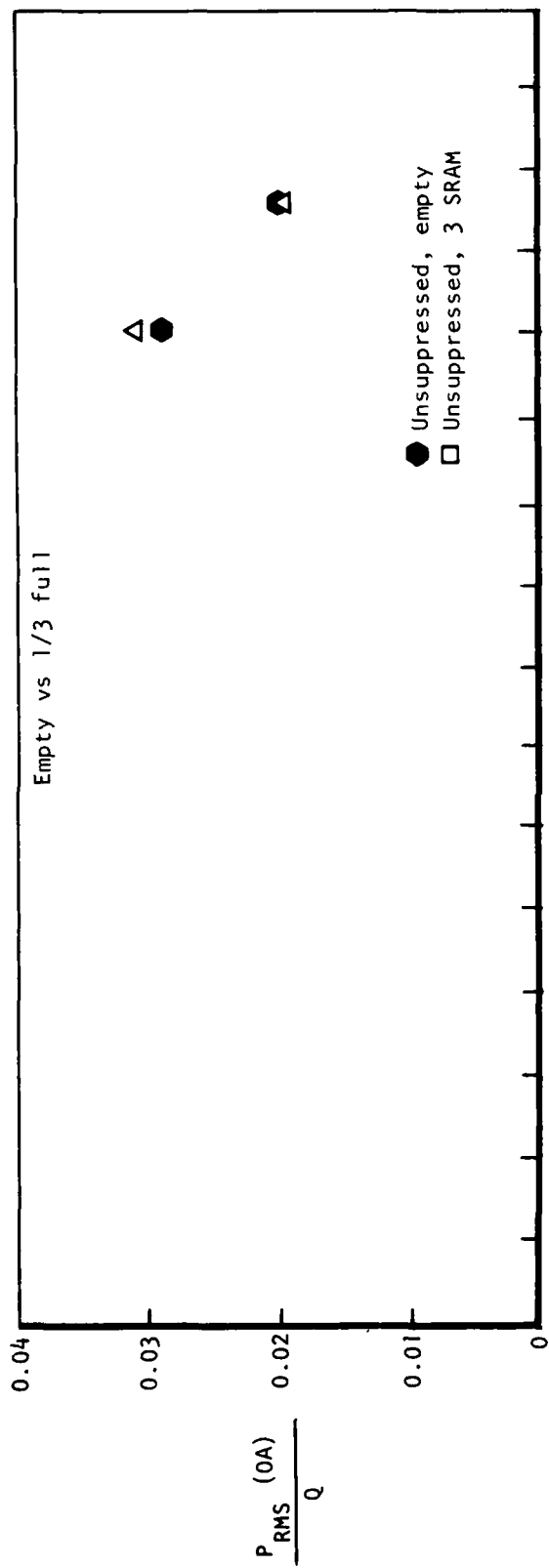
Figure 109. Cavity Noise Internal Stores, Full-Scale Flight Data, Lower Forward
Sidewall - Full-Open

120
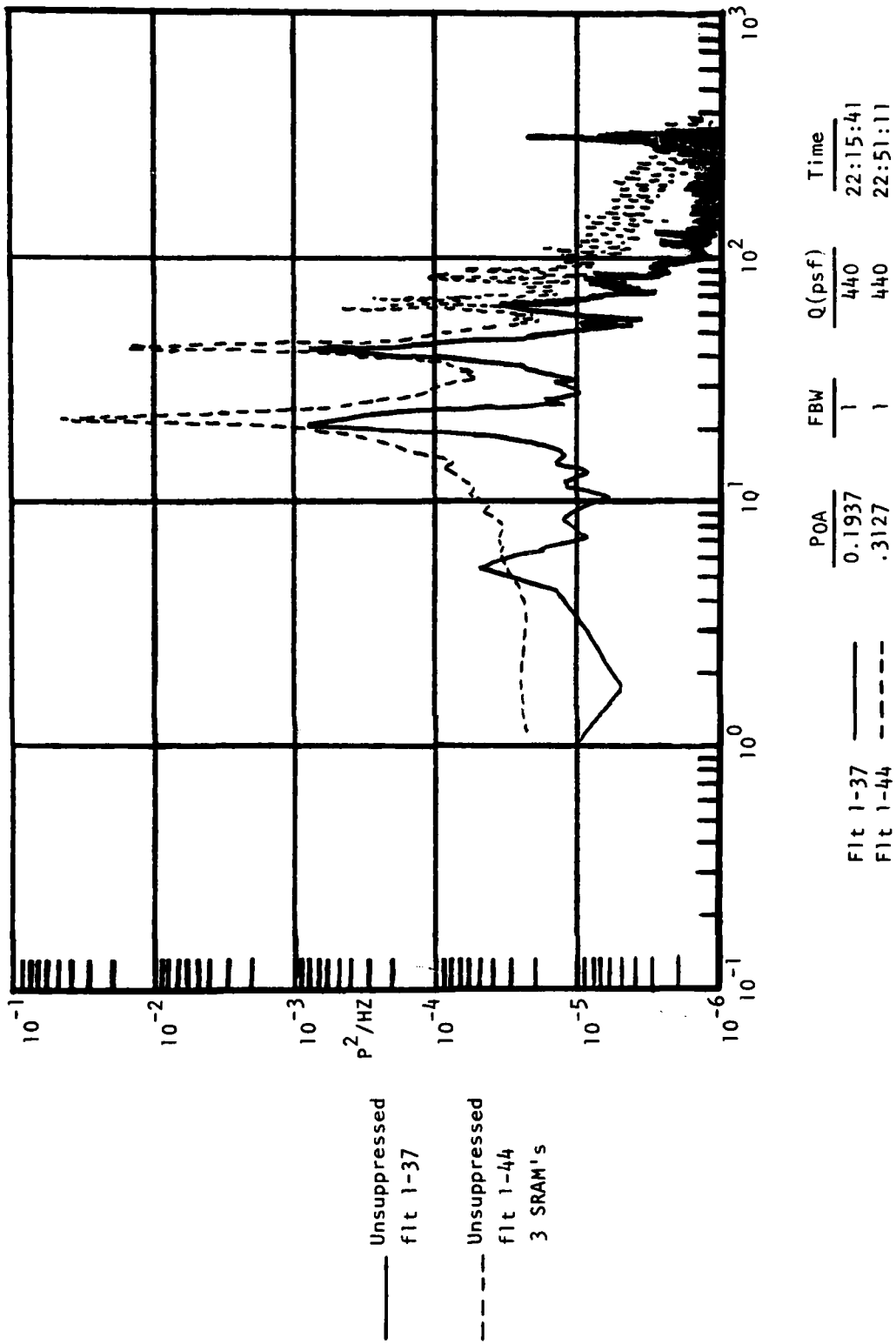
Figure 110. Full-Scale Flight Data, Unsuppressed, Stores, Mach 1.2, Full-Open, Aft Bulkhead Upper

SINGLE-STORE CAVITY CONFIGURATION

The data shown in Figures 111 through 115 are for a single store at the 6 o'clock position near the cavity opening with a 90-degree porous noise-suppression spoiler. The empty bay baseline data are shown on each data plot to determine the effects of the store on cavity noise level. The data indicate a slight increase in noise level relative to an empty bay. The increase in noise is close to the scatter factor of noise level measurement and may not be a significant trend. The spectral density plots show essentially broadband random noise levels. The 90-degree porous spoiler attenuated the narrow-band cavity resonances typical of unsuppressed cavities. A typical spectral density plot is shown in Figure 116.

TWO SUCCESSIVE OPEN CAVITIES

Cavity noise data are presented for two open bays in close proximity for suppressed and unsuppressed bays The successive weapon bay cavities are shown in Figure 117. The bay noise suppressors employed are 90-degree porous, at the forward edge of the cavities. The cavity noise data are shown in Figures 118 through 129 for the suppressed and unsuppressed cavity configurations at various mach numbers and dynamic pressures for several locations inside the cavities. The data for two open cavities shown on all plots are referenced to a baseline configuration of a single open cavity.

The unsuppressed cavity data are shown on Figures 118 through 129. Full-scale aircraft data are shown at mach 0.6 with 0.10-scale model data at mach 0.85 and 1.2. In general, the broadband noise for two open cavities does not vary significantly from the baseline of a single open cavity. The discrete cavity modes, however, are affected by the presence of an adjacent open cavity. The full-scale data at mach 0.6 show a slight reduction in levels in the downstream cavity when an upstream cavity is open. The model data, however, show that the amplitude of the fundamental cavity mode is slightly higher in the downstream cavity than for a single open cavity. The second cavity mode for the model data is lower in the downstream cavity with an open upstream cavity and agrees with the trend of the full-scale data. Mach number variations may exist which influence the relative amplitudes of the cavity discrete modes. The model data are in the mach 0.85 to 1.2 range, with the only full-scale data at mach 0.6. With the available limited data for two adjacent open cavities, final conclusions or data trends cannot be established with certainty.

The cavity noise for suppressed cavities are shown in Figures 130 through 135 for 90-degree porous spoilers. In general, the noise data for the suppressed cavities indicated increases in the amplitude of the discrete frequencies for two open cavities relative to the baseline condition of a single open cavity. The broadband cavity noise level is unaffected by the presence of an additional open cavity in close proximity.
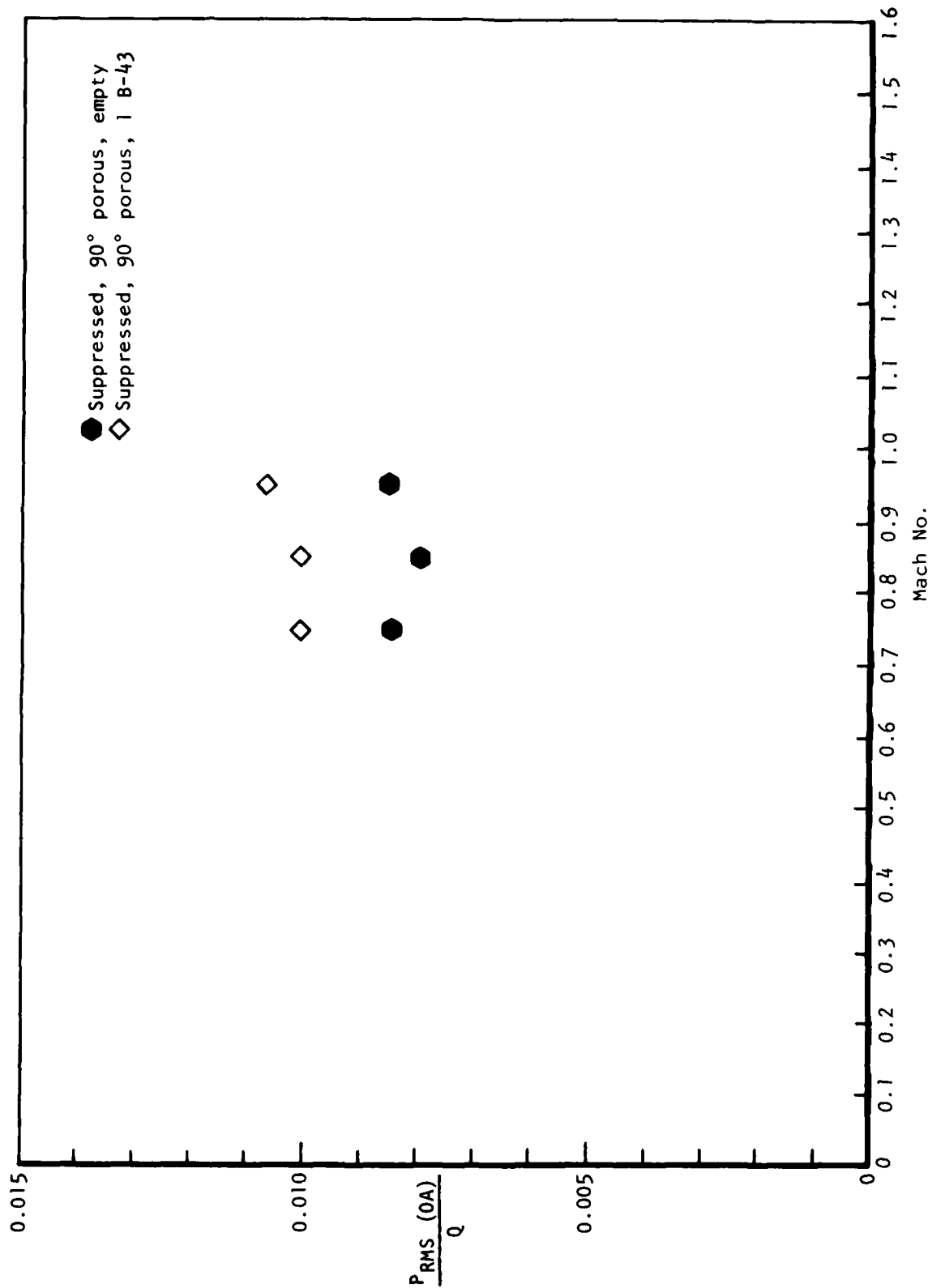
Figure 111. Cavity Noise Internal Stores, Full-Scale Flight Data, Lower Aft Bulkhead Part-Open Empty Versus One Store

123
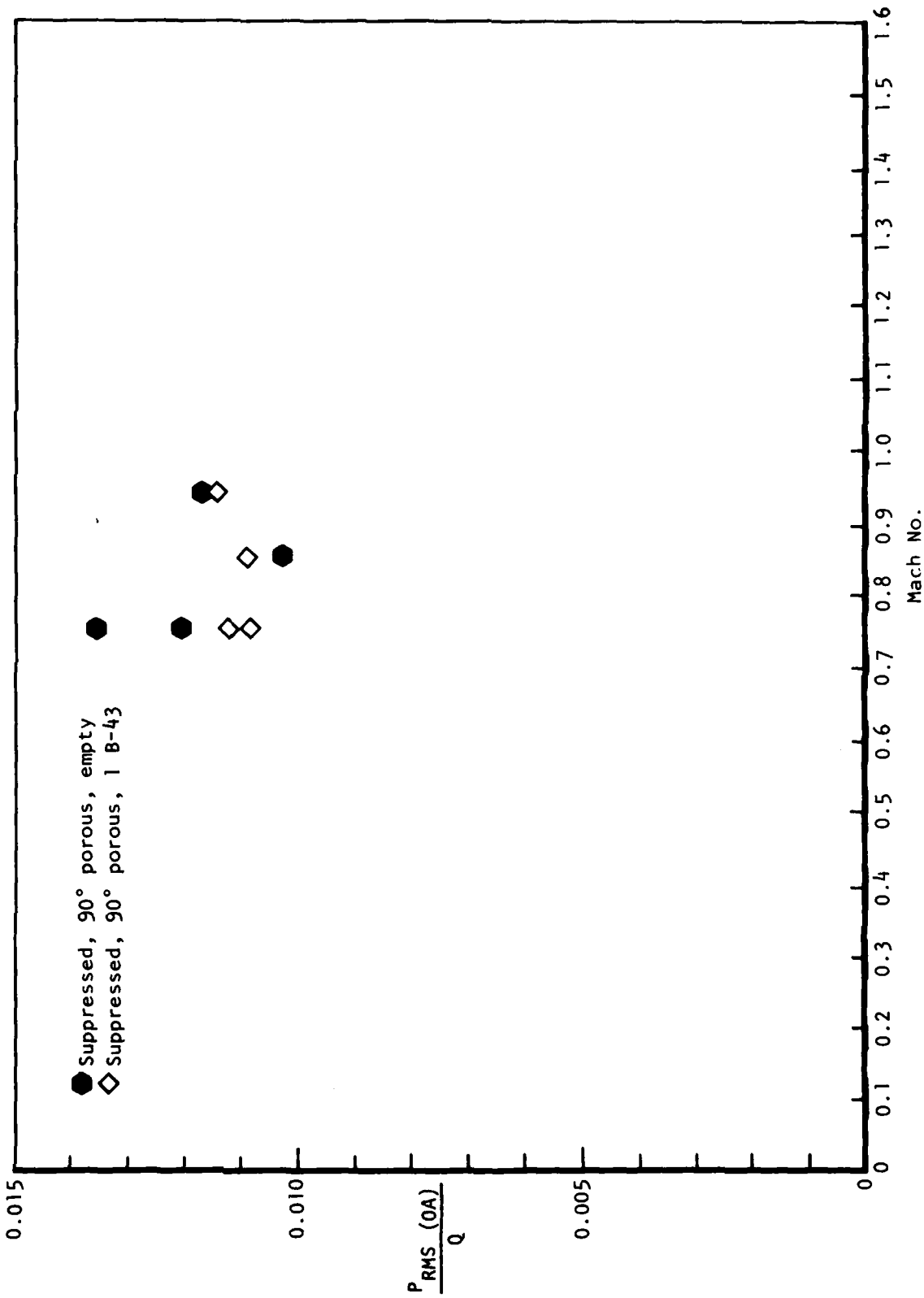
Figure 112. Cavity Noise Internal Stores, Full-Scale Flight Data, Lower Aft Sidewall Part-Open Empty Versus One Store

● Suppressed, 90° porous, empty
◇ Suppressed, 90° porous, 1 B-43

Mach No.

$\dfrac{P_{RMS}\ (OA)}{Q}$
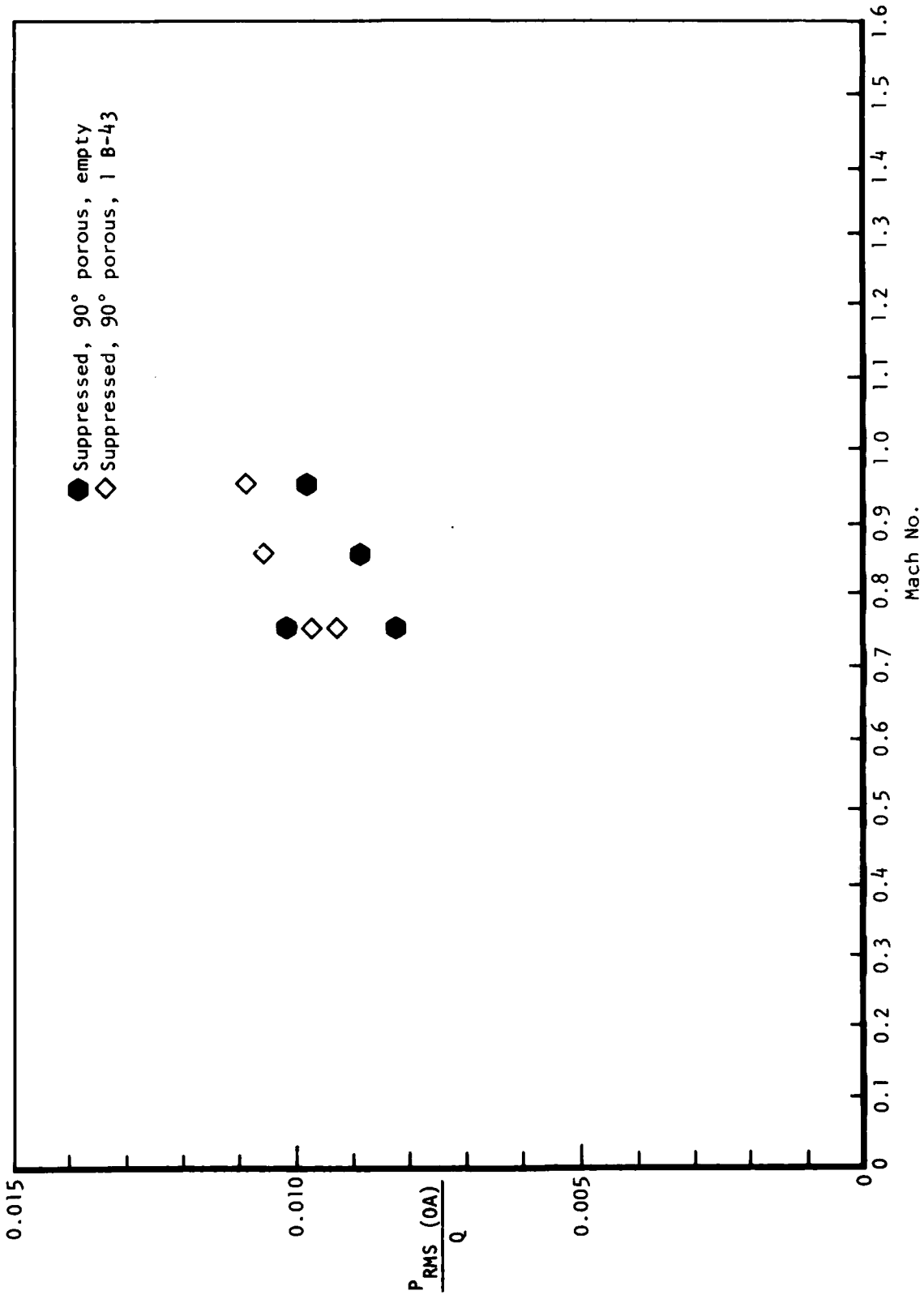
Figure 113. Cavity Noise Internal Stores, Full-Scale Flight Data, Upper Aft Sidewall
Part-Open Empty Versus One Store
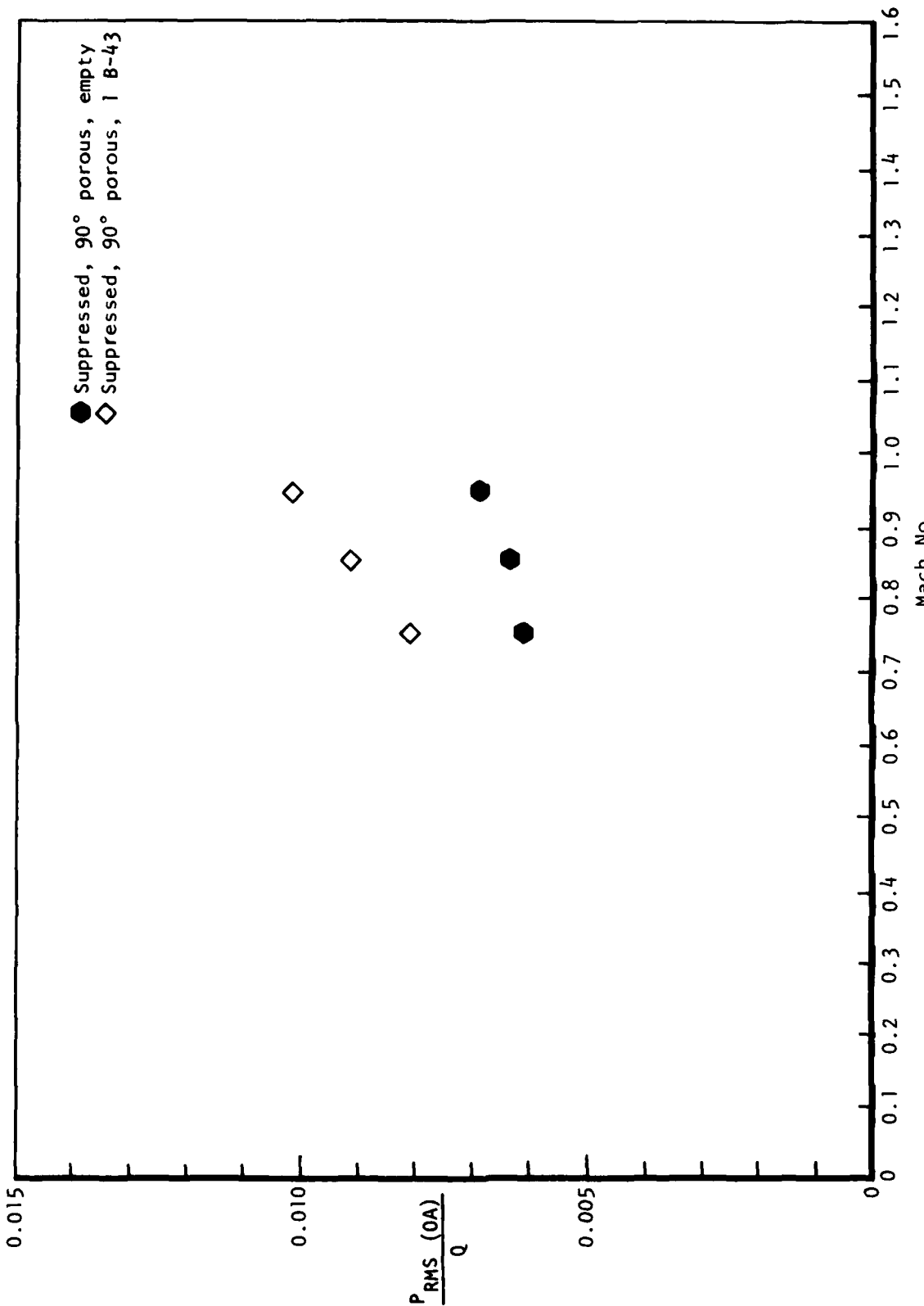
Figure 114. Cavity Noise Internal Stores, Full-Scale Flight Data, Upper Forward Sidewall Part-Open Empty Versus One Store

126
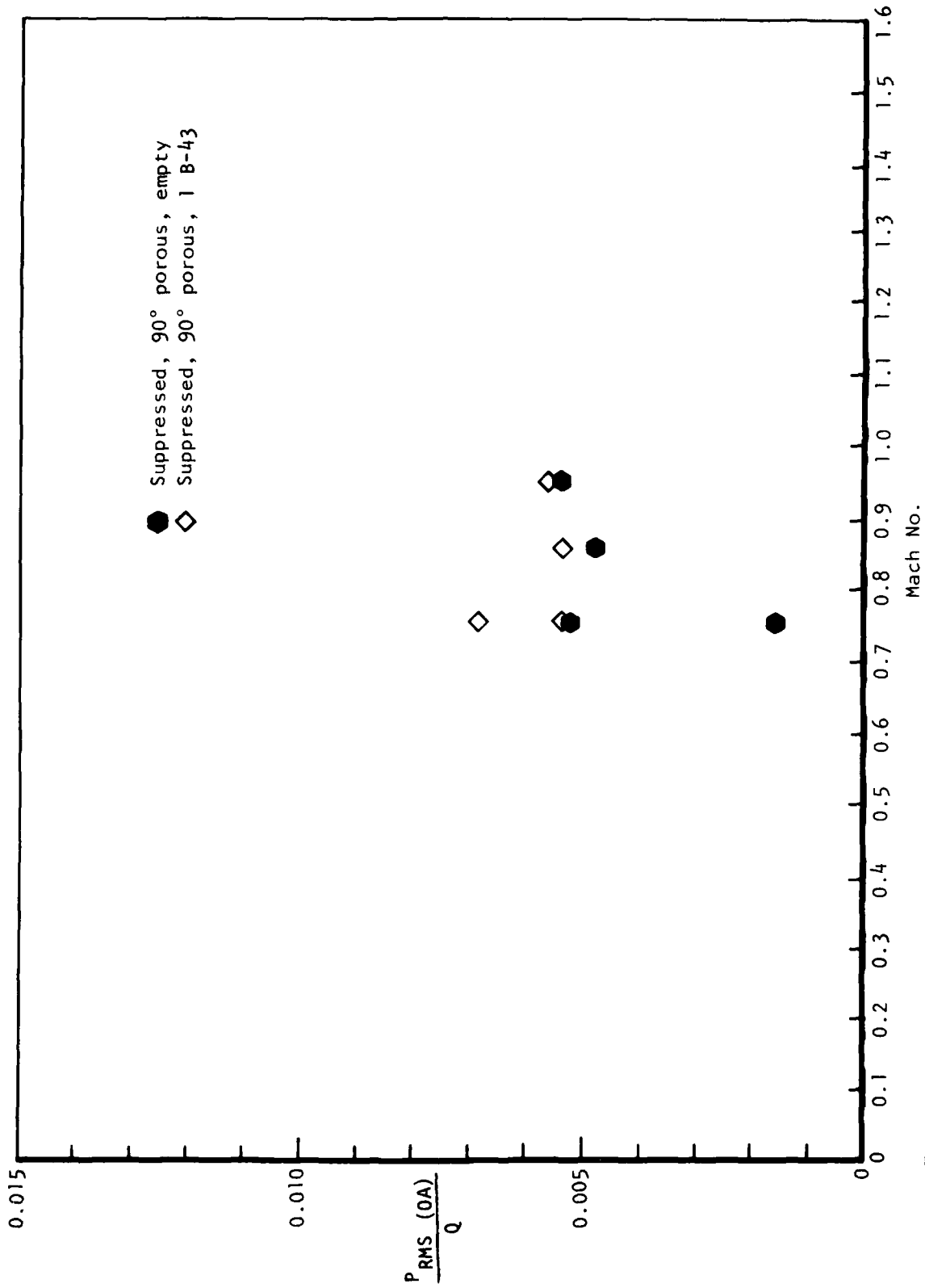
Figure 115. Cavity Noise Internal Stores, Full-Scale Flight Data, Lower Forward Bulkhead Part-Open Empty Versus One Store
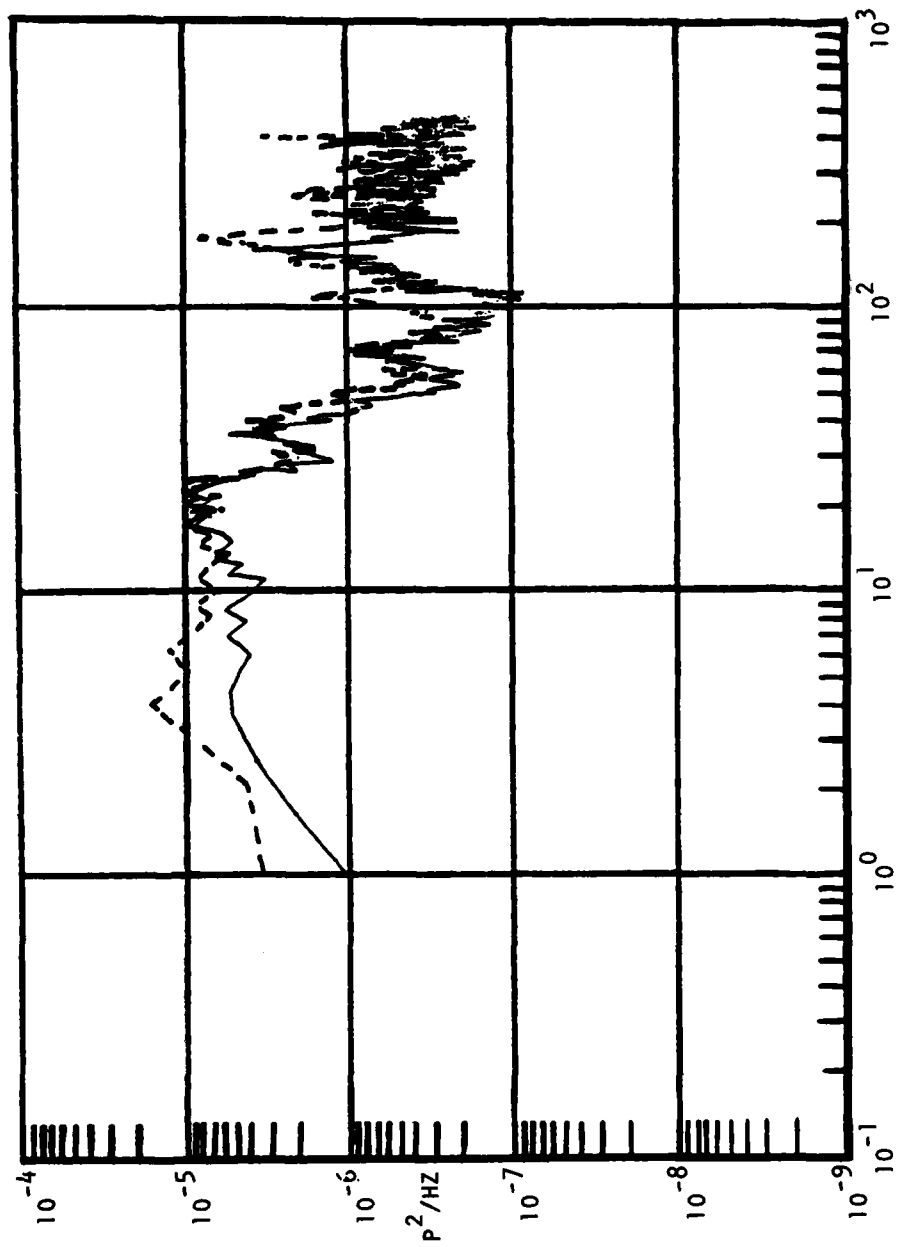
Figure 116. Full-Scale Flight Data, Mach 0.85, Part-Open, Aft Bulkhead Lower

Figure 117. Double-Bay, 90-Degree Porous Spoiler, Part-Open

Figure 118. Full-Scale Flight Data, Adjacent Open Cavities, Mach 0.6, Part-Open, Forward Bulkhead Lower

130
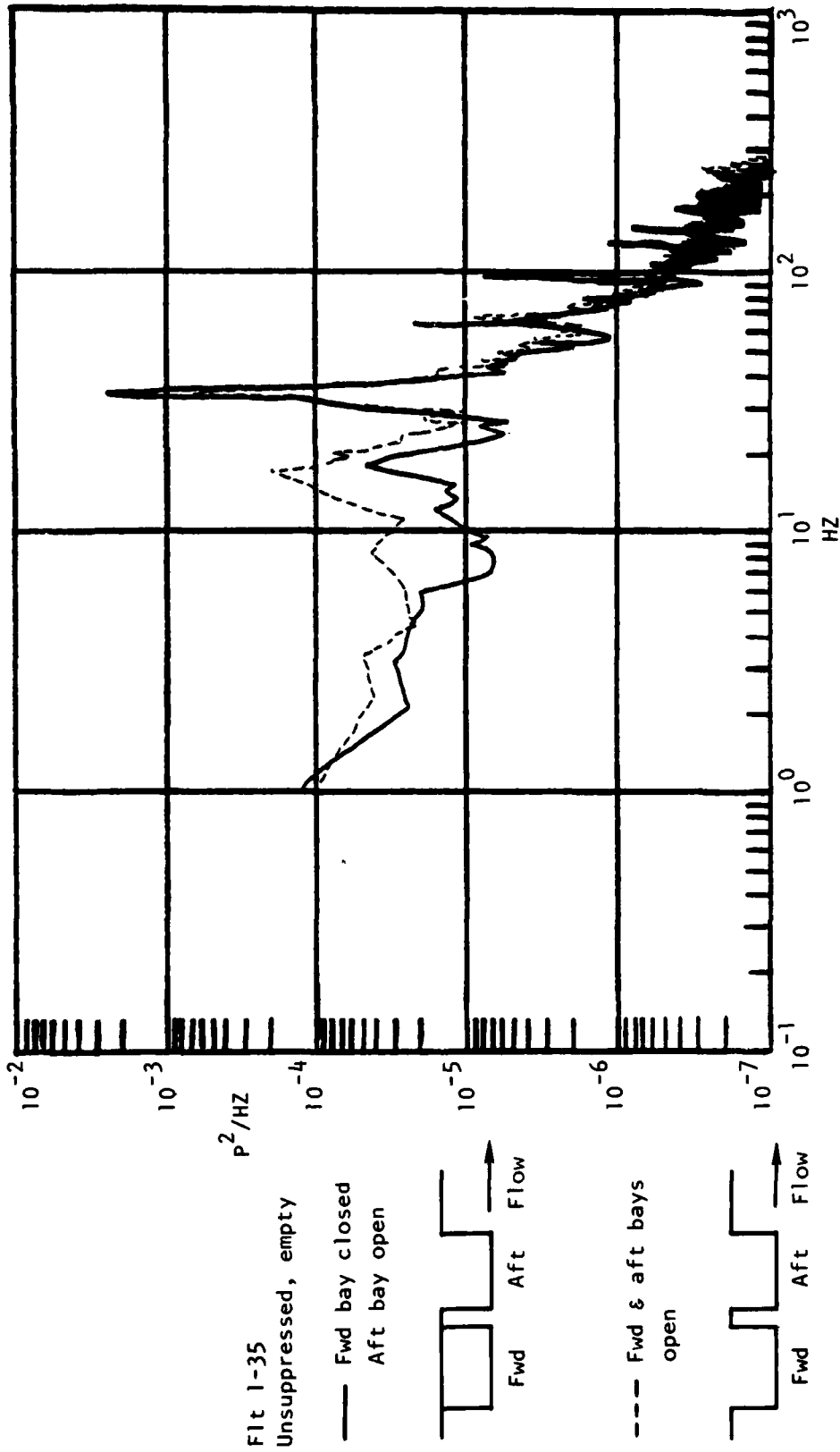
Figure 119. Full-Scale Flight Data, Adjacent Open Cavities, Mach 0.6, Part-Open Aft Bulkhead Upper

Flt 1-35
Unsuppressed, empty

P^2/HZ

—— Fwd bay closed
      Aft bay open

Fwd   Aft   Flow

- - - Fwd & aft bays
         open

Fwd   Aft   Flow

	POA	FBW	Q(psf)	Time
——	.1884	1	250	19:13:18
- - -	.1173	1	250	19:27:10

10^{-2} 10^{-3} 10^{-4} 10^{-5} 10^{-6} 10^{-7}

10^{-1} 10^0 10^1 10^2 10^3
HZ

132
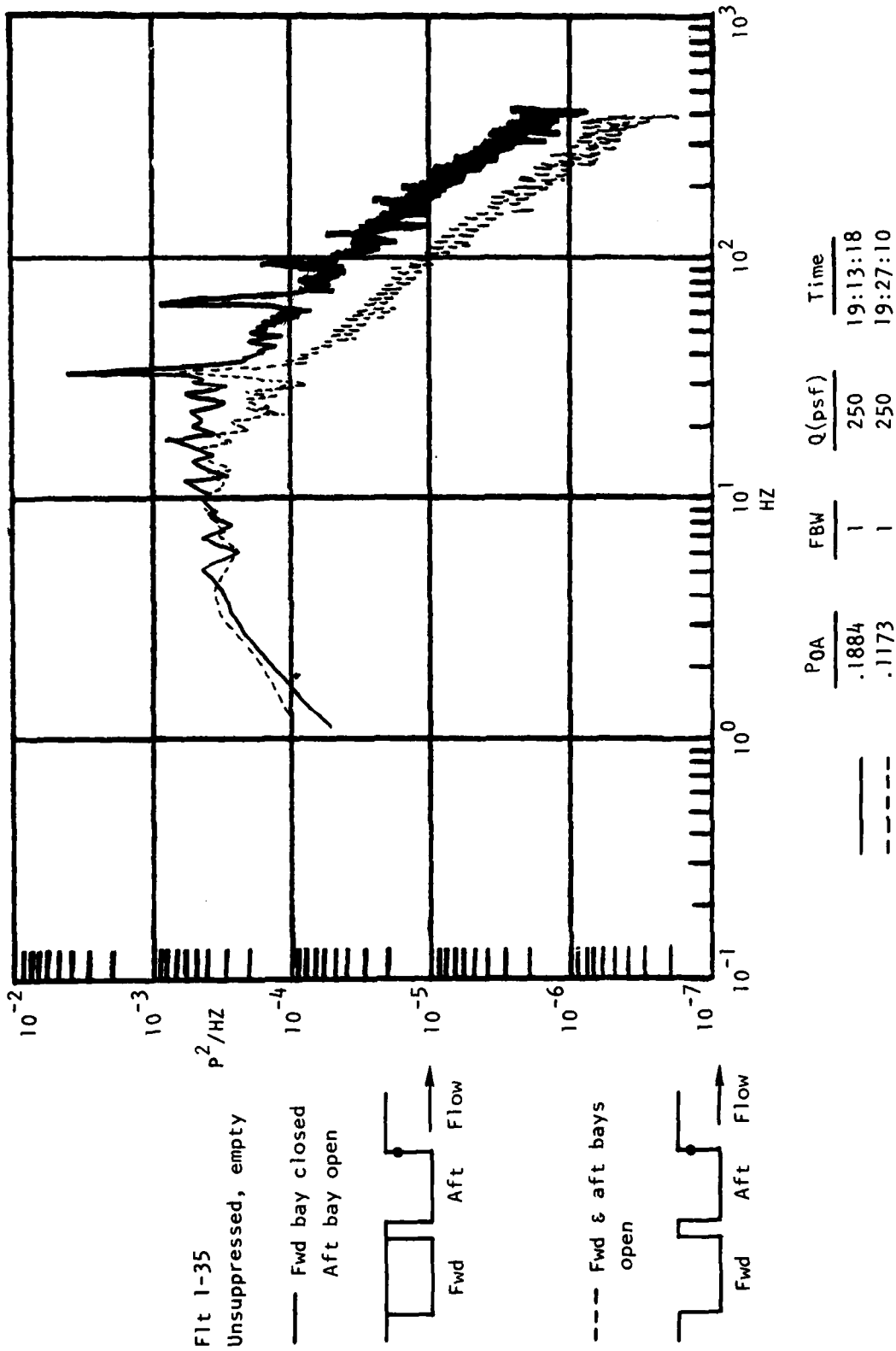
Figure 120. Full-Scale Flight Data, Adjacent Open Cavities, Mach 0.6, Part-Open, Aft Bulkhead Lower
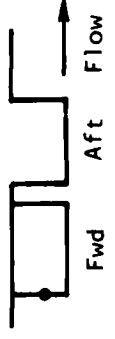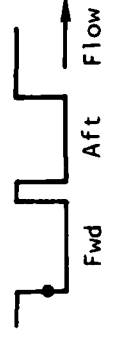
Figure 121. Full-Scale Flight Data, Adjacent Open Cavities, Mach 0.6, Full-Open, Forward Bulkhead Upper

133

Flt 1-35
Unsuppressed, empty

—— Fwd bay closed
     Aft bay open

Fwd | Aft | Flow →

--- Fwd & aft bays
     open

Fwd | Aft | Flow →

	POA	FBW	Q(psf)	Time
——	0.1062	1	250	19:19:42
---	0.05991	1	250	19:28:37

P^2/HZ

10^{-2} 10^{-3} 10^{-4} 10^{-5} 10^{-6} 10^{-7}

10^{-1} 10^0 10^1 10^2 10^3

HZ
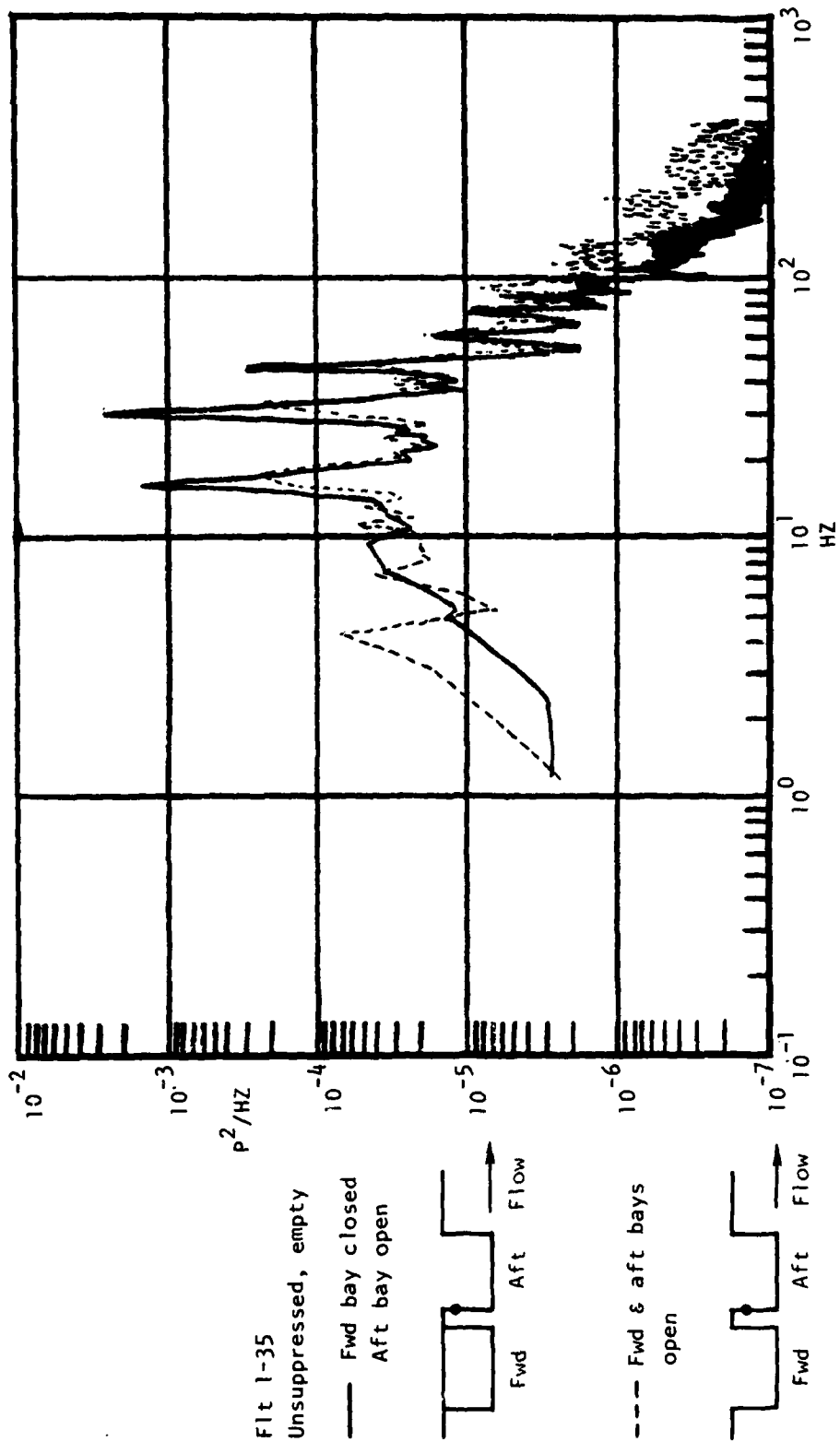
Figure 122. Full-Scale Flight Data, Adjacent Open Cavities, Mach 0.6, Full-Open, Forward Bulkhead Lower

134
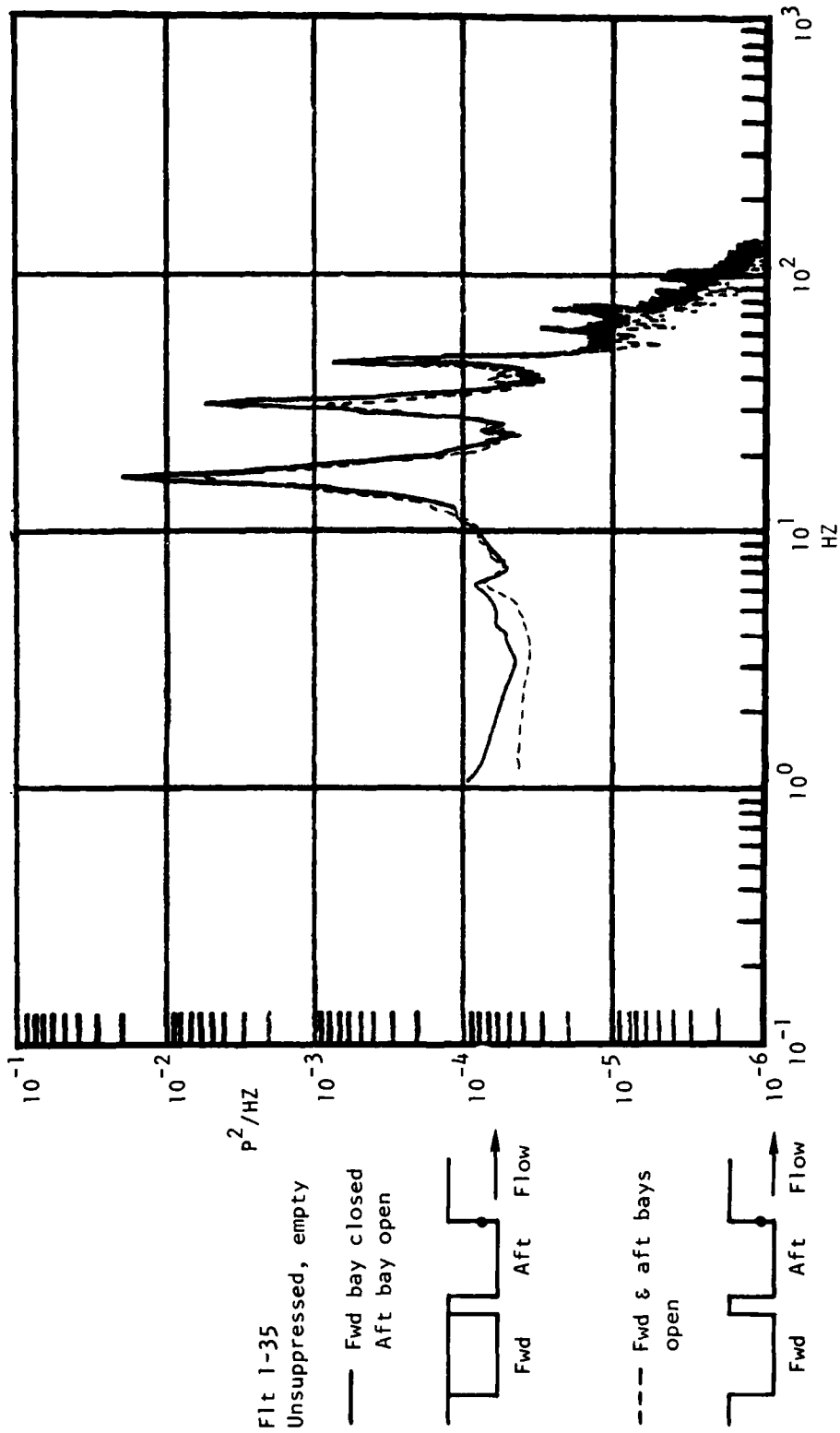
Figure 123. Full-Scale Flight Data, Adjacent Open Cavities, Mach 0.6, Full-Open Aft Bulkhead Upper

135
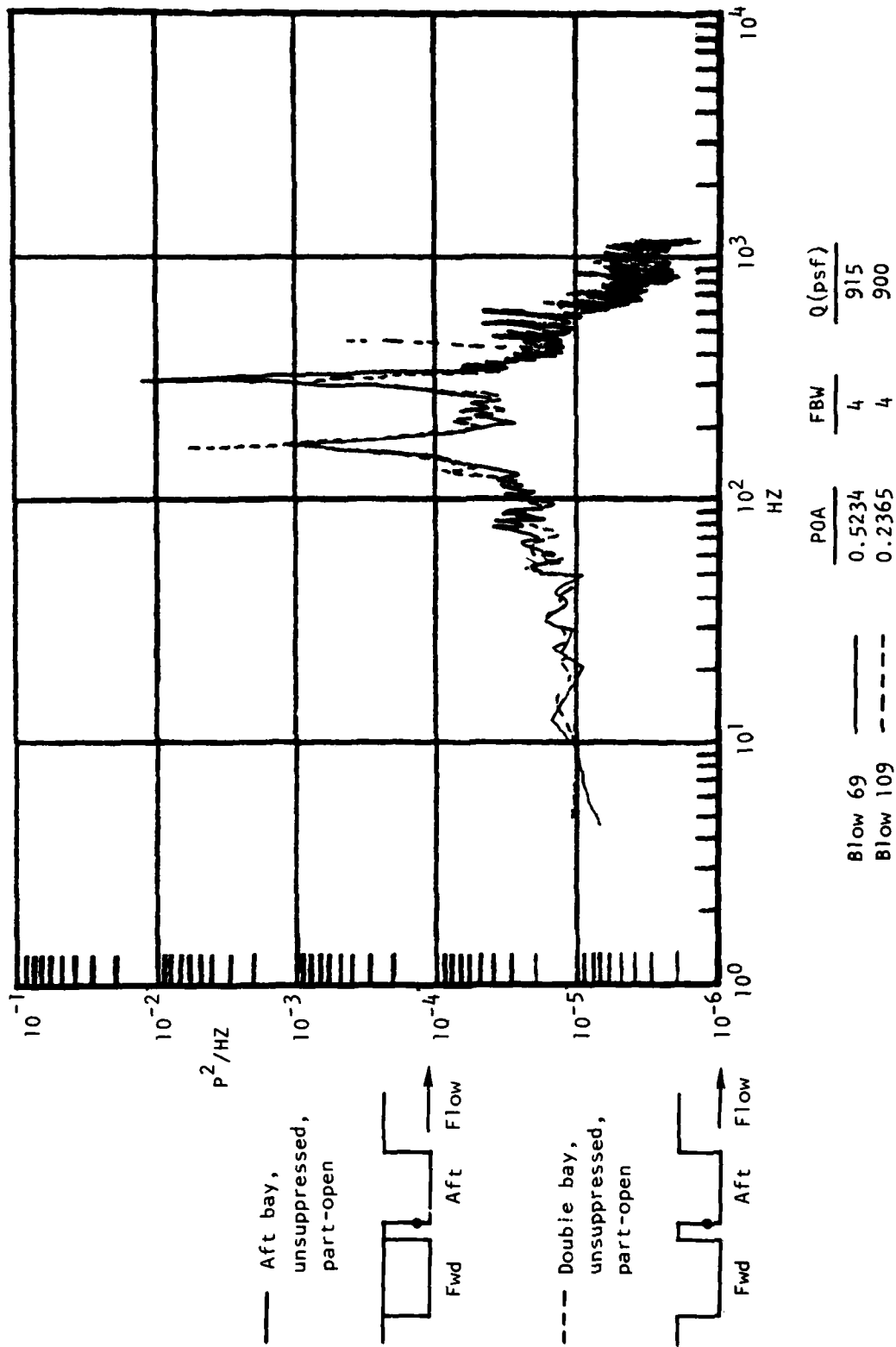
Figure 124. Adjacent Open Cavities, TWT 302 0.1-Scale Model Data, Mach 0.85, Part-Open, Forward Bulkhead Upper

136
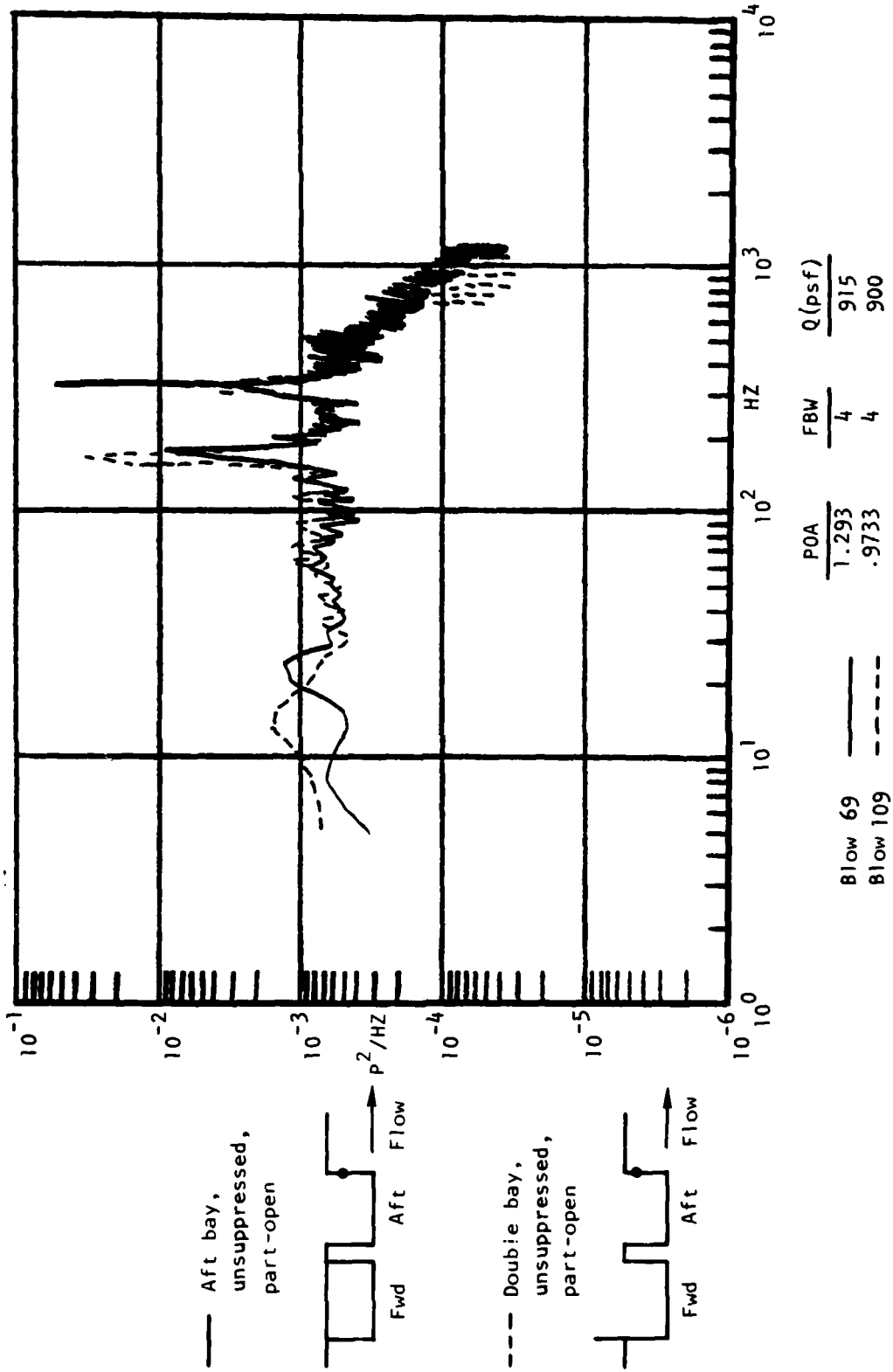
Figure 125. Adjacent Open Cavities, TWT 302 0.1-Scale Model Data, Mach 0.85, Part-Open, Aft Bulkhead Lower

137
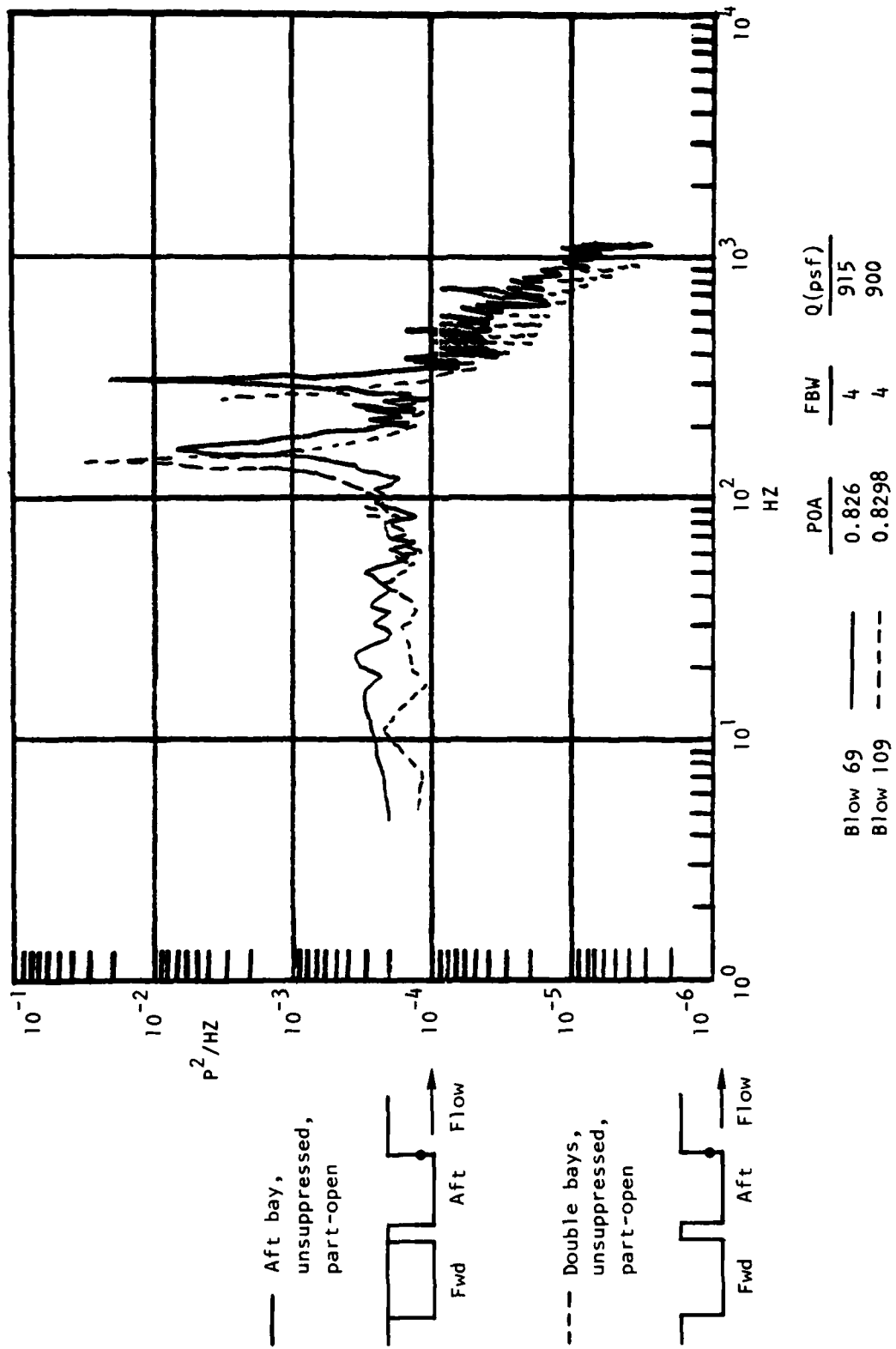
Figure 126. Adjacent Open Cavities, TWT 302 0.1-Scale Model Data, Mach 0.85, Part-Open, Aft Bulkhead Upper
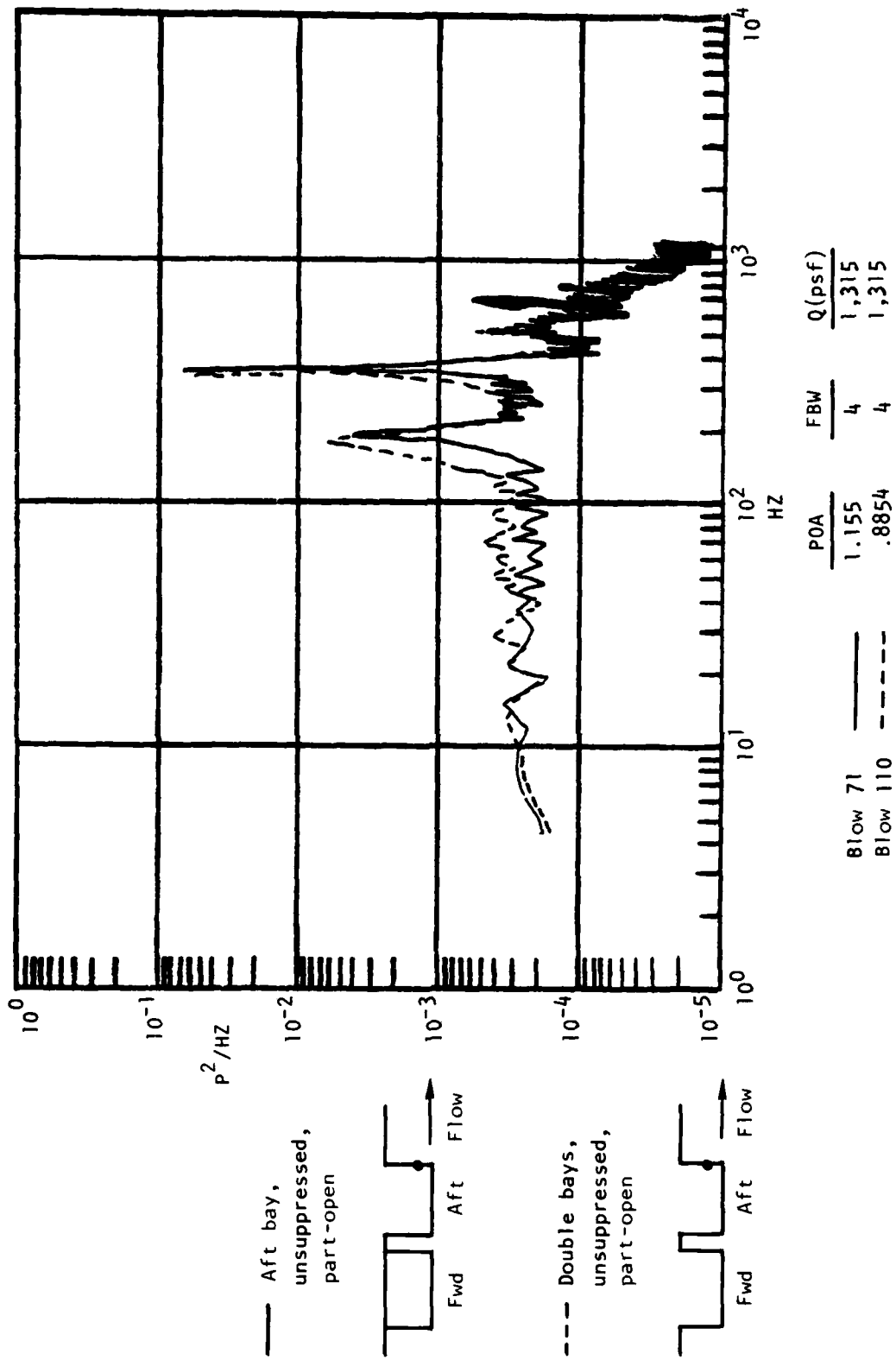
Figure 127. Adjacent Open Cavities, TWT 302 0.1-Scale Model Data, Mach 1.2, Part-Open, Aft Bulkhead Upper

139

Figure 128. Adjacent Open Cavities, TWT 302 0.1-Scale Model Data, Mach 1.2, Part-Open, Aft Bulkhead Lower
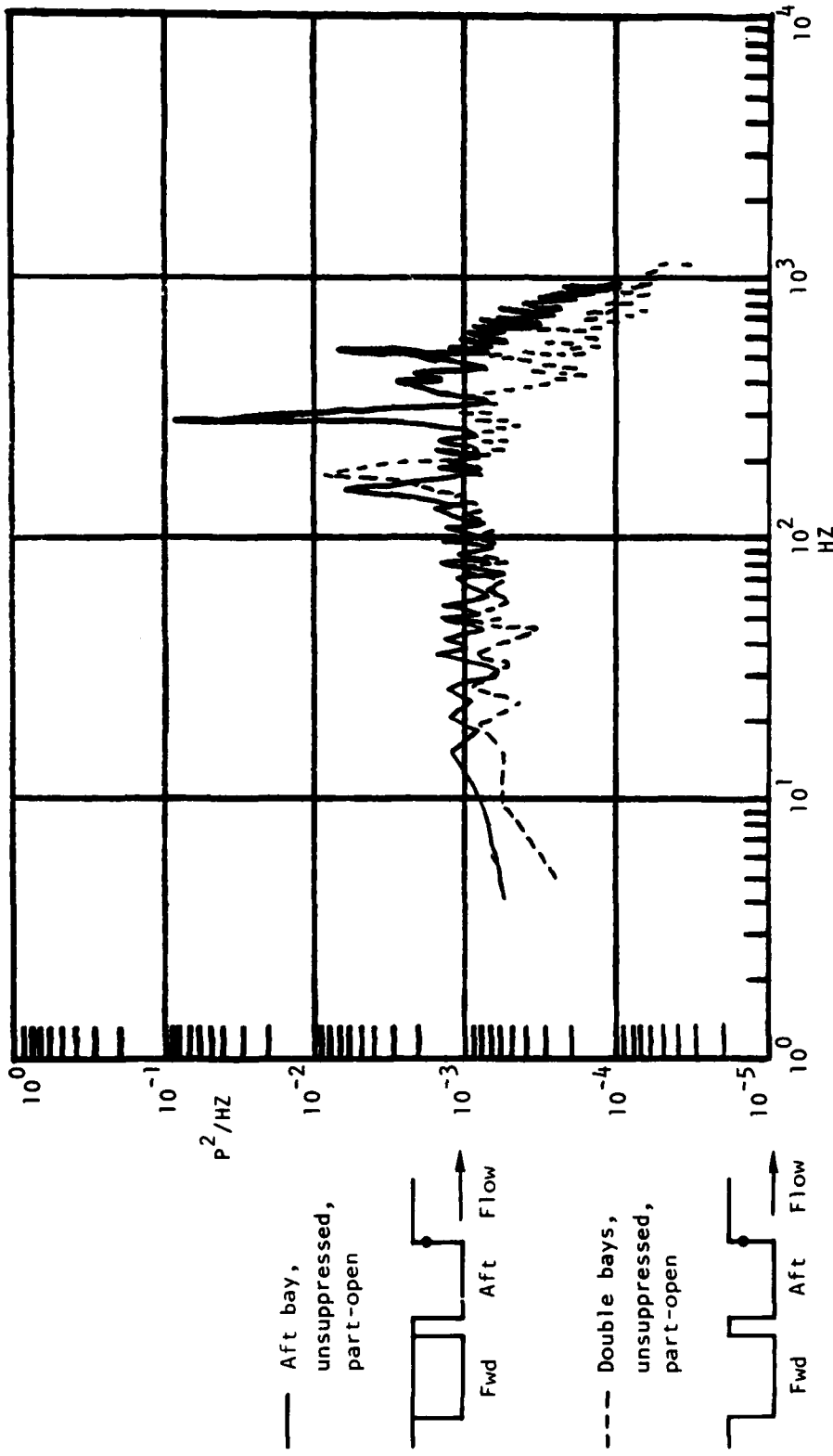
	POA	FBW	Q(psf)
Blow 71	1.67	4	1,315
Blow 110	1.123	4	1,315

Aft bay, unsuppressed, part-open

Double bays, unsuppressed, part-open

140
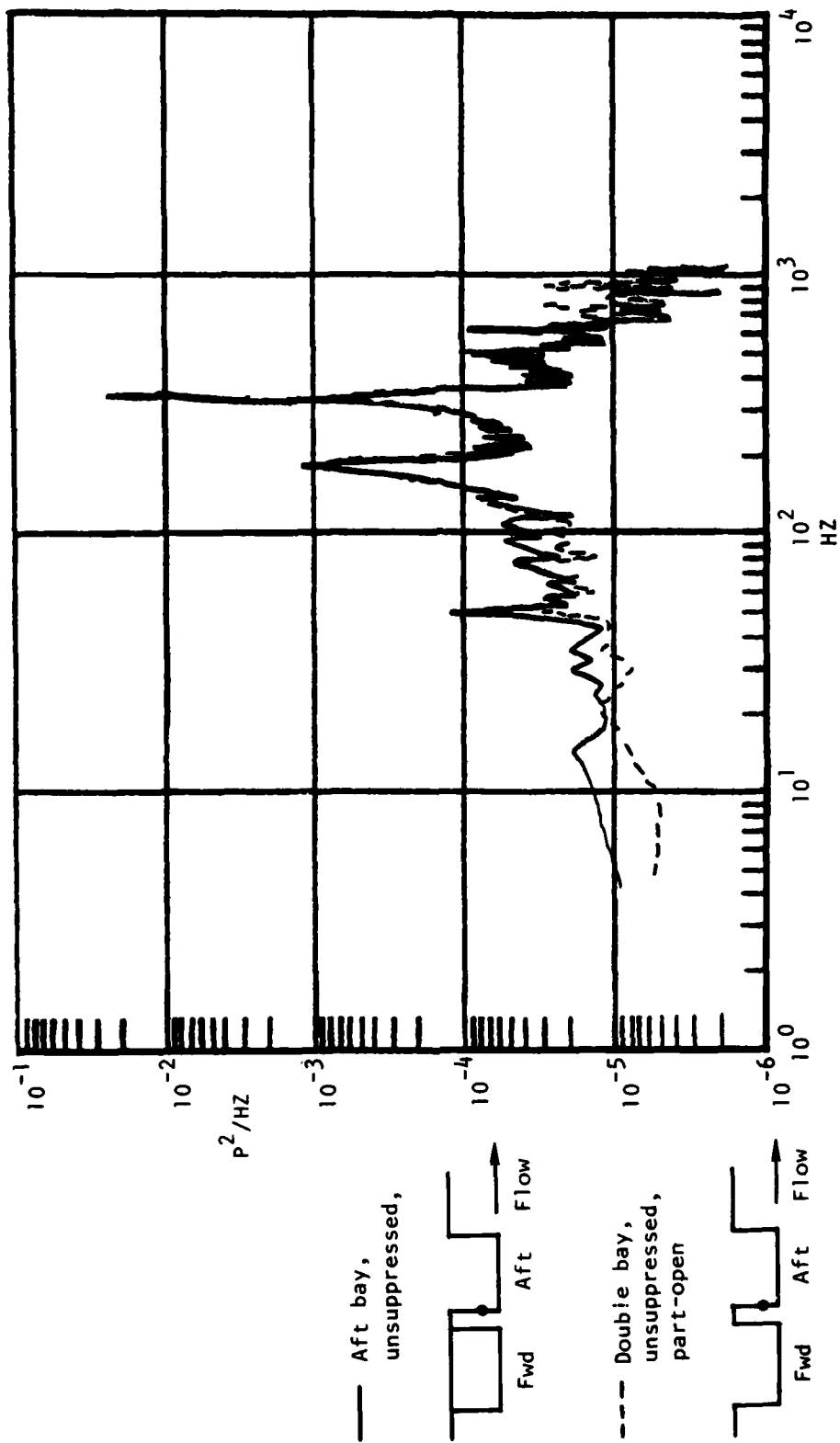
Figure 129. Adjacent Open Cavities, TWT 302 0.1-Scale Model Data, Mach 1.2, Part-Open, Forward Bulkhead Upper
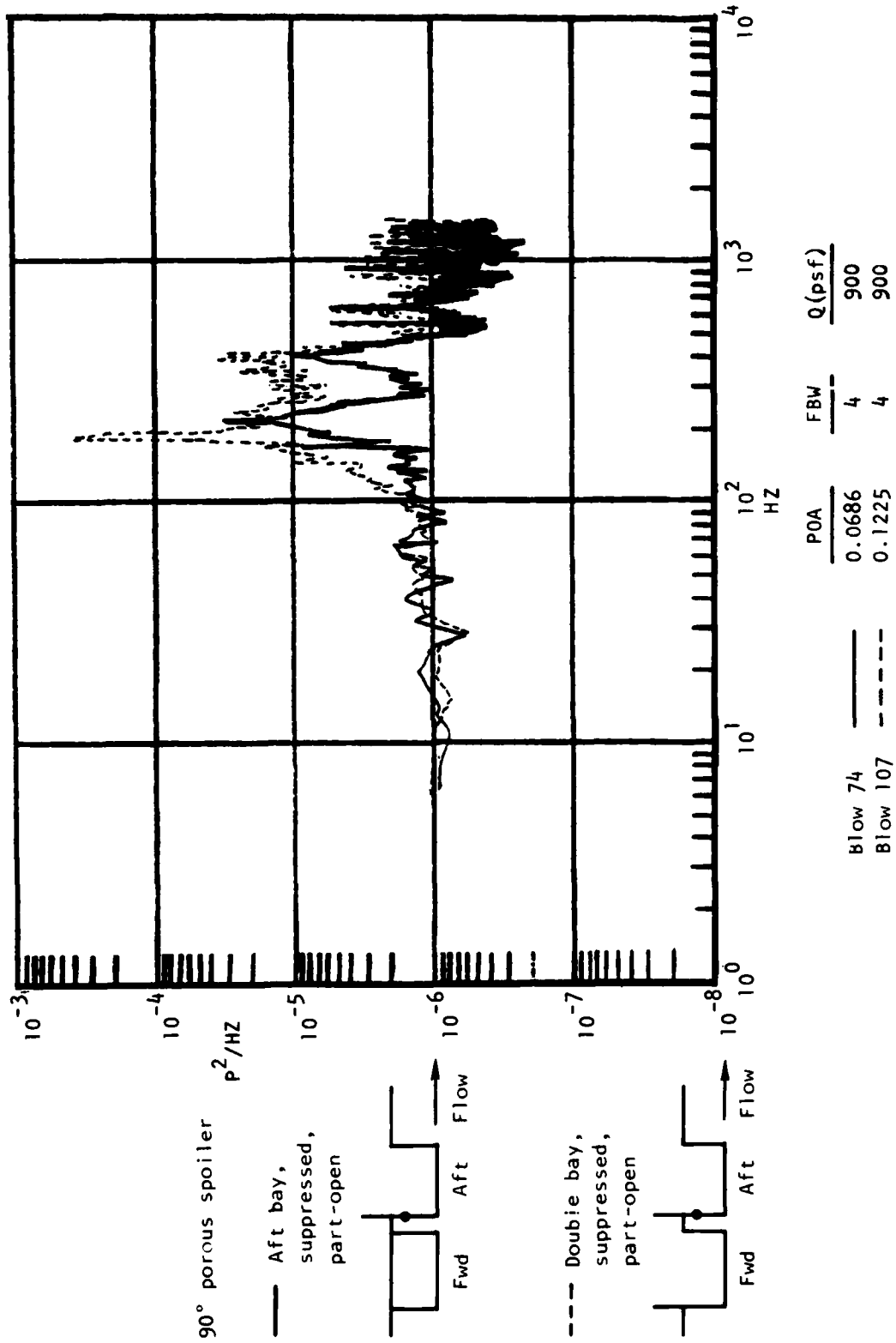
Figure 130. Adjacent Open Cavities, TWT 302 0.1-Scale Model Data, Mach 0.85, Part-Open, Forward Bulkhead Lower

142

Figure 131. Adjacent Open Cavities, TWT 302 0.1-Scale Model Data,
Mach 0.85, Part-Open, Aft Bulkhead Lower
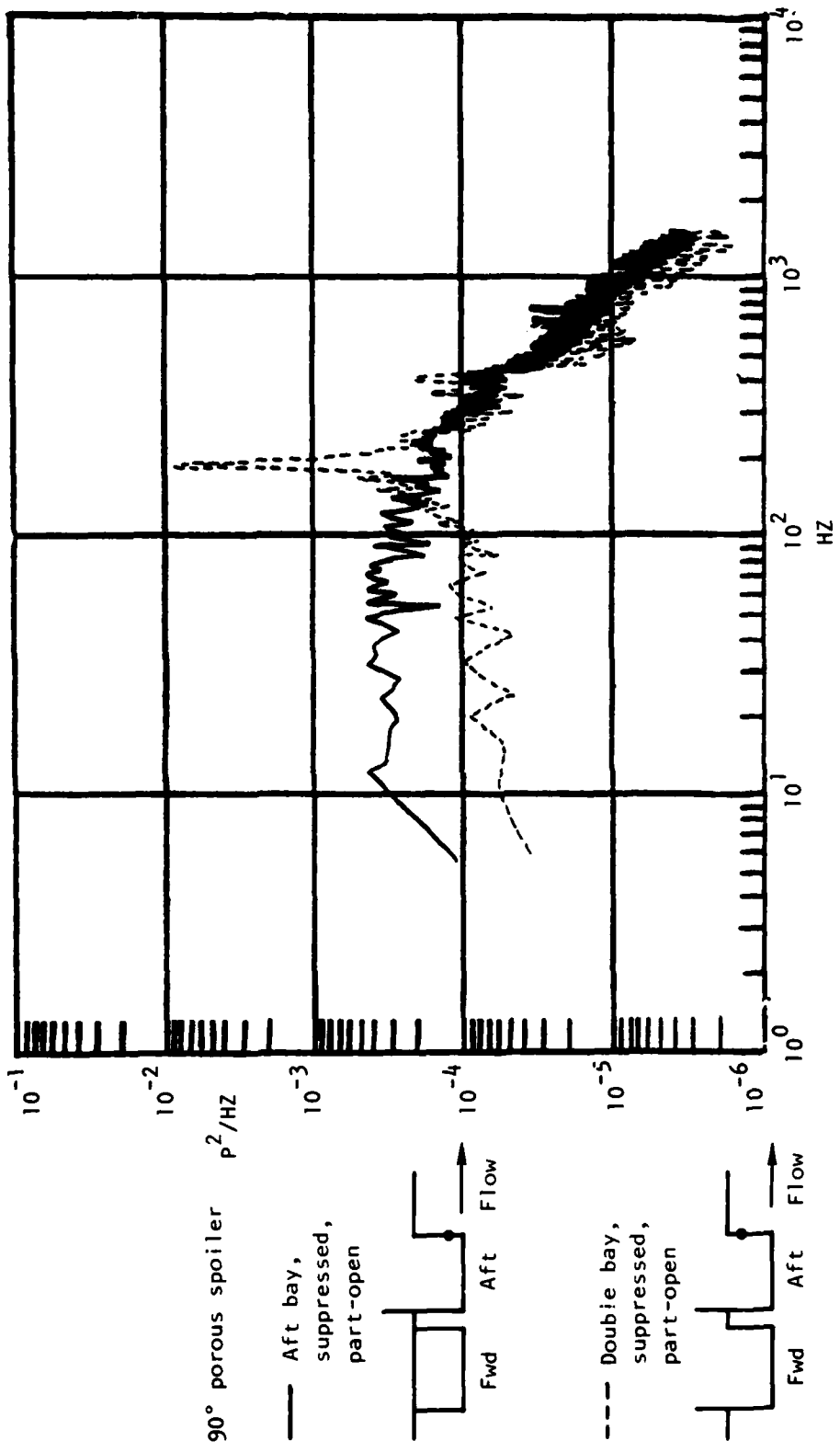
Figure 132. Adjacent Open Cavities: TWT 302 0.1-Scale Model Data
Mach 0.85, Part-Open Aft Bulkhead Upper
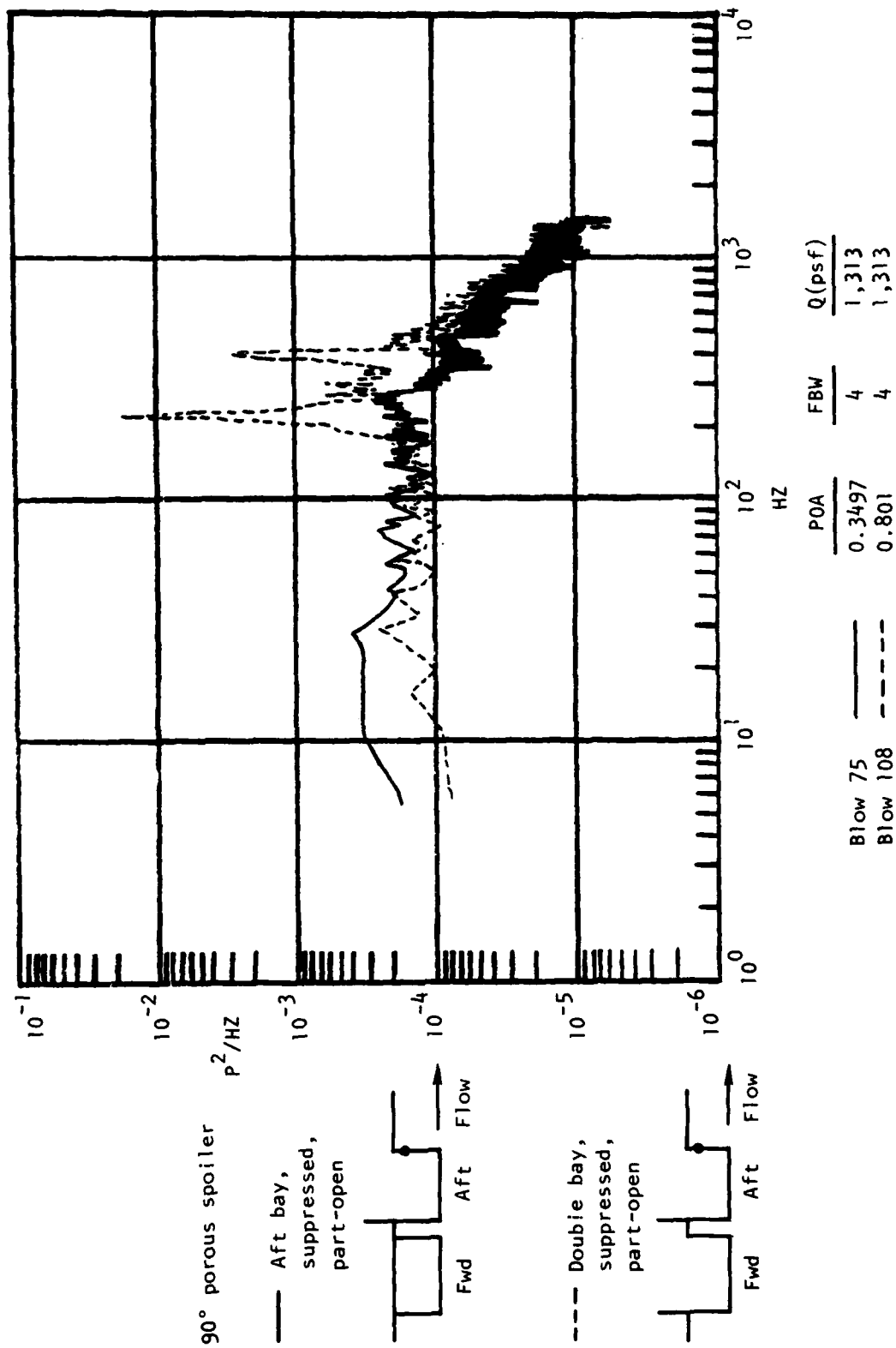
Figure 133. Adjacent Open Cavities, TWT 302 0.1-Scale Model Data, Mach 1.2 Part-Open, Aft Bulkhead Lower
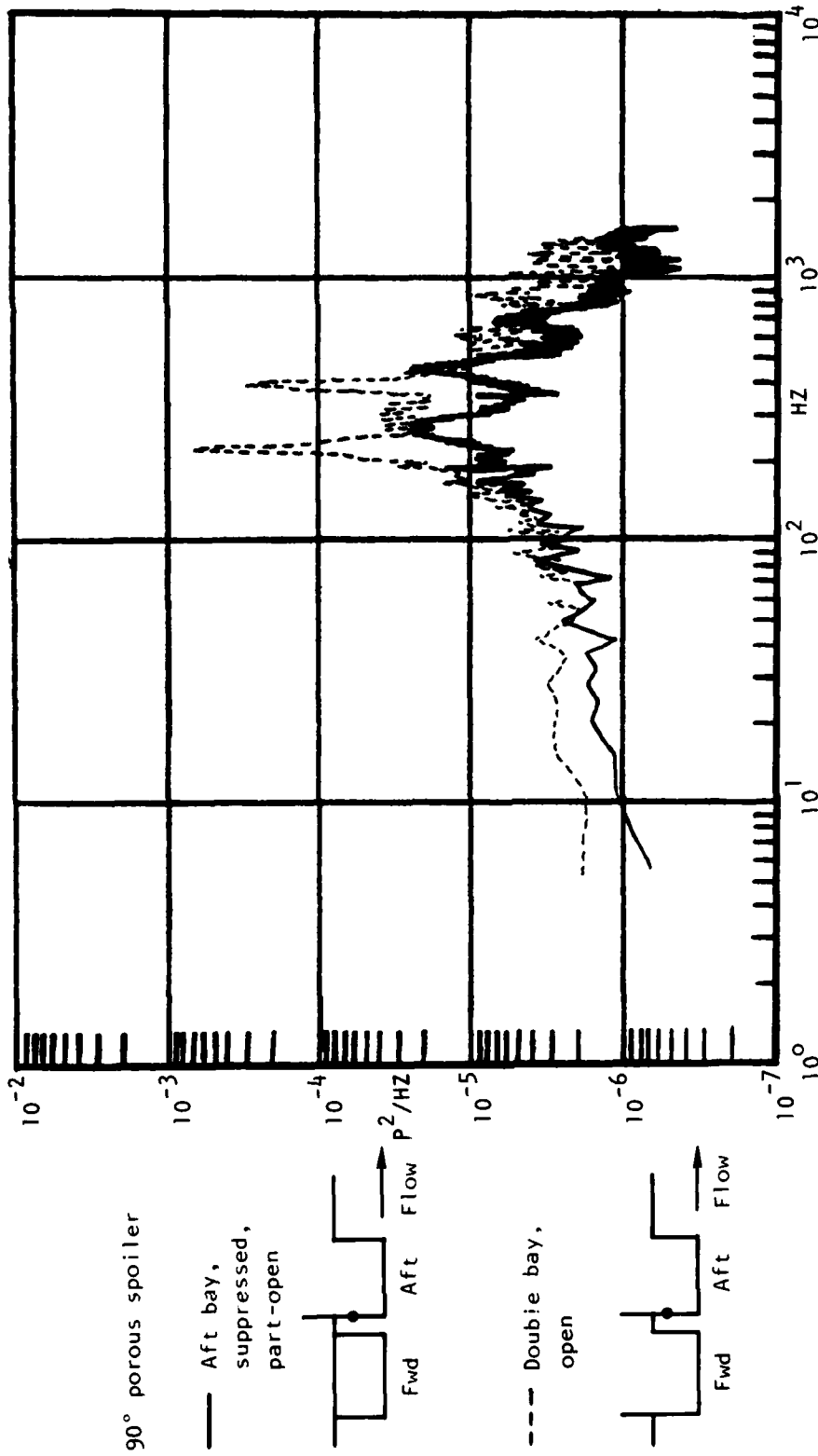
Figure 134. Adjacent Open Cavities, TWT 302 0.1-Scale Model Data, Mach 1.2, Part-Open, Forward Bulkhead Lower

146

Figure 135. Adjacent Open Cavities, TWT 302 0.1-Scale Model Data, Mach 1.2, Part-Open, Aft Bulkhead Upper

	P_{OA}	FRW	Q(psf)
Blow 75	0.3454	4	1,313
Blow 108	.5642	4	1,313
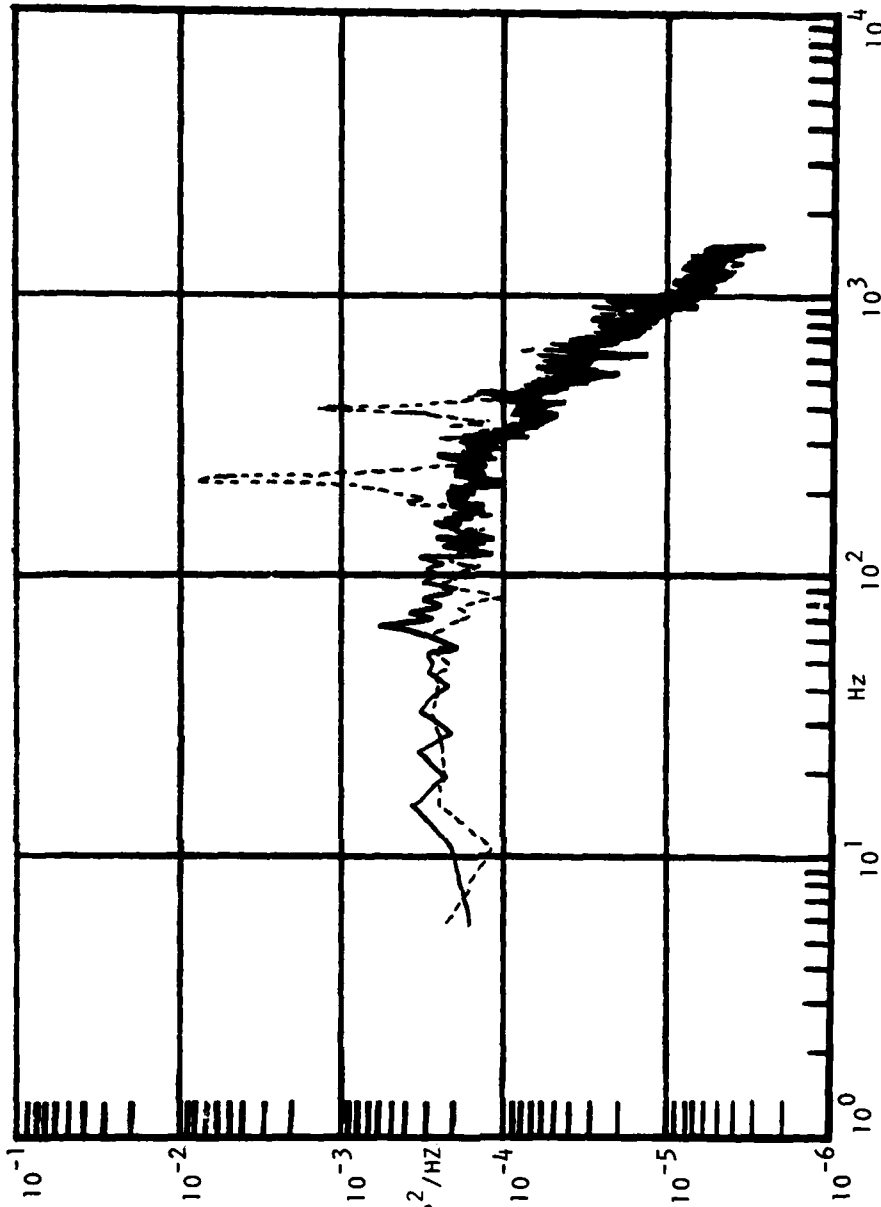
90° porous spoiler

— Aft bay, suppressed, part-open

Fwd Aft Flow
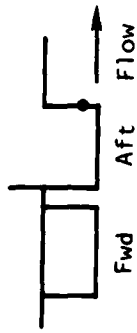
- - - Double bay, suppressed, part-open

Fwd Aft Flow

P^2/HZ

Hz

SECTION IV

EVALUATION OF PREDICTION METHODS

The prediction of cavity noise levels has been addressed by many investigators and is documented in the literature. Analytical and empirical prediction methods have been presented in the literature for empty unsuppressed cavities. Noise-prediction guidelines based on empirical data have been suggested for cavities with internal stores and two adjacent cavities in the streamline direction. The existing noise-prediction methods will be evaluated and correlated with B-1 empirical data. The evaluation of prediction methods and guidelines will address empty unsuppressed cavities, cavities with noise suppression devices, cavities with internal stores, and two streamwise adjacent cavities.

REVIEW OF PREDICTION METHODS

The cavity noise environment consists of discrete frequencies of resonating cavities and broadband noise for resonating and nonresonating cavities.

Prediction methods for cavity noise address the frequencies of cavity oscillation, amplitude and spatial distribution of the discrete resonances, and spectrum shape and spatial distribution of the random broadband cavity noise level.

Analytical cavity noise-prediction methods appear in References 1, 2, and 3. The techniques in Reference 1 use classical theoretical acoustic analysis in which the cavity responds to a forcing function at the natural frequencies of the enclosure. It is assumed that the boundary pressures in the shear layer at the cavity opening are the forcing function. Graphs and charts are presented to obtain estimates of the cavity noise level. The methods employed in References 2 and 3 use fluid elements with appropriate boundary conditions and numerical analysis techniques to obtain cavity response. Both methods seem to correlate well with the empirical data presented in References 2 and 3.

The numerical analysis methods seem promising, based on the initial published results, and perhaps could be expanded to include cavities of any shape with internal stores and possibly cavity noise-suppression mechanisms. The numerical analysis methods are more sophisticated than the classical methods of Reference 1 and include coupling effects of the shear layer and cavity internal acoustic response which is necessary for long shallow cavities L/D 2. These methods require a higher degree of analytical and programming skill to obtain solutions, but perhaps additional effort could result in a series of standard solutions for general cavity configurations that could be used by design personnel.

The prediction methods in Reference 4 through 12 are based on empirical techniques. The empirical techniques employ wind tunnel or full-scale data which are expressed in terms of flow paremeters such as dynamic pressure, mach number, and the cavity length/depth (L/D) ratio. The cavity response characteristics consist of fluctuating pressure amplitude variations throughout the cavity for discrete cavity oscillation frequencies and the broadband random noise levels. The empirical noise-level prediction methods provide estimates of the cavity frequencies and mode shapes, amplitude of the resonant responses, and amplitude and spectral content of the broadband noise.

148

Initial empirical cavity noise-prediction methods were presented in Reference 4 for shallow cavities. Improved prediction methods of References 5 and 6, based on flight-test data, include the effects of cavity L/D ratio, amplitude variation of each resonant mode, and updated pressure-level distribution within the cavity. Several investigations ([7], [8], and [9]) preceded that of Reference 6 in which several cavity L/D ratio ranges from 4 to 7 were evaluated. Several expressions for the amplitude of the cavity oscillation were presented. All reference materials use the same Strouhal number relationship to predict the cavity oscillation frequencies. The methods presented in Reference 6 extended the applicability of the prediction methods from L/D of 4 to L/D of 2. The prediction method in Reference 5 is based on small-scale wind tunnel data in the L/D range from 2 to 7. Additional prediction methods are also presented in References 10, 11, and 12. The prediction methods identified previously use different relationships for noise prediction in some cases. The various prediction methods will be compared using the B-1 weapon bay cavity noise levels recorded in small-scale wind tunnel models and full-scale aircraft.

CORRELATION OF PREDICTION METHODS WITH B-1 DATA

The B-1 weapon bay has a L/D ratio of 2, which is in the low range of shallow cavities and the high range of deep cavities. The B-1 cavity could be considered to be in the transition region between shallow and deep cavities.

Open cavities exposed to external flow fields basically fall into two categories, short deep cavities L/D 1 and long shallow cavities L/D 1. Depth modes are predominant for deep cavities, and longitudinal modes are dominant in shallow long cavity. A sharp distinction between short deep cavities and long shallow cavities obviously does not exist, and a gradual transition takes place between the two cavity types. From a practical point of view, the transition region between long and short cavities occurs at approximately L/D=2. For long cavities, the internal acoustic modes of the enclosure are coupled and cannot be considered separately with the shear layer motion in the cavity opening. For short cavities with a much smaller opening, the effects of the shear layer coupling are less important, and the cavity response approaches that of a hard-wall acoustic enclosure. For cavities in the transition region, L/D = 2, characteristics of short and long cavities may occur.

Prediction methods have been developed for deep and shallow cavities. The B-1 data presented in Section III will be correlated with prediction methods for deep cavities with predominant depth modes and shallow cavities with predominant longitudinal modes.

The data correlations with the various prediction methods will address empty unsuppressed cavities, noise-reduction devices, internal stores, and two adjacent streamwise cavities. The cavity noise level for discrete oscillation and broadband noise will be evaluated independently.

The prediction methods for empty unsuppressed cavities will be evaluated first. This is considered to be a baseline case, and the effects of noise reduction devices, internal stores, and adjacent cavities will be expressed in terms of noise-level differences relative to an empty unsuppressed cavity.

149

EMPTY UNSUPPRESSED CAVITIES

The unsuppressed empty cavity which is considered a baseline for subsequent evaluations will address all characteristics of the cavity noise environment. Depth and longitudinal modes will be considered. The frequency of the discrete modes, mode shapes, and pressure amplitudes for cavity oscillations will be evaluated. Evaluation of the broadband noise component of the cavity noise environment will address the spectral content, pressure amplitude, and distribution within the cavity.

CAVITY DEPTH MODE - DEEP CAVITIES

It is possible that depth modes could occur in cavities of L/D = 2. These cavities are in the transitional regions between deep and shallow cavities. The frequency of the first cavity depth mode was predicted using the methods of References 1 and 10. The predicted depth modes are shown in Figures 136 and 137. The method of Reference 1 shown in Figure 136 predicts a depth mode at 24 Hz. The method of Reference 10 shown in Figure 137 predicts a depth mode at 40 Hz which has maximum intensity at the bottom of the cavity away from the open side.

The B-1 cavity noise data do not show frequencies at 24 Hz as shown in Figure 136. The B-1 data in Figure 137 are shown for various cavity depths and compared to the predicted fundamental cavity depth mode at 40 Hz. The predicted depth mode noise level varies from maximum at the cavity bottom away from the open side to minimum at the cavity opening. The B-1 data at 40 Hz (Figure 137) do not show a consistent variation as a function of cavity depth and do not correlate with the predicted cavity depth mode. It is concluded that the cavity depth modes do not exist in the B-1 cavities of L/D = 2. The preceding evaluation and characteristics of the noise presented in Section III indicate the B-1 cavity is acting like a shallow cavity, with longitudinal oscillation modes dominant. The remainder of the prediction method evaluation will, therefore, address longitudinal pressure oscillations of a shallow-type cavity.

DISCRETE FREQUENCY OSCILLATIONS - SHALLOW CAVITY

The cavity oscillation frequencies are correlated using a modified Rossiter formula which is derived from the Strouhal number and characteristics of the vortex flow field convected over the cavity opening.

$$f_m = \frac{V}{L} \left[\frac{m - 0.25}{\frac{M}{(1 + \frac{K-1}{2} M^2)^{1/2}} + 1.75} \right]$$

f = frequency
L = cavity length
V = free-stream velocity
M = free-stream mach no.
m = mode No. 1, 2, 3,...

150
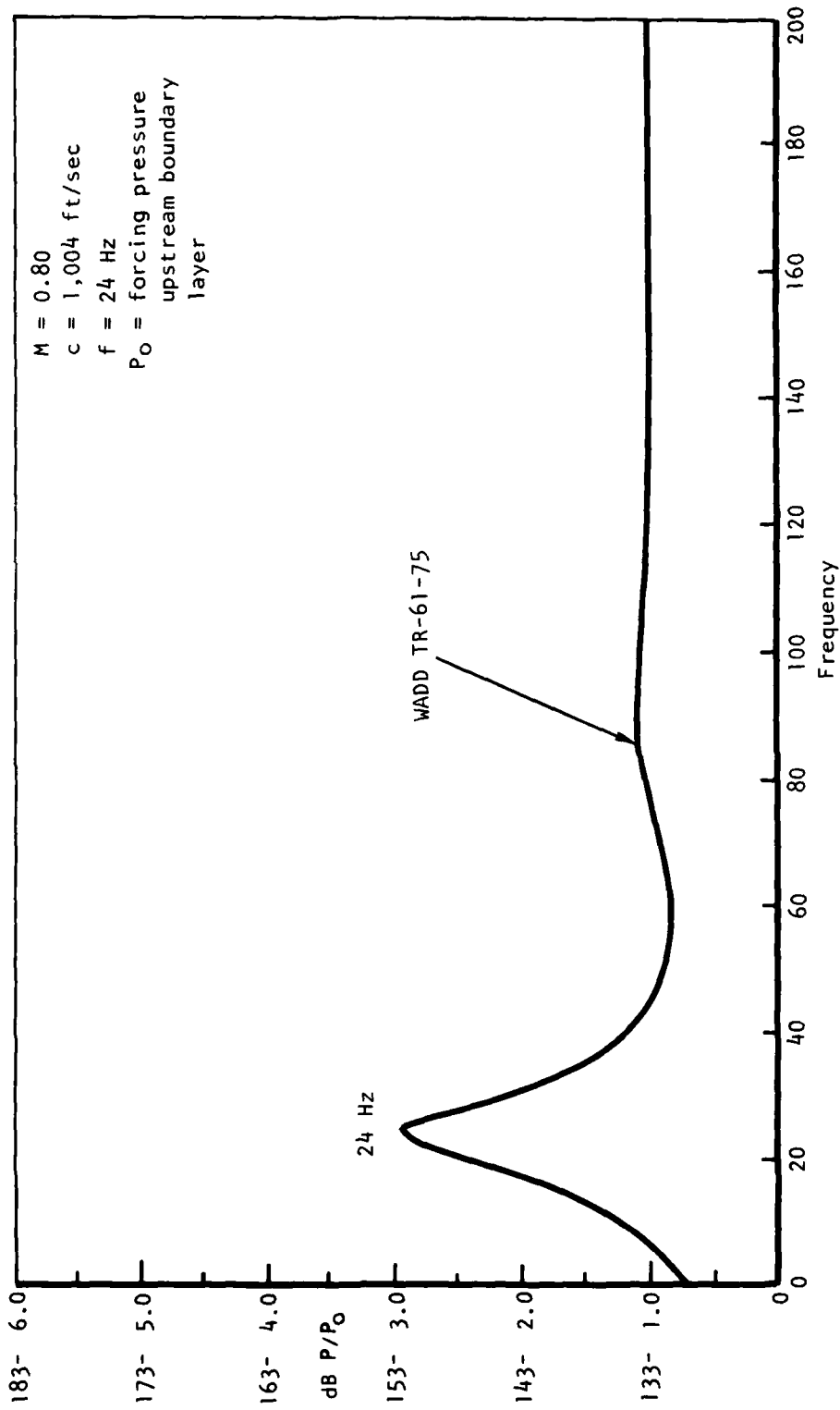
Figure 136. Fundamental Depth Mode

151
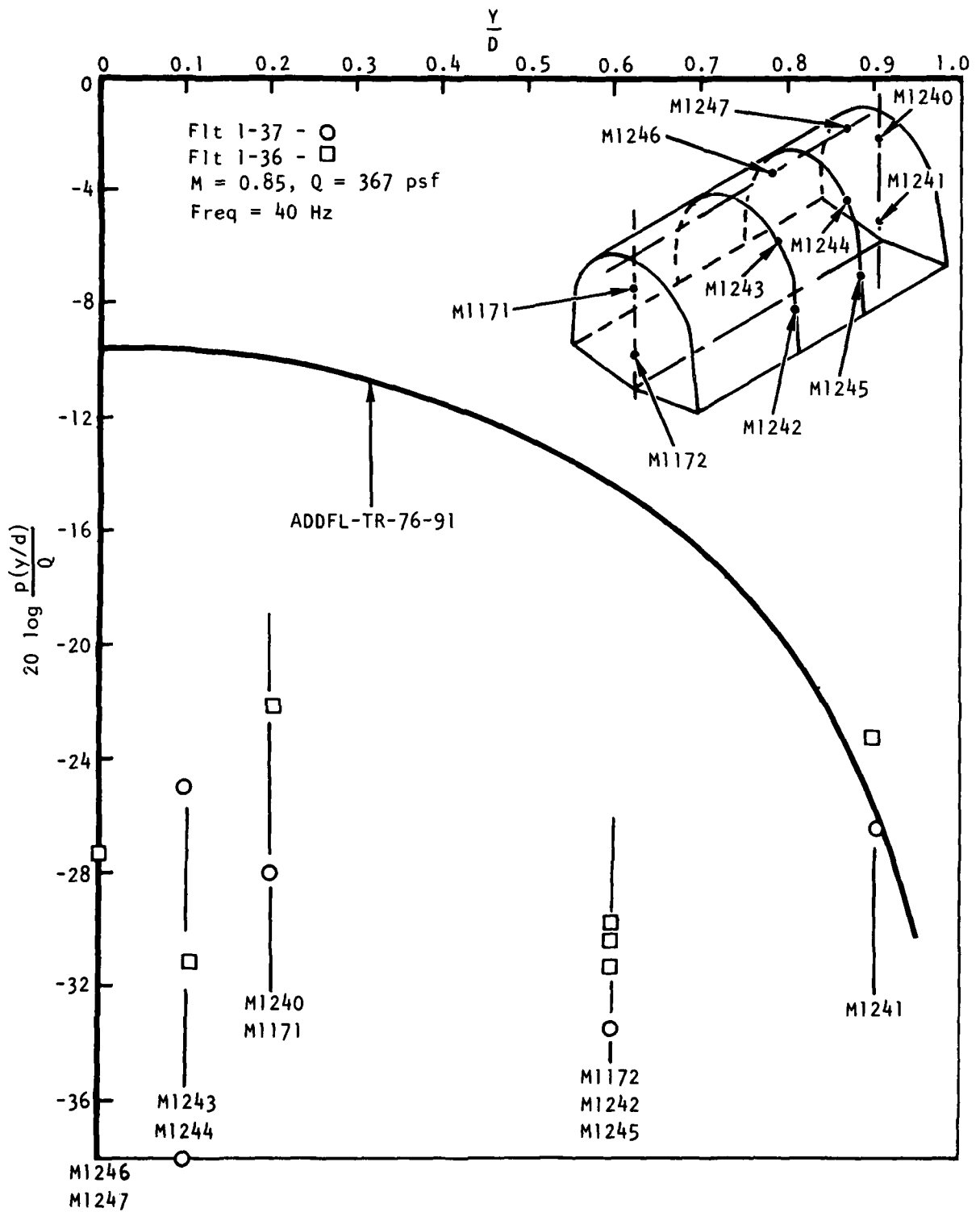
Figure 137.   Fundamental Depth Mode, Theoretical
Prediction Versus Experimental

152

The frequency of the cavity oscillations are shown in Figures 138 and 139 for the first four resonant modes for part- and full-open door positions. The data are correlated with Strouhal number and plotted as a function of mach number. The modified Rossiter equation is currently used in Reference 4, 5, and 6 to predict the cavity oscillation frequencies.

The B-1 data correlate very well with the modified Strouhal number relationship for the full-scale and wind tunnel data as shown in Figures 138 and 139 for the first four cavity modes. The B-1 data are plotted for each mode and identified by symbols in Table 1 of Section III. The B-1 cavity data indicate no appreciable difference in the cavity oscillation frequencies for part- or full-open doors. The frequency prediction shows good correlation between model and full-scale data when relative cavity scale factors are considered. The accuracy of predicting the cavity oscillation frequencies with the modified Rossiter equation is considered excellent.

PRESSURE AMPLITUDE-DISCRETE FREQUENCIES

The B-1 cavity noise-level data for the full-scale aircraft and the wind tunnel models were recorded with part- and full-open doors at numerous locations inside the weapon bay cavity. Table 1 identifies the flight conditions and type of empirical data presented on subsequent data plots.

The amplitudes of the first four cavity resonances are shown in Figures 140 through 155 on the aft bulkhead for lower and upper locations for part- and full-open door positions. The cavity noise-prediction methods of References 4, 5, and 6 are shown for comparison with the measured full-scale and wind tunnel B-1 cavity noise levels. The pressures recorded at various mach numbers and dynamic pressures for the full-scale and wind tunnel models are normalized to dynamic pressure and plotted as a function of mach number for each of the first four cavity resonant frequencies.

The normalized pressures for the wind tunnel and the full-scale data show considerable scatter for the same mach number. In some cases, reasonable correlation exists at the same mach number for the normalized full-scale and wind tunnel pressure amplitudes, but on the average, the small-scale wind tunnel data shown higher pressure amplitudes.

In general, the prediction method of Reference 6 best matched the empirical B-1 cavity noise data. The initial method of Reference 4 predicts a very conservative envelope for the B-1 cavity noise data. Both of these methods predict maximum levels for all modes in the transonic speed range, decreasing to lower levels at supersonic mach numbers. The prediction method of Reference 5, however, predicts an increasing magnitude as a function of mach numbers, leading to conservative estimates of cavity noise at supersonic speeds.
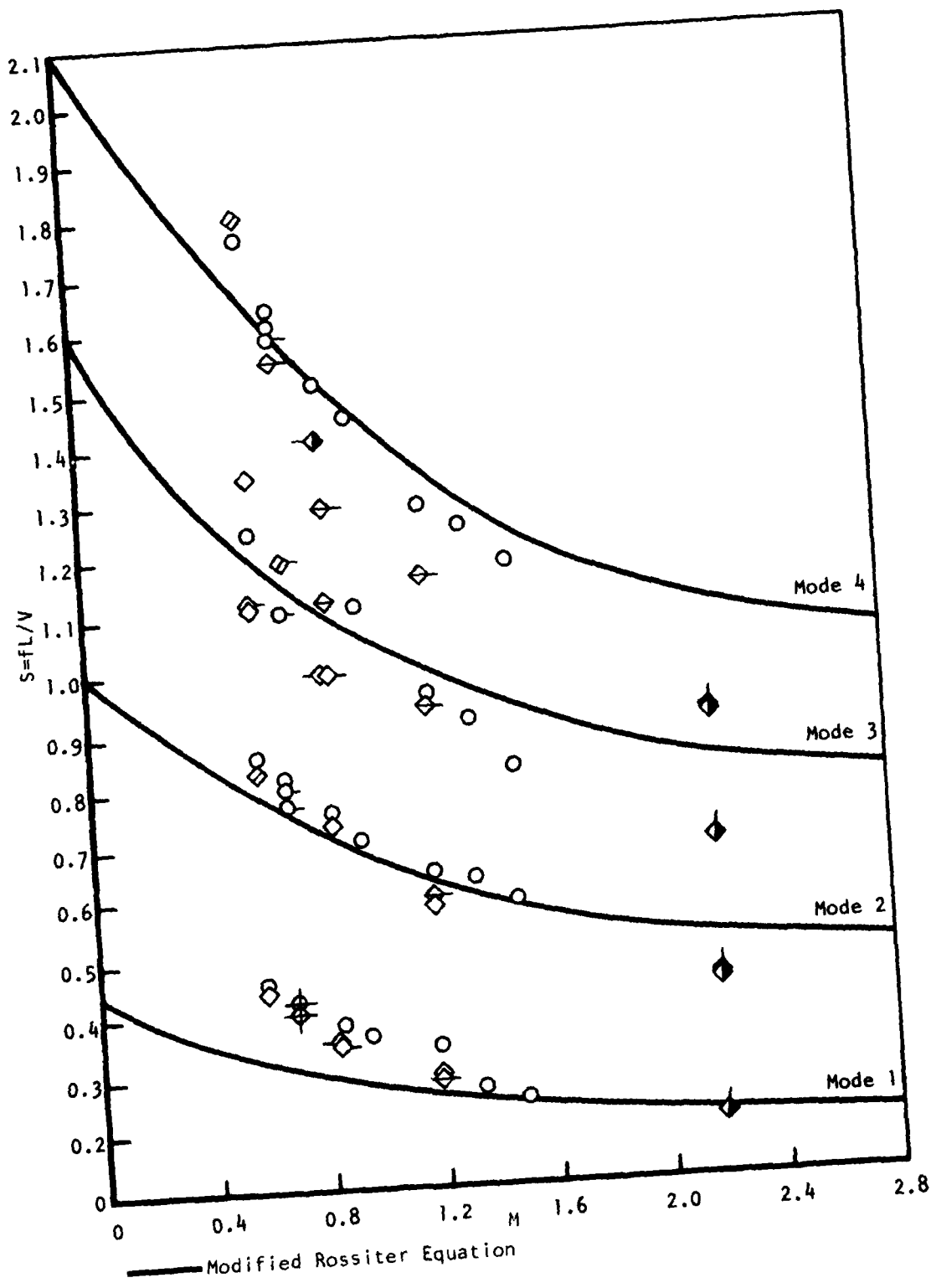
Figure 138. Part-Open Doors, Cavity Discrete Frequency, L/D = 2.0

154
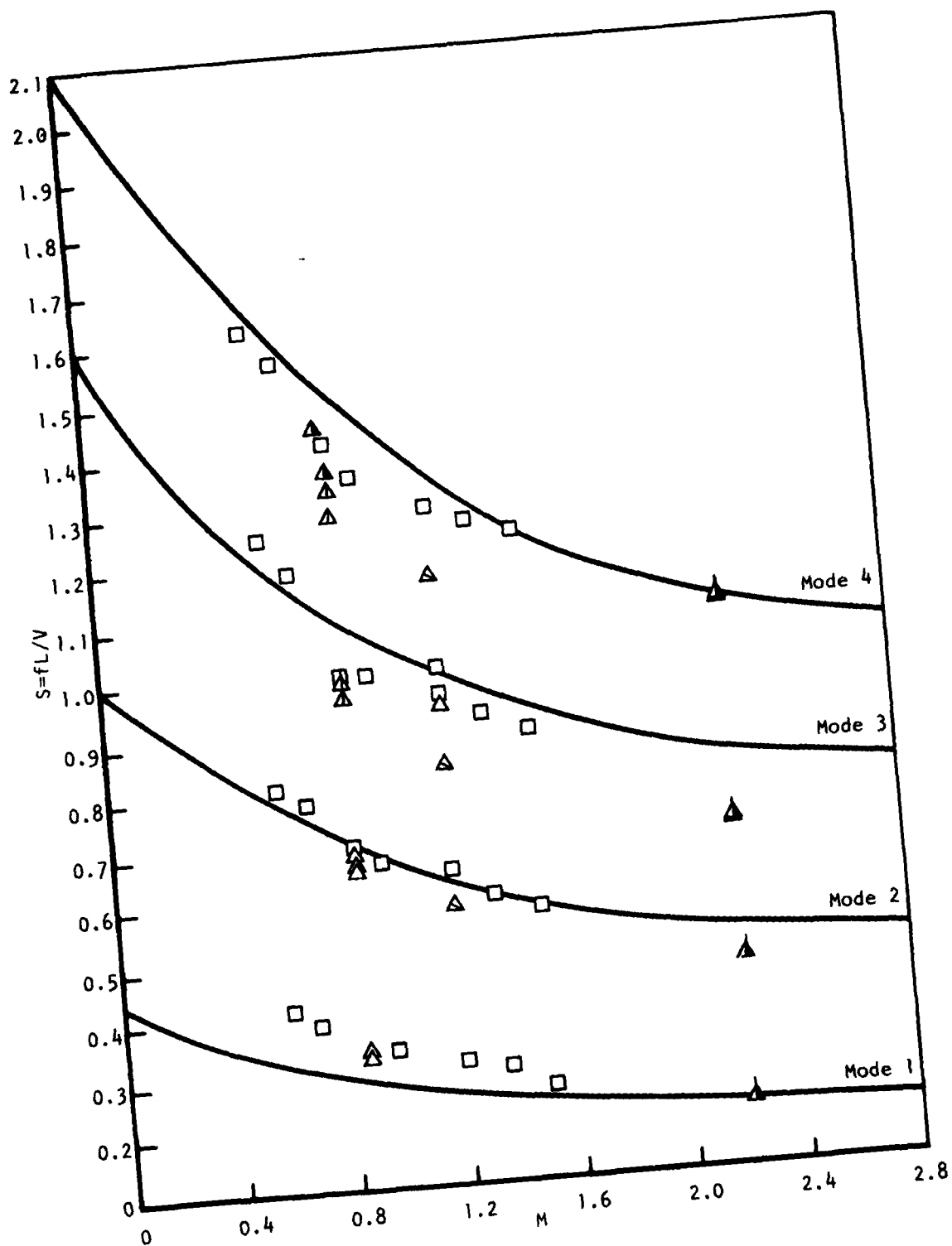
Figure 139. Full-Open Doors, Cavity Discrete Frequency, L/D = 2.0

155
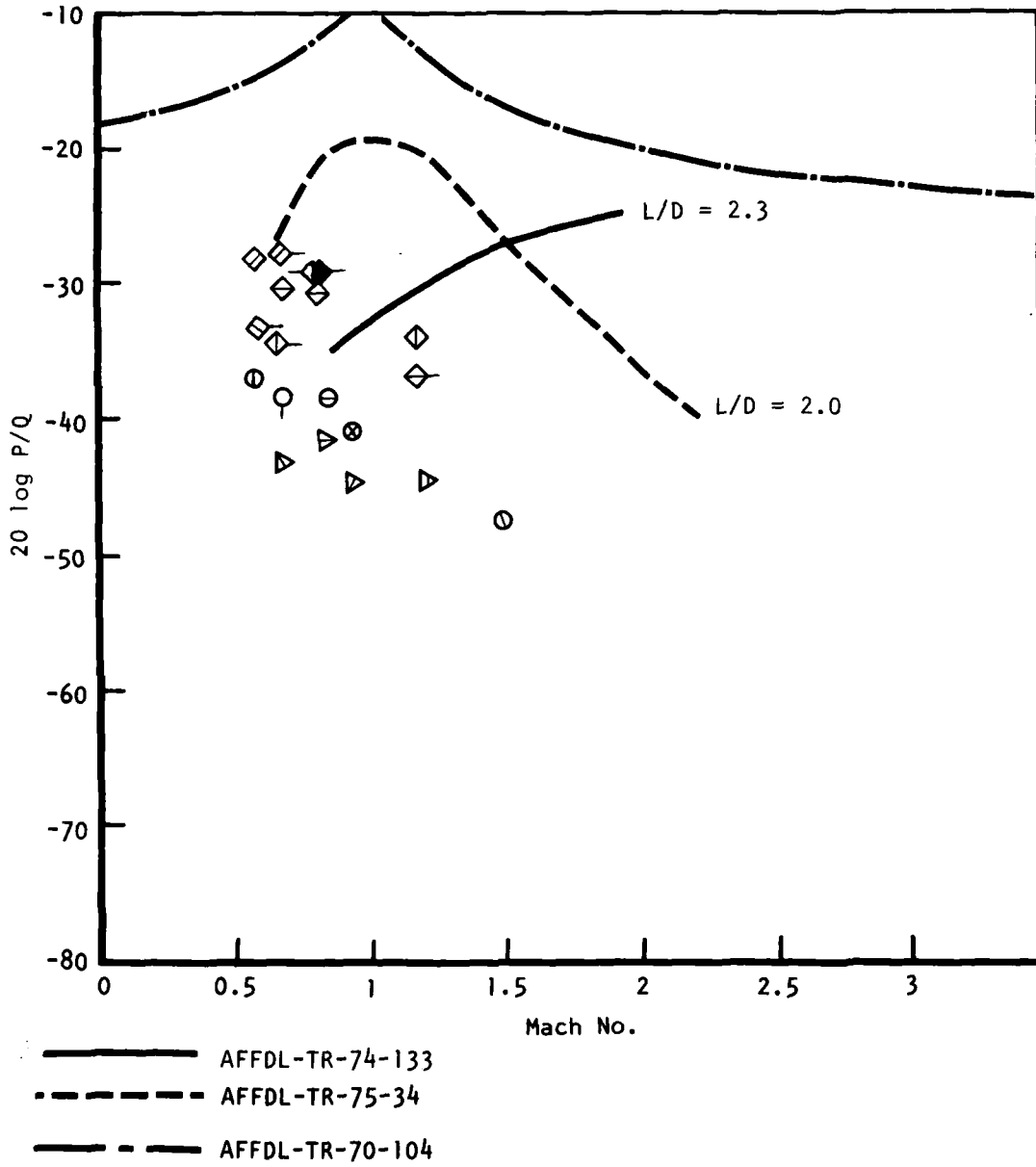
Figure 140. Mode 1 PO Aft Bulkhead, Lower
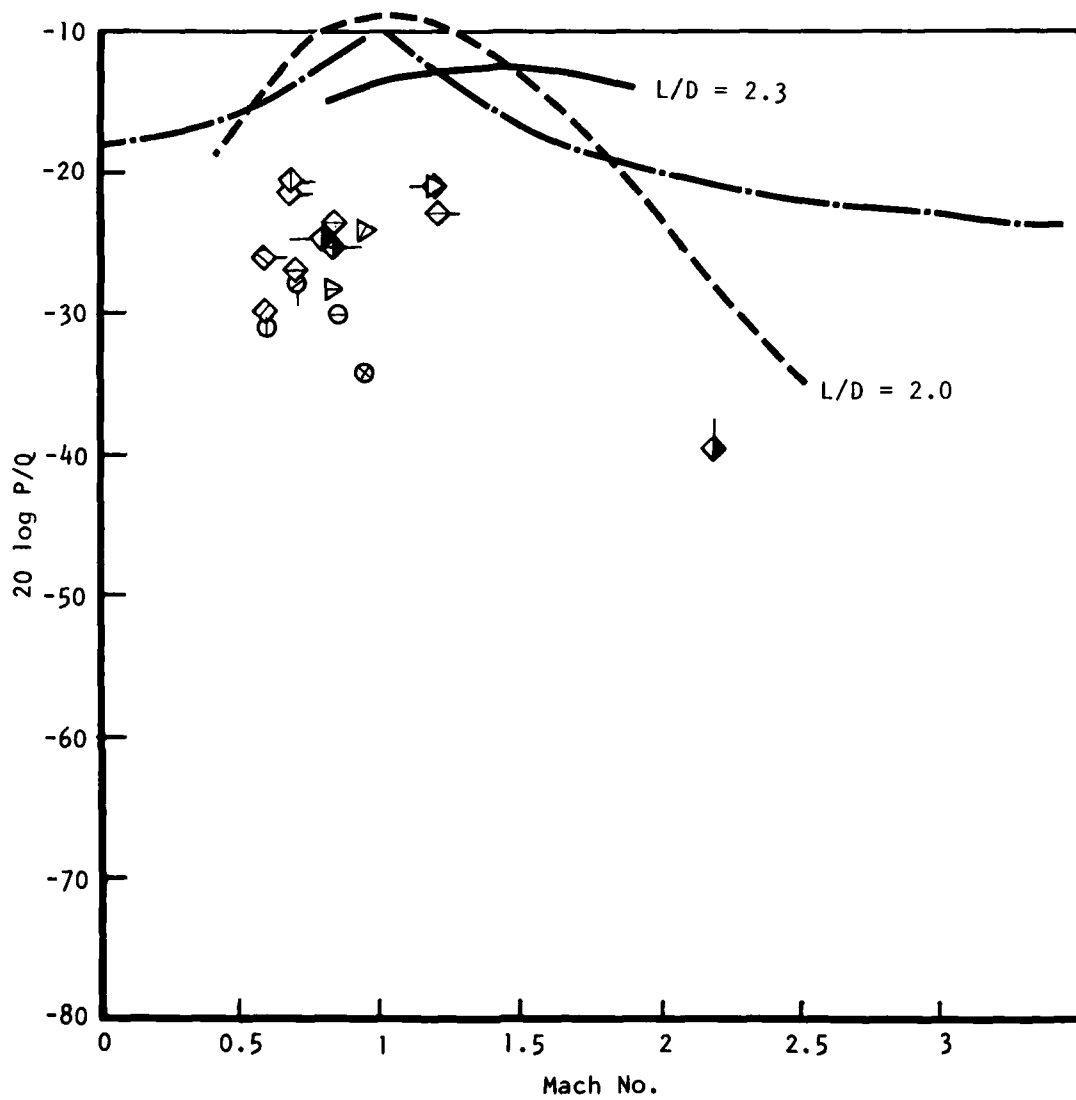
Figure 141. Mode 2 PO Aft Bulkhead, Lower

157
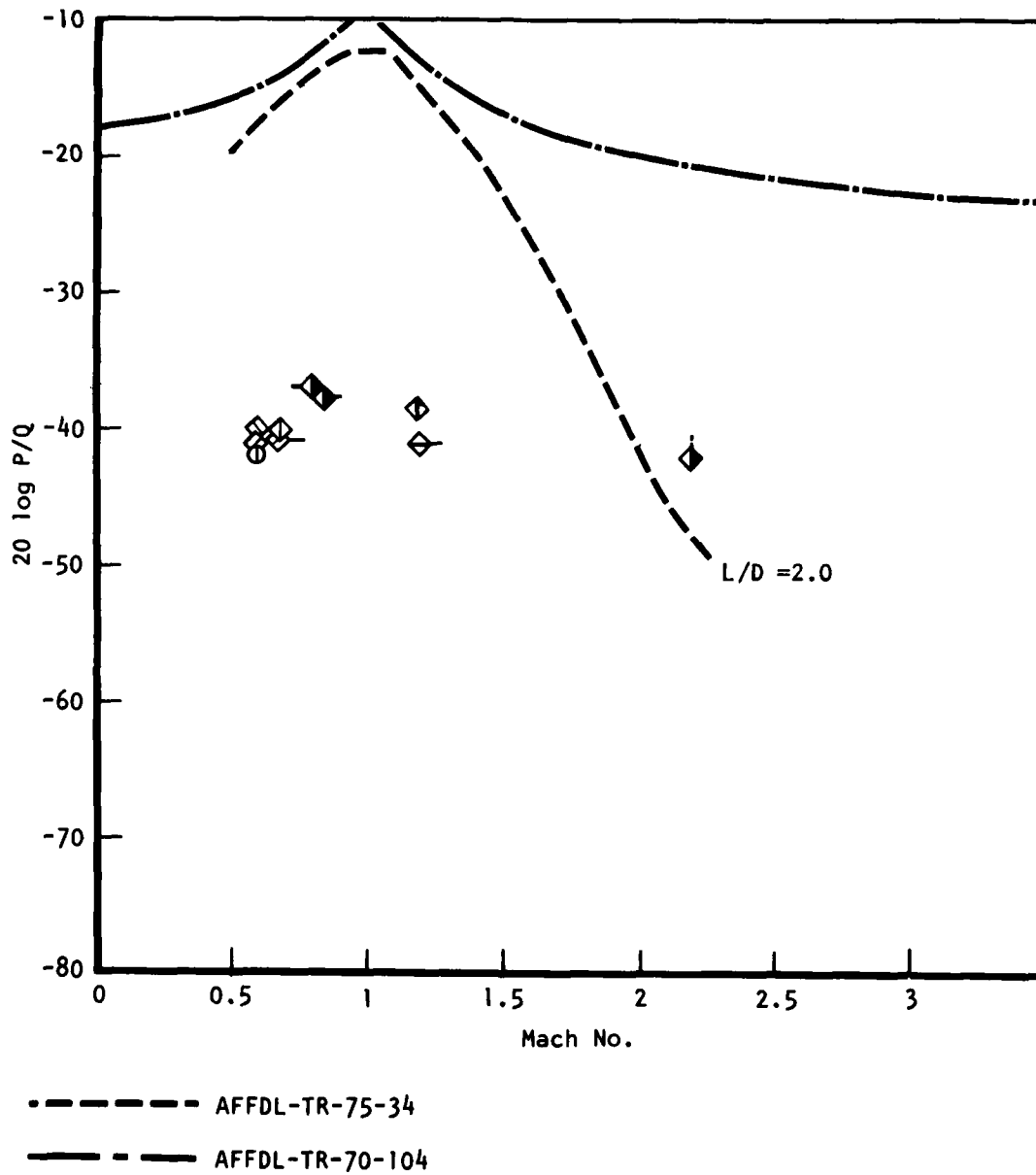
Figure 142. Mode 3 PO Aft Bulkhead, Lower

158
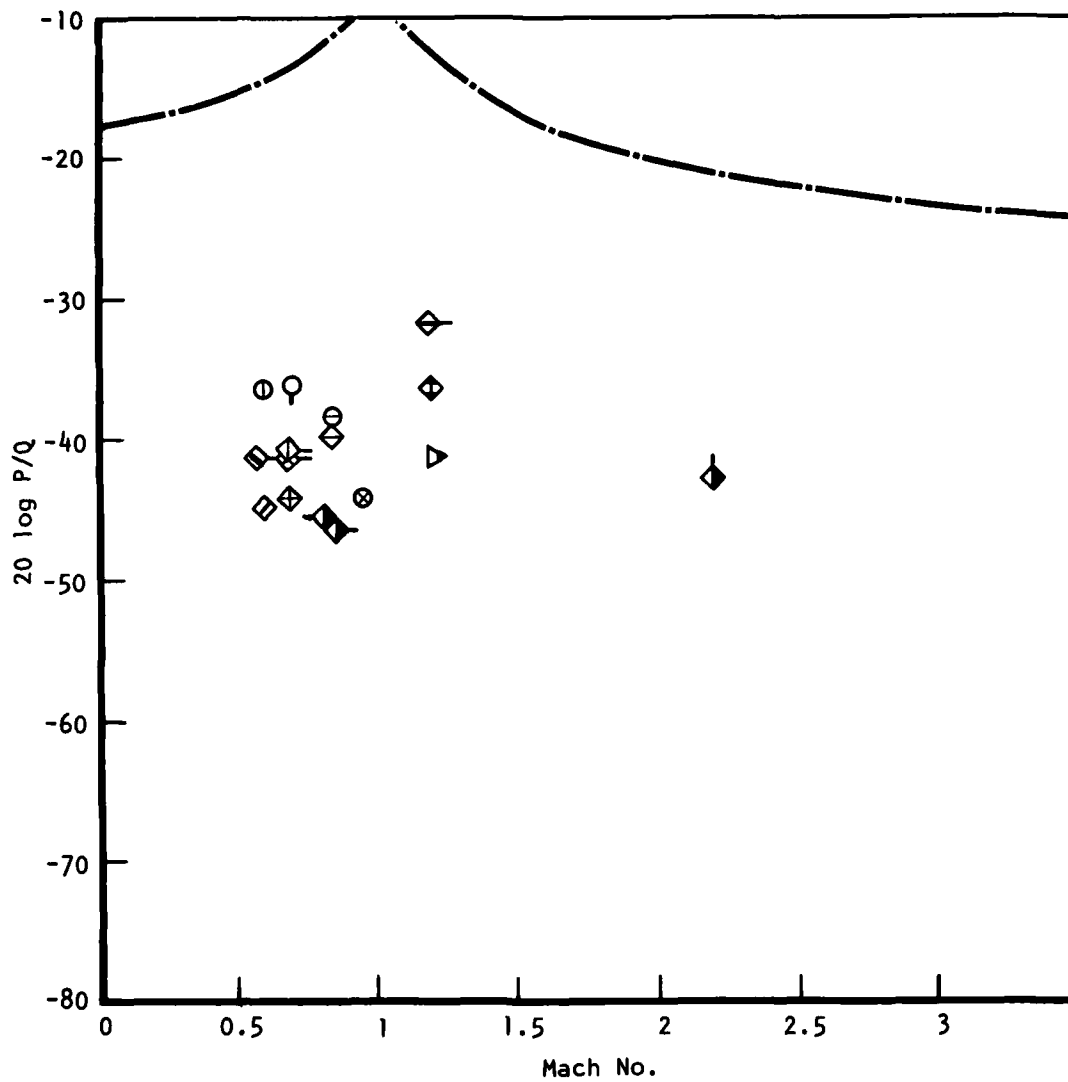
Figure 143. Mode 4 PO Aft Bulkhead, Lower
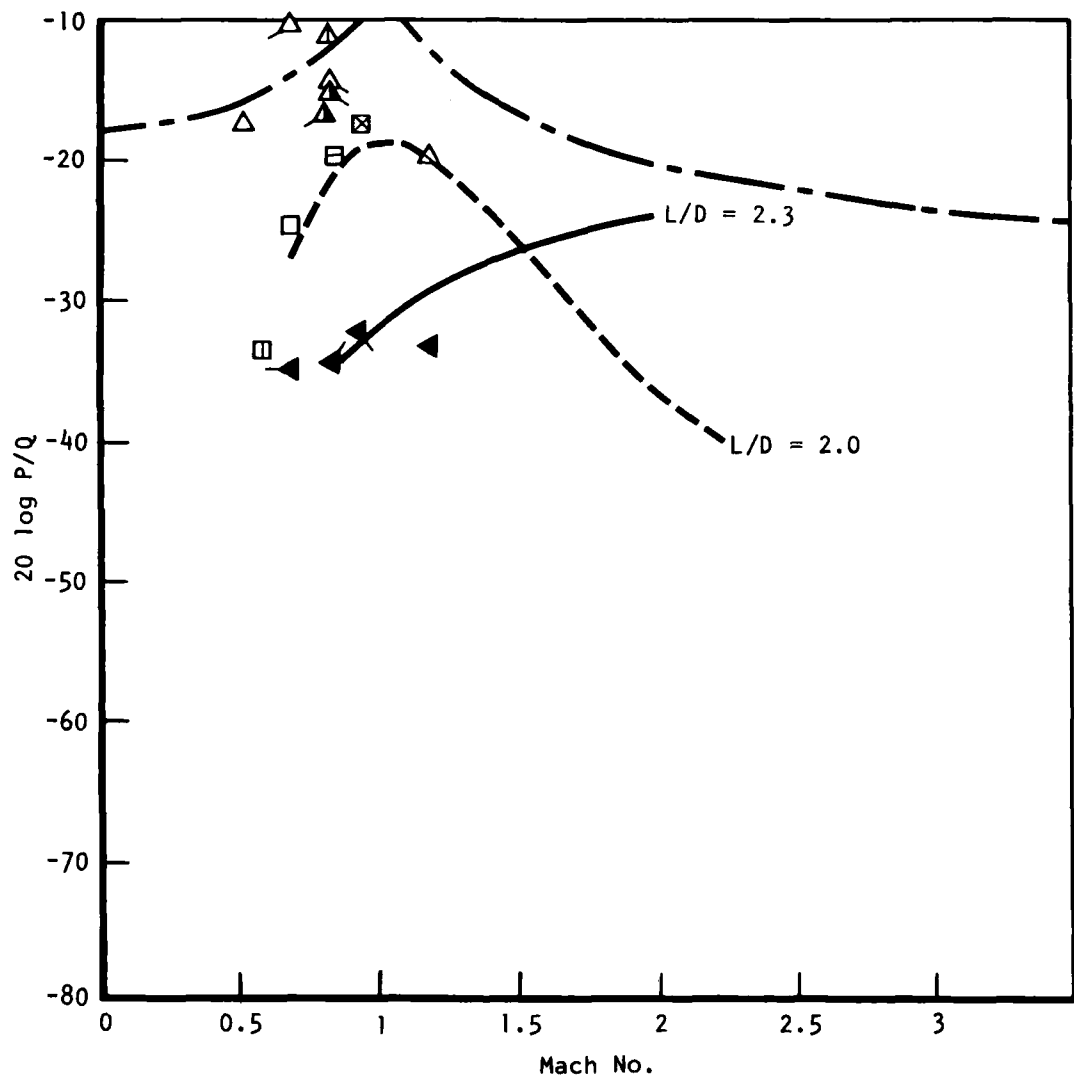
Figure 144. Mode 1 FO Aft Bulkhead, Lower
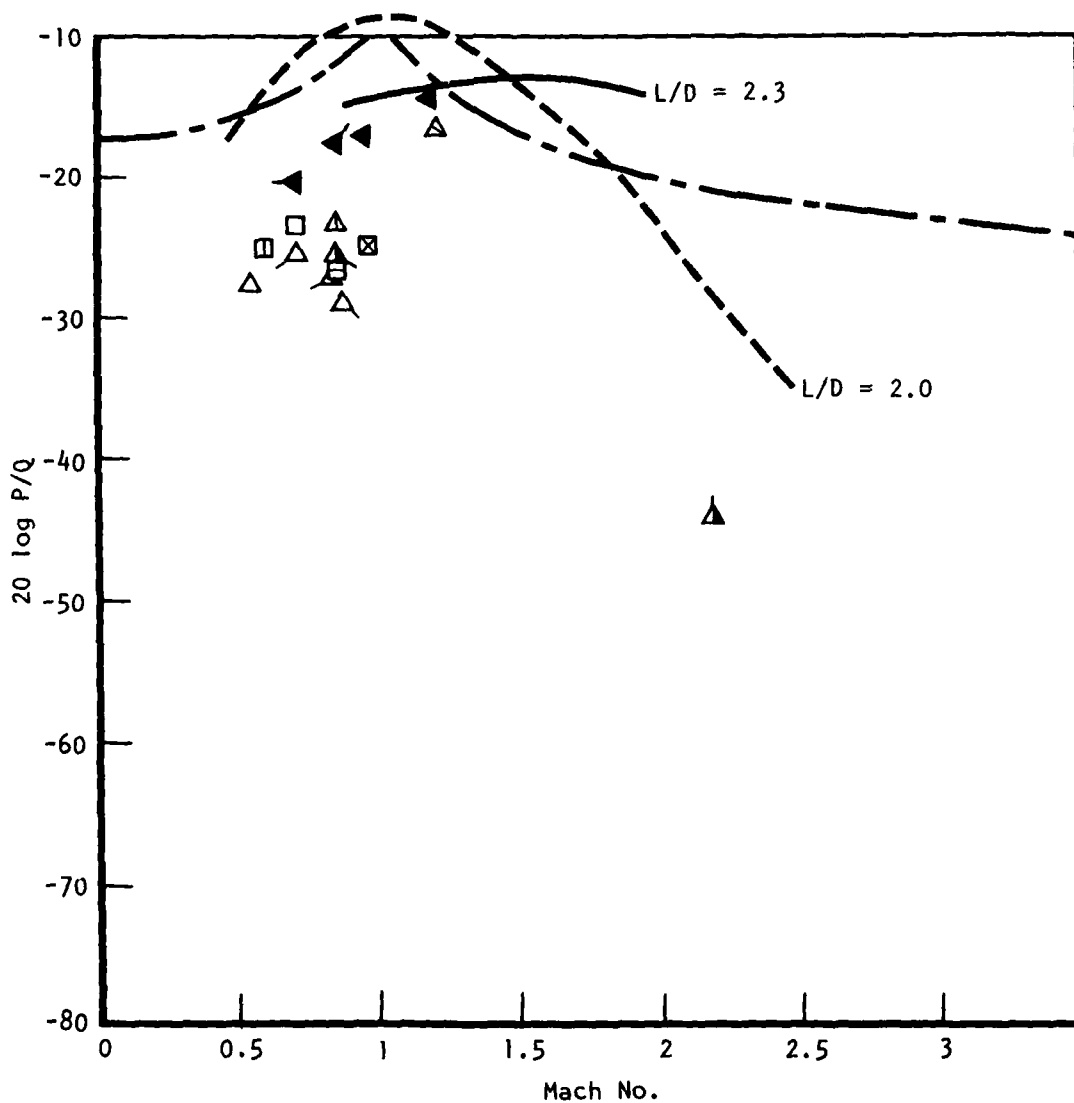
Figure 145.   Mode 2 FO Aft Bulkhead, Lower
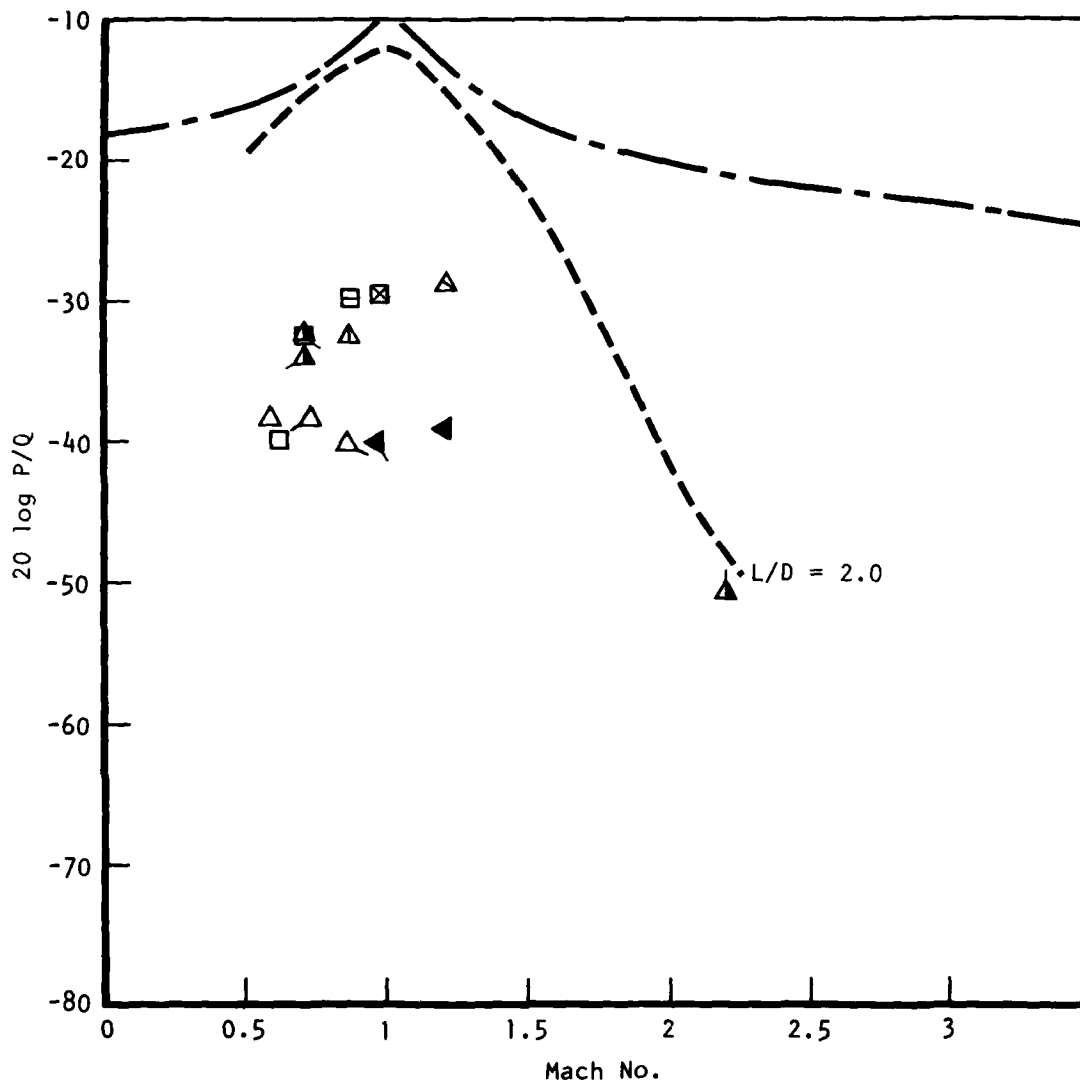
Figure 146. Mode 3 FO Aft Bulkhead, Lower
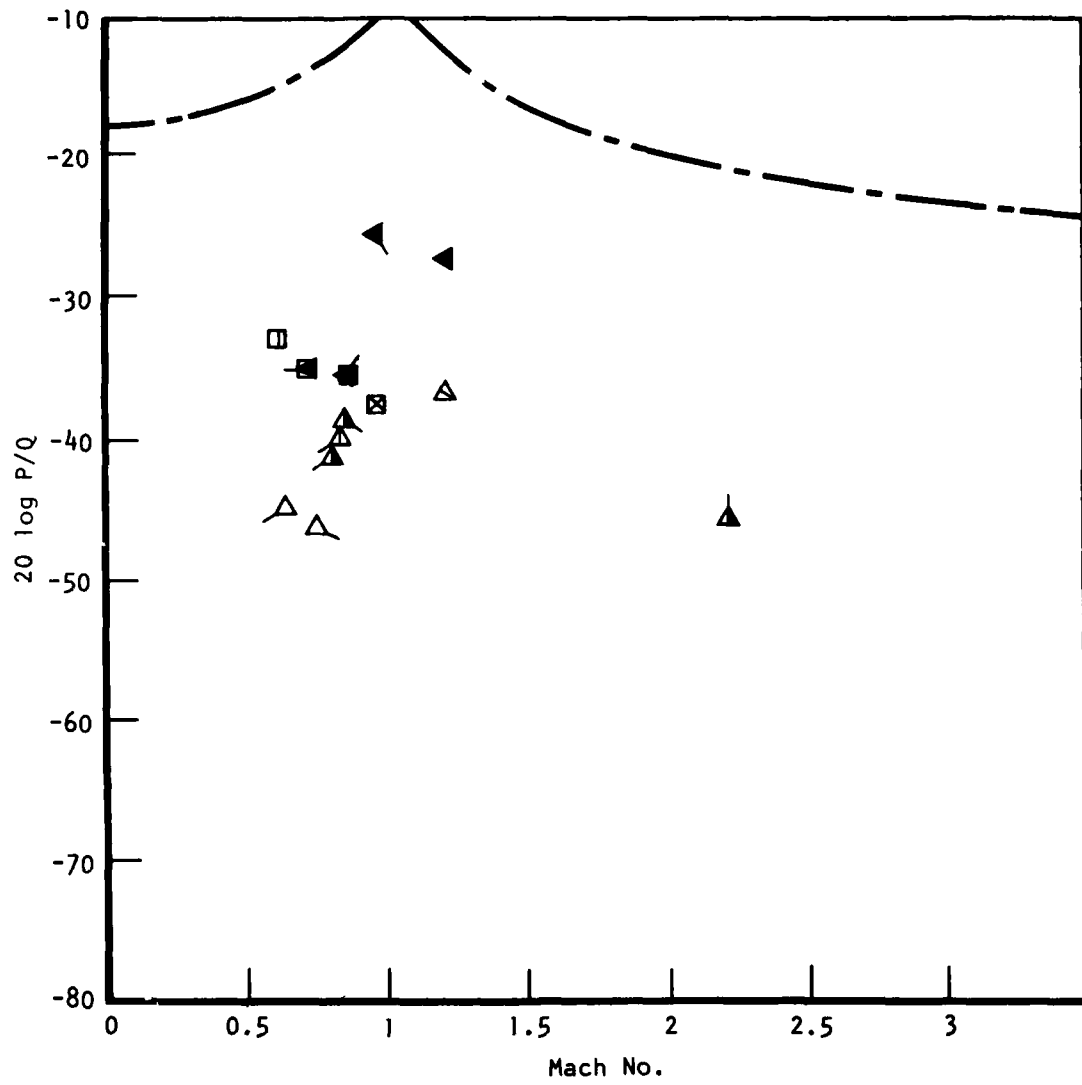
Figure 147. Mode 4 FO Aft Bulkhead, Lower
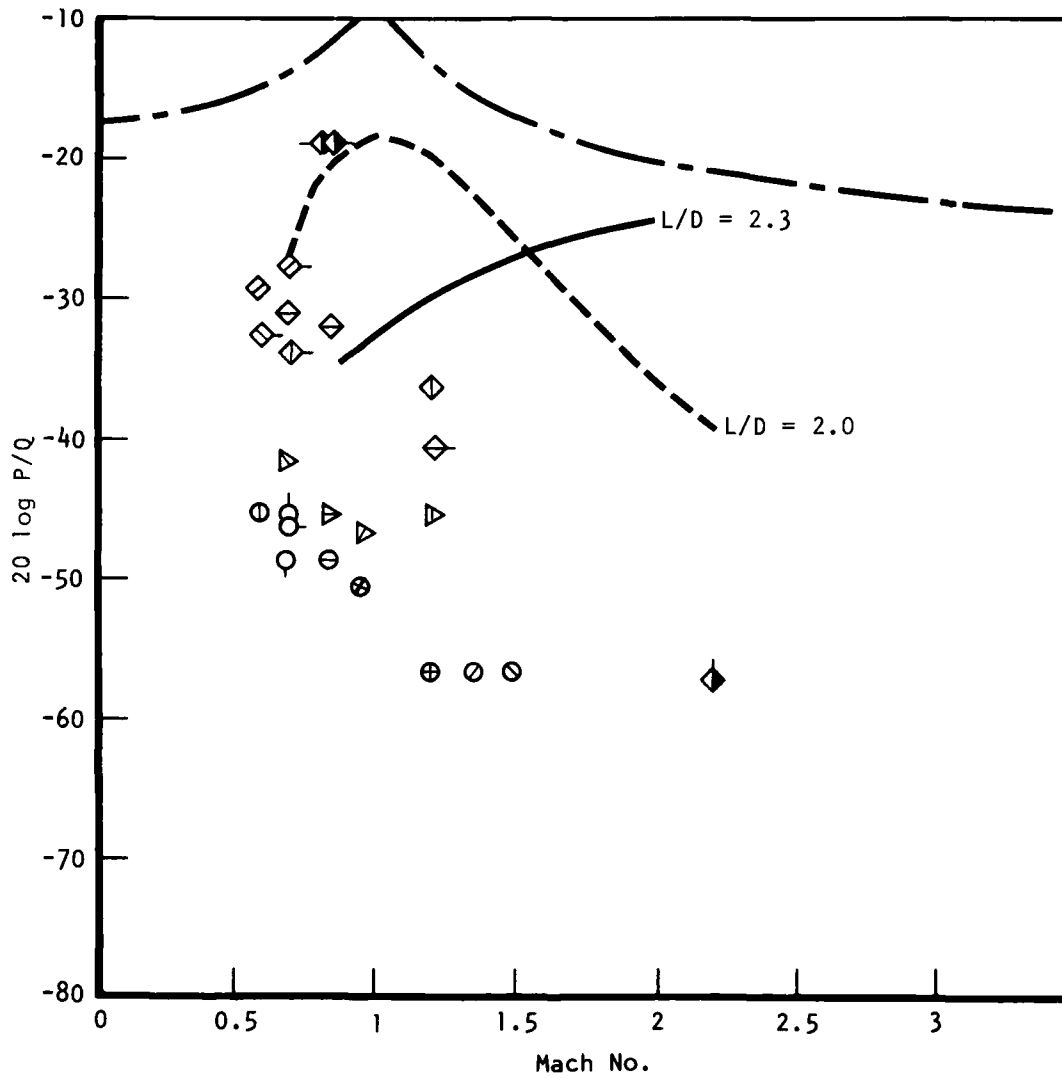
163

Figure 148.   Mode 1 PO Aft Bulkhead, Upper
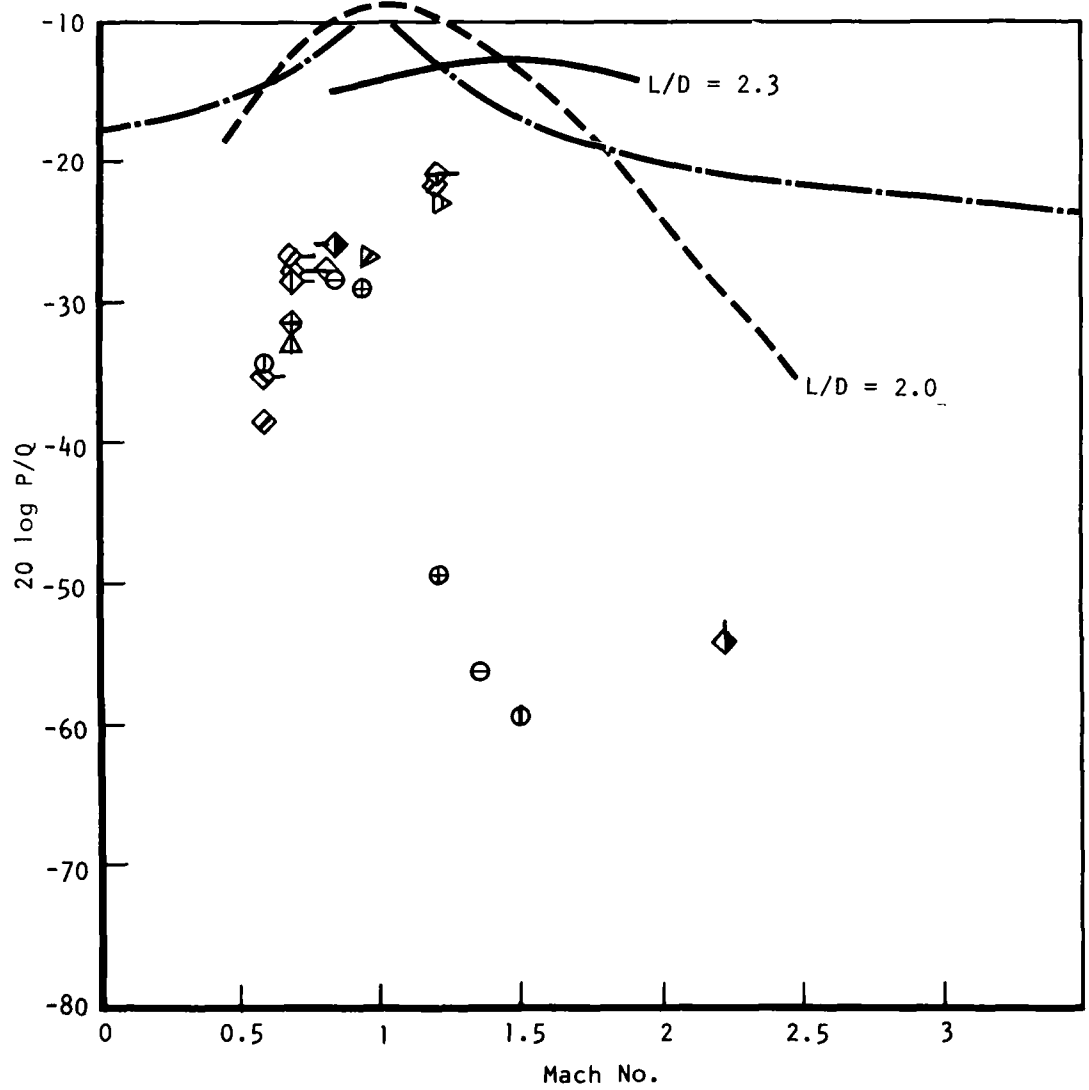
Figure 149.   Mode 2 PO Aft Bulkhead, Upper
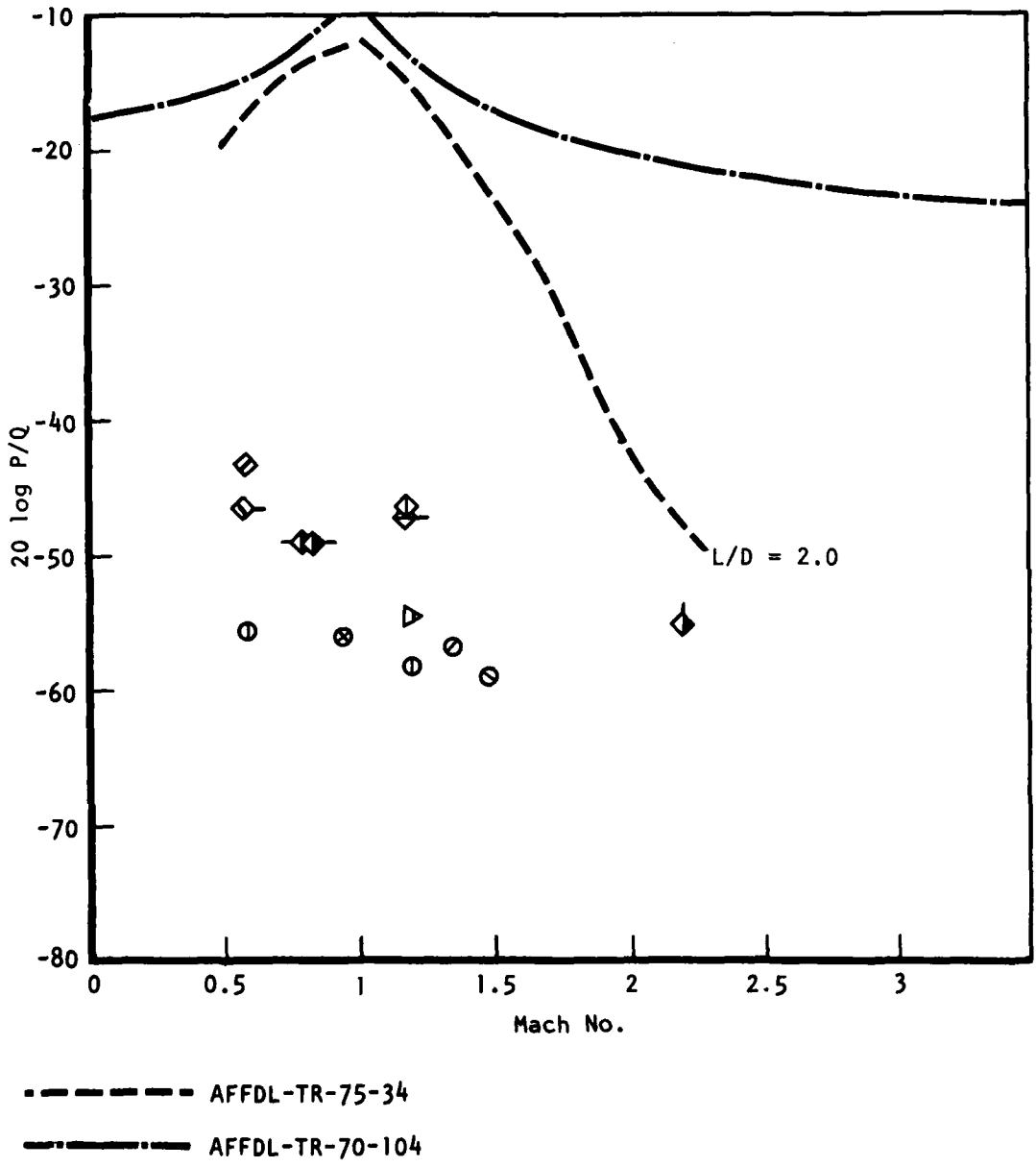
Figure 150. Mode 3 PO Aft Bulkhead, Upper
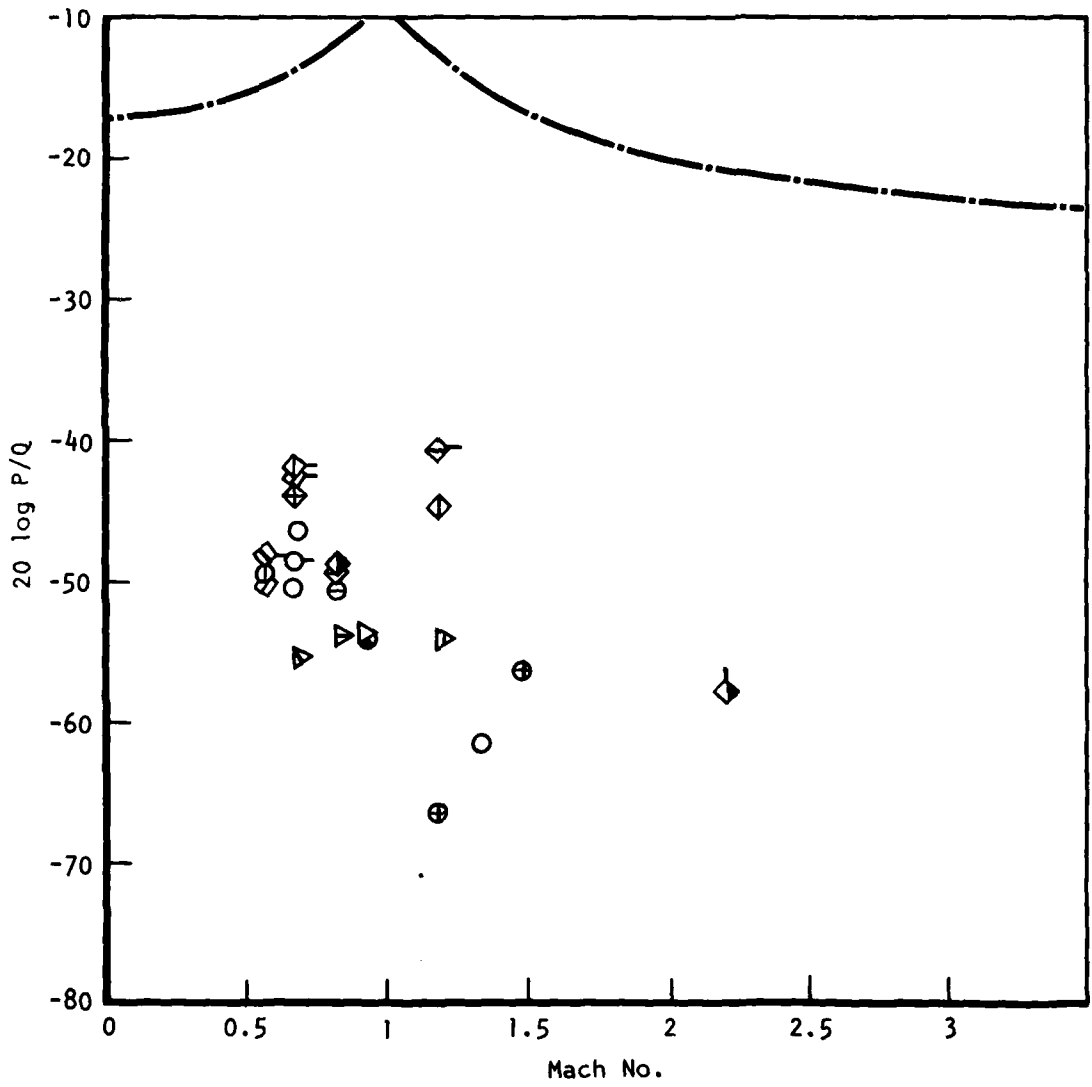
Figure 151. Mode 4 PO Aft Bulkhead, Upper

167
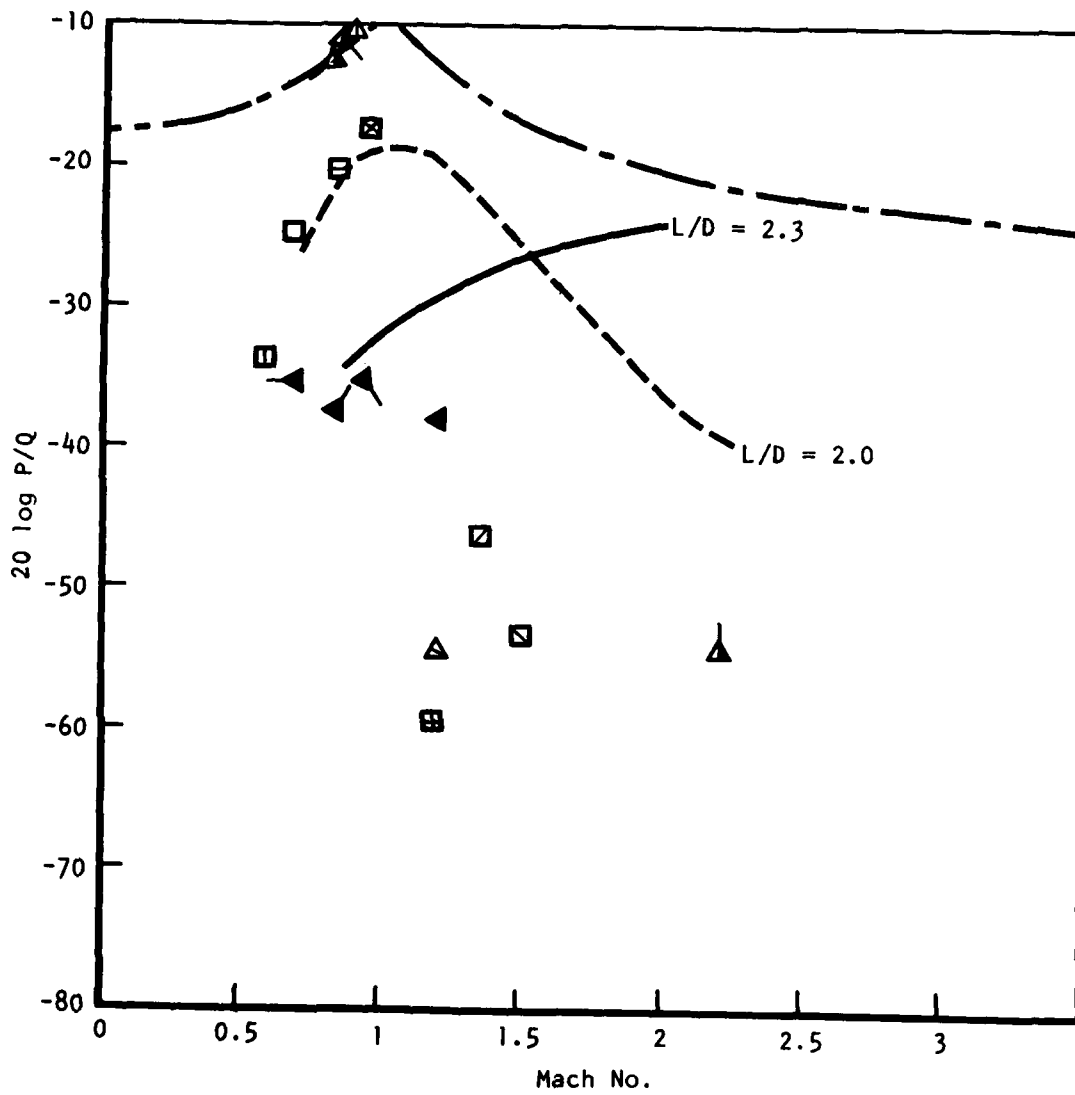
Figure 152.   Mode 1 FO Aft Bulkhead, Upper

168
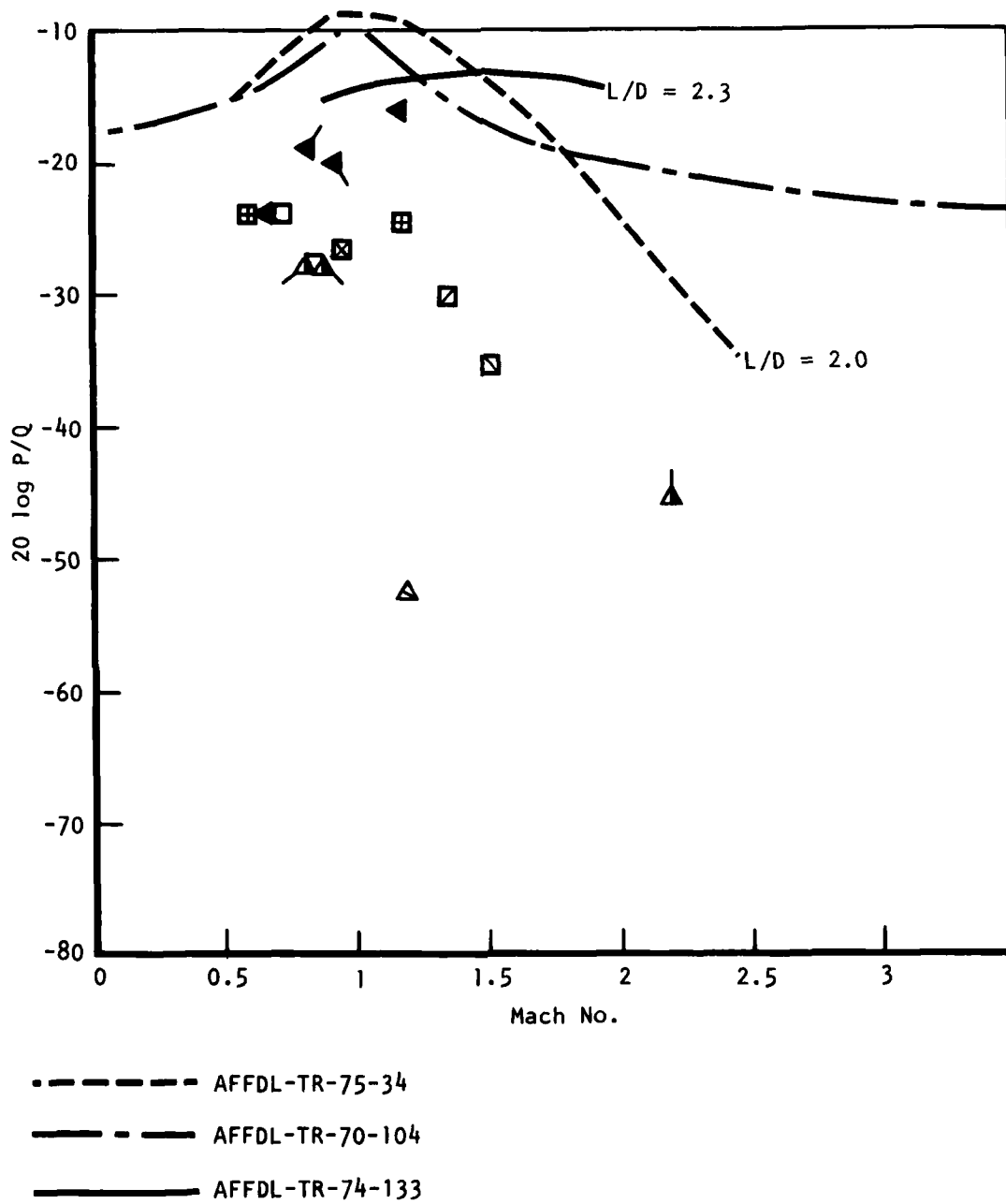
Figure 153. Mode 2 FO Aft Bulkhead, Upper

169
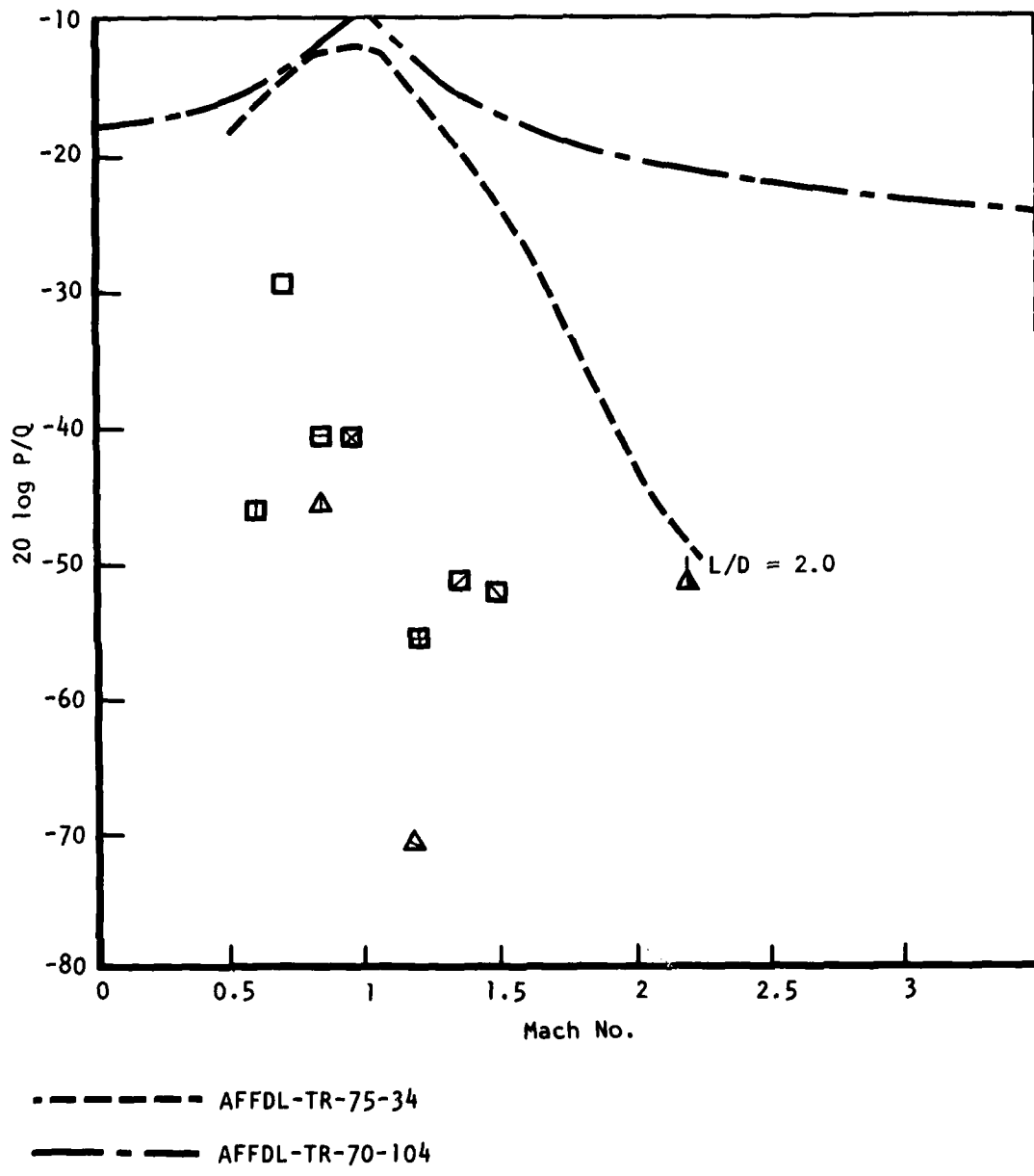
Figure 154.   Mode 3 FO Aft Bulkhead, Upper
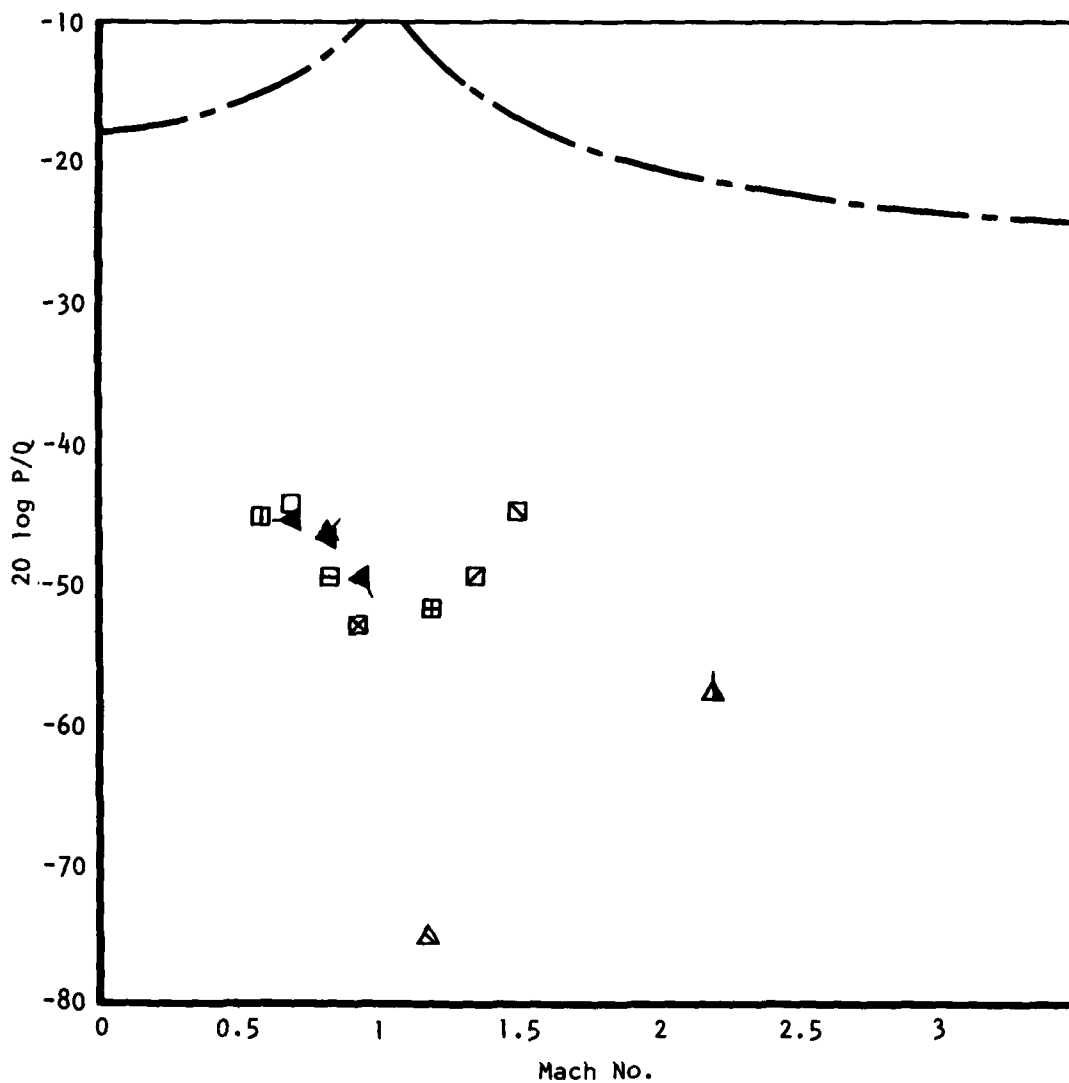
Figure 155. Mode 4 FO Aft Bulkhead, Upper

The pressure amplitude of the discrete frequencies appears to be a complex variable which is affected by a multitude of parameters. Even though it was concluded that the prediction method of Reference 6 provides a better match to the B-1 cavity noise data than the other prediction methods certain differences should be noted. The method in Reference 6 is based on cavity mode 2 as the dominant and highest pressure-level mode, with the magnitude of the other lower pressure-level modes (1 and 3) ratioed to the dominant mode 2. The B-1 data, however, shows that the mode 2 is not always dominant, and in some cases, cavity mode 1 is the highest pressure-level mode. The magnitude and dominance of one mode relative to another for the B-1 cavity is affected by mach number, door position, and possibly flow disturbances. Noise levels presented in Section III illustrate the variations typical of the B-1 data. In general, the full-open door position resulted in higher pressure amplitudes for all modes than the part-open door position. For part-open doors, cavity mode 2 was dominant, which is consistant with the data in the Reference 5 prediction method. For full-open doors, however, modes 1 and 2 are usually dominant, except for the levels in the aft bay located between the engine nacelles. Cavity mode 1 in the aft bay was lower, and cavity mode 2 was higher in the aft bay than for the forward bays on the B-1 aircraft. It is thought that the flow disturbances induced by the nacelles affect the aft bay noise levels. Modes 1 and 2 show the highest pressure amplitudes at transonic mach numbers. The higher order modes (3 and 4) show lower amplitude pressures than for modes 1 and 2. The magnitude of modes 3 and 4 is relatively constant as a function of mach number.

The currently published prediction methods for discrete cavity resonant amplitudes are derived by formulating equations that describe the trend of the measured data. Equations could be formulated which describe the B-1 data in like fashion; however, modifications to the existing prediction method [6] are recommended. The prediction method incorporates the empirical data trends for a range of mach numbers and cavity L/D ratios of several previous investigations and also matches the trend of the B-1 data. In some cases, however, the magnitude of the modal pressures predicted by Reference 6 may need refinement to provide a closer match to the B-1 cavity noise data.

It has been observed that considerable scatter exists in cavity noise measurements, especially for the discrete tones. It is not understood why particular cavities show mode 2 dominance and other cavities show mode 1 dominance. Modal dominance also appears to be a function of door position, mach number, and upstream flow disturbances, and it is not possible at this time to formulate expressions that would reliably predict these effects. It is therefore recommended that modifications to the prediction method of Reference 6 be accomplished and a range of levels, or accuracy of prediction, be identified to account for data scatter and uncertainties in modal pressure variations.

The aft lower bulkhead has been identified as the location of maximum pressure inside open cavities; therefore, the noise-prediction methods use this location as a baseline and the noise-level variation throughout the cavity is expressed relative to the aft lower bulkhead position. B-1 data are shown in Figures 140 through 147 for the lower aft bulkhead position.

The magnitude of the B-1 data in Figures 140 through 147 is generally lower than predicted by the method in Reference 6. The prediction method in Reference 6 could be modified to provide a better fit to B-1 data by subtracting 5 decibels from mode 2 noise-level estimates and to use the same curve for cavity modes 1 and 2 noise predictions. These modifications would be applicable to the full-open door positions.

For the part-open door positions, an additional 5-decibel reduction for each mode would better match the B-1 data. The door position influences the cavity noise level, and it suggests that the presence of the door closeout along the cavity walls has an effect on cavity noise levels. Unfortunately, B-1 data were not recorded without weapon bay doors to evaluate the effects on noise level.

The accuracy of predicting cavity noise levels is a concern. It appears that considerable data scatter exists after the pressures have been normalized with dynamic pressure and effects of cavity L/D ratios and mach number have been taken into consideration. The data in Figures 156 through 161 were taken from Reference 6, which illustrates the prediction accuracy relative to the published cavity noise data base. The B-1 cavity noise data are superimposed on the data in Figures 156 through 161 for comparison with the prediction method of Reference 6 and the scatter of experimental data in the published cavity noise data bank. The envelope for B-1 data (model and full-scale) shown previously in Figures 140 through 147 is identified by the cross-hatched region. The full-scale data are identified separately on each plot. The B-1 data for each cavity mode and for full- and part-open doors are shown on separate plots. In general, the magnitude of the B-1 data fall in the low range of the published data base and also below the levels predicted using methods in Reference 6. The data range for cavity mode 1 with full-open doors, however, is higher in amplitude than the rest of the B-1 data and falls within the range of the published data base, with the full-scale data correlating closely with the prediction methods of Reference 6. All the other B-1 data consistently fall in the low end of the published data scatter. All previously published data shown (Figures 156 through 161) are for cavities without doors. The B-1 cavities have doors adjacent to the cavity walls along the entire length of the cavity, and it is suspected that the doors may help stabilize the shear layer, resulting in reduced cavity noise levels. The shear layer stabilizing effect of the part-open doors may be greater than full-open doors, which would result in lower noise levels for part-open doors. The effect of full-open doors on cavity noise is shown in Reference 15. The data show that adding full-open doors to the cavity has no effect on noise level. Empirical data are not currently available for cavities with and without part-open doors.

Noise-level variation within the cavity is another possible factor in data scatter. The highest level occurs in the aft portion of the cavity, and most data bases confirm this. The B-1 data show a variation between the upper and lower aft bulkhead position of up to 10 decibels. When the maximum cavity noise levels of various data bases which were recorded at different locations in the aft portion of the cavity are compared and if the B-1 data is typical, then data scatter occurs. Variations between wind tunnel and flight data also occur, with wind tunnel data generally slightly higher in amplitude than the flight data. The general trend of the B-1 wind tunnel and full-scale data indicated the same trend. This also contributes to data scatter and is not currently understood.

Figure 156. Correlation of B-1 Data With Previous Data Base - Mode 1, Full-Open Doors

174

Figure 157. Correlation of B-1 Data With Previous
Data Base - Mode 2, Full-Open Doors

Figure 158. Correlation of B-1 Data With Previous
Data Base - Mode 3, Full-Open Doors

1.0

1.1

1.25   1.4   1.6

4.5
5.0
5.6
6.3
7.1

2.8   2.5

3.2   2.2

3.6

4.0   2.0

1.8
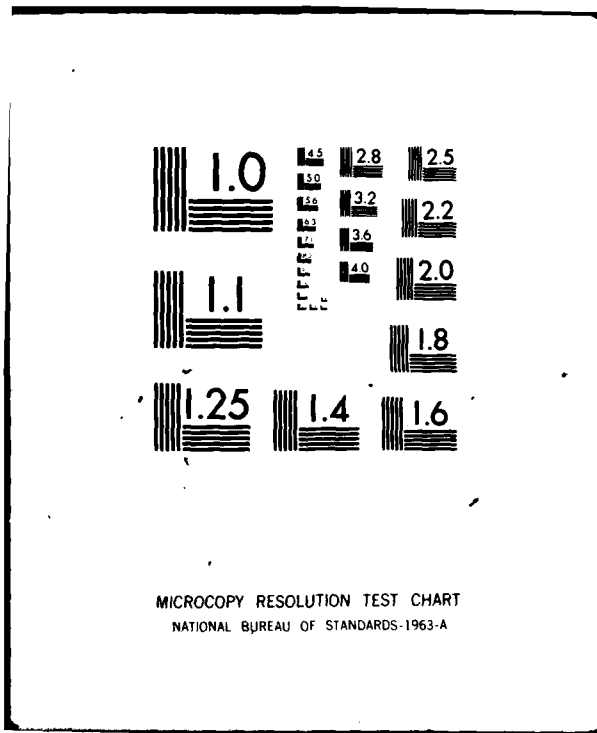
MICROCOPY RESOLUTION TEST CHART
NATIONAL BUREAU OF STANDARDS-1963-A
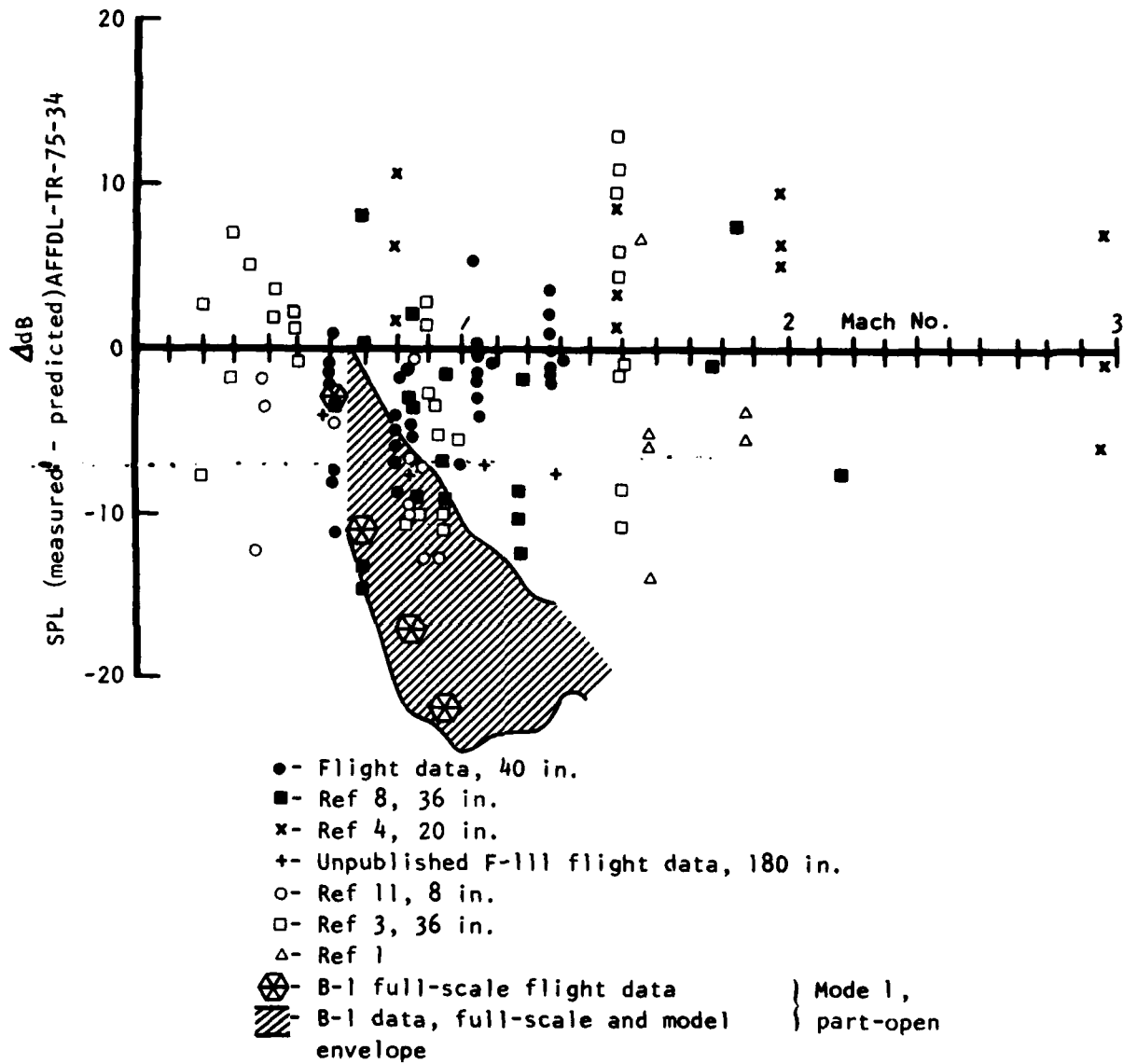
Figure 159. Correlation of B-1 Data With Previous
Data Base - Mode 1, Part-Open Doors
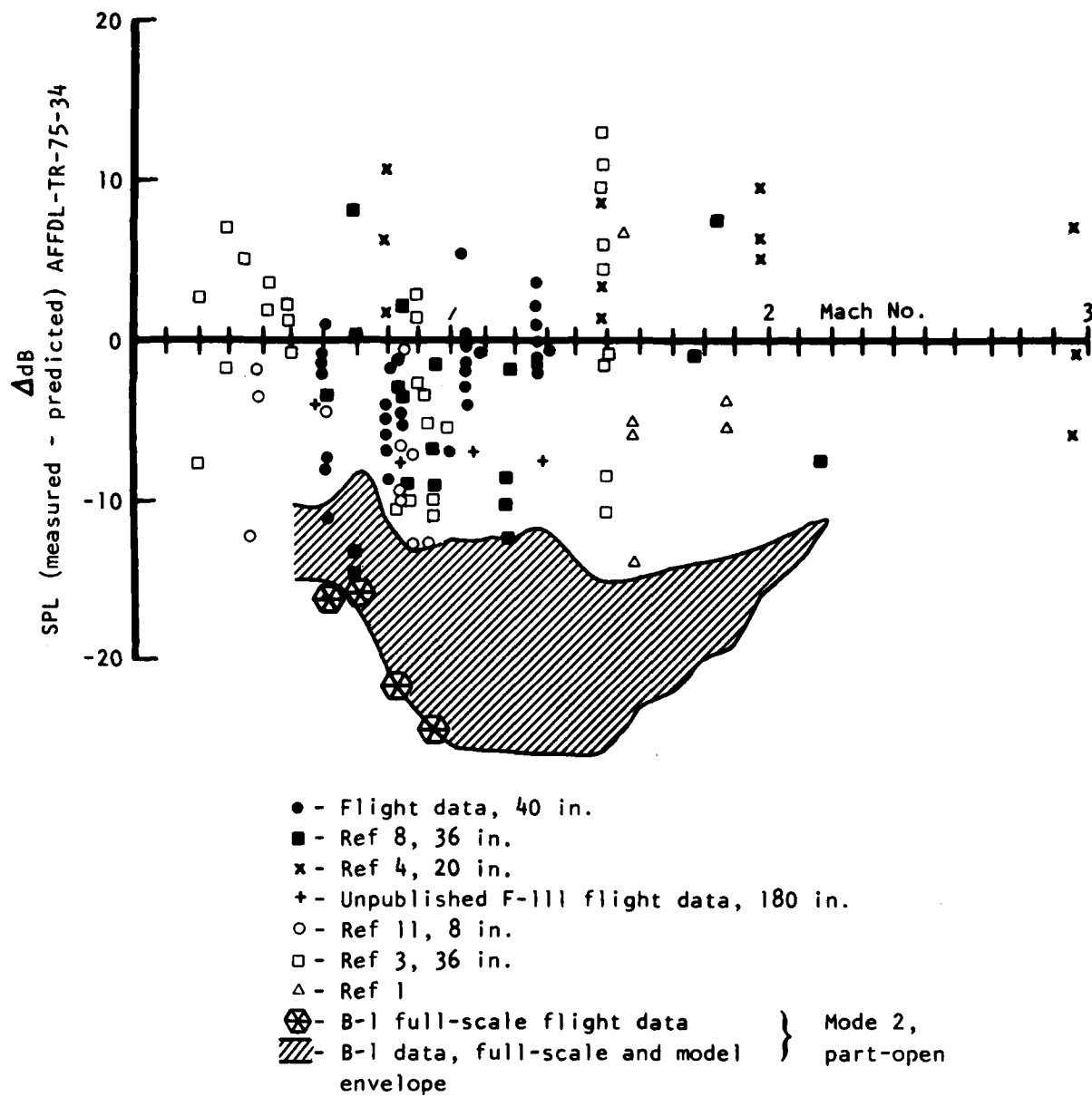
Figure 160. Correlation of B-1 Data With Previous
Data Base - Mode 2, Part-Open Doors

ΔdB   SPL (measured - predicted)AFFDL-TR-75-34

20

10

0

-10

-20

Mach No.

2

3

● - Flight data, 40 in.
■ - Ref 8, 36 in.
x - Ref 4, 20 in.
+ - Unpublished F-111 flight data, 180 in.
○ - Ref 11, 8 in.
□ - Ref 3, 36 in.
△ - Ref 1
⊗ - B-1 full-scale flight data   } Mode 3,
▨ - B-1 data, full-scale and model   } part-open
      envelope
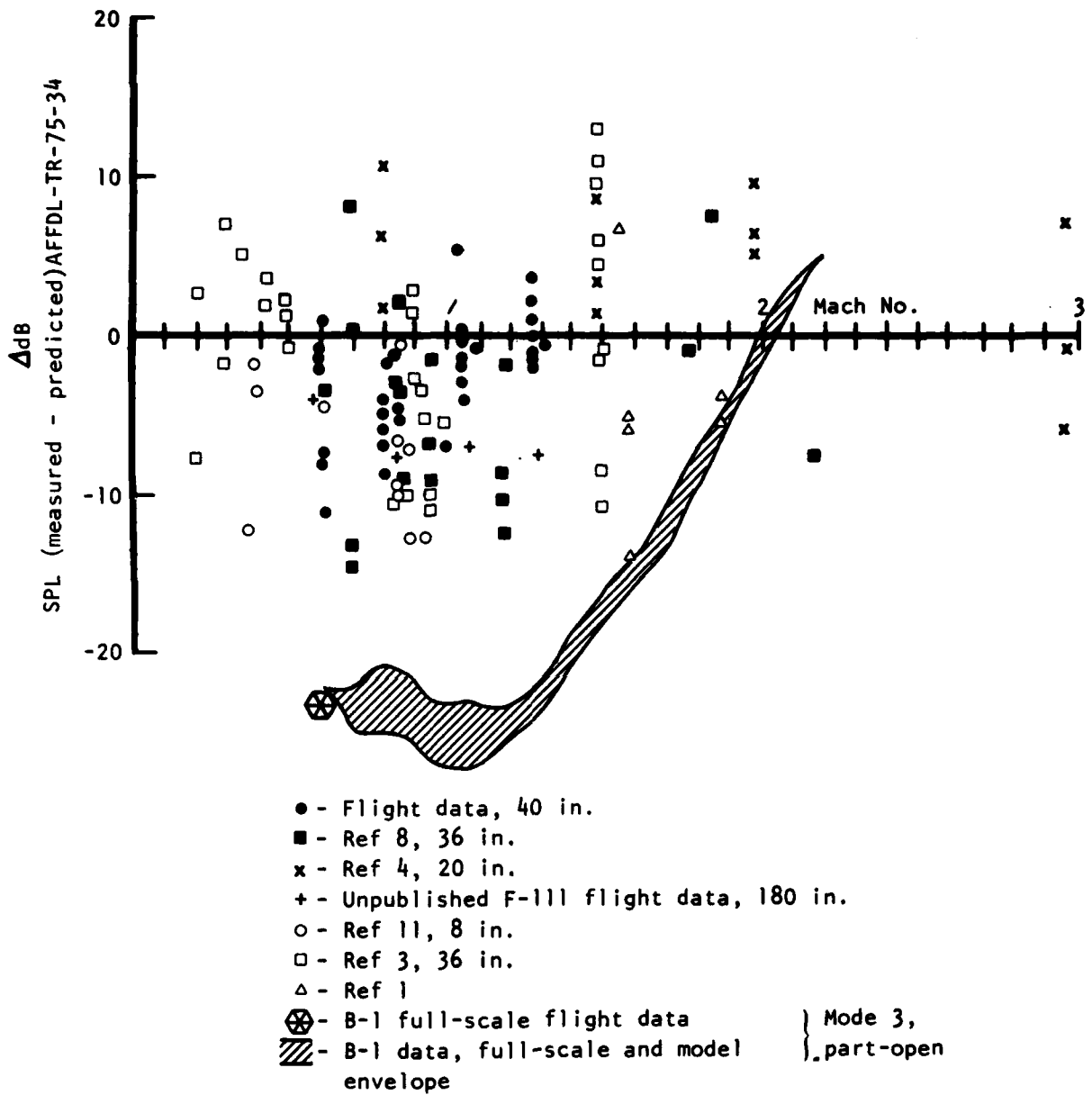
Figure 161.   Correlation of B-1 Data With Previous Data
Base - Mode 3, Part-Open Doors

179

In summary, considering the current scatter in the data bases, accurate prediction methods for discrete cavity pressure oscillation are not possible. It appears that in general 10 decibels is the current prediction accuracy. If the B-1 data were included in the current data base without determining the effects of doors on cavity noise level, even greater data scatter would result. It is not recommended that changes be made to the methods of Reference 6 for discrete tones until the scatter factor in the data bases can be reduced.

DISCRETE CAVITY NOISE LEVEL VERSUS CAVITY LENGTH

The longitudinal variation of the amplitude of the discrete cavity oscillation was shown in Section III. The prediction method of Reference 6 is superimposed on the B-1 data for cavity modes 1 and 2 (Figures 162 and 163). Comparing the B-1 data and predicted longitudinal variation, it's rather difficult to determine whether good correlation was achieved or not. The mode 1 data seem to indicate the same trend of the predicted data with a node point (minimum level) near the center of the cavity and maximum levels occurring at each bulkhead. Mode 2 data were harder to correlate due to an insufficient number of data points in the longitudinal axis. It is concluded, however, that the predicted variation of the modal pressure is reasonable with the B-1 data showing similar trends for cavity mode 1.

BROADBAND CAVITY NOISE

Broadband random noise levels are generated in open cavities and correlated with dynamic pressure, mach number, and Strouhal number. The maximum noise level within the cavity occurs on the aft bulkhead. The spectral content of the broadband noise is expressed in terms of Strouhal number and nondimensional P/Q ratios. The pressure level P is in terms of 1/3 octave bands. The prediction methods of Reference 4, 5, and 6 are correlated with the B-1 cavity wind tunnel and full-scale data.

The overall noise level as a function of mach number is shown in Figure 164. The three prediction methods are correlated with B-1 data and show somewhat different overall noise-level trends with mach number. In general, the maximum cavity broadband overall noise level decreases with increasing mach number, and the methods in Reference 6 seems to best correlate with the trend of the B-1 data for the overall levels illustrated in Figure 164. Considerable scatter exists in the broadband cavity noise data. It seems that a ±5-decibel prediction accuracy relative to Reference 6 methods would envelope most of the empirical data points, although some data would fall outside this range.

The 1/3 octave band spectra are nondimensionalized to dynamic pressure and plotted as a function of Strouhal number in Figures 165, 166, and 167. The B-1 data are correlated with the prediction methods of References 4, 5, and 6. The maximum noise level occurs at Strouhal numbers in the vicinity of 1, and all the prediction methods in Reference 4, 5, and 6 seem to correlate reasonably well with the empirical B-1 data.

Considerable scatter exists in the overall and spectrum-level broadband cavity noise data. It seems that a 5-decibel prediction accuracy relative to Reference 6 method would envelope most of the empirical data points, although some data would fall outside this range.
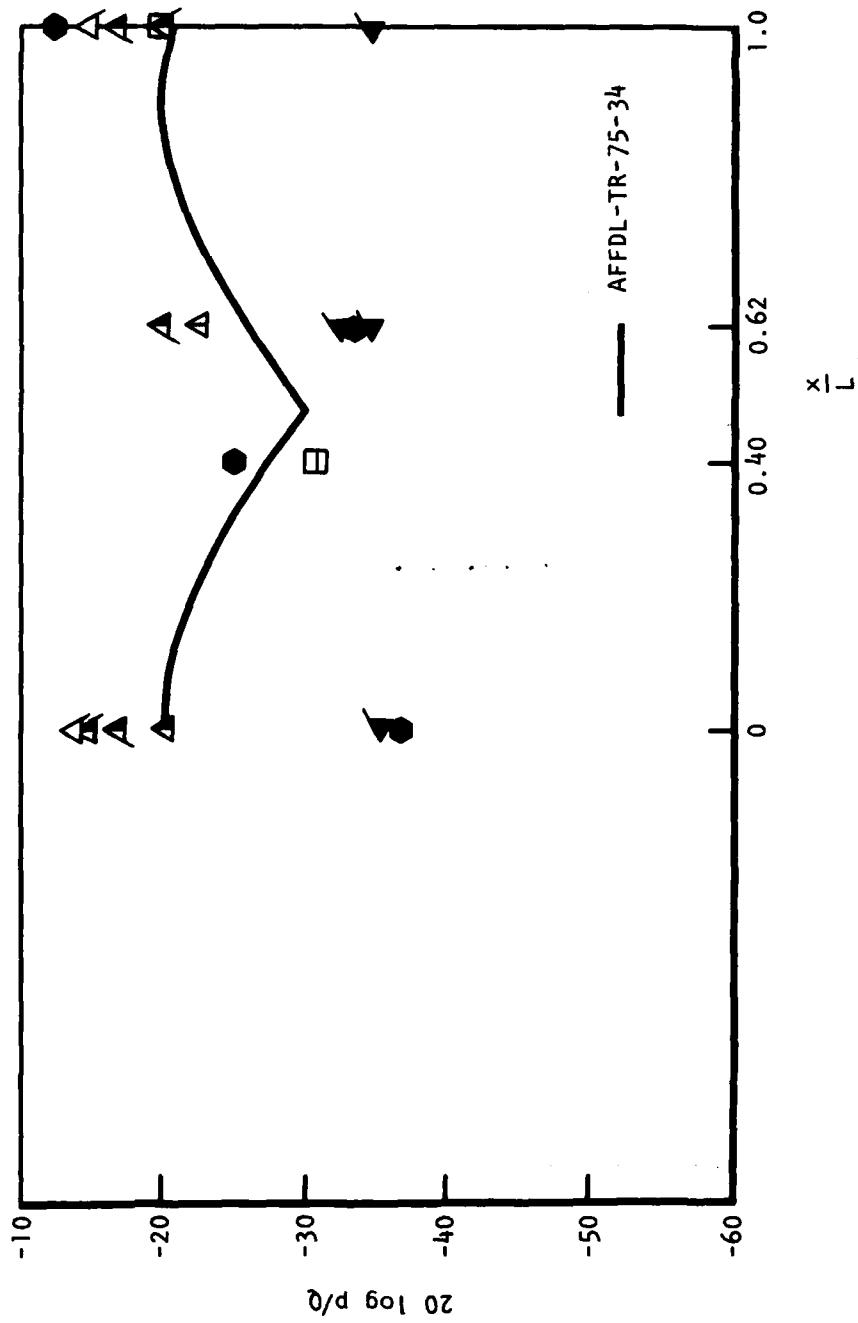
Figure 162. Bulkhead/Sidewall Lower, Mode 1, M 0.85, Full-Open, Discrete Levels Versus Bay Length

181
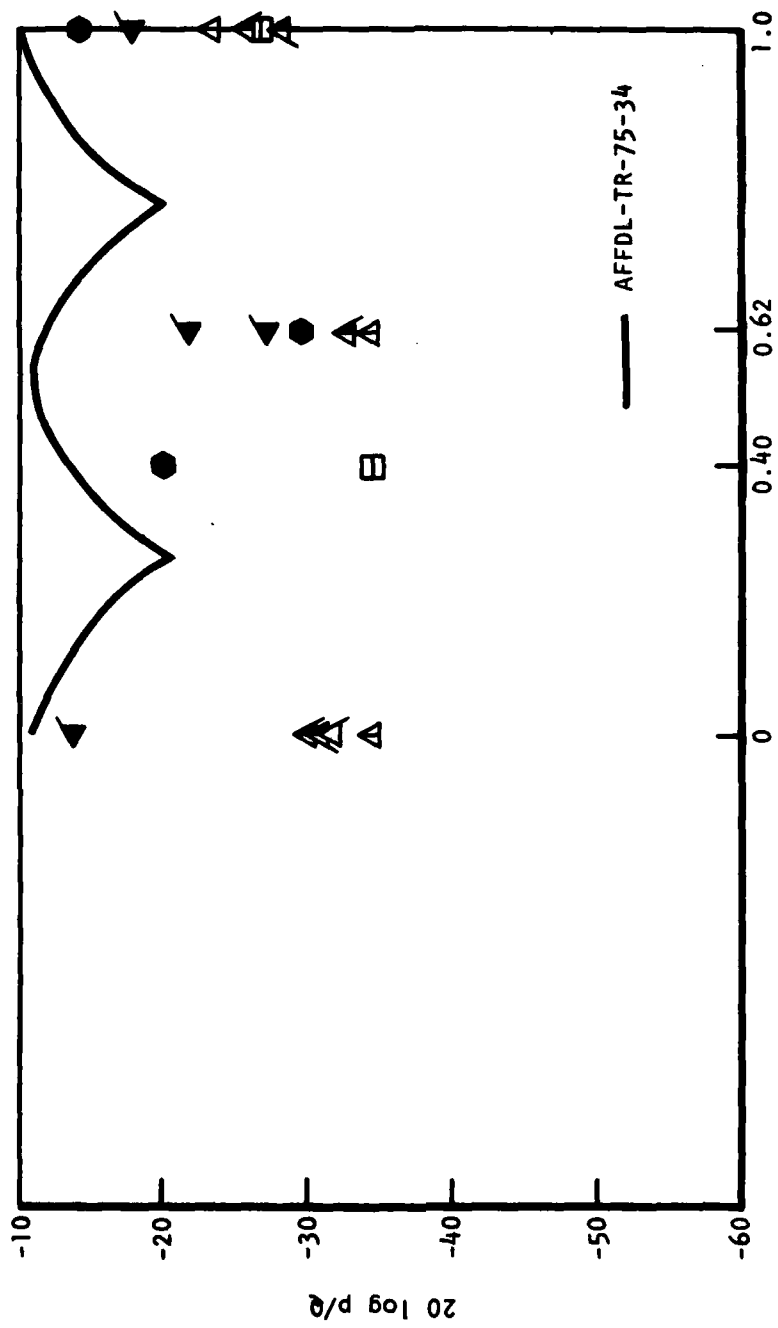
Figure 163. Bulkhead/Sidewall Lower, Mode 2, M 0.85, Full-Open, Discrete Levels Versus Bay Length

182
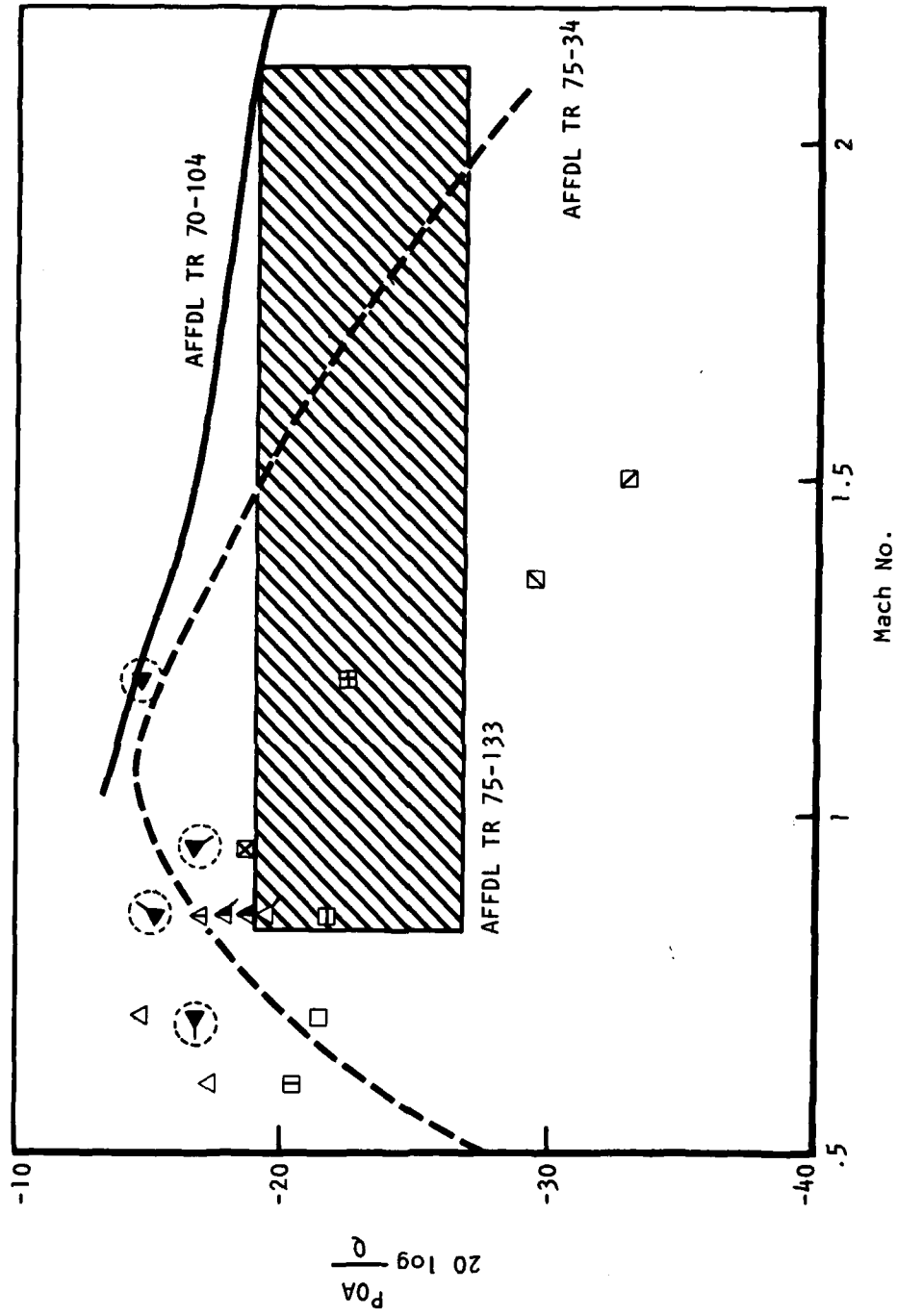
Figure 164. Overall Broadband Pressure Level Full-Open, Aft Bulkhead Lower
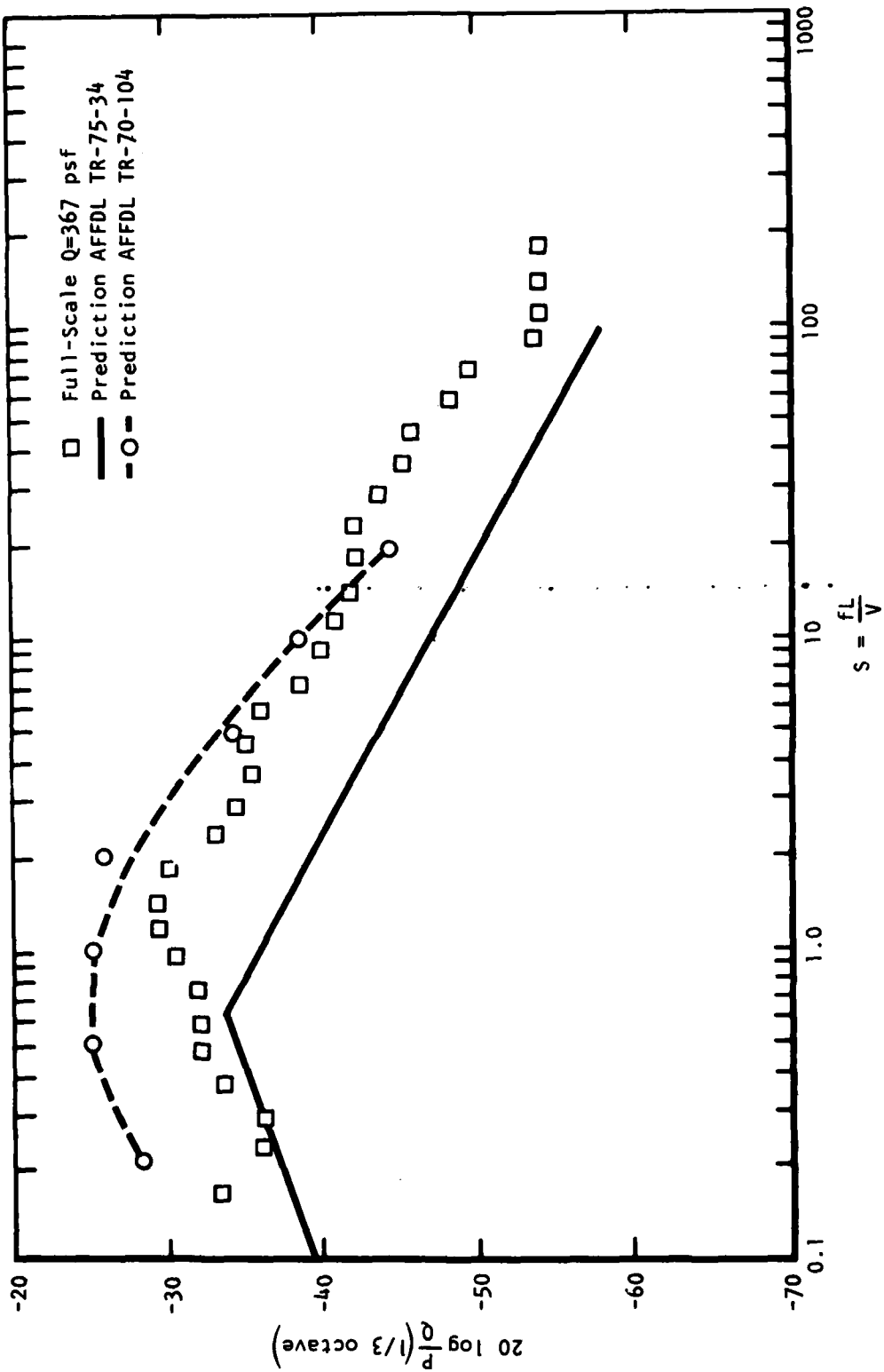
Figure 165. Broadband Pressure Versus Strouhal Number, Full-Open, Mach 0.6, Aft Bulkhead Lower
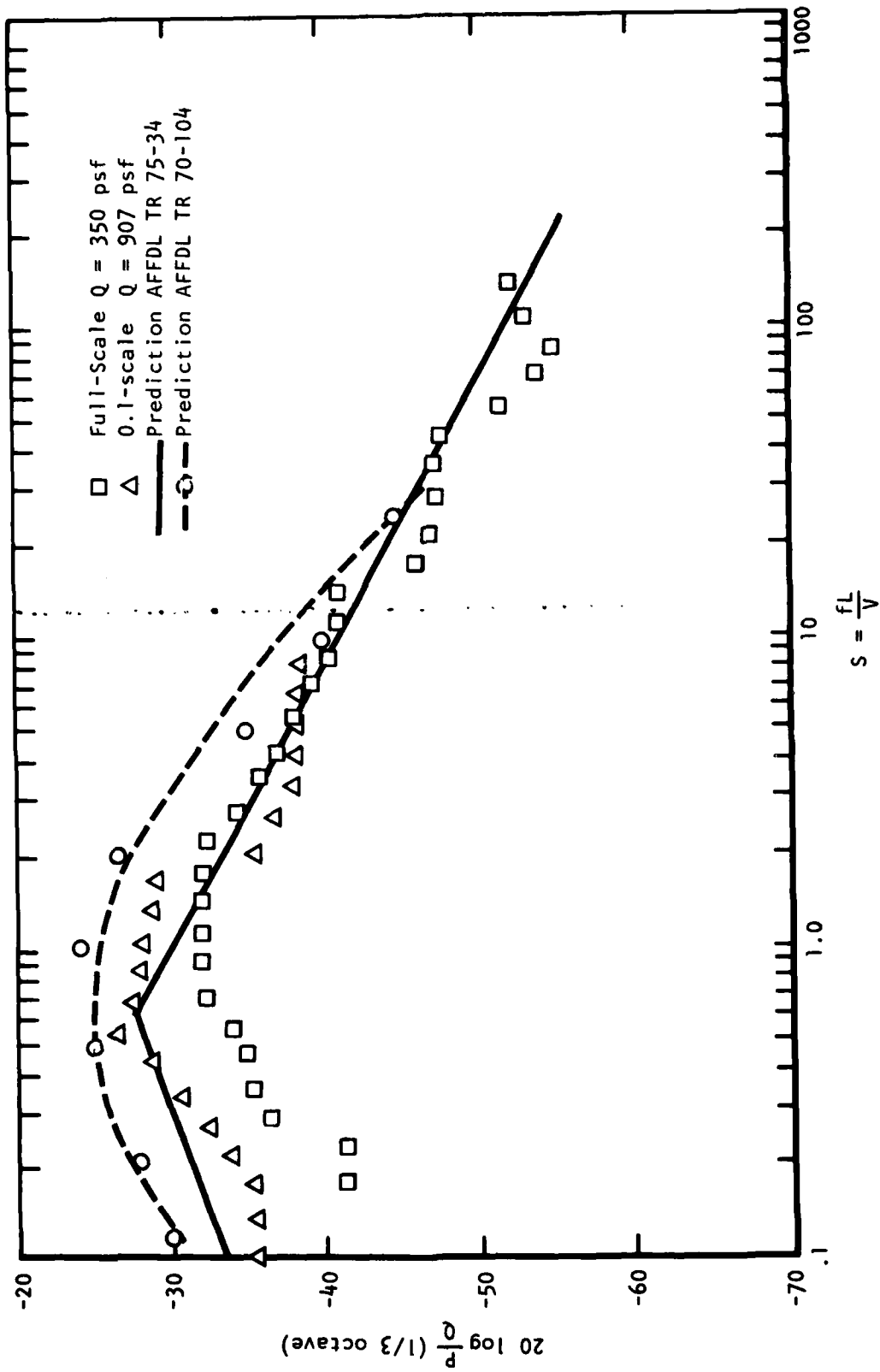
Figure 166. Broadband Pressure Versus Strouhal Number, Full-Open, Mach 0.85, Aft Bulkhead Lower

185
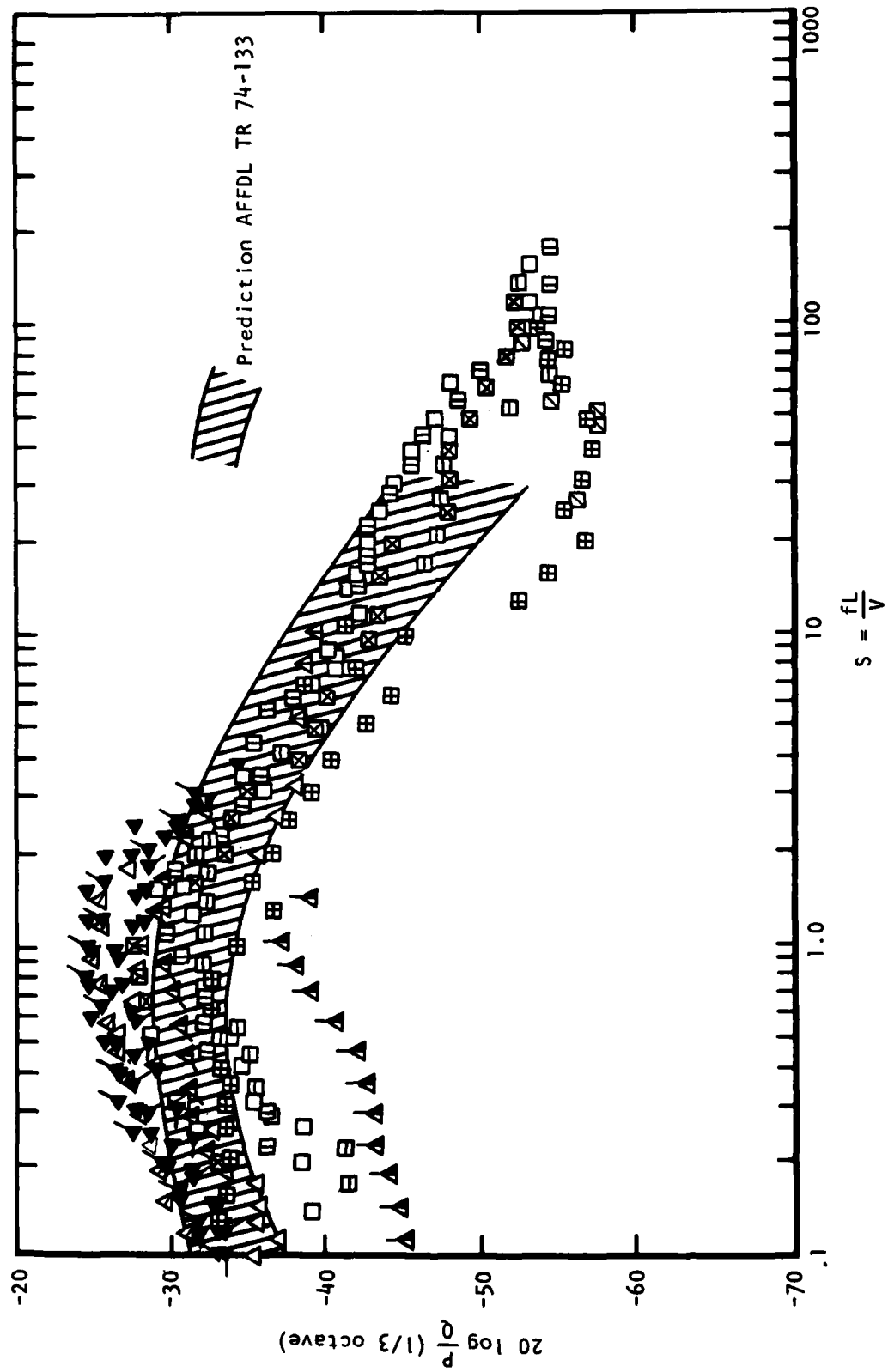
Figure 167. Broadband Pressure Versus Strouhal Number, Full-Open, Aft Bulkhead Lower

The broadband noise-level distribution within the cavity has been briefly discussed in the literature. The overall noise level has been found to be reduced by up to 10 decibels in the forward part of the cavity. The method of Reference 6 predicts a 2- to 3-decibel reduction for the forward bulkhead, relative to the aft bulkhead. The B-1 data show approximately a 10-decibel noise-level reduction in the lower part of the bay near the opening and approximately a 5-decibel noise-level reduction between the forward and aft bulkheads in the top portion of the cavity. The noise level on the lower portion of the aft bulkhead is usually higher, with approximately a 10-decibel reduction near the top of the cavity. The B-1 data do not show a clear trend of noise-level variation as a function of cavity depth for the forward bulkhead.

In summary, the broadband noise prediction of Reference 6 seems to best predict the trend of the B-1 data for overall and spectra pressure levels. A ±5-decibel tolerance is recommended, due to the scatter in cavity noise-level data. The longitudinal noise-level variation along the length of the cavity appears greater than that predicted by Reference 2, and it is recommended to decrease the noise level predicted for the lower aft bulkhead position by 10 decibels for the forward bulkhead. The B-1 data show a noise level variation of 10 decibels with cavity depth for the aft bulkhead, and it is recommended that the noise level predicted by reference 6 be reduced by 10 decibels for the top of the aft bulkhead. The B-1 data do not show reduced noise level with cavity depth for the forward bulkhead; therefore it is recommended that the noise level of the entire forward bulkhead area be 10 decibels below the aft lower bulkhead prediction. The broadband noise levels for part-open doors are approximately the same amplitude within normal data scatter ±5 decibels as for full-open doors. The broadband cavity noise prediction for full- and part-open doors is therefore the same.

CAVITY NOISE-REDUCTION DEVICES

Various cavity noise-reduction devices have been evaluated in the literature. The most successful of these devices induce vorticity into the flow forward of the cavity and employ canted aft bulkheads as shown in Reference 15. Not all cavity noise suppression devices that show appreciable noise reduction in wind tunnel tests are easily incorporated in the aircraft. The canted bulkheads and detached airfoils would entail real design challenges for aircraft where space is a limiting factor. The relatively simple retractable spoilers located near the forward bulkhead of the open cavity have been shown to be an effective noise-suppression device. Due to the practicality of this type noise suppressor, a noise-reduction prediction guideline will be recommended.

Evaluations of the forward bulkhead spoiler-type noise-reduction device have been documented in Reference 5, 13, and 14. The geometry of the spoiler varies somewhat between the various investigators but is believed to accomplish the same basic results of shear layer stabilization by inducing vorticity at the cavity leading edge. Some of the results of References 13 and 14 are summarized in Figures 168 and 169. Varying degrees of noise level reductions are shown for the various types of noise-reduction devices. The noise reduction for various fences is illustrated in Figure 168, and all show good noise reduction. Some of the devices shown in Figure 169 show little if any noise reduction, except for the saw-tooth fence which indicated good noise reduction throughout the mach number range.

187

Sym	TP	Mach	Alpha (deg)	$R_N \times 10^{-6}/ft$	Fence
□	38	0.8	3	5.0	None
○	51	0.79	3	4.9	I
◇	53	0.79	3	4.9	II
△	55	0.79	3	4.9	III
◇	56	0.79	3	5.0	IV

Fwd bulkhead →   Rear bulkhead →

$\frac{P_{OA}}{Q}$

0.3

0.2

0.1

0.025

0

Basic (no fence)

III

II

I

IV

$\Delta dB = -8.5$

0   0.5   1.0

Reference AFFDL-TM-75-147-FXM   X/L
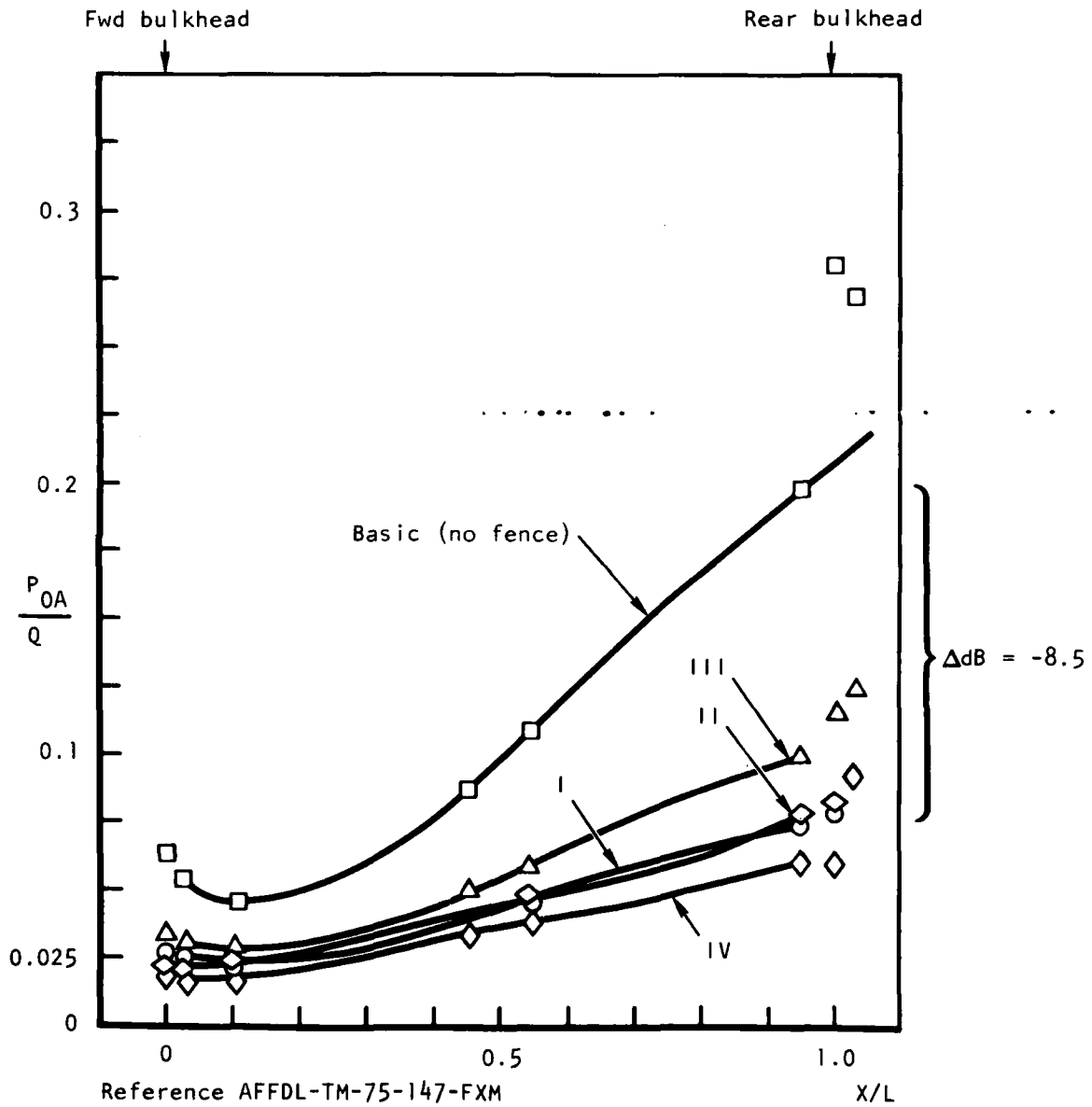
Figure 168. Comparison of Fences I Through IV With Basic
(No Fence) Turbulence Distribution

Sym	X/L	Left bay	Right bay	Suppressor
□	0.5	B-43	Empty	None
△	0.5	B-43	Empty	A (saw-tooth)
■	0.5	B-43	Empty	B (vortex gen)
▽	0.5	B-43	Empty	C (step)
○	0.5	B-43	Empty	D (ramp)

$\dfrac{P_{OA}}{Q}$

Mach No.
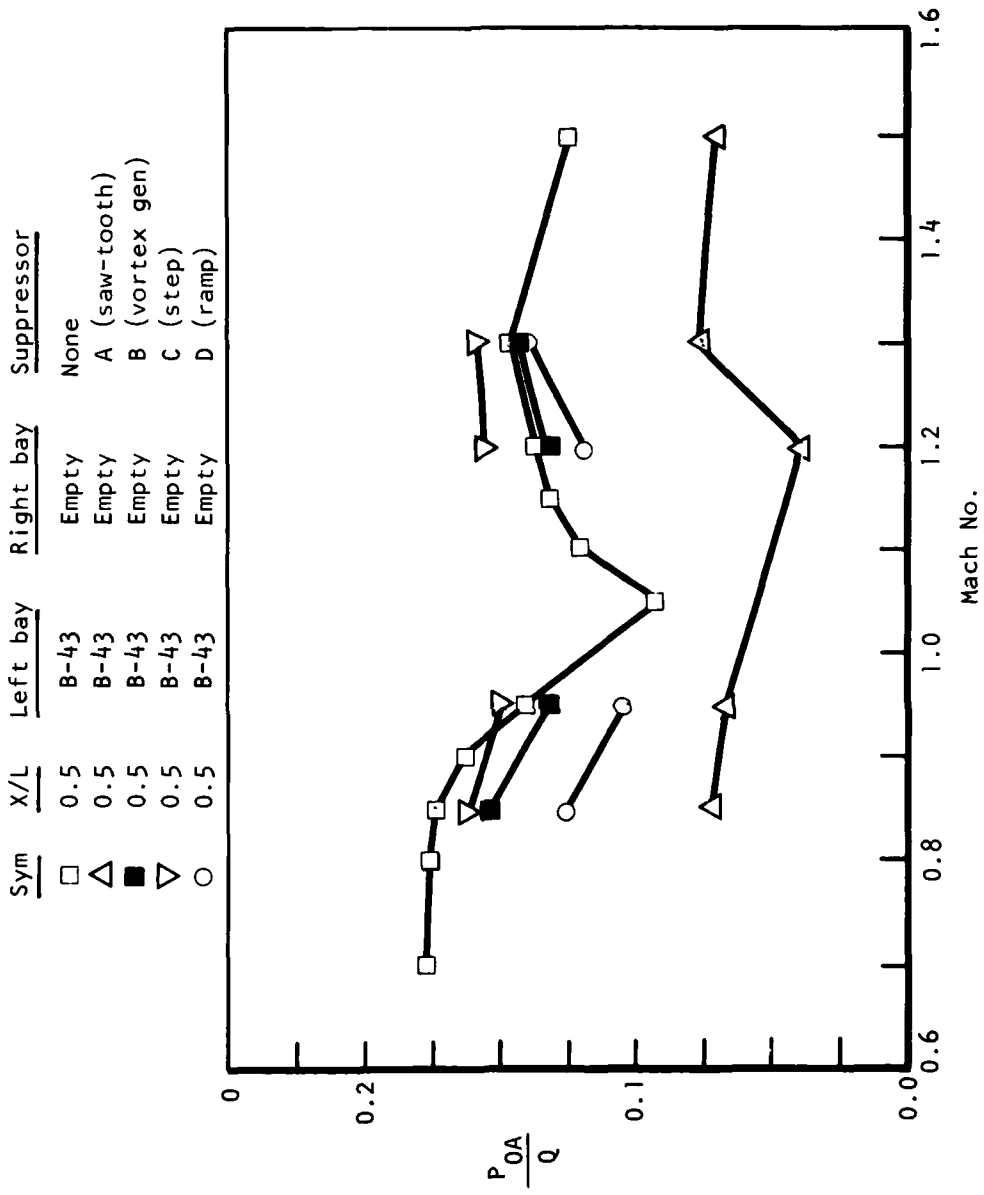
Reference AFFDL-TR-79-3003

Figure 169. Comparison of Suppressor Effectiveness, Left Wall, Mid-Bay Location

A spoiler was developed for the B-1 weapon bay which significantly reduced the cavity noise level. A summary of the various B-1 spoiler configurations is illustrated in Section III. The overall noise level is nondimensionalized with dynamic pressure and plotted as a function of mach number. Comparisons are shown relative to the unsuppressed bay for part- and full-open doors. The various types generally showed about the same noise reduction, except at supersonic speeds where none of the B-1 spoilers appeared effective in reducing the cavity noise level. The unsuppressed cavity noise level at supersonic speeds is much lower than at transonic speeds where the noise suppressors are very effective. The noise level in the B-1 weapon bay with spoilers deployed is shown in Section III for the cavity discrete resonant frequencies. Full-scale and wind tunnel data are shown for 90-degree porous and solid and 70-degree porous and solid spoilers. The noise level for each spoiler configuration was compared to unsuppressed cavity noise levels for full- and part-open doors and plotted as a function of mach number. Generally, the wind tunnel data showed noise reduction at subsonic and supersonic speeds while the full-scale data showed appreciable reduction at subsonic speeds but no reduction at supersonic speeds. This effect is not currently understood.

A prediction guideline for spoilers (located immediately forward of the cavity) which extend at least one local boundary thickness from the aircraft mold line is recommended based on evaluation of the data published in Section III. The prediction guideline is restricted to subsonic speeds due to the conflicting trends in some of the supersonic data.

The noise level of the dominant cavity resonant frequencies (modes 1 and 2) with noise-reduction spoilers located at the forward bulkhead is reduced 15 decibels, relative to the predicted levels for an unsuppressed cavity. The 15-decibel reduction applies throughout the cavity in the longitudinal and depth directions. The maximum broadband noise level in the cavity, which occurs on the aft lower bulkhead, is reduced 10 decibels, relative to the prediction of an unsuppressed cavity. The broadband noise level in the forward and top of the cavity is not attenuated by the spoiler and is equal to the predicted levels for an unsuppressed cavity.

CAVITIES WITH INTERNAL STORES

Noise-prediction methods for single cavities with internal stores have not been formalized in terms of equations relating noise level to the flow field and cavity configuration parameters for empty cavities. Guidelines have been established, however, that illustrate the effects of internal stores relative to empty cavities.

Cavity noise measurements with internal stores configurations have been published in the literature. The consensus of opinion in the literature on the effects of inserting stores in open cavities is that noise-level reductions occur when the store interacts with the shear layer and that little, if any, reduction occurs when shear layer store interaction does not occur. In some cases noise-level increases have been observed. Most of the published data are for unsuppressed cavities which in some cases shown high-amplitude discrete cavity resonances. The greatest noise-level reduction occurs for cavities with dominant resonant frequencies, in some cases, the intensity of the discrete resonance frequencies is reduced to the level of the broadband noise.
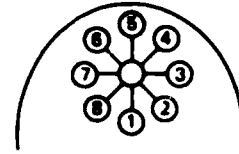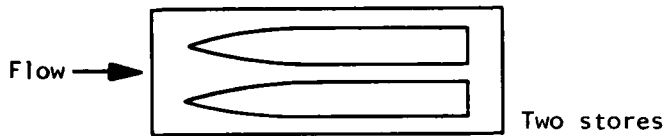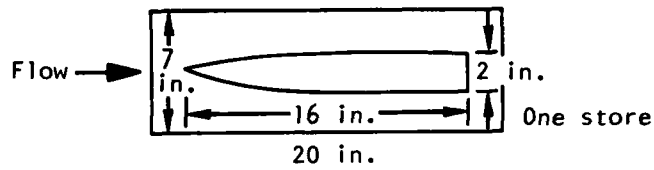
190
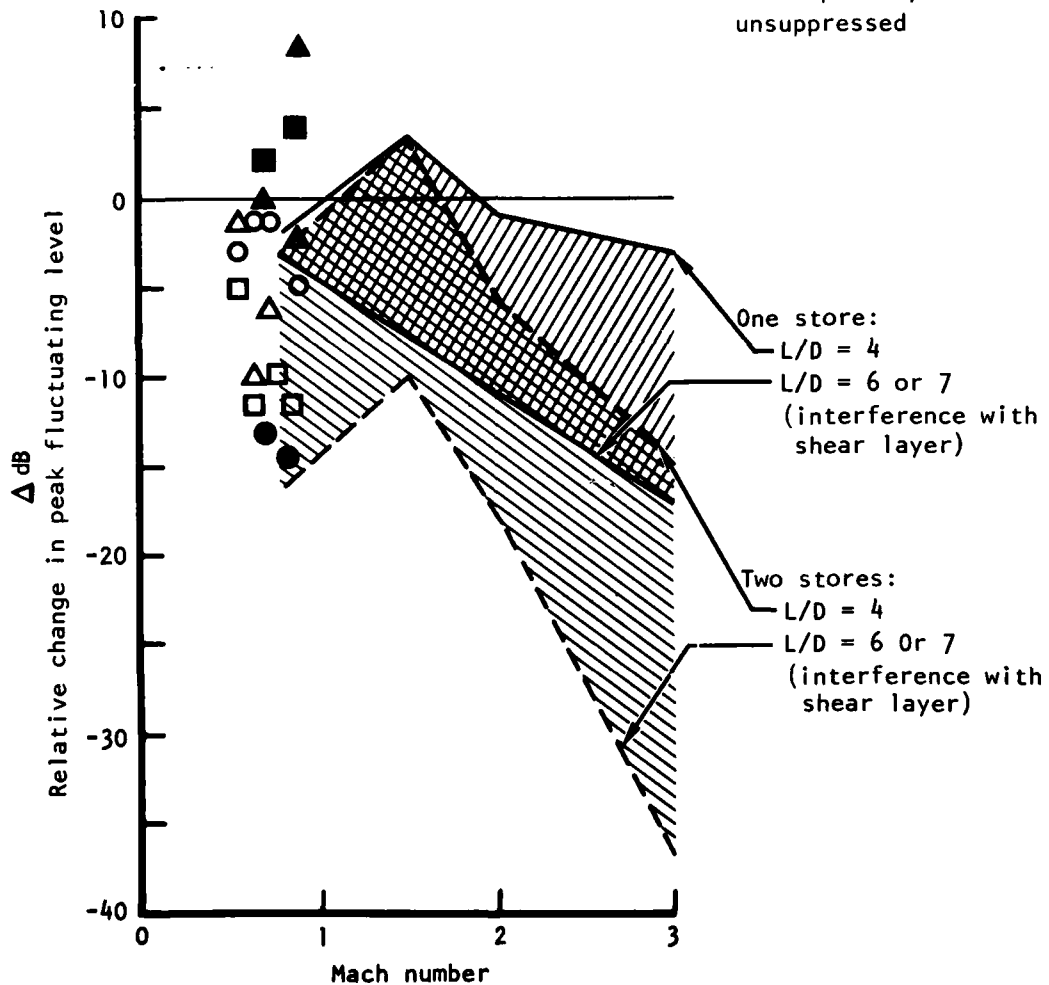
Figure 170. Effects of Stores on Peak Pressure Fluctuation Levels in Cavities - Full Weapon Bay, Eight Stores
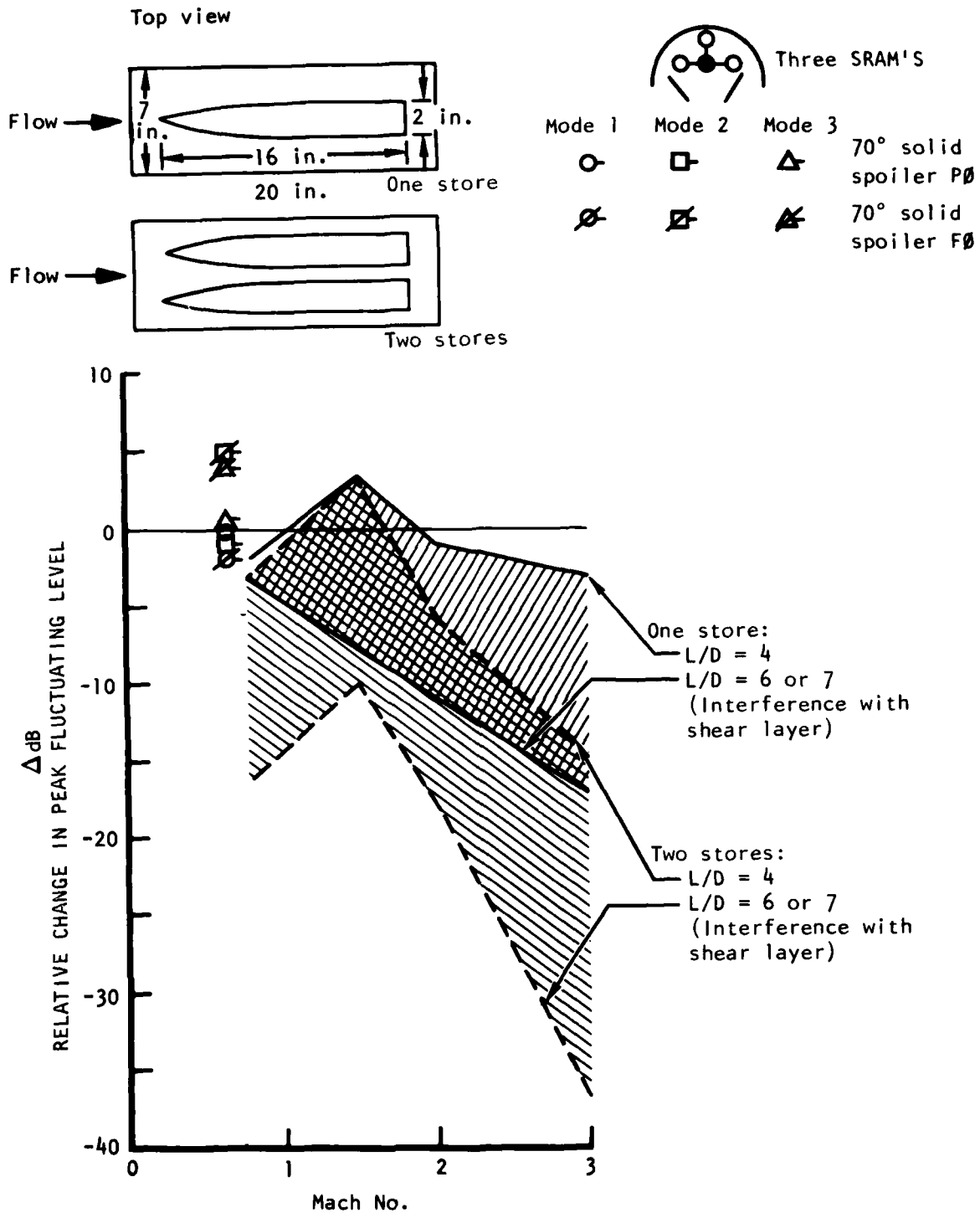
Figure 171. Effects of Stores on Peak Pressure Fluctuation Levels in Cavities - Partial Open Door, Three Stores
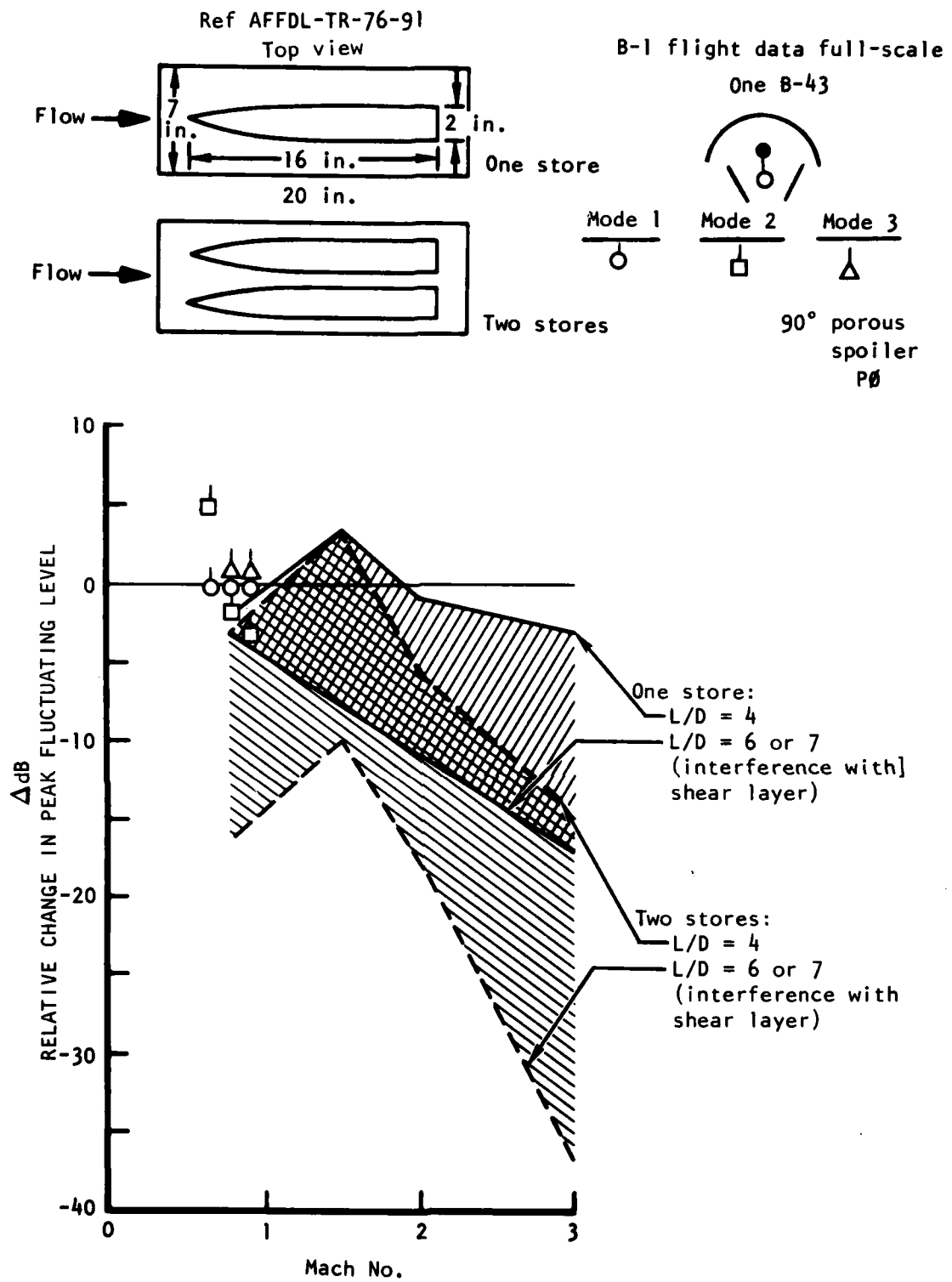
Figure 172. Effects of Stores on Peak Pressure Fluctuation Levels in Cavities - Partial Open Door, One Store

193

The data shown in Figure 170 through 172 illustrate the noise-level difference of various store configurations, relative to an empty cavity. The B-1 data are superimposed on summary plots published in Reference 11. The cavity/store configurations with noise-level suppressors show little noise-level difference between empty cavities and cavities with internal stores. The configurations without noise-level suppressors (Figure 170) show substantial noise-level reduction from the baseline empty cavity configuration. The data in Figure 170 for a full load of internal stores shows noise-level reduction for the discrete frequencies, but the broadband noise level shown in previous reports is unaffected by insertion of internal stores. The bottom stores in this configuration probably interact with the shear layer, which has been identified with reduced noise levels.

In summary, the effect of internal stores for unsuppressed cavities when the store configuration interacts with the shear layer is that the discrete resonances are reduced to broadband levels. For cavities where the internal stores do not interact with the shear layer, the discrete resonances are not effected and are equal to the empty cavity values. The broadband cavity noise level is not affected for either case and is equal to the empty cavity values.

For cavities with noise suppressors, the effects of store shear layer interaction are insignificant, and the cavity noise levels with internal stores are equal to the empty cavity noise levels.


MULTIPLE CAVITIES

Noise-prediction methods for single cavities have been formulated in the literature, with equations relating cavity geometry and flow field parameters. For multiple cavities, prediction methods have not been established, but empirical data illustrating the effects of multiple cavities have been published in the literature. These data have been used to establish noise-prediction guidelines to account for the effect of multiple cavities.

The B-1 cavity noise data (Section III) are correlated with the published guideline data. The multiple cavity noise levels are expressed relative to a baseline condition of a single cavity. These values can be added or subtracted from the predicted noise level of a single cavity to obtain multiple cavity noise levels.

CONSECUTIVE CAVITIES - EMPTY UNSUPPRESSED

The noise level inside open cavities located in close proximity is anticipated to interact, especially in the downstream cavities. Noise levels have been measured for two cavities in close proximity and documented in Reference 5. The data are summarized in Reference 11 and presented in terms of mach number and differential decibel level between the forward and aft bays for each of the three discrete cavity resonant frequencies.

The B-1 cavity noise data for two open cavities in close proximity are superimposed on the summary plots of Reference 11 in Figures 173 and 174 for full- and part-open B-1 cavity door positions, respectively. The initial data published in Reference 5 were obtained from a small-scale wind tunnel model. The B-1 data shown in Figures 173 and 174 were obtained from the 0.10-scale wind tunnel model and the full-scale aircraft. The multiple cavity data shown are for unsuppressed empty cavities.
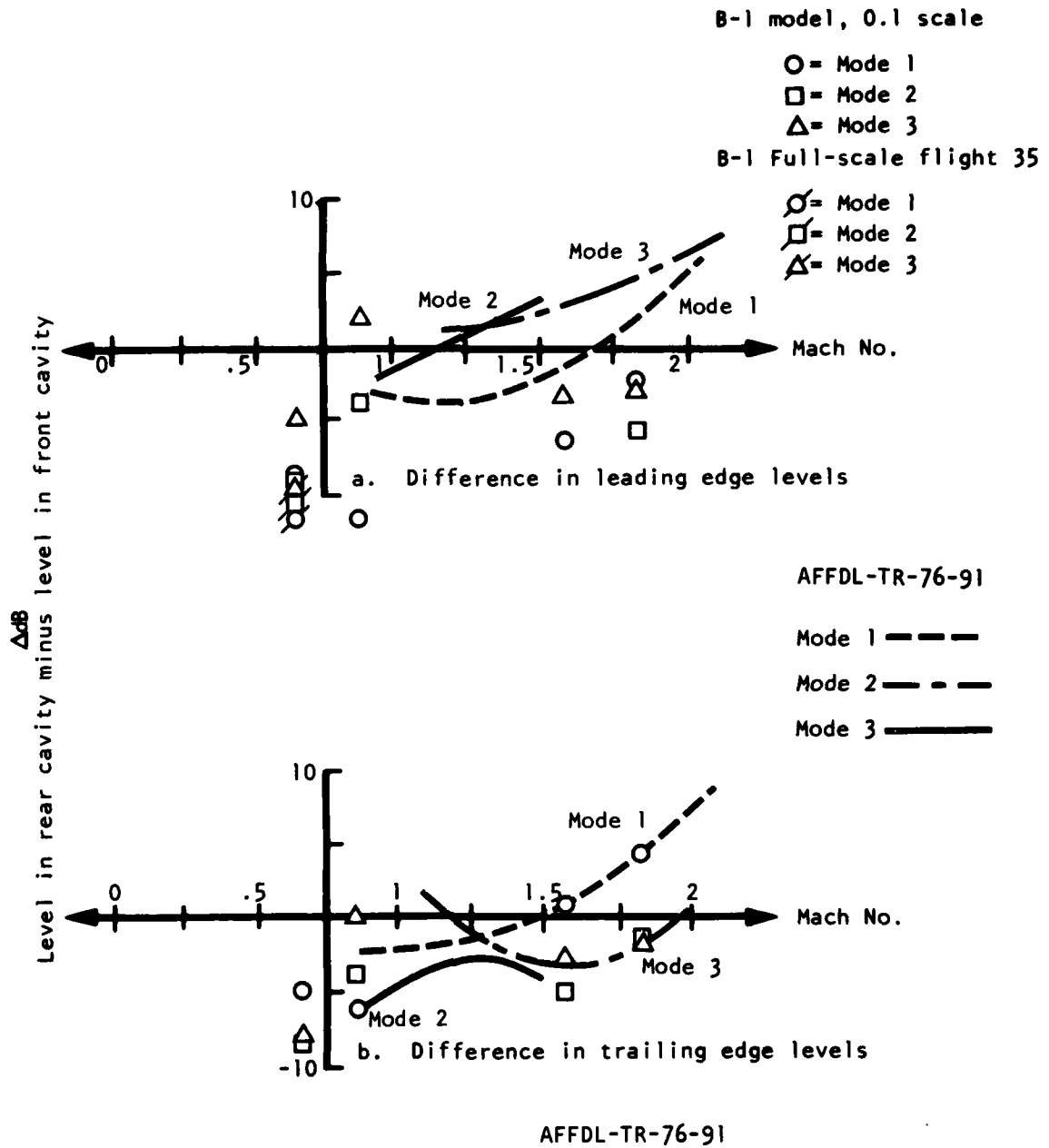
194

Figure 173. Comparison of Modal Pressure Levels in Consecutive
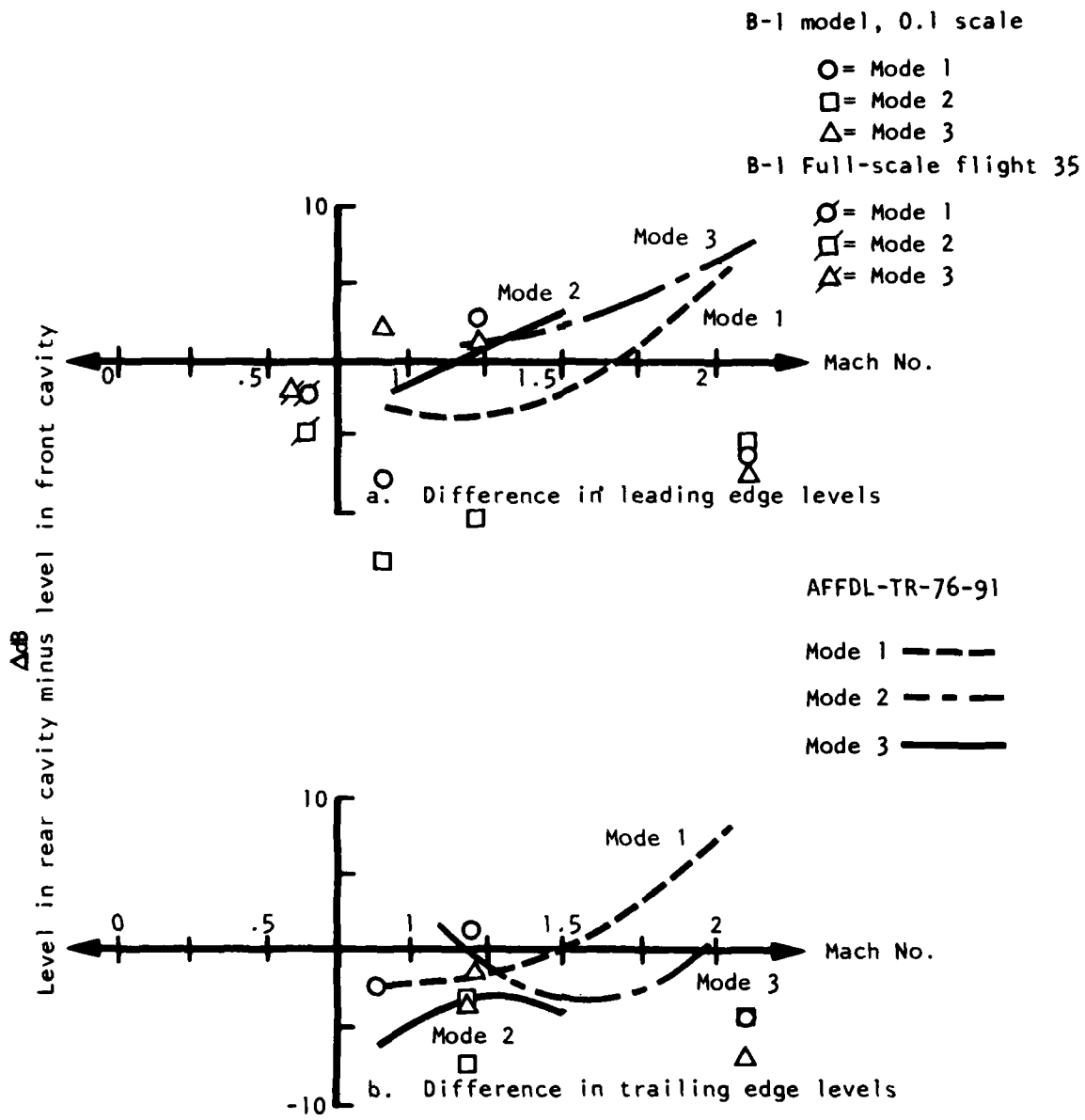Cavities - Full-Open Empty, Unsuppressed

195

Figure 174. Comparison of Modal Pressure Levels in Consecutive
Cavities - Part-Open Empty, Unsuppressed

196

Noise levels are shown for the forward and aft bulkheads for the forward and aft bays as a function of mach number. The previously published data indicate an increasing noise level in the aft cavity, with increasing mach number. The B-1 data show lower noise levels in the aft cavity at subsonic speeds, particularly near the cavity leading edges, but do not show the increased aft cavity noise level at supersonic speeds. A good deal of scatter exists in measured cavity noise levels; often, it is difficult to identify meaningful trends. The B-1 data on the average show that the noise level in the aft cavity is reduced in amplitude due to the presence and interaction of the forward cavity.

The noise level in the forward cavity of the two open cavity configurations compares favorably with a single open cavity (Section III). The forward cavity is therefore unaffected by the presence of the downsteam cavity, and the downsteam cavity noise level is generally reduced by the presence of an upstream cavity. The noise level for multiple cavities is summarized and a noise prediction guideline curve is shown in Figure 175.

CONSECUTIVE CAVITIES - EMPTY SUPPRESSED

The presence of spoilers on the leading edges of open cavities has been shown in Section III to greatly attenuate noise levels for single cavities. Cavity noise levels for two open bays are shown in Figures 176 through 184. Comparing the noise levels for suppressed and unsuppressed multiple cavities (Section III) shows substantial noise reduction.

The cavity noise data for unsuppressed cavities (Section III) indicated only slight cavity interaction. the forward cavity noise level was equal to a single open cavity and the noise level in the aft cavity of the two open cavity configurations showed slightly reduced levels relative to the forward cavity and baseline single cavity. The noise data for multiple cavities with noise suppressors shown considerable interaction. The fundamental cavity resonance (mode 1) is higher for two open cavities than for the single open cavity. The broadband noise levels and the higher order cavity modes are approximately the same for single and multiple cavities. The data in Figures 176 through 184 show the interaction of the forward and aft bay for several suppression devices. In general, the noise levels are higher in the aft cavity, expecially at supersonic speeds. It is apparent that even though the spoilers reduce the magnitude of the multiple cavity noise levels, they induce significant cavity interaction effects.

In summary a noise-prediction guideline for multiple cavities with suppression is to add 5 decibels to all discrete cavity resonances in the forward cavity and 10 decibels to all resonances in the aft cavity. The broadband level is the same as for a single open cavity.
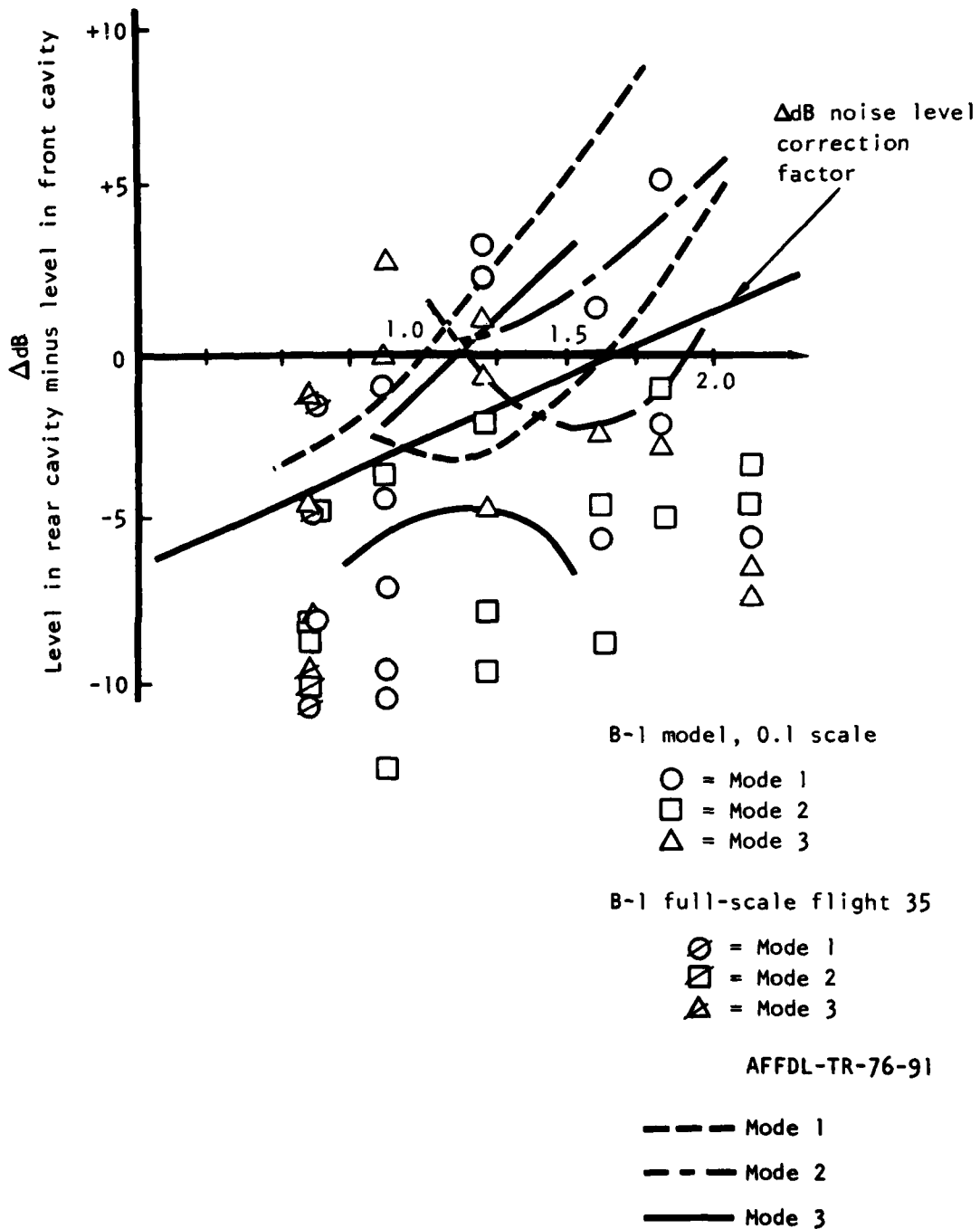
Figure 175. Multiple-Cavity Noise Level Correction

Figure 176. Comparison of Modal Pressure Levels in Consecutive Cavities -
Suppressed, 90° Porous Spoiler, Part-Open Empty

199

Figure 177. Comparison of Modal Pressure Levels in Consecutive Cavities -
Suppressed, 90° Porous Spoiler, Full-Open Empty

Figure 178. Comparison of Modal Pressure Levels in Consecutive Cavities -
Suppressed, 90° Solid Spoiler, Part-Open Empty
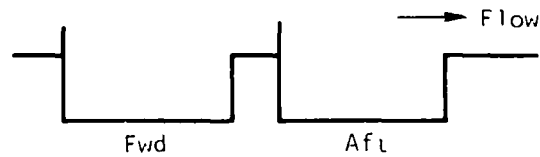
Figure 179. Comparison of Modal Pressure Levels in Consecutive Cavities -
Suppressed, 90° Solid Spoiler, Full-Open Empty
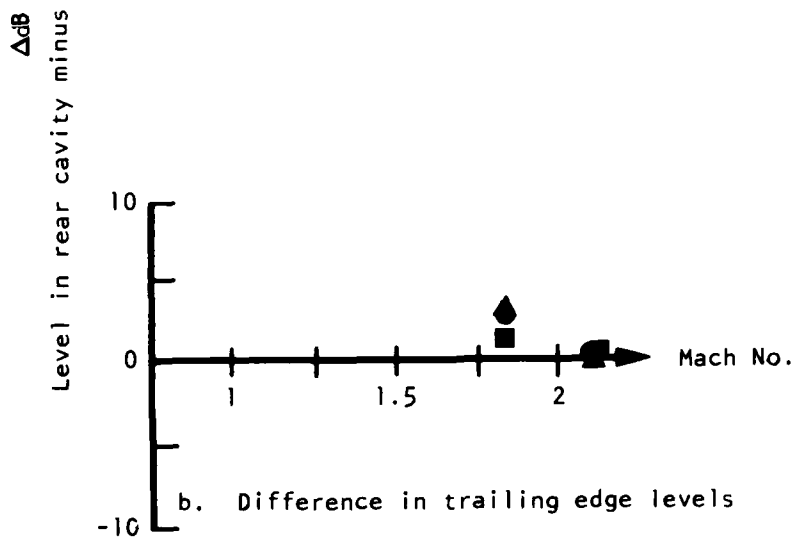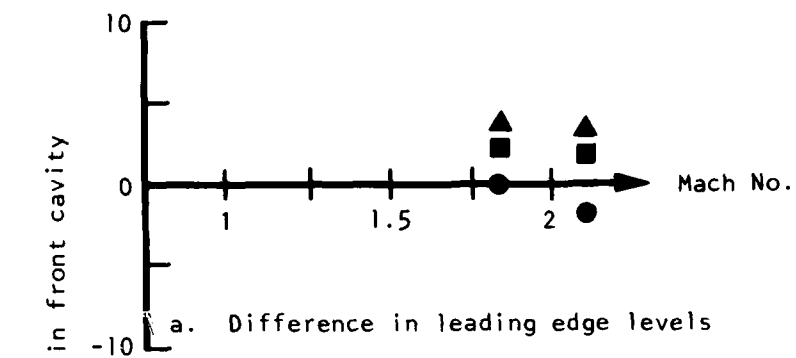
Figure 180. Comparison of Modal Pressure Levels in Consecutive Cavities - Suppressed, 70° Solid Part-Span Spoiler, Full-Open Empty

203

Figure 181.   Comparison of Modal Pressure Levels in Consecutive Cavities -
Suppressed, 70° Solid Full-Span Spoiler, Full-Open Empty
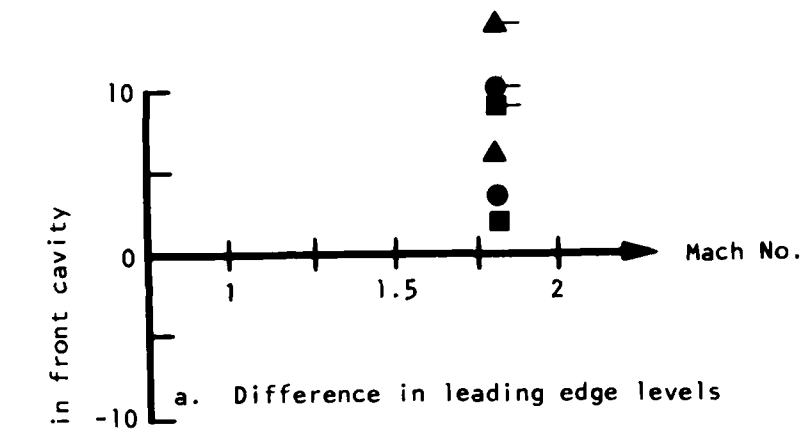
204

Figure 182. Comparison of Modal Pressure Levels in Consecutive Cavities - Suppressed, 70° Solid Spoiler, Full-Span, Part-Open Empty

205
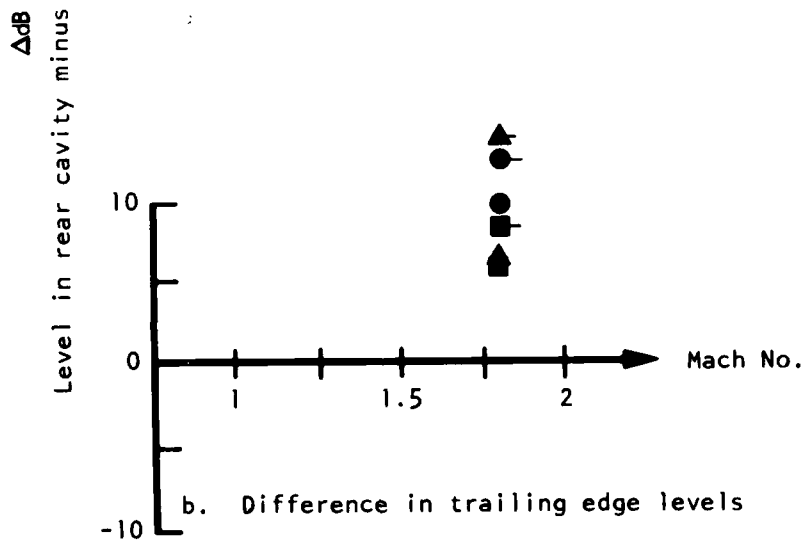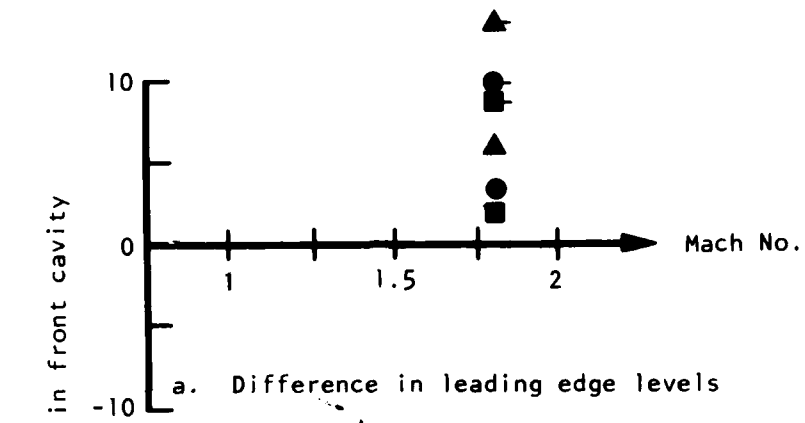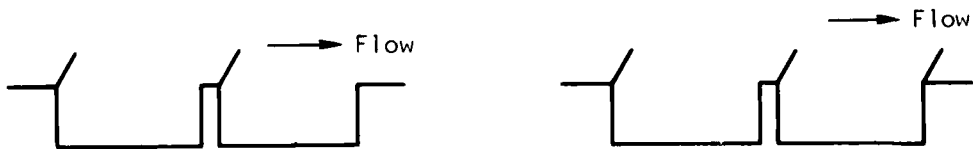
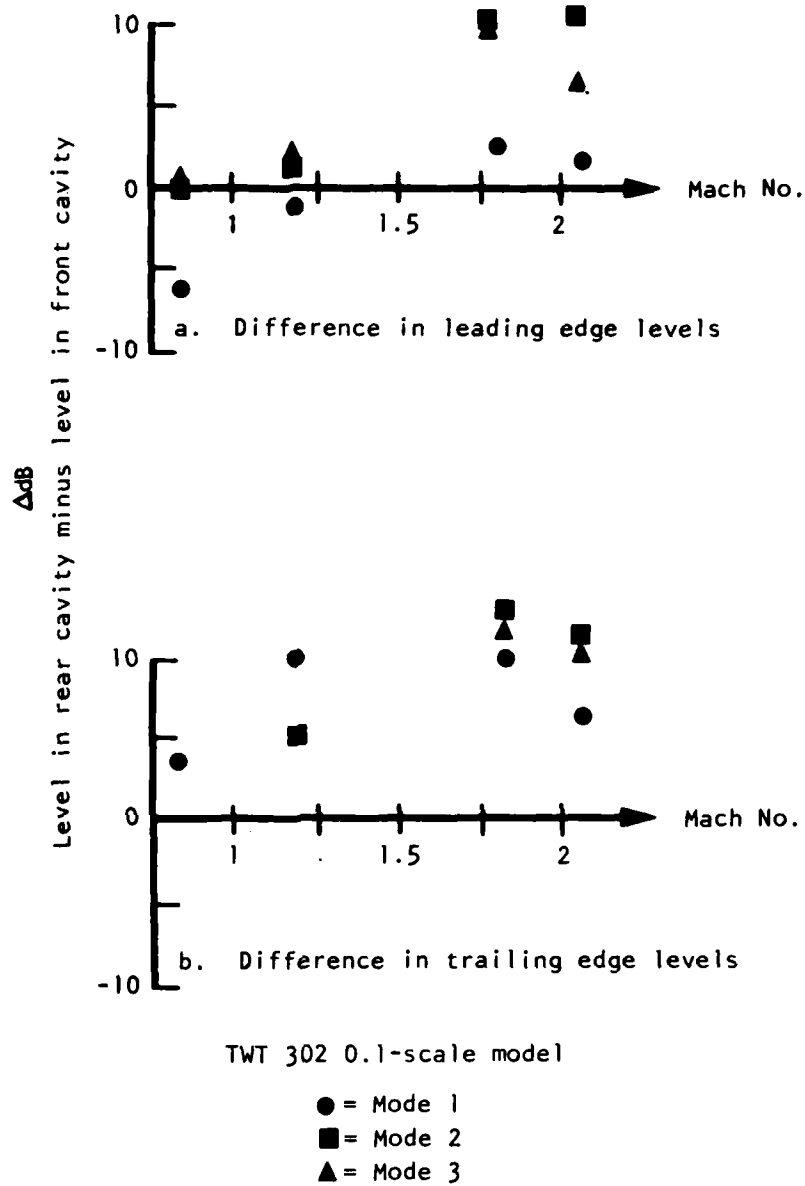Figure 183.   Comparison of Modal Pressure Levels in Consecutive Cavities - Suppressed, 70° Solid Spoiler, Full-Span, Part-Open Empty

206
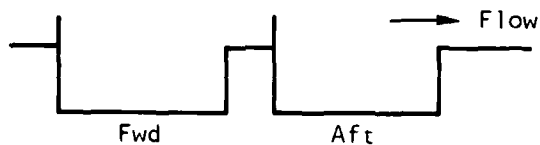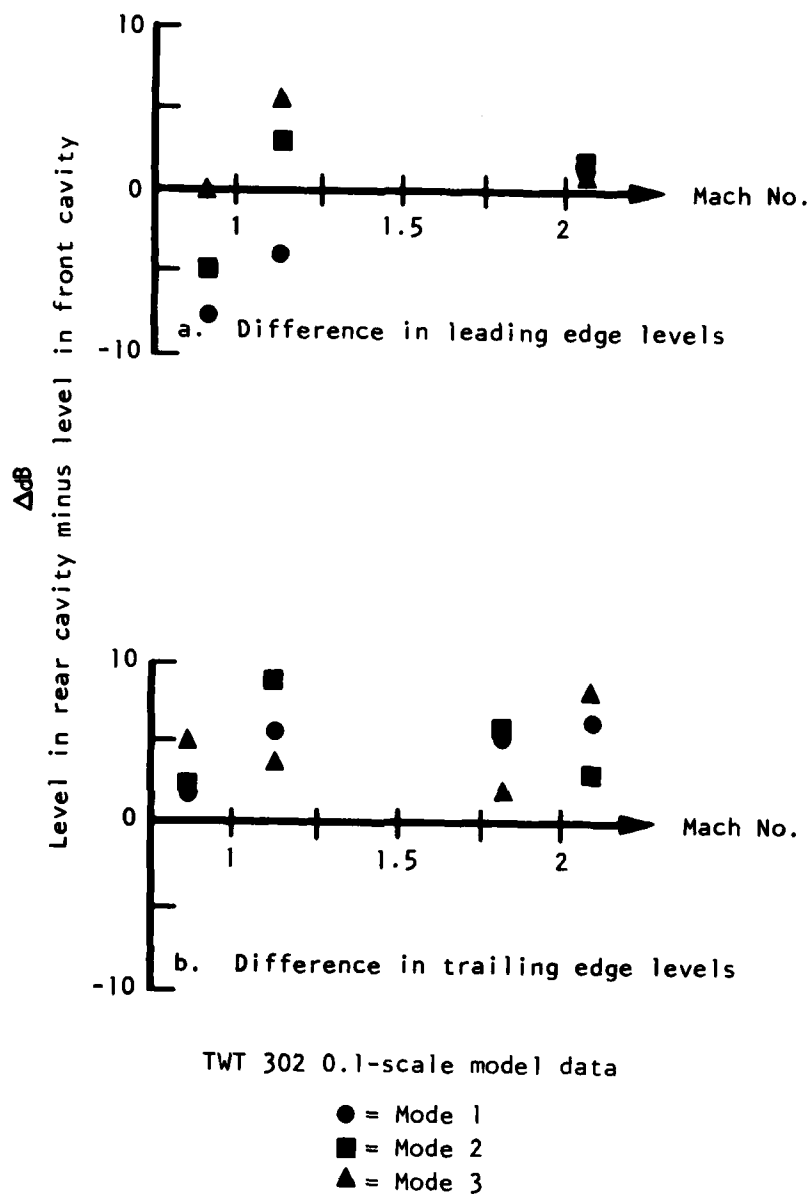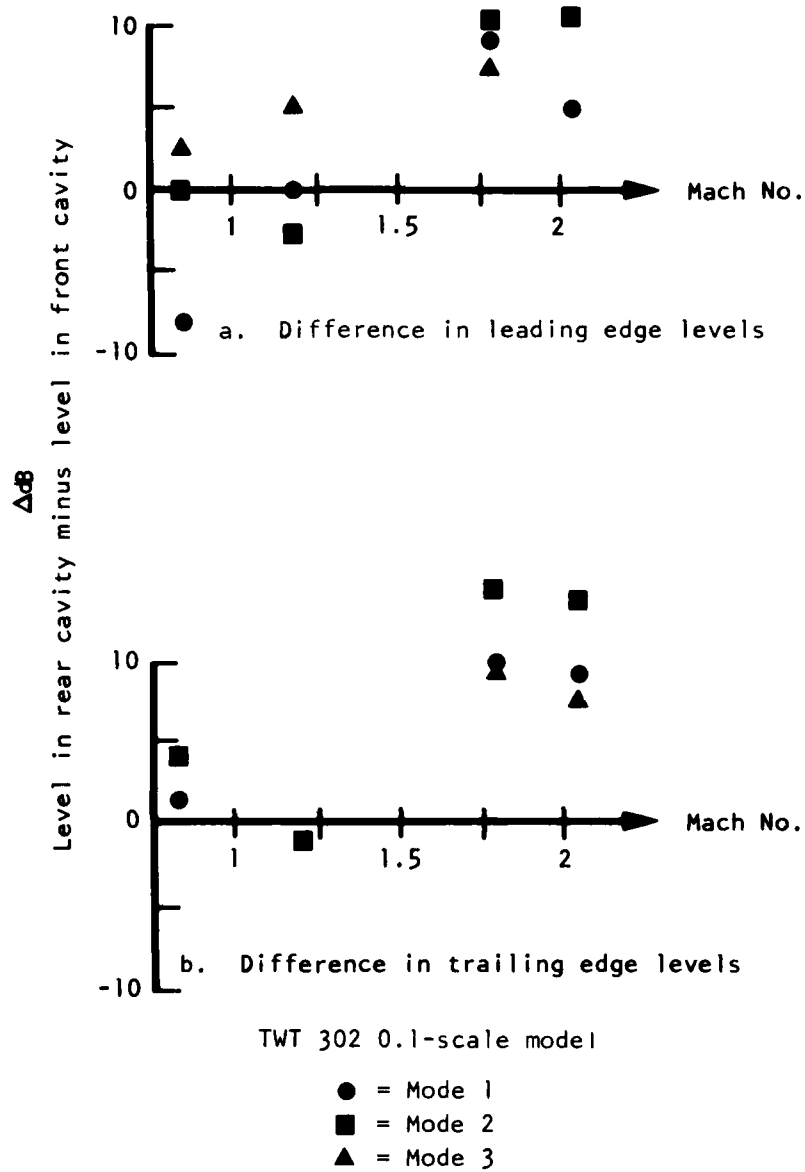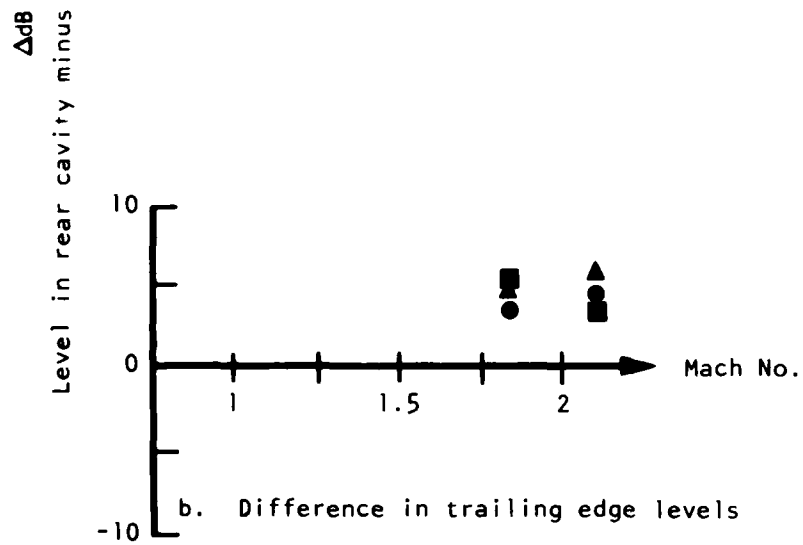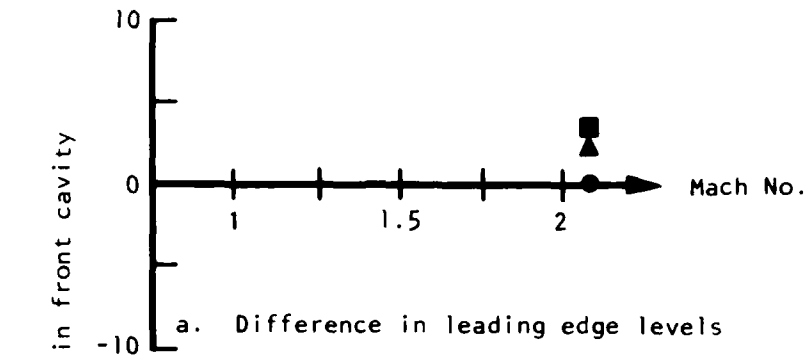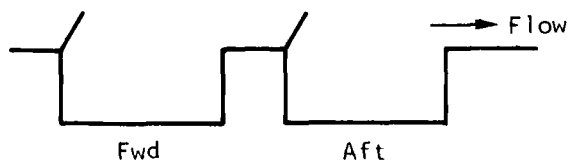
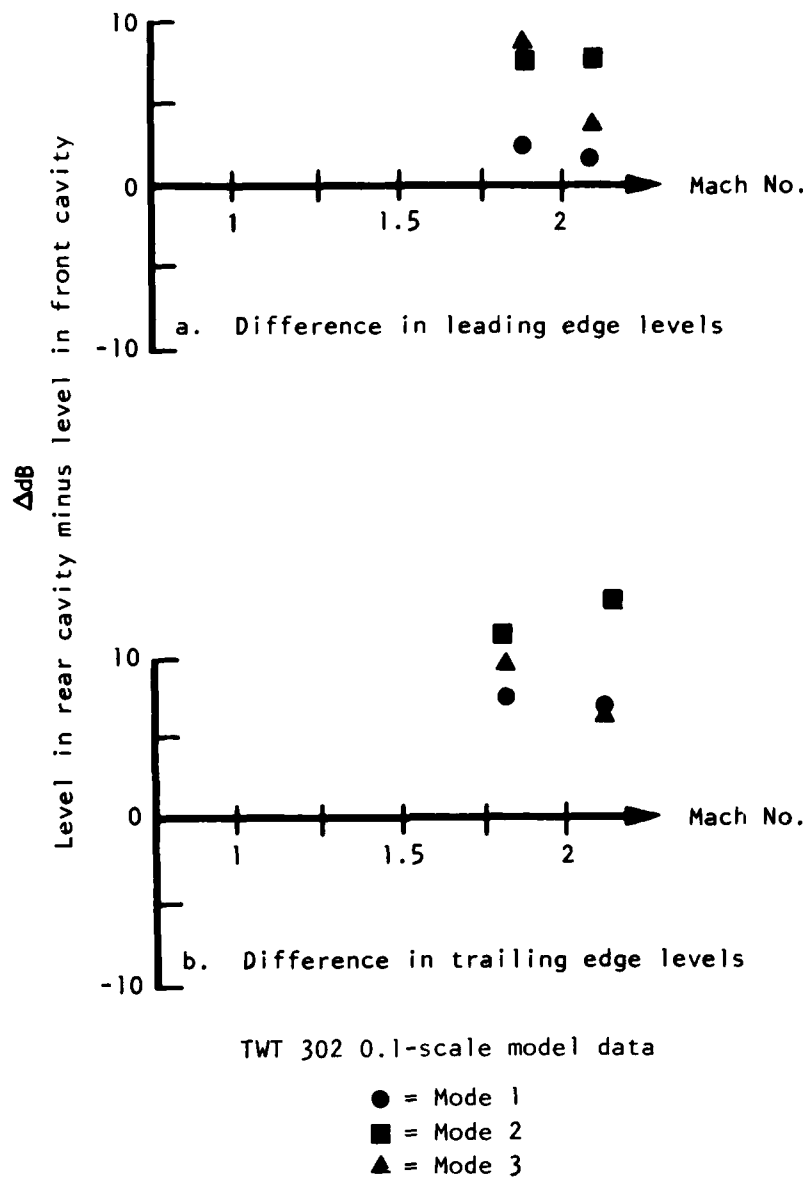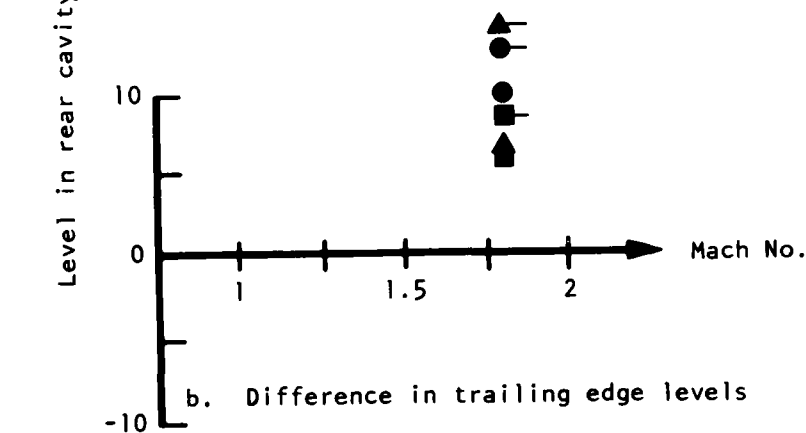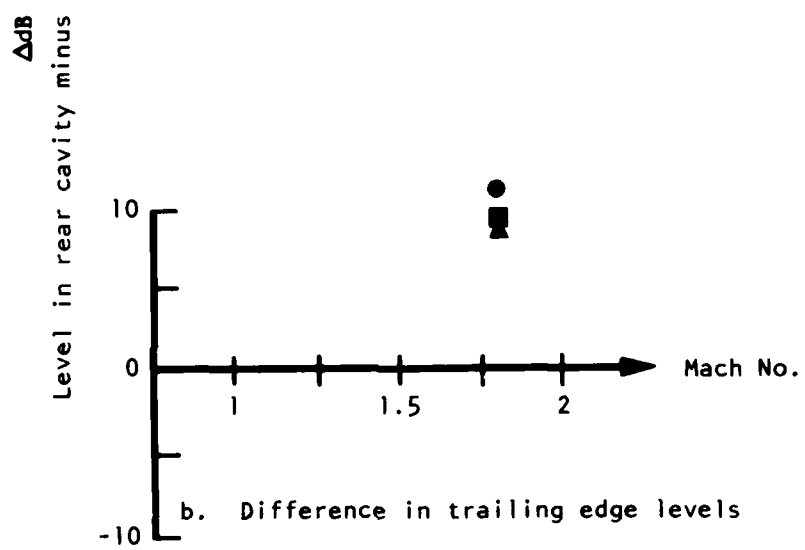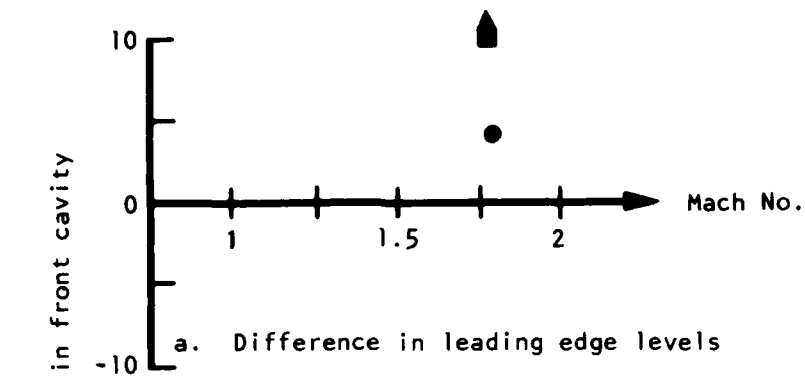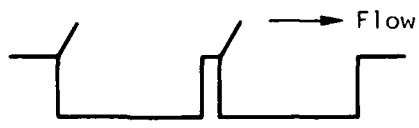Figure 184. Comparison of Modal Pressure Levels in Consecutive Cavities -
Suppressed, 70° Solid Spoiler, Part-Span, Part-Open Empty

SECTION V

RECOMMENDATIONS AND PREDICTION METHOD IMPROVEMENT

Prediction methods are evaluated in Section IV, and final recommendations are presented for empty-cavities, noise suppression device, internal stores, and two adjacent streamwise cavities. The single empty unsuppressed cavity is the baseline configuration, and the effects of noise suppressors, internal stores, and multiple cavities are expressed in terms of noise level differences relative to the baseline. A noise-level prediction of the baseline cavity is obtained, and the noise-level differences are added or subtracted from the baseline to obtain estimates for cavities with noise suppressors, internal stores, and multiple cavities.

EMPTY UNSUPPRESSED CAVITIES

Evaluation of the published prediction methods relative to B-1 data indicates the method of Reference 6 best fits the empirical B-1 data. The methods of Reference 6 result in conservative estimates of noise level for the B-1 cavities. In Section IV the noise-level conservatisms are illustrated and data scatter is discussed. Due to the scatter in cavity noise data, it is suspected that a ±10 decibel error could result in discrete cavity noise prediction and a ±5 decibel error for broadband noise prediction. The noise prediction methods of Reference 6 could be refined as previously discussed to provide a less conservative estimate of B-1 cavity noise level. The B-1 data are for a cavity of L/D = 2, and the data trends may not be applicable to other cavity L/D ratios on which the Reference 6 prediction method is based. In view of this and data scatter typical of cavity noise, it is recommended that the methods of Reference 6 be used without modification to obtain conservative predictions of empty cavity noise level. The prediction methods of Reference 6 are summarized in the following paragraphs for convenience.

MODAL FREQUENCIES

The modal or resonant frequencies are predicted with the modified Rossiter equation:

$$f_m = \frac{V}{L} \left[\frac{m - 0.25}{\dfrac{M}{(1 + \frac{K-1}{2} M^2)^{1/2}} + 1.75} \right] \quad m = 1,2,3,4$$

The equation can be used to predict modal frequencies for m as large as desired; however, this prediction scheme only concerns itself with the first four frequencies; i.e., m = 1, 2, 3, or 4.

NORMALIZED MODAL SOUND PRESSURE AMPLITUDES

The following expressions are used to determine the maximum normalized 1/3 octave-band sound pressure amplitude of the first three modal frequencies. The maximum value occurs at the rear of the cavity for each frequency.

$$20 \log (P_2 \text{ max}/Q) = 25 \text{ sech } [2(M-1)] - (3.3 \text{ L/D}) - 27$$

$$20 \log. (P_1 \text{ max}/Q) = 20 \log. (P_2 \text{ max}/Q) + 1.5 \text{ L/D} - 13$$

$$20 \log. (P_3 \text{ max}/Q) = 20 \log. (P_2 \text{ max}/Q) - 13 M + 9$$

For convenience to the user values of the "sech" function are included as Table 2.

LONGITUDINAL DISTRIBUTION

The longitudinal sound pressure distribution for the first three modes is determined by the following expression:

$$20 \log. (P_m/Q)_{X/L} = 20 \log. (P_m \text{ max}/Q) -$$

$$10[1- |\cos\alpha_m \text{ X/L}| + (0.33\text{L/D} - 0.6)(1 - \text{X/L}]$$

$$\alpha_1 = 3.5 \text{ rad} \qquad \alpha_3 = 10.0 \text{ rad}$$

$$\alpha_2 = 6.3 \text{ rad} \qquad \alpha_4 = 13.3 \text{ rad}$$

This expression describes the standing modes that were observed in the cavities for flight and wind tunnel data.

BROADBAND LEVELS

The final step in the prediction scheme is to determine the broadband levels. This is accomplished with the aid of the following equation

$$20 \log. (P_b \text{ max}/Q) = 20 \log. (P_2 \text{ max}/Q) +$$

$$[3.3 \text{ L/D} - 28 + 3(1 - \text{L/D}) (1 - \text{X/L})][1.2 - 0.4M]$$

to determine the maximum level for the peak 1/3-octave band.

With this maximum level determined by the preceding equation and Figure 185, the broadband spectrum can be defined, based upon Strouhal number, where the frequency spectrum is a function of cavity length and the free-stream velocity.

209

TABLE 2. VALUES OF THE "SECH" FUNCTION[a] - SECH $x = 2/ (e^x + e^{-x})$

x	"sech" x	x	"sech" x
0	1.000		
.1	.995	2.1	0.241
.2	.980	2.2	.219
.3	.957	2.3	.199
.4	.925	2.4	.180
.5	.887	2.5	.163
.6	.844	2.6	.148
.7	.797	2.7	.134
.8	.748	2.8	.121
.9	.698	2.9	.110
1.0	.648	3.0	.099
1.1	.599	3.1	.090
1.2	.552	3.1	.081
1.3	.507	3.3	.074
1.4	.465	3.4	.067
1.5	.425	3.5	.060
1.6	.388	3.6	.055
1.7	.354	3.7	.049
1.8	.322	3.8	.045
1.9	.293	3.9	.040
2.0	.266	4.0	.037

[a]Refer to Reference 6.

$$20 \log(P_b max/Q) = 20 \log(P_2 max/Q) + [3.3 \, L/D - 28 + \sigma$$
$$3 \, (1 - L/D)(1 - X/L)][1.2 - 0.4M]$$

Strouhal number, $S = \dfrac{fL}{V}$
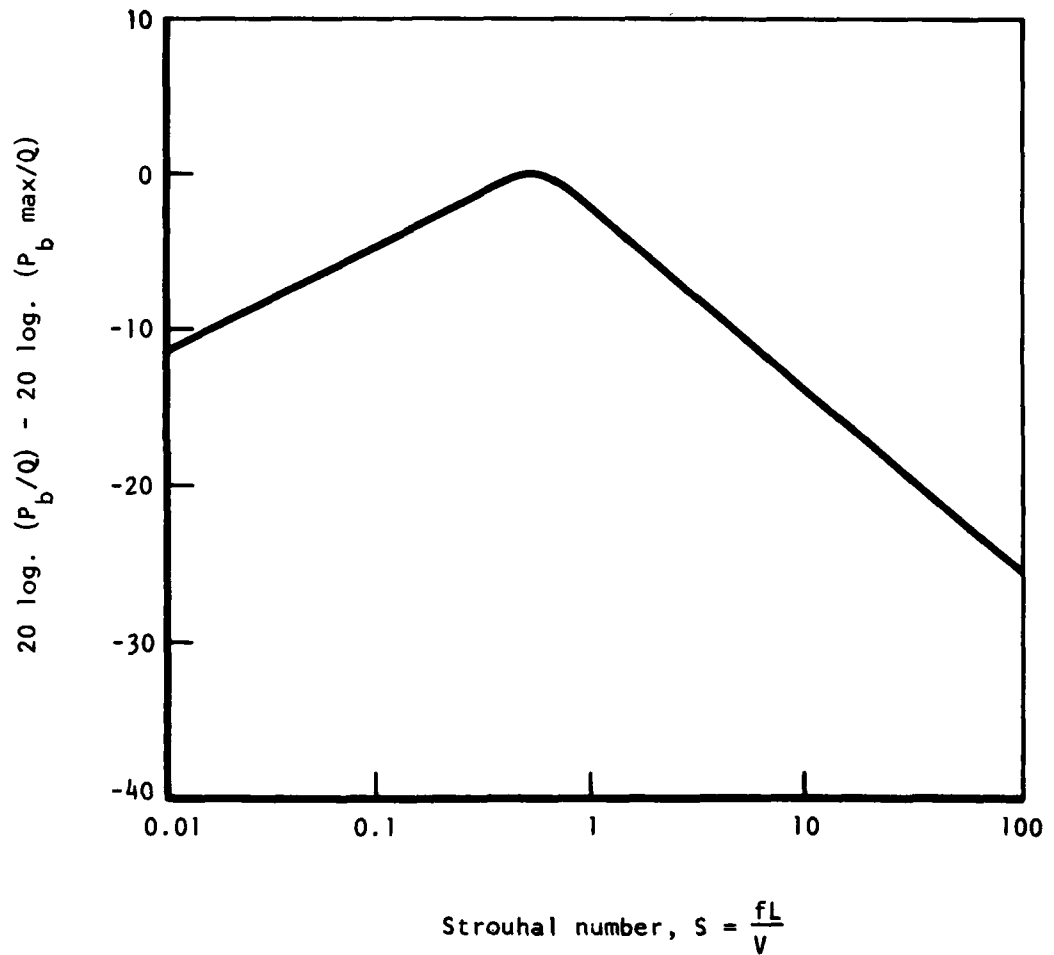
(Reference 6)

Figure 185.   One-Third Octave Broadband Level Versus Strouhal Number

211

CAVITY NOISE-REDUCTION DEVICES

A noise-prediction guideline for spoilers located immediately forward of the cavity which extend at least one local boundary thickness from the aircraft mold line is recommended, based on B-1 data. The prediction guideline is restricted to subsonic speeds, due to the conflicting trends in some of the supersonic data.

The noise level of the dominant cavity resonant frequencies (modes 1 and 2) with noise-reduction spoilers located at the forward bulkhead is reduced 15 decibel relative to the predicted levels for an unsuppressed cavity. The 15-decibel reduction applies throughout the cavity in the longitudinal and depth directions. The maximum broadband noise level in the cavity which occurs on the aft lower bulkhead is reduced 10 decibels relative to the prediction of an unsuppressed cavity. The broadband noise level in the forward and top of the cavity is not attenuated by the spoiler and is equal to the predicted levels for an unsuppressed cavity. The broadband noise-level spectrum shape is the same as for the baseline unsuppressed cavity.

CAVITIES WITH INTERNAL STORES

For cavities with internal stores without noise-reduction spoilers:

1. Predict baseline noise level for empty cavity.

2. For cavities with store configuration that interacts with the shear layer, broadband noise is equal to the baseline, and discrete cavity resonances are reduced in amplitude to the broadband levels.

3. For cavities with store configurations that do not interact with the shear layer, broadband noise is equal to the baseline, and discrete cavity resonances are equal to the baseline.

For cavities with internal stores with noise-reduction spoilers:

1. Predict baseline noise level for empty suppressed cavity.

2. For all internal store configurations, broadband and discrete noise levels are equal to the baseline, and effects of shear layer and store interaction are insignificant.

TWO ADJACENT STREAMWISE CAVITIES

The cavity separation distance in the streamwise direction is a significant parameter in cavity interaction effects. Not much data are available to assess this variable. The multiple cavity noise-level prediction guideline in the following paragraphs is derived with two immediately adjacent open cavities. It is anticipated that when two open cavities are located greater than four cavity depths apart, cavity interaction is minimized, and the cavity noise level is equal to a single open cavity.

For multiple cavities without noise-reduction spoilers, the following procedure is recommended.

1. Predict baseline noise level for single open cavity.

2. Forward cavity noise equal to baseline.

3. Aft cavity noise level is obtained by adding noise-level correction factors in Figure 184 to the baseline.

For multiple cavities with noise-reduction spoilers:

1. Predict baseline noise level for a single open cavity with spoilers.

2. Add 5 decibels to all discrete cavity resonances for the forward cavity. Broadband noise level is equal to baseline.

3. Add 10 decibels to all discrete cavity resonances for the aft cavity. Broadband noise level is equal to baseline.

SAMPLE PROBLEM

Two weapon bays are located in close proximity (less than four cavity depths apart) and are opened to deploy stores at mach 0.8 Q = 950 psf. The bays are 24-feet long and 6.5-feet deep. Determine maximum noise level inside open weapon bay for the following conditions.

1. Single open bay unsuppressed

    a. Full internal stores

    b. Empty

2. Single open bay suppressed

    a. Full internal stores

    b. Empty

3. Both bays open unsuppressed

    a. Empty

4. Both bays open suppressed

    a. Empty

SAMPLE PROBLEM SOLUTION - BASELINE CAVITY EMPTY UNSUPPRESSED

First, the four modal or resonant frequencies are calculated from the modified Rossiter equation

$$f_m = \frac{V}{L} \left[\frac{\frac{m - 0.25}{M}}{(1 + \frac{K-1}{2} M^2)^{1/2}} + 1.75 \right]$$

where

m = 1, 2, 3, and 4 (mode number)
M = 0.8 (free-stream mach number)
Q = 950 psf (free-stream dynamic pressure)
L = 24 feet (cavity length)
K = 1.4
V = 893.15 ft/sec (free-stream velocity)

Therefore for mode 1:

$$f_m = \frac{893.15}{24} \left[\frac{\frac{1 - 0.25}{0.8}}{(1 + \frac{1.4-1}{2} 0.8^2)^{1/2}} + 1.75 \right]$$

$$= (37.2) \left[\frac{0.75}{2.5} \right]$$

$$= 11.16 \text{ Hz}$$

Correspondingly, modes 2, 3, and 4 are calculated as:

Mode 2 = 25.8 Hz

Mode 3 = 40.6 Hz

Mode 4 = 55.4 Hz

Second, the predicted discrete pressure levels for modes 1, 2, and 3 are calculated, starting with the mode 2 level:

$$20 \log. (P_2 \text{ max}/Q) = 25 \text{ sech } [2(M-1)] - (3.3 \text{ L/D}) - 27$$

Where

$$L/D = \left(\frac{24 \text{ ft}}{6.5 \text{ ft}}\right) = 3.7$$

$$20 \log. (P_2 \text{ max}/Q) = 25 \text{ sech } [2(.8-1)] - [3.3(3.7)] - 27$$

$$= 25 \text{ sech } [-0.4] - [12.2] - 27$$

From Table 2 sech $[-0.4] = 0.925$

$$20 \log. (P_2 \text{ max}/Q) = 25(0.925) - [12.2] - 27 = -16.1$$

$$P_2 \text{ max} = (0.157)Q = 0.157(6.6) = 1 \text{ psi or } 171 \text{ dB re } 0.0002 \frac{\text{dyne}}{\text{cm}^2}$$

From the mode 2 level, the mode 1 level can then be calculated

$$20 \log. (P_2 \text{ max}/Q) = 20 \log. (P_2 \text{ max}/Q) + 1.5 \text{ L/D} - 13$$

$$= -16.1 + 1.5(3.7) - 13$$

$$= -23.56$$

$$P_1 \text{ max} = (0.066)Q = 0.066(6.6) = 0.44 \text{ psi or } 163.5 \text{ dB re } 0.0002 \frac{\text{dyne}}{\text{cm}^2}$$

From the mode 2 level the mode 3 level can also be calculated

$$20 \log. (P_3 \text{ max}/Q) = 20 \log. (P_2 \text{ max}/Q) - 13M + 9$$

$$= -16.1 - 13(.8) + 9$$

$$= -17.54$$

$$P_3 \text{ max} = (0.13)Q = 0.13(6.6) = 0.87 \text{ psi or } 169.6 \text{ dB re } 0.0002 \frac{\text{dyne}}{\text{cm}^2}$$

Third, the maximum 1/3-octave broadband level in the cavity is calculated from:

$$20 \log. (P_b \text{ max}/Q) = 20 \log. (P_2 \text{ max}/Q) +$$

$$[3.3 \text{ L/D} - 28 + 3(1 - \text{L/D})(1 - \text{X/L})][1.2 - 0.4M]$$

where $X/L = 1$ corresponds to the maximum predicted 1/3-octave broadband predicted level in the cavity at the aft edge of the cavity.

$$20 \log. \ (P_b \ \text{max}/q) = -16.1 + [3.3(3.7) - 28 + 3(1 - 3.7)(1 - 1)][1.2 - 0.4(0.8)]$$

$$= -16.1 + [12.2 - 28][1.2 - 0.3]$$

$$= -30.3$$

$$P_b \ \text{max} = (0.031)(q) = (0.031)(6.6) = 0.2 \ \text{psi or 157 db re 0.0002} \ \frac{\text{dyne}}{\text{cm}^2}$$

Using Figure 185, the 1/3-octave-band spectrum can be generated, based upon the Strouhal number values, and the relationship:

$$S = \frac{fL}{V}$$

where

    V = free-stream velocity

    L = cavity length

    f = 1/3-octave-band center frequency

The empty cavity baseline noise levels are shown in Figure 186. The effects of internal stores in accordance with prediction guidelines are shown in Figure 187. The effects of noise suppressors are illustrated in Figure 188. The multiple bay noise levels are shown in Figures 189, 190, and 191 in accordance with the noise-prediction guidelines.
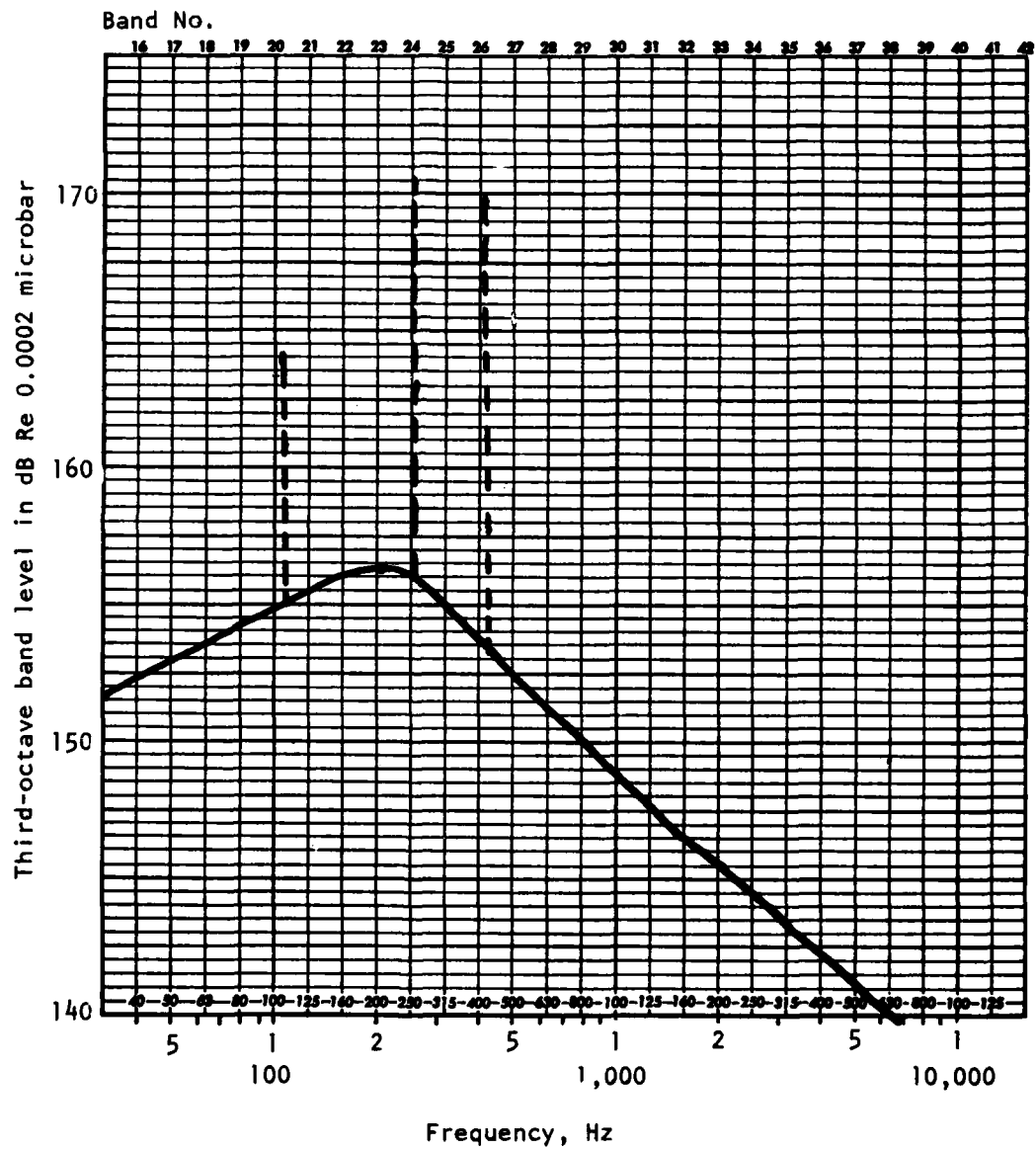
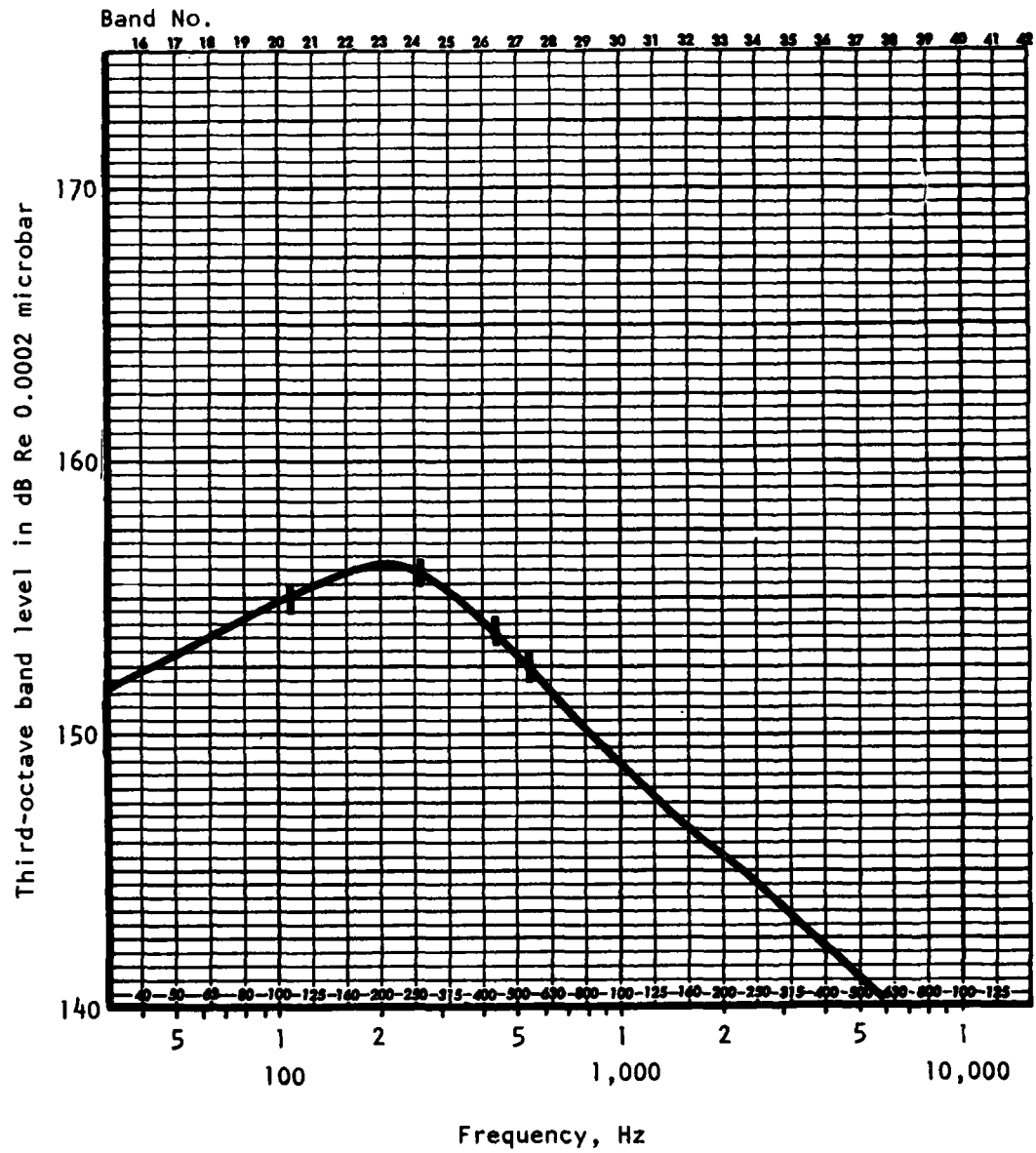Figure 186. Aft Bulkhead Lower, Unsuppressed Empty Single Open Bay

Figure 187. Aft Bulkhead Lower, Single Open Bay Unsuppressed -
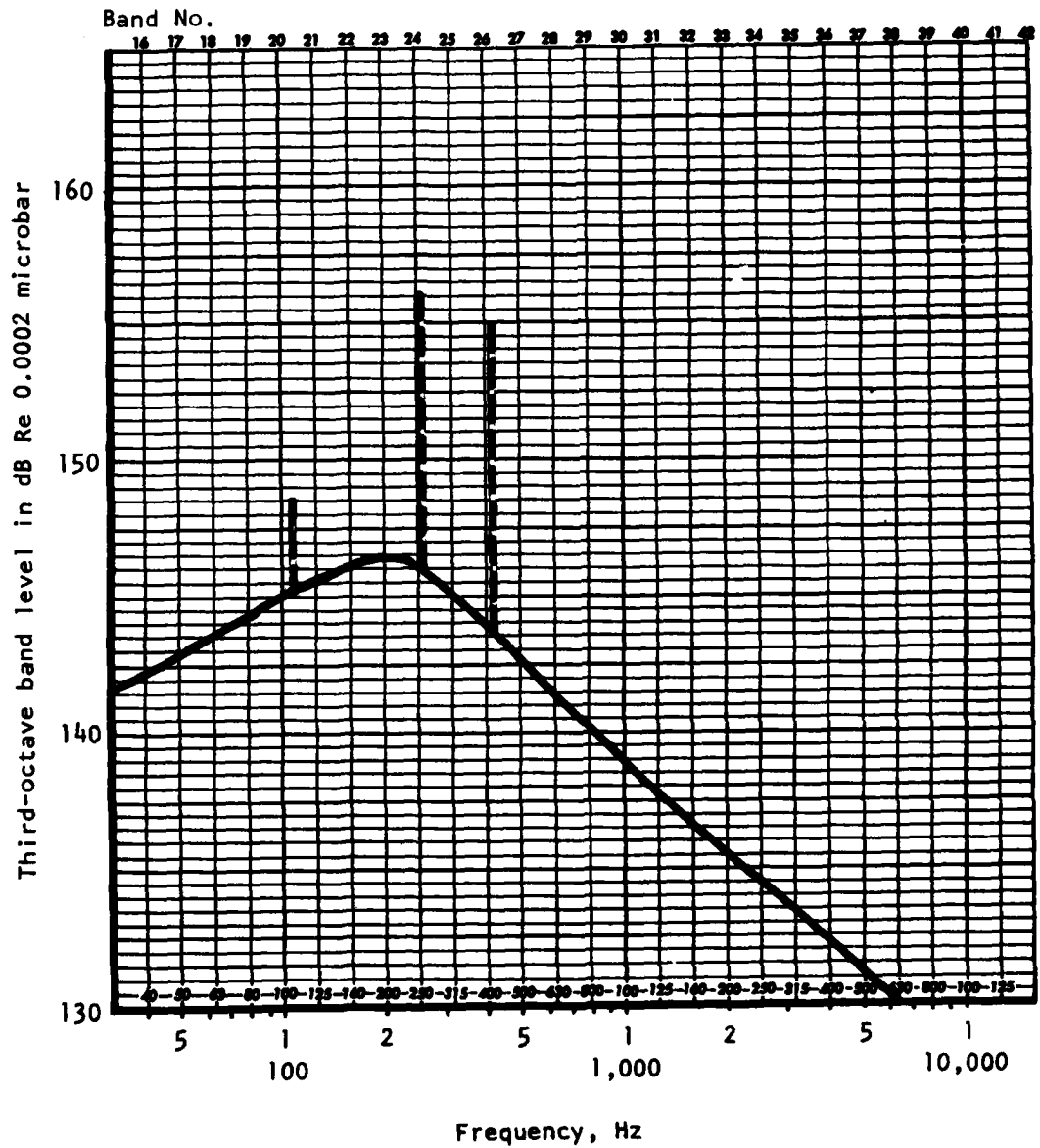Full Internal Stores With Shear Layer Interaction

218

Figure 188. Aft Bulkhead Lower Single Open Bay -
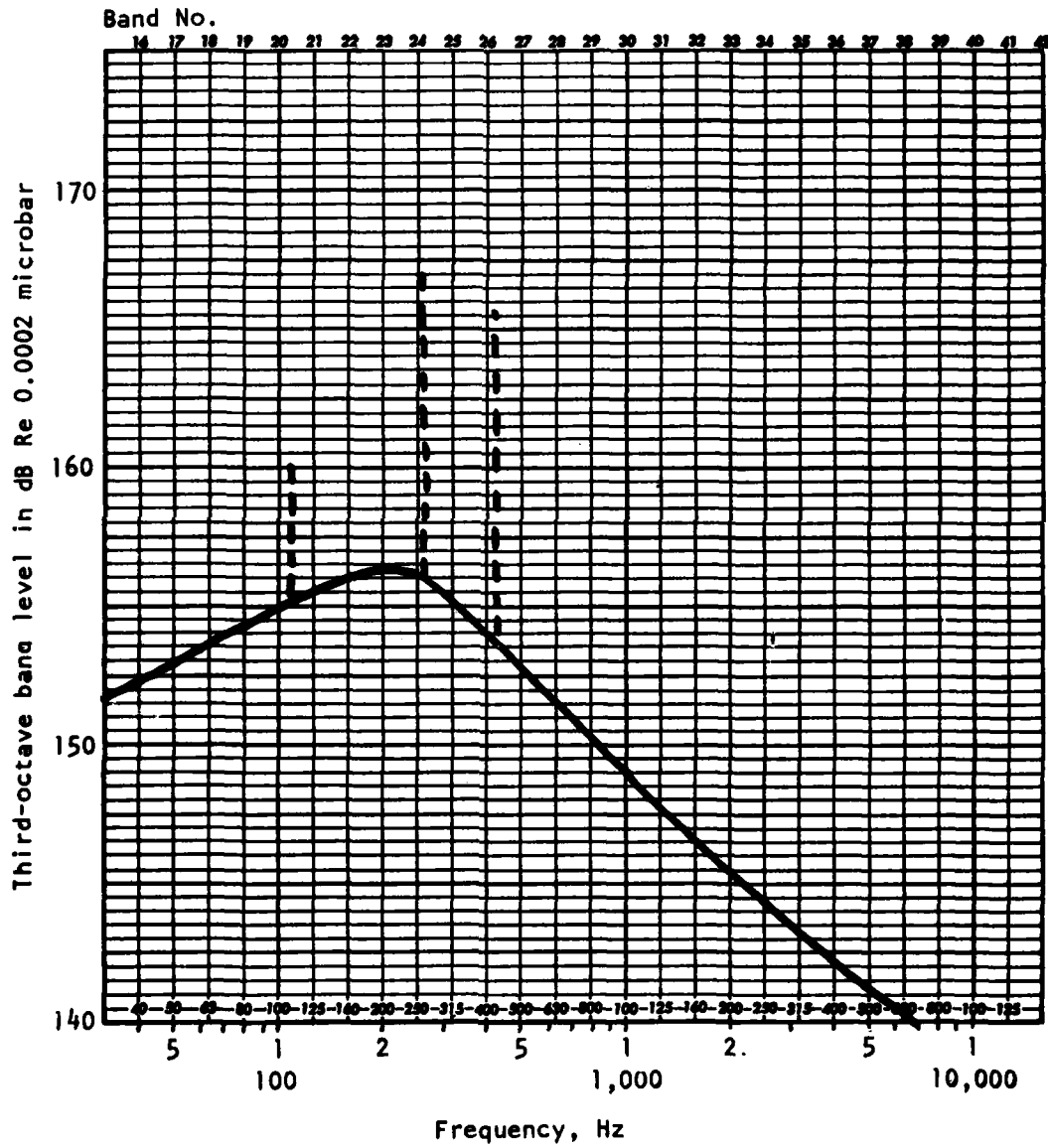Suppressed Empty and Suppressed With Stores

219

Figure 189. Aft Bulkhead Lower Multiple Bay -
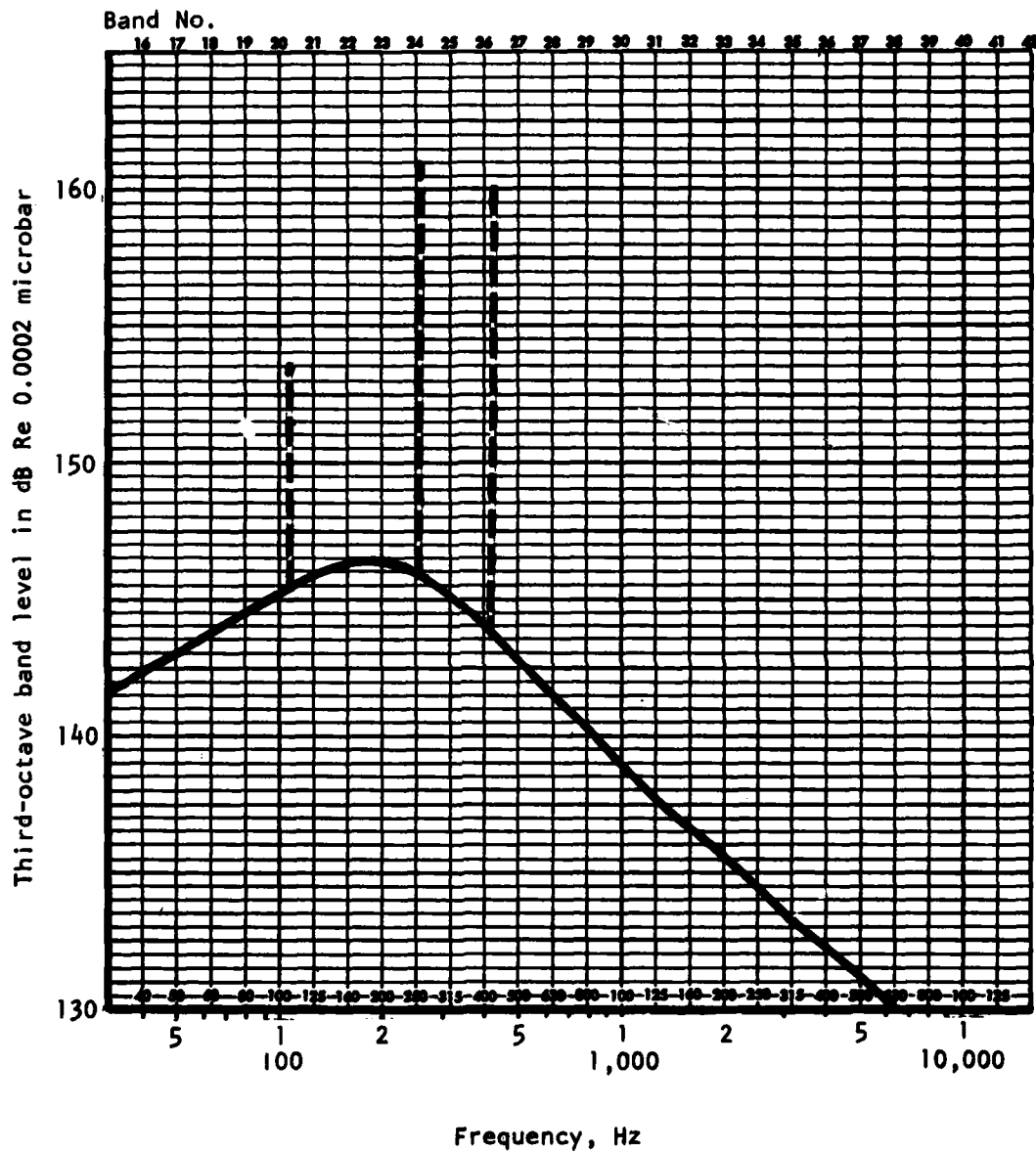Trailing Cavity - Unsuppressed Empty

Figure 190. Aft Bulkhead Lower Multiple Bay -
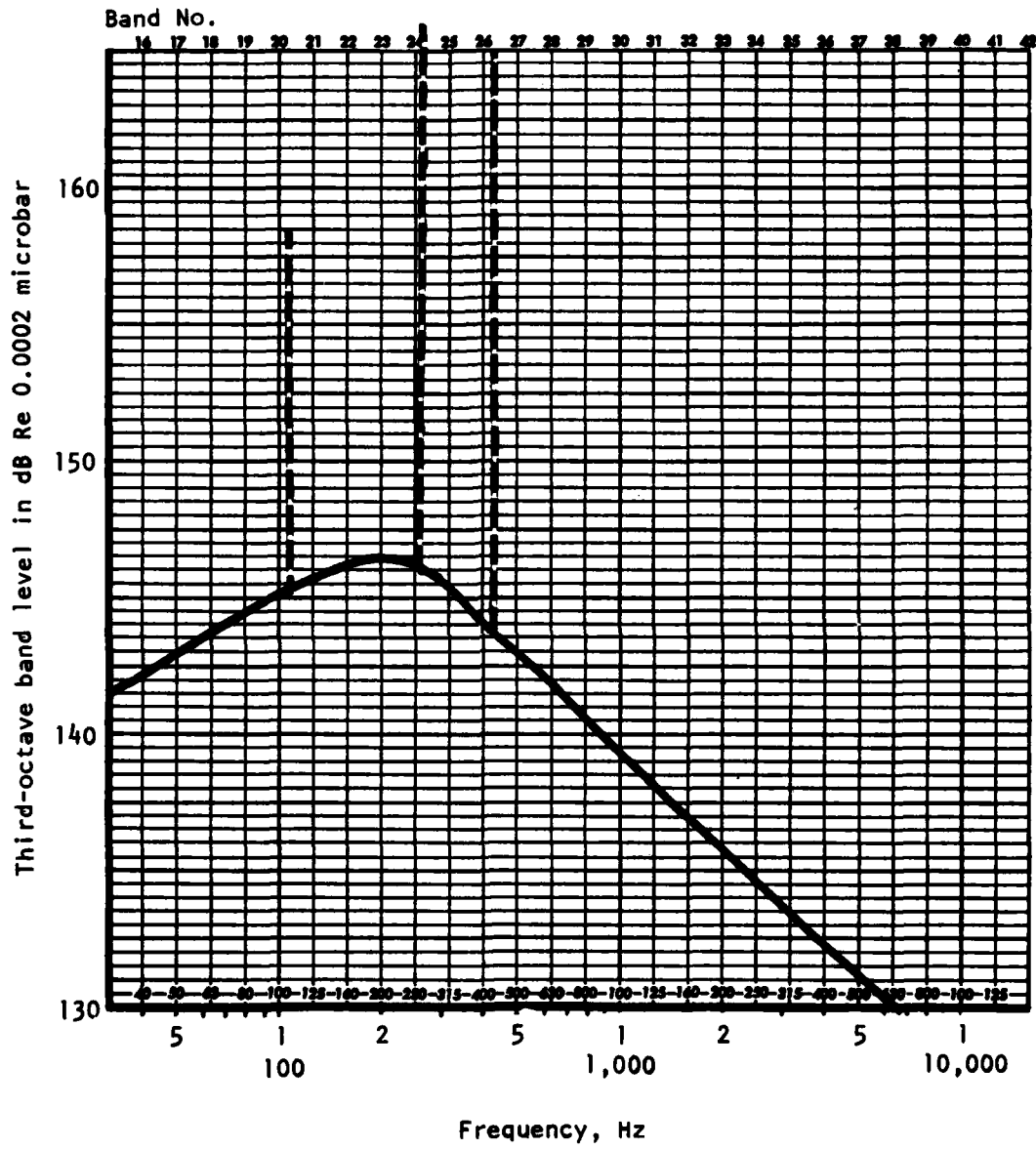Leading Bay - Suppressed Empty

221

Figure 191. Aft Bulkhead Lower Multiple Bay
Trailing Bay - Suppressed Empty

REFERENCES

1. Plumblee, H.E., et al, "A Theoretical and Experimental Investigation of the Acoustic Response of Cavities in an Aerodynamic Flow," WADD TR-61-75, March 1962

2. Borland, C.J., "Numerical Prediction of the Unsteady Flowfield in an Open Cavity," AIAA 77-673, June 1977

3. Hankey, W.L., and Shang, J.S., "The Numerical Solution to Pressure Oscillations in an Open Cavity," AIAA 79-0136, January 1979

4. Heller, H.H., et al, "Flow-Induced Pressure Oscillation in Shallow Cavities," AFFDL TR-70-104, December 1970

5. Heller, H.H., and Bliss, D.B., "Aerodynamically Induced Pressure Oscillations in Cavities-Physical Mechanisms and Suppression Concepts," AFFDL TR-74-133, February 1975

6. Smith, D.L., and Shaw, L.L., "Prediction of the Pressure Oscillations in Cavities Exposed to Aerodynamic Flow," AFFDL TR-75-34, October 1975

7. Shaw, L.L., et al, "Aero-Acoustic Environment of a Rectangular Cavity With a Length to Depth Ratio of Four," AFFDL TM-74-19 FYA, January 1974

8. Smith, D.L., et al, "Aero-Acoustic Environment of Rectangular Cavities With Length to Depth Ratios of Five and Seven," AFFDL TM-74-79 FYA, April 1974

9. Shaw, L.L., and Smith, D.L., "Aero-Acoustic Environment of Rectangular Cavities With Length to Depth Ratios in the Range of Four to Seven," Shock and Vibration Bulletin 45, Part 3, June 1975

10. Ungar, E., et al, "A Guide for Estimation of Aeroacoustic Load on Flight Vehicle Surfaces Volume I," AFFDL TR-76-91, Vol I, February 1977

11. Ungar, E., et al, "A Review of Methods for Estimation of Aeroacoustic Loads on Flight Vehicle Surface, Volume II," AFFDL TR-76-91, Vol II, February 1977

12. Bliss, D. B., and Hayden, R., "Landing Gear and Cavity Noise Prediction," NASA CR 2714, July 1976

13. Clark, R. L., "Weapons Bay Turbulence Reduction Techniques," AFFDL TM 75-147 FXM, December 1975

14. Clark, R. L., "Evaluation of F-111 Weapon Bay Aero-Acoustic and Weapon Separation Improvement Techniques," AFFDL TR 79-3003, February 1979

15. Shaw, L. L., "Suppression of Aerodynamically Induced Cavity Pressure Oscillation," AFFDL TR 79-3119, November 1979